2004-04-30

Self-Assembled Systems for Molecular Device Applications

Christopher G. F. Cooper
Worcester Polytechnic Institute

Self-Assembled Systems for Molecular Scale Device Applications

By

Christopher G.F. Cooper

A Dissertation

Submitted to the Faculty

of the

WORCESTER POLYTECHNIC INSTITUTE

in partial fulfillment of the requirements for the

Degree of Doctor of Philosophy

in

Chemistry

by

_____

April 5, 2004

APPROVED

_____	_____
Dr. W.Grant McGimpsey, Major Advisor	Dr. John C. MacDonald, Co-Advisor
_____	_____
Dr. James P. Dittami, Committee Member and Department Head	Dr. Nicholas K. Kildahl, Committee Member

_____

Dr. Danial D.M. Wayner, External Examiner

Abstract

The rational design, synthesis, and characterization of several systems that undergo self-assembly are described. Systems were chosen based on their ability to self-assemble in a highly ordered and predictable fashion that imparts order on the structure such that it is able to perform a given device function. Herein we describe self-assembled multilayered thin films on gold that can behave as molecular wires with tunable length, photocurrent generating films, and surfaces with photoswitchable wettability, and self-assembling peptide nanotubes that can potentially function as long range energy and electron transfer conduits.

A non-covalent, modular approach to multilayered thin film fabrication was used to generate three thin film systems that function as molecular scale wires, photocurrent generating devices, and photoswitchable thin films, respectively. These films were based on 4-[(10-mercaptodecyl)oxy]pyridine-2,6-dicarboxylic acid self-assembled monolayers on gold. These monolayers are able to chelate metal (II) ions, and thus multilayers were assembled based on metal-ligand coordination chemistry. The three systems described were characterized by contact angle measurements, electrochemical methods, and grazing angle IR spectroscopy. All three systems emphasize the versatility of a modular approach to thin film construction, and provide proof-of-concept for future studies.

A cyclic octapeptide architecture was employed as a scaffold for the predictable self-assembly of photoactive groups within a nanotubular structure. The degree of cyclic

peptide aggregation in stacking nanotube systems and non-stacking monomer systems, was studied via fluorescence emission spectroscopy. Based on the spectral results, it was determined that peptide nanotubes can be constructed such that photoactive side chains can be assembled in stacks. Future experiments for the determination of long range energy and/or charge transfer in these systems are also discussed.

Acknowledgements

I would like to sincerely thank my advisor Dr. W. Grant McGimpsey for allowing me to work in his laboratory for the past four years. I have learned more under his tutelage than I have during any other period of my life. Besides being a fantastic mentor, and an incredibly astute scientist, Dr. McGimpsey has also been a friend, always willing to take time out from a busy schedule to discuss science over a beer. It's hard to imagine having a better graduate experience than I have had working for his group.

I would also like to thank all my friends and colleagues at WPI. In particular, I'd like to thank Mr. Ernesto Soto. Ernesto has collaborated on a great deal of the work that is presented in this thesis. Ernesto is an excellent chemist with a very sharp mind, and excellent musical tastes. Thanks also go to Dr. Hubert Nienaber, who has always been willing to share his voluminous knowledge of organic chemistry, or debate world politics for hours on end. Dr. John Benco has also played a crucial role in my graduate career. It was John who took me under his wing when I first came into the McGimpsey group, and taught me all about photochemistry. Without John to initially get me started, who knows how things may have turned out. Additionally, I'd like to thank Dr. Christopher Lambert, Dr. John MacDonald, Mr. Mustafa Guler, Ms. Nantanit Wanichacheva and Ms. Cheryl Nowak. All of you have made my days at WPI very enjoyable.

I would also like to thank my family. Both my father (Christopher Cooper, Sr.), and my mother (Gail Sroka) have been inspirational throughout my life. They have

always been supportive, and really encouraged me to attend graduate school. Without their lifelong support, I certainly would not be in the position that I am today.

Finally, I'd like to thank Kathy Dennen. She has helped me keep my sanity throughout graduate school, and certainly through the thesis writing stage, in more ways than I could possibly detail here.

Table of Contents

List of Figures

List of Tables

List of Synthetic Schemes

I. INTRODUCTION

Arguably, there have been few topics in recent scientific history that have received as much attention as molecular nanotechnology. More than any other field within the sciences, nanotechnology has been the focus of the government, the media, the general public, the academic world, and industry. By its simplest definition, nanotechnology refers to the development and use of devices that have dimensions on the order of nanometers (1×10^{-9} m). Devices of this exceptionally small size begin to be governed by quantum mechanics, which entirely changes their characteristics and properties. Because of this, nanodevices will be fundamentally different than their macroscopic counterparts, and nanotechnology will provide the researcher with an entirely new "toolbox" with which to solve problems in fields such as computing, medicine, and electronics.

Nanotechnology was first conceptualized in 1959 by Richard Feynman during his now famous "There's Plenty of Room at the Bottom" lecture to the American Physical Society.[1] Briefly, the lecture served as an open invitation to the scientific community to begin thinking about the manipulation of matter at the atomic scale, because it could be theoretically done:

> "I am not inventing anti-gravity, which is possible someday only if the laws [of physics] are not what we think. I am telling you what could be done if the laws are what we think; we are not doing it simply because we haven't yet gotten around to it…..The principles of physics, as far as I can see, do not speak against the possibility of maneuvering things atom by atom."[1]

In addition to proposing the idea of moving individual atoms, Feynman also addressed the notion of developing what he called "small but movable machines".[1]

Feynman's vision of being able to precisely position atoms and molecules has been partially realized more recently through the development of probe microscopy. A classic example was provided by IBM Zurich in 1990 when Iegler and Schweizer successfully maneuvered xenon atoms on a metal surface using scanning tunneling microscopy (STM).[2] (Figure 1)

Figure 1.[2] Xenon atoms deposited on a platinum surface via STM.

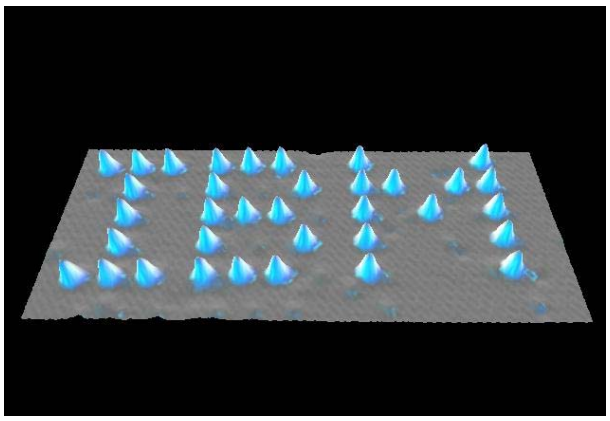

In 1996, a separate group at IBM illustrated that larger molecules could be manipulated using the same technique and constructed a molecular scale abacus.[3] In this abacus, the beads are C_{60} units, and are moved via an STM tip. (Figure 2)

Less progress has been made towards Feynman's prediction of "small but movable machines". Theorists have generated a considerable body of literature describing the

possibility of atomically precise machinery. Both Drexler and Merkle have spent the majority of their careers providing eloquent explanations as to how the laws of physics allow the construction of complicated machines at the atomic level.[4,5,6,7]

Figure 2.[3] A molecular scale abacus.

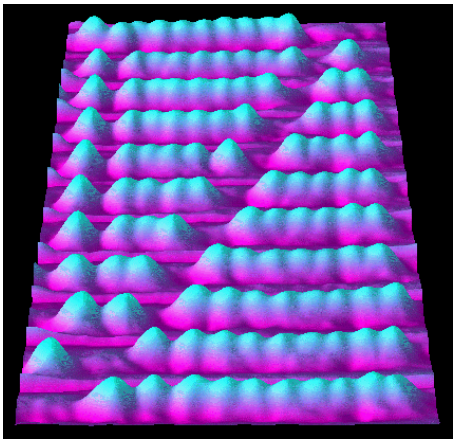

However, as with any new technology, there is a disagreement between theorists and experimental scientists over the potential of nanotechnology and the best routes towards its realization.

The debate often centers around a 1986 book by Drexler entitled "*Engines of Creation*".[8] Although not overly scientific in nature, the book describes the advent of so called "molecular assemblers" that are capable of constructing anything by positional atomic assembly. The book also details the possible dangers of nanotechnology as these "assemblers" would be capable of reproducing by assembling themselves. The

disagreement between "Drexlerian" nanotechnologists and the rest of the scientific community focuses upon whether or not molecular assemblers will one day be possible. Drexlerian nanotechnologists believe that positional assembly is the future of all technology, where machines can be assembled by simply placing atoms near one another in the correct spatial coordinates. Although many noted scientists have publicly debated Drexler, including both Whitesides[9,10] and Smalley[11], the disagreement appears to be far from resolved. Drexler has published a variety of books since *Engines of Creation* that have given reasonable explanations as to how assemblers could work based on physics. Opponents simply point out that there is absolutely no empirical evidence for the possibility of molecular assemblers with atomic precision.

Both sides agree that the construction of nanoscale devices is indeed possible, but they have different views as to how construction should be accomplished. Any device, regardless of size, has a variety of components that need to be assembled in a particular order for the device to perform its function. For example, a computer certainly won't operate if its components are randomly assembled. The same argument can be made for nanoscale devices; there needs to be a way to arrange the device components in a highly ordered fashion; there needs to be molecular precision. This can be accomplished via either a "top-down" or "bottom-up" approach.

A "top-down" approach involves starting with a macroscopic construct and reducing it to a nanoscopic device through lithography and etching. This differs significantly from Drexler's view of assembling machines one atom at a time. The top-down approach is

currently used by many research groups and by chip makers with great success. For example, through micromachining Reed and co-workers were able to prepare an atomically sharp break junction and thus were able to measure the conduction of a single molecule spanning the break (Figure 3).[12]

Figure 3. An atomically sharp break junction[12]: a pictorial representation (left) and an electron microscope image (right).

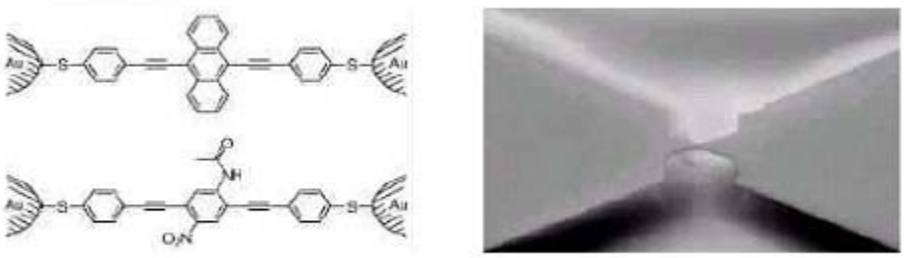

A "bottom-up" approach, seeks to assemble molecular devices one atom or one molecule at a time. This can be achieved by the manipulation of atoms or molecules using an external force (e.g. probe microscopy, lithography) to order the molecules in a specific way. Alternatively, synthetic chemists take a "bottom-up" approach by synthesizing molecules. Here, the tool that imparts order on the structure is the covalent bond and the manipulation is accomplished by the energetics of the bonds formed. Either approach is time consuming and labor intensive, prohibitively so if large numbers of bottom-up assembled systems are to be manufactured. Mass production at the atomic and molecular scale can really only be achieved in a rational way by designing systems that can self-assemble into the desired arrangements.

Molecular self-assembly refers to the spontaneous organization of molecules into well defined aggregates. This organizational event is typically an energetically driven process. In other words, a well ordered aggregate of molecules forms because it is the lowest energy structure, and therefore the most stable. Usually some type of non-covalent interaction (e.g. hydrogen bonding, ionic interactions, size-fit interactions) triggers the assembly process. The concept of self-assembly is certainly not new, and numerous examples can be seen throughout nature. Protein folding, DNA coiling, ionic crystal formation, and inclusion complexes are all examples of systems that self-assemble into well defined structures.

Figure 4. Some examples of common self-assembling systems: ice (left) and double helical DNA (center) adopt their structures based on hydrogen bonding interactions. Sodium Chloride forms its crystal structure based on ionic interactions. All these examples represent energy minima.

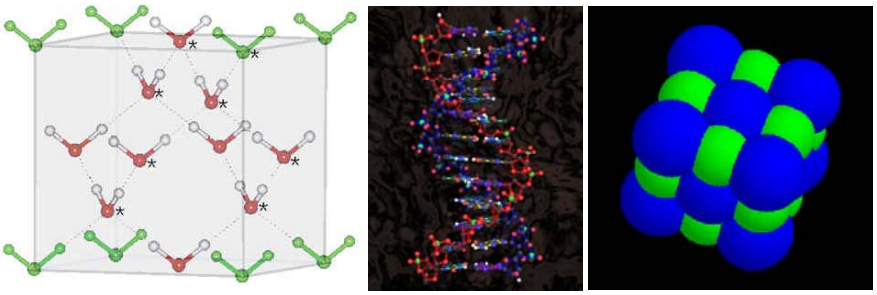

Self-assembly can be considered a bottom-up approach towards nanotechnology, as it provides a new path towards achieving precise structures starting at the molecular level. We previously noted that all devices require a particular arrangement of their components in order to function. Through the appropriate modification of molecules that are already known to assemble, it is possible to incorporate device components into self-assembling

networks at regular intervals. Upon self-assembly, the components assemble in a predictable fashion, and the molecular scale device essentially builds itself. The ability to self-assemble devices therefore can partially eliminate the time-consuming steps of other bottom-up approaches. For example, instead of covalent synthesis of a linear molecule containing 400 carbon-carbon bonds to produce a 50 nm construct, self-assembly could allow for the spontaneous arrangement of ten 5 nm subunits into an overall 50 nm construct. (Figure 5)

Figure 5. A pictorial representation of how self-assembly (bottom) can be used to build a structure analogous to a large construct (top).

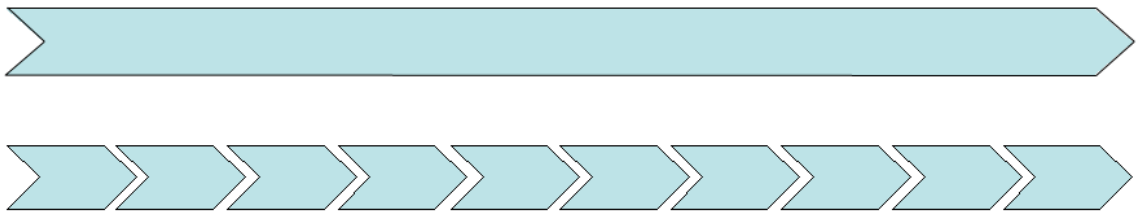

Self-assembly has been successfully used by a variety of groups to construct molecular scale devices. These devices have included, amongst others, thin film transistors,[13] quantum dots,[14] and molecular wires.[15] For example, the Marks group from Northwestern has used hydrogen bonding to promote self-assembly of organic light emitting diodes (OLEDs).[16] (Figure 6)

Regardless of "top-down" or "bottom-up", it is clear that nanoscopic devices can be manufactured that perform specific functions. However, nanotechnology is an emerging technology, and therefore, most of the devices made to date are very rudimentary and

mimic macroscopic constructs. Indeed, much of the work in the field to date has sought to provide "proof-of-concept" as opposed to commercially viable devices.

Figure 6.[16] An SPM image of an array of self-assembled organic light emitting diodes. Each island consists of several thousand OLEDs.

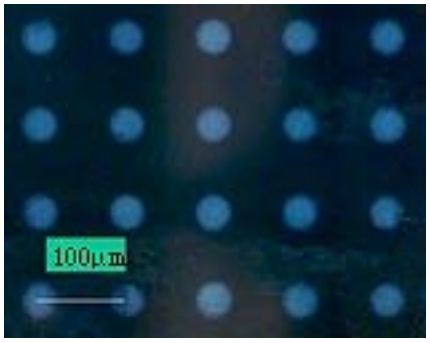

Our group's work in the field of nanotechnology began with the synthesis and photophysical characterization of molecules containing donor-acceptor pairs that were models for molecular wires and switches. Specifically the effects of linking architecture (rigid linkers such as adamantly, and norbornyl; flexible linkers such as ester, and methylene) on the efficiency of electron or energy transfer were investigated. (Figure 7)

Figure 7. Sample molecules used for energy transfer studies.

These initial studies showed that systems with rigidly linked donor-acceptor pairs generally transfer energy and charge with higher efficiency than those systems that are linked with flexible bridges. Thus, in order to build a molecular wire that conducts

charge or energy efficiently, the donor and acceptor must be held rigidly relative to each other, since conformational freedom causes a decrease in transfer efficiency. However, the synthesis of rigidly linked molecules was time consuming and had poor yields. This initial work pointed out the drawbacks of "assembling" molecular wires with well defined geometries and conformations by organic or covalent synthesis (lengthy synthesis, low yields) and led to our investigation of self-assembly approaches to device fabrication. Self-assembled architectures can be very stable, with well defined conformations and can be created with larger dimensions more easily than covalently assembled systems. The work described in the following pages represents our attempts to make self-assembled nanodevices with specific architectures and functionalities. In general, two approaches have been taken – self assembly on surfaces and self assembly into "free standing" structures. In section II-A we describe the use of metal-ligand interactions to assemble multilayers on gold and other surfaces. The films assembled showed efficient long range electronic conduction, photocurrent generating capacity, and photoinduced changes in surface wettability. In section II-B we describe the results of attempts to assemble cyclic peptide nanotubes from solution. These nanotubes were created with the view to their use as scaffolds for electro- and photoactive substituents that have a variety of potential applications, including molecular wires.

II. SELF ASSEMBLING SYSTEMS

A. SELF ASSEMBLING MONO- AND MULTILAYER THIN FILMS ON GOLD

1. Background

A variety of techniques have been developed over the past several decades to assemble highly ordered thin films that consist of only a few atomic layers. These methods include chemical vapor deposition (CVD),[17] self-assembled monolayers (SAMs),[18,19] and Langmuir-Blodgett films (LB films).[18,20] The driving force behind this research is the understanding that thin films with thicknesses on the order of nanometers could have properties previously unobserved at the macroscopic level.

We have undertaken the development of methods to promote self-assembly of multilayers on gold for specific device applications. Using a modular, non-covalent approach, we have been able to construct a supramoleuclar architecture that allows control of surface morphology and surface chemistry through the careful selection of component layers. In particular, we have constructed self-assembling thin films that can act as tunable length molecular wires, photovoltaic devices, and photoswitchable interfaces. In this section we introduce the concepts of self-assembled monolayers on gold and their characterization, and will discuss the results obtained for each of the multilayer thin films that have been assembled.

Thin films consisting of a single molecular layer were first realized in the 1920's by Langmuir and Blodgett, who developed a method of forming highly ordered layers of

organic molecules at a liquid-air interface.[21,22] By compressing the liquid and transferring the organic layer to a substrate, a single layer, or multiple organic layers could be produced.

Langmuir-Blodgett films (LB Films) have a variety of commercial applications in the coatings industry, sensor technology, and display manufacturing. However, the technique is limited because the binding of the LB film to the substrate is typically via a weak electrostatic interaction. As a result, the films formed are not very robust, and can often be mechanically removed, making them undesirable from a device standpoint.

In 1983, Nuzzo and Allara reported that monolayers of alkane thiols can be formed on gold substrates.[23] Sulfur has a natural affinity for gold, and upon exposure to a clean gold surface, self-assembly of sulfur containing molecules rapidly takes place. Since the chemistry of sulfur compounds is well established, it is possible to incorporate almost any organic compound or functionality into a self-assembled monolayer (SAM). These SAMs were found to be highly ordered, having a well-defined thickness, and orientation relative to the surface. (Figure 8)

Figure 8. Picture of a SAM on gold. The S atoms are 5 Å apart on the gold surface.

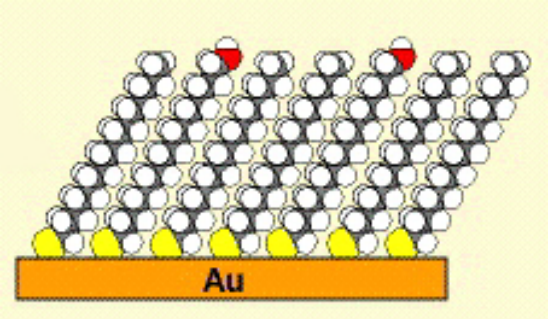

SAM formation involving alkane thiols is believed to take place via a two step process (Figure 9), where the first step involves the formation of gold thiolates that remain mobile on the surface, leading to formation of growth islands, and eventually a complete surface of bound thiolates, all lying flat on the surface. [24] The second step involves a slower, rate-determining, surface reorganization in which packing of the alkane chains yields a stable "quasi-crystalline" surface. [25,26] Reorganization also causes the alkyl chains to cant from the surface at an angle of between 20-30º.[27]

The stability and order of SAMs makes them an attractive vehicle for designing thin films. Monolayers on gold have been shown to be stable to both protic and aprotic solvents, as well as to light and to sonication although in the presence of intense radiation and oxygen, it *is* possible to oxidize the surface bound thiolate.[28] However, a variety of photochemical studies have been performed on assembled monolayers of chromophores where irradiation in solvents for multiple hours showed no degradation of the monolayer.[29,30] In addition, monolayers are very stable under typical laboratory conditions, making it unnecessary to shield the sample from ambient light or to keep it in an oxygen free atmosphere.[28]

Characterization of SAMs is possible by a wide variety of techniques that can give insight as to their physical and chemical properties. Probe microscopy yields information about the surface morphology of a given monolayer, and when combined with microcontact printing can give very accurate measures of monolayer thickness.[31,32]

Figure 9.[28] Illustration of the self-assembly mechanism for alkanethiols on gold. Steps A-C correspond to the first kinetic step, where 60-80% of the alkanethiol is adsorbed. Steps D and E represent alkanethiol reorganization producing a dense monolayer.

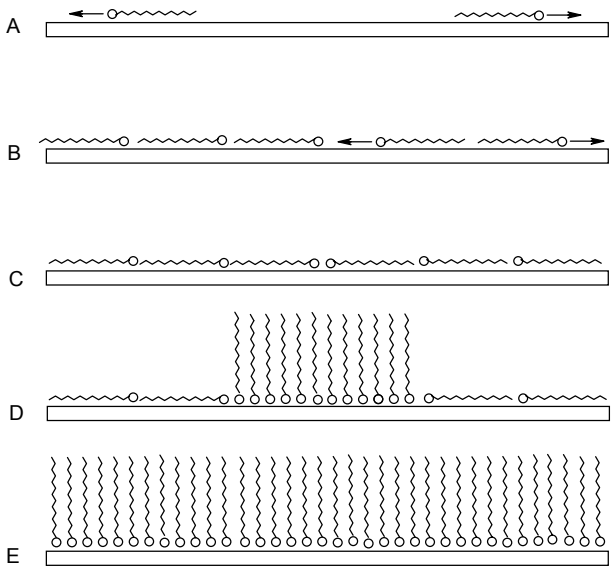

In addition, ellipsometry, secondary ion mass spectrometry, and quartz crystal gravimetry have been successfully used in giving precise values for monolayer thickness and coverage. Additional non-destructive characterization can be achieved by a combination of electrochemical, IR, and contact angle measurements. The most qualitative of these methods listed is contact angle goniometry. The contact angle of a thin film, measured using a goniometer, involves placing a small drop of a liquid (10 μL) with known surface tension on the SAM. The angle formed between the water droplet and the substrate provides information as to the hydrophilic or hydrophobic character of the surface (Figure 10). The size of the measured angle indicates the hydrophobic character of the surface, with increasing angles indicating more hydrophobicity.

Figure 10. A typical contact angle measurement. The angle measured is shown in red.

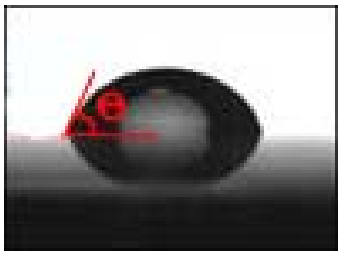

This method is useful in monitoring monolayer formation. A clean bare gold substrate is very hydrophilic, whereas an assembled alkane thiol monolayer is significantly less so. Therefore, completeness of a monolayer can be estimated by taking several contact angle measurements during the course of monolayer formation and determining when the contact angle ceases to change. This method has been widely used in the literature.[27,33,34]

Functional group identification in monolayers can be achieved by using grazing angle IR spectroscopy. This technique has proven to be critical for monolayer characterization particularly because it provides both basic functional group information, as well as the degree of ordering. For example, upon self-assembly, alkane thiols form quasi-crystalline packing arrangements that can be evidenced by a shifting in the asymmetric CH_2 stretch in the IR to ~ 2925 cm^{-1}.[28] This shift is attributed to a lack of gauche-gauche interactions upon monolayer formation.

Cyclic voltammetry (CV) measurements are also valuable in determining the completeness of monolayer formation. Alkane thiols are known to electrically insulate gold upon ordered SAM assembly. By setting up a standard electrochemical cell with the

SAM as the working electrode, the completeness of a monolayer can be studied by monitoring the disappearance of a CV redox wave.

Finally, impedance spectroscopy quantifies the ionic permeability of a given monolayer and therefore provides a measure as to how densely it is packed. By its simplest definition, impedance is a measure of the total opposition to current flow in an alternating current circuit.8 Impedance measurements therefore model the monolayer after an AC circuit (Figure 11).[25,35,36]

Figure 11. The simple Randles circuit used to model the SAM for impedance measurements.

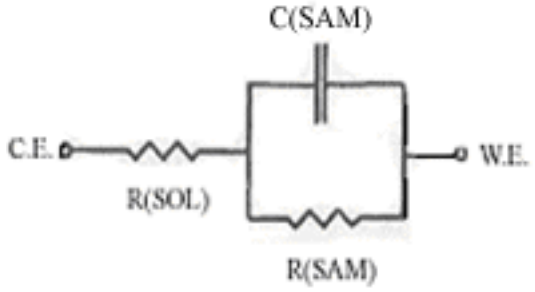

The model circuit exists between the working electrode (W.E. – the monolayer), and the counter electrode (C.E. – platinum wire). Based on the circuit design presented in Figure 11, there are three quantities that oppose current flow in this system; the resistance of the solution (R(SOL)), the capacitance of the monolayer (C(SAM)), and the resistance of the monolayer (R(SAM)). Since the solution resistance should be constant for all monolayers (assuming the electrolyte is constant), the quantities of importance are R(SAM) and C(SAM). Typically, capacitance values between 3-11 $\mu F/cm^2$ are considered to represent well ordered monolayers, implying that there is no diffusion of

ions into the monolayer.[35,36] Higher values are typically indicative of a disordered monolayer, although conducting monolayers will also give rise to increased capacitance values.

As the value of impedance is actually a complex number, impedance plots are typically viewed as a Nyquist plot (Figure 12). In such a plot, the real component of the impedance is plotted on the x axis with the imaginary component being represented on the y axis. The two x-intercepts on this plot give information as to the resistance of the solution used and the surface studied. The maximum y value gives the maximum capacitance (Wmax) for the surface being studied. Multiple points are generated, as the impedance changes for different applied AC frequencies. Figure 12 illustrates an impedance plot for an actual AC circuit. In practice, impedance data is gathered and then modeled after such a circuit.

Figure 12. An example of a Nyquist plot from an impedance experiment for a simple Randles circuit.

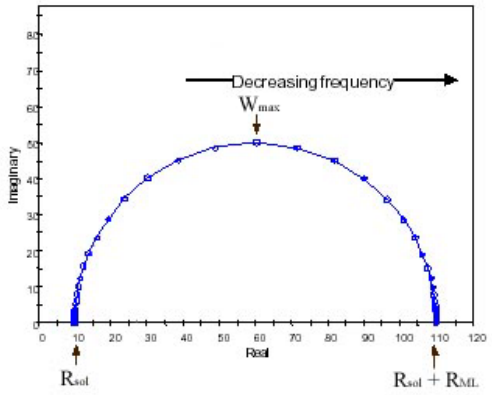

While much work has been reported for monolayers, relatively few papers have been published on multilayer thin films based on a SAM architecture. However, multilayer systems are of interest because they may allow controllable assembly of three dimensional structures, in turn leading to the assembly of molecular electronic devices, microfluidic channels, optical waveguides, and other devices.

For a multilayer to be incorporated into a commercial device, it must be stable. While it is possible to make multilayer thin films by a variety of different methods, it has been suggested that the construction of films based on ionic interactions maintain the optimal balance between ease of preparation and durability. Several systems have been developed that illustrate this point. Mallouk has published several papers outlining methodologies for the assembly of multilayer films based on zirconium ion/organophosphate interactions.[37,38] Both Ulman[39] and Bard[40] have published work on multilayers assembled on gold based on interactions between copper ions and either mercaptoalkanoic acids or alkanedithiols (Figure 13).

While these systems are interesting, they lack stability. Multilayers of either system degrade during electrochemical studies and neither is stable to prolonged exposure to the atmosphere.[40] In Bard's work, this lack of stability is believed to stem from the ability of copper ions to oxidize adjacent thiol groups into disulfides, and thus be reduced to Cu(I). Electrochemical studies performed on systems where copper ions were ligated only by carboxyl groups showed stability over multiple redox cycles, suggesting that multilayer stability can be achieved by employing non-thiol containing ligands.

Figure 13. Multilayer systems based on ionic interactions with copper ions. Bard's system is shown on the left, Ulman's on the right.

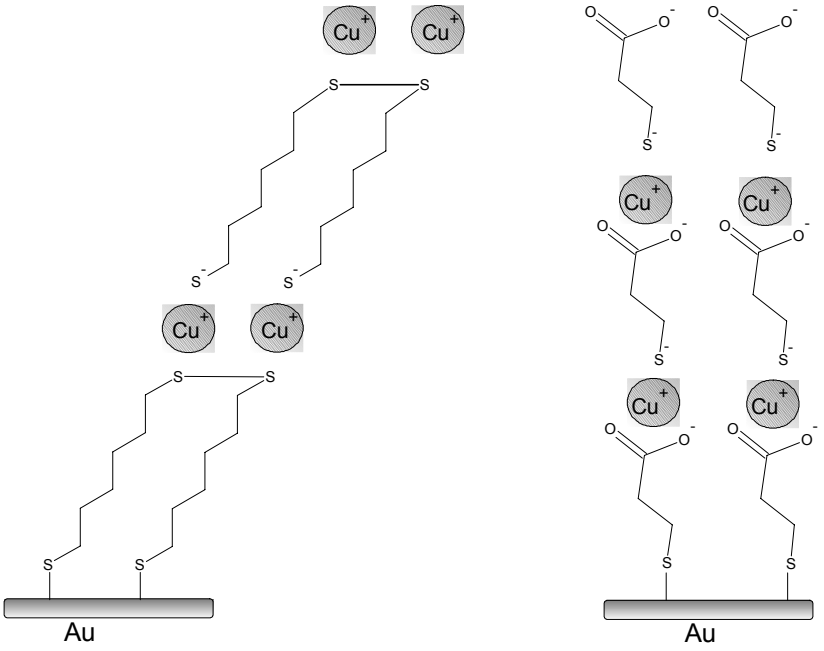

Based on the work by Bard and Ulman, we sought to develop a system that would take advantage of similar self-assembly processes to construct multilayer films, but would employ ligands that would not cause monolayer degradation during electrochemical studies.

MacDonald and co-workers have developed a supramolecular scaffold based on transition metal complexes with 2,6-pyridinedicarboxylic acids, illustrating that crystal structures could be formed with a variety of transition metal ions (M^{2+}), in which crystal structure was independent of the metal used.[41] This system provides a new architecture for multilayer assembly because unlike the thiol ligands employed by Bard, pyridine dicarboxylic acid groups cannot be easily oxidized. In addition, based on studies in bulk

systems the metal ions used can be interchanged without causing significant changes in the overall structure of the system. Using this non-covalent strategy of ligation, structures similar to those in Figure 14 can be constructed.

Figure 14. The proposed design for the construction of multilayer systems.

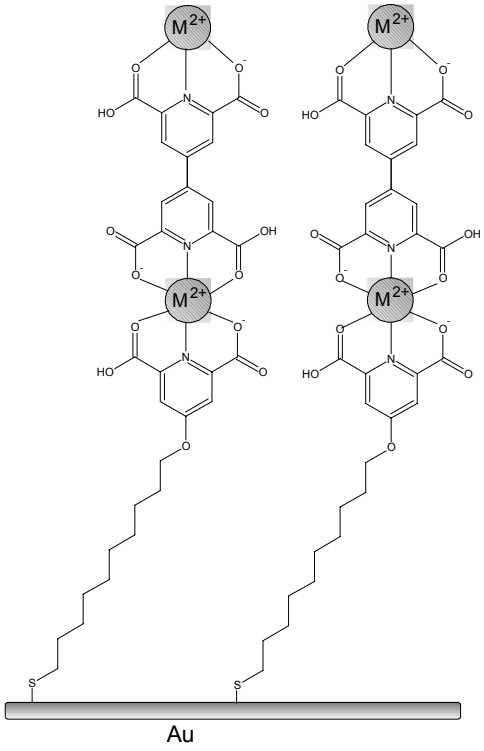

The advantages of this system over traditional multilayer architectures on gold are substantial. Besides the stability of the chelating groups, which should leave the redox states of the metal centers unaffected, the rigid linking group between layers should promote ordering. More importantly, the approach is modular; the characteristics of the multilayer can be easily changed by simply exposing the layer to different solutions. For example, the thickness of the films can be controlled based on how many metal ion layers and tetracarboxy dipyridyl linker layers are used. The surface characteristics can also be

simply altered, as the chemistry of chelidamic acid (4-hydroxy-2,6-pyridinedicarboxylic acid) is well established, thus making it possible to terminate the SAM with any head group desired (Figure 15). Additionally, the interlayers (any layer between the gold surface and the exposed surface) of the system can be changed by building linking groups with different functionalities as shown in Figure 14.

Figure 15. A modular approach towards multilayer films. By choosing what groups are exposed to the substrate, the surface characteristics can be altered (left). Additionally, different components can be incorporated into the film below the surface, in its interlayers (right).

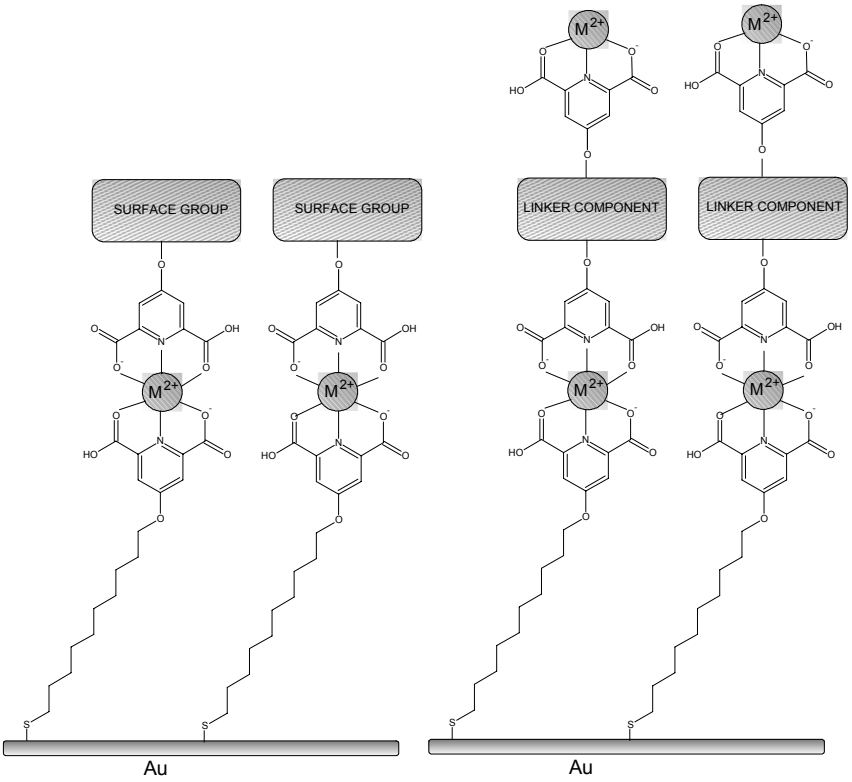

Thus far, only dicarboxy pyridyl chelates have been discussed. However, ligands known to chelate transition metals can also be used within these films.

To date, we have used this approach to assemble thin films that can conduct charge, can function as photovoltaic devices, and can switch their wetting properties when irradiated. Although none of these phenomena are completely new, the fact that these systems can be quickly and easily prepared is novel.

2. Results and Discussion

(i) Multilayer Thin Films as Molecular Scale Wires

-Materials and Methods and Experimental Data are provided in Section II-3 and II-4-

The construction of multi-layered films with predictable electrochemical properties has been investigated by several groups because of their potential as molecular scale wires and switches. Bharathi has shown that conduction through thin films is dependent upon the surface functionalities of the film.[42,43] In particular, alkyl-based films that are capped with metal complexes can be made to conduct. This was particularly apparent in multilayer systems constructed containing iron hexacyanoferrate groups, coordinated to a surface. In similar work, Lin and co-workers have shown that layer by layer growth of metal-metal bonded thin films leads to predictable electrochemical properties.[44] Based on their predictability, these types of systems have been suggested as possible molecular junctions in nanoelectronics applications. The results reported here demonstrate that conducting multilayer films can be assembled with our noncovalent approach.

Films **I-VI** (Figure 16) were constructed by the step-wise deposition of their individual layers. These films take advantage of ionic interactions to assemble the film, which have been previously shown to be highly stable.[45,46,47] Besides offering a tunable thickness, the conducting properties of the films can also be controlled. Through impedance and conductivity measurements performed on the films, we have found that conductivity can be switched on and off simply by terminating the surface with either a metal ion or an alkyl capping unit.

Figure 16. A schematic illustrating the sequential buildup of conducting and non-conducting thin film layers. For this study, Multilayers **I-VI** were constructed that alternate between insulating and conducting. Here, the metal used (M) was copper(II).

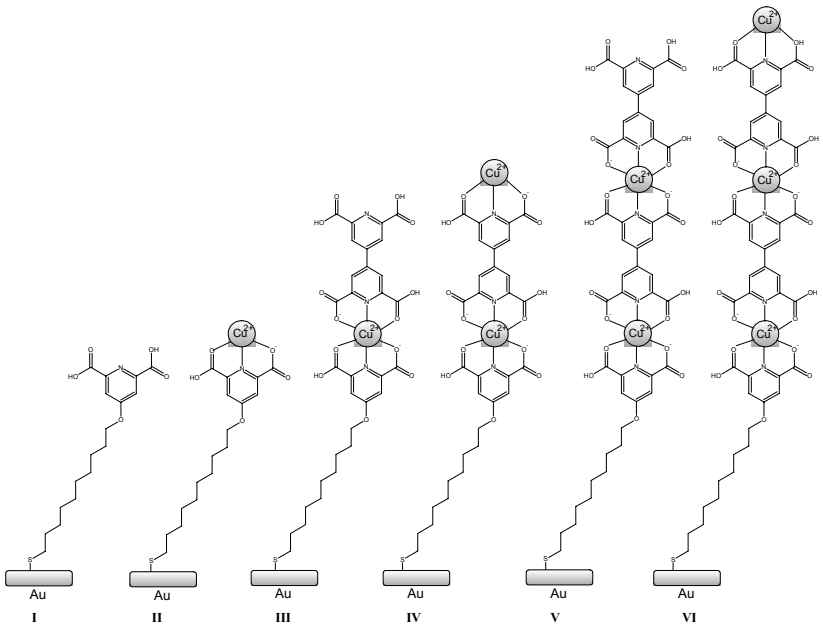

The sequential construction of films **I-VI** was monitored via contact angle, grazing angle IR, cyclic voltammetry, and impedance measurements. The grazing angle IR data was initially useful in detecting layer by layer construction. (Figures 17 and 18)

For thin films **I-III**, IR spectra were obtained after the deposition of each layer. After deposition of the initial SAM, symmetric and asymmetric vibration bands are observed at similar frequencies to those observed in the spectrum of dodecanethiol (2852 and 2924 cm^{-1} respectively).[48] This suggests that the packing arrangement for film **I** is similar to that of dodecanethiol. A broad, structureless band is observed for the carboxylic acid group above 3000 cm^{-1} and the characteristic carbonyl band is observed at 1726 cm^{-1}. With deposition of Cu(II) ions (Film **II**), two resolved peaks appear between 3300 – 3500

cm^{-1} and another band at 2088. These bands are related to carboxylic acid/carboxylate anion units in the complex.

Figure 17. IR spectra of films **I** (top) and **II** (bottom)**.**

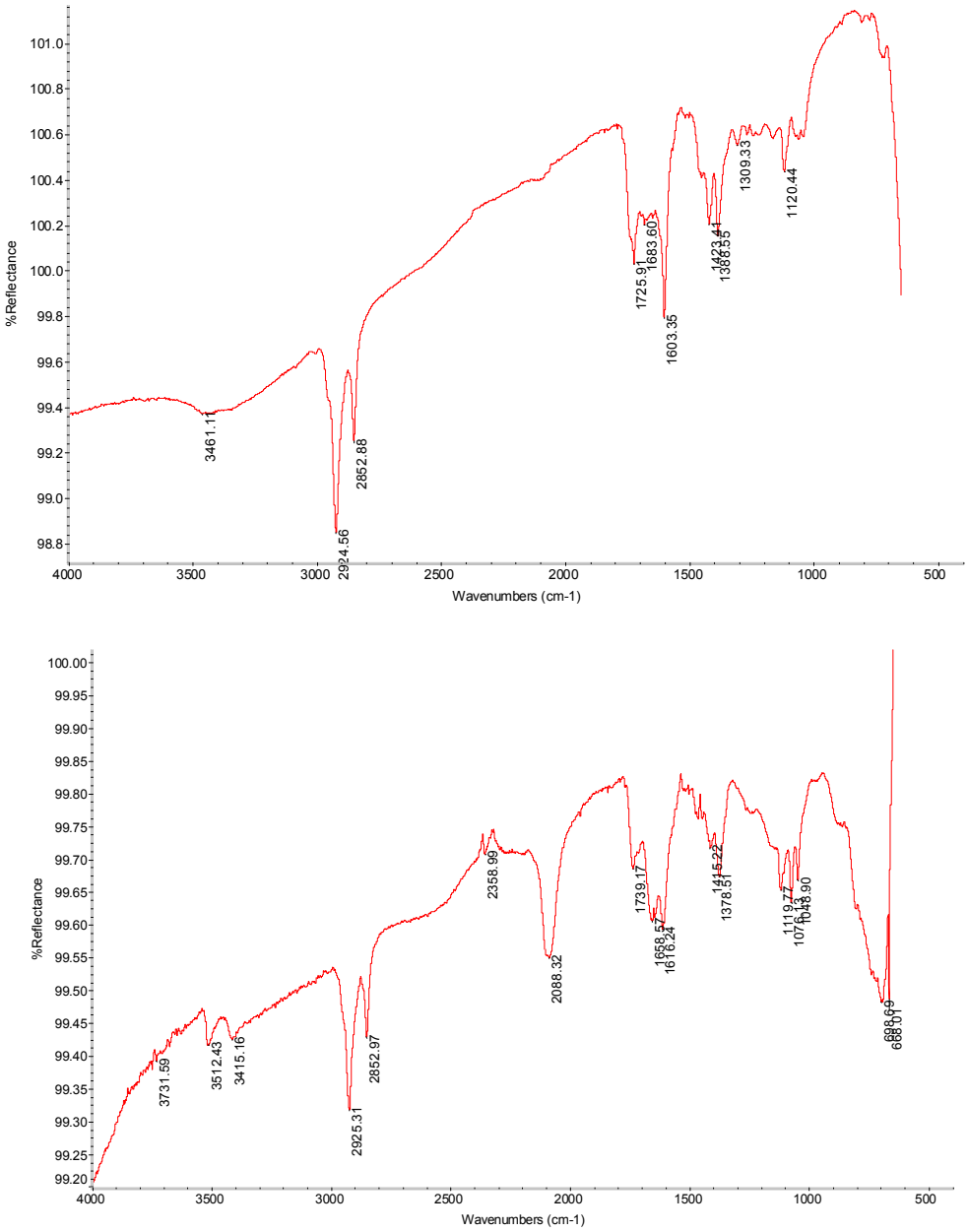

Figure 18. The IR Spectrum for Film **III**.

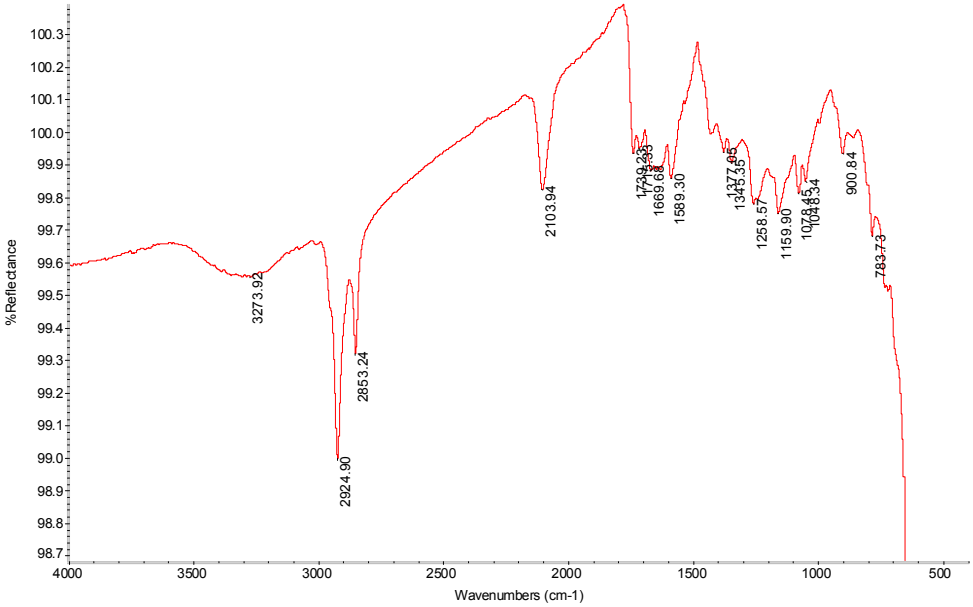

The altering of the carboxylic acid absorption bands upon complexation has been well documented in the literature. Hatzor, et al. have shown that different carbonyl bands arise in spectra for multilayers of bis-hydroxamate with Zr(IV) and Ce(IV) ions, depending upon whether or not they are complexed.[49,50] The resolved bands between 3300-3500 cm^{-1} disappear in film **III**, likely because they are masked by the uncomplexed carboxylic acids in the tetracarboxy dipyridyl ligand. Grazing angle IR data for films **IV-VI** is increasingly difficult to interpret, as additional layers absorb in very similar areas to the layers that are already deposited. Because of this limitation, additional data was required to accurately characterize the films.

Contact angle measurements confirmed substantial changes in the hydrophilicity of the surface upon the addition of each layer. These results are summarized in Table **1**.

Table 1. The contact angle values obtained for Films **I-VI**.

Film	Contact Angle (Degrees)
Gold	76 +/- 1.0
Film **I**	69 +/- 0.5
Film **II**	54 +/- 1.5
Film **III**	67 +/- 2.0
Film **IV**	51 +/- 1.0
Film **V**	67 +/- 2.0
Film **VI**	55 +/- 1.5

There is a clear difference in contact angle depending on whether the surface is composed of dicarboxypyridyl groups or complexed Cu(II) ions. The Cu(II) ion surface has a much smaller contact angle, differing from the dicarboxypyridyl capped surface by ~15º. This is possibly due to the ability of water to complex with Cu(II), which would make the surface considerably more hydrophilic, and hence decrease the contact angle.

Impedance measurements were performed on films **I-VI** and are summarized in Table **2** (some examples of experimental impedance plots are provided on page 78). The initial SAM (Film **I**) shows high values of resistance and low values of capacitance for the monolayer. These values are consistent with the literature on SAMs, and are indicative of a well ordered monolayer. Film **II** shows very different behavior, with significantly lower resistance and much higher capacitance values. These results are expected if the

multilayer is conducting. Although this result could also be interpreted as a disordered layer, contact angle, IR, and CV measurements eliminate this as a possibility. Throughout the measurements, it is clear that films terminated with dicarboxypyridyl surface groups have higher resistance values and lower capacitance values, indicating that they are insulating compared to Cu(II) terminated films.

Table 2. Impedance data for thin films **I-VI**.

Layer	R_{SOL} (ohms)	R_{SAM} (ohms)	C_{DL} (μF)
I	147 (21)	12533 (510)	4.55 (.97)
II	93 (8.3)	3591 (274)	19.2 (4.5)
III	114 (15)	6133 (628)	11.2 (1.6)
IV	198 (18)	4487 (55)	17.1 (2)
V	87 (18)	5920 (628)	16.4 (3.5)
VI	58 (9)	4012 (673)	26.2 (10.7)

This assumption is confirmed by studying the conductivity behavior of films **I-VI**. Conductivity measurements were obtained in an aqueous solution of $K_3[Fe(CN)_6]$ and exhibited markedly different behavior depending upon their surface group. Figure 19 displays the cyclic voltammograms for film **I-VI** with respect to bare gold.

The redox wave corresponding to the bare gold electrode shows the expected oxidation and reduction of ferricyanide measured in the range from 0 V - + 0.6 V. Upon self-assembly of a monolayer on that electrode (film **I**), the redox wave is significantly

attenuated, signifying the formation of a well packed insulating SAM. When the monolayer is allowed to ligate Cu(II) ions (film **II**), the redox wave returns to nearly the same peak current as seen with bare gold.

Figure 19. The cyclic voltammograms of films **I-II** (top) and **III-VI** (bottom) with respect to a gold electrode.

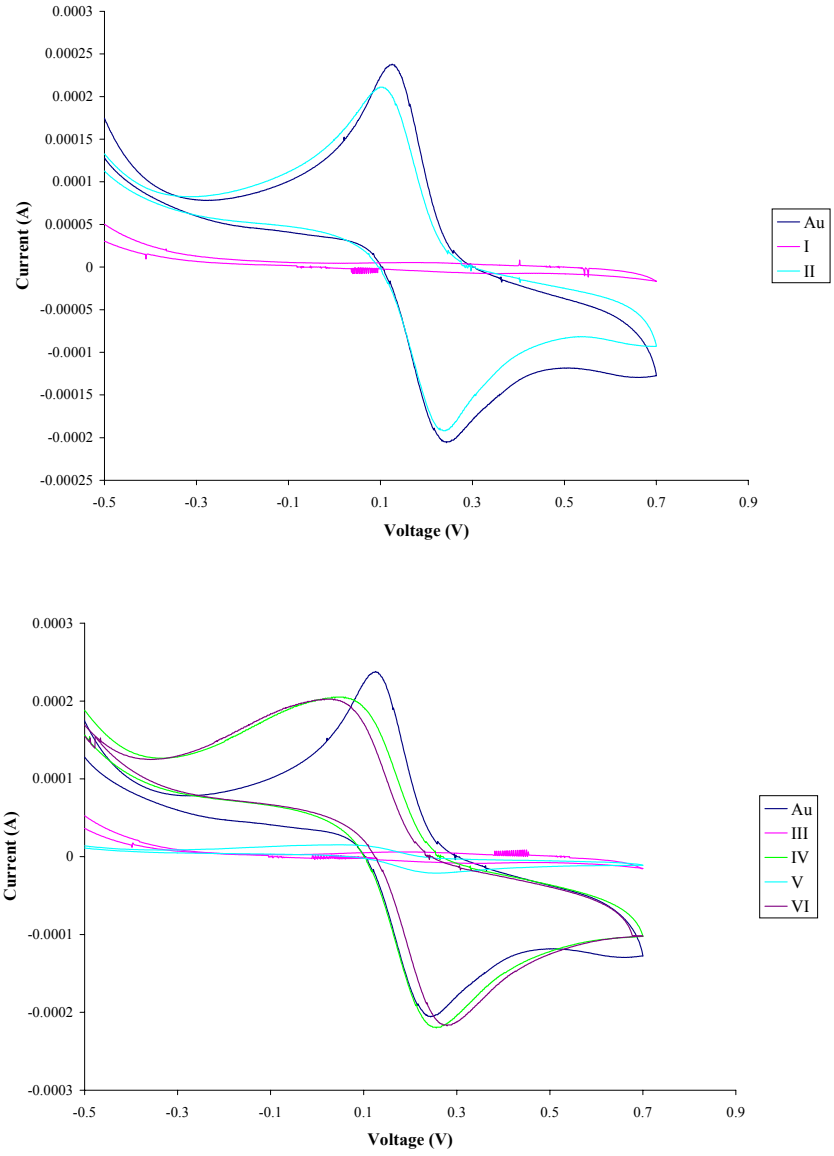

When film **II** is capped with a tetracarboxy dipyridyl ligand (film **III**), the conduction of the electrode is again attenuated. Exposure of film **III** to copper ions again results in a noticeable increase in current, as shown in Figure 19. This trend continues for up to six deposited layers, with the conducting ability of the electrode being determined by the surface group. As the number of deposited layers increases, the position of the redox peaks begin to shift slightly. This shift could be due to a higher barrier for inelastic tunneling of electrons through the layers. Alternatively, the surface for these larger multilayers may have defects. The latter possibility is arguably more likely since Film **V** exhibits some slight conducting behavior. Films **I-VI** alternate between insulating and conducting depending on their exposed surface group. This relationship is presented graphically in Figure 20.

Figure 20. A plot of ΔE vs. film number. ΔE is a measure of the total amount of current flow in a given redox cycle. The larger the value of ΔE, the more conducting a given film is. All even numbered films have Cu surface groups, whereas all odd films have dicarboxypyridyl surface groups.

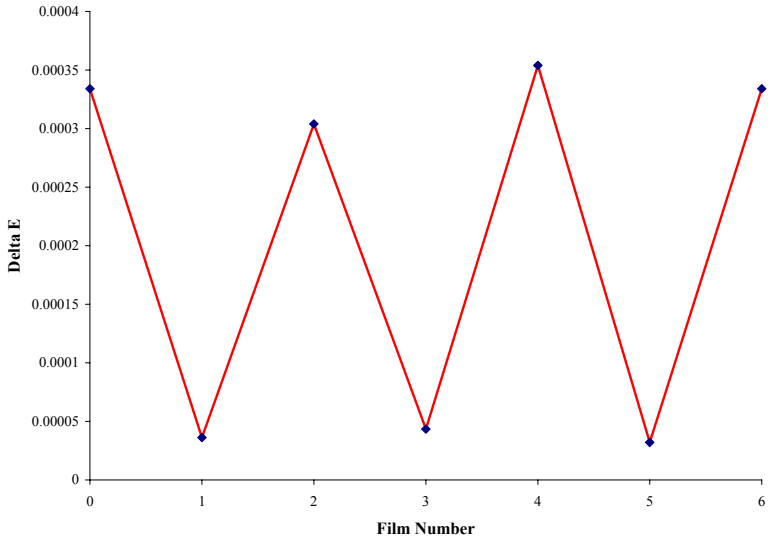

In conclusion, we have provided evidence that a non-covalent strategy can be used for the construction of multilayer thin films with tunable thickness and with switchable conducting properties. We realize that this system is not optimized, in that multilayer films of greater thickness than presented here suffer from disorder as evidenced by impedance and conductivity measurements. However, this work illustrates proof of concept that architectures similar to this can be used to develop tunable thin films. Future work will focus on developing linker groups that will impart added order in the films in two dimensions, thus increasing its stability and the likelihood of observing the trends presented here in films with much greater thicknesses and numbers of layers.

(ii). Photocurrent Generation in Multilayer Thin Films

McGimpsey, W.G.; MacDonald, J.C.; Cooper, C.G.F.; Soto, E.R. *J. Am. Chem. Soc. (Comm. Ed.)* **2003**, *125*, 2838.

-Materials and Methods and Experimental Data are provided in Section II-3 and II-4-

The construction of photovoltaic devices, systems that convert light energy into electricity, has been of interest since the 1950's when the first commercially available photovoltaic device was introduced. Since their introduction, many light-harvesting devices have been developed that are based on inorganic semi-conductor technology. Currently, commercial photovoltaics are inorganic thin films on the order of a few microns in thickness. Several systems have been constructed that have shown reasonable light-harvesting ability and have provided insight towards the nature of the light harvesting reaction and charge separation processes.[51,52,53] However, the realization of a system that can efficiently generate electrons from photons based on organic assemblies has not been realized.

In attempting to design a photovoltaic with a reasonably high quantum efficiency it is essential to construct a system in which the light harvesting components are organized in a highly ordered arrangement that optimizes both the transfer efficiency (the percentage of electrons that participate in charge transfer) and the conversion efficiency (the percentage of incident photons that are absorbed to produce the excited state). Several groups have fabricated self-assembling systems based on gold-thiol chemistry that produce highly organized networks. Imahori et al created self-assembled monolayers (SAMs) on gold by depositing a covalently linked, multicomponent molecule containing

alkanethiol, ferrocene, porphyrin, and C_{60} subunits. (Figure 21)[54,55,56] These SAMs possessed both light-harvesting and charge separation character as evidenced by the generation of electrical current upon photoexcitation of the SAM in the presence of methyl viologen (an electron acceptor).

Figure 21. The photocurrent generator published by Imahori. Monolayers were formed by functionalizing R^1 with a thiol terminated chain and exposing to a gold surface in solution.

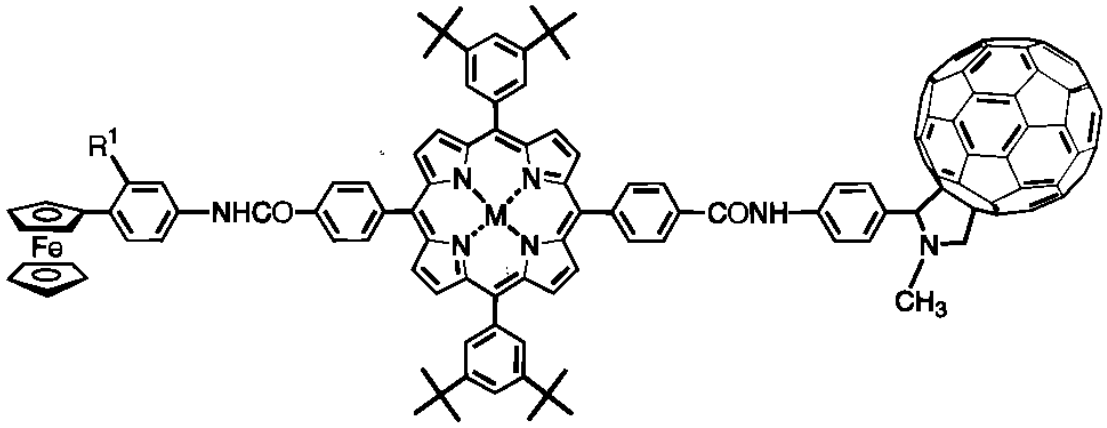

1a: M=H_2; 1b: M=Zn, R^1=O$(CH_2)_{11}$SH

Additionally, Kimura and co-workers have constructed photocurrent generating films based on monolayers of α-helical peptides terminated with amino acids containing light absorbing groups. (Figure 22)[52] While this work has yielded systems able to generate photocurrent, the synthetic effort involved in producing them was considerable.

Figure 22. Helical peptide based photocurrent generators. Here, ECz represents the photo-oxidizable ethyl carbazolyl head group.

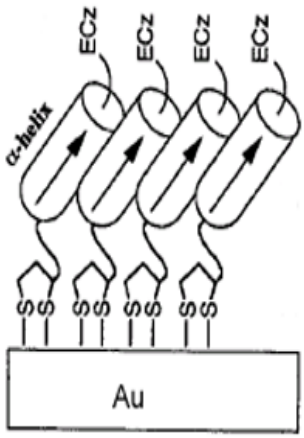

Based on the non-covalent, modular assembly of multilayer thin films described earlier, we have fabricated two types of photocurrent generating thin films on a gold surface. (Figure 23) SAM **VII**, partially synthesized by E. R. Soto of our group, consists of a pyrene chromophore coupled to a helical peptide that is attached to a gold surface through a disulfide linkage. This system serves as a model for comparison to films **VIII** and **IX**, and is analogous to the systems previously reported by Kimura, et al. Films **VIII** and **IX** were assembled in an analogous fashion to the thin films previously mentioned. A SAM of 4-[(10-mercaptodecyl)oxy]pyridine-2,6 dicarboxylic acid was deposited on a clean gold surface. The monolayer was then exposed to Cu(II) ions that are chelated by the monolayer. From this point, the multilayer can either be extended in thickness by capping with a tetracarboxy dipyridyl linker unit, or terminated by capping with a pyrenyl substituted chelidamic acid unit.

Figure 23. Structures of SAM **VII**, and multilayer thin films **VIII** and **IX**.

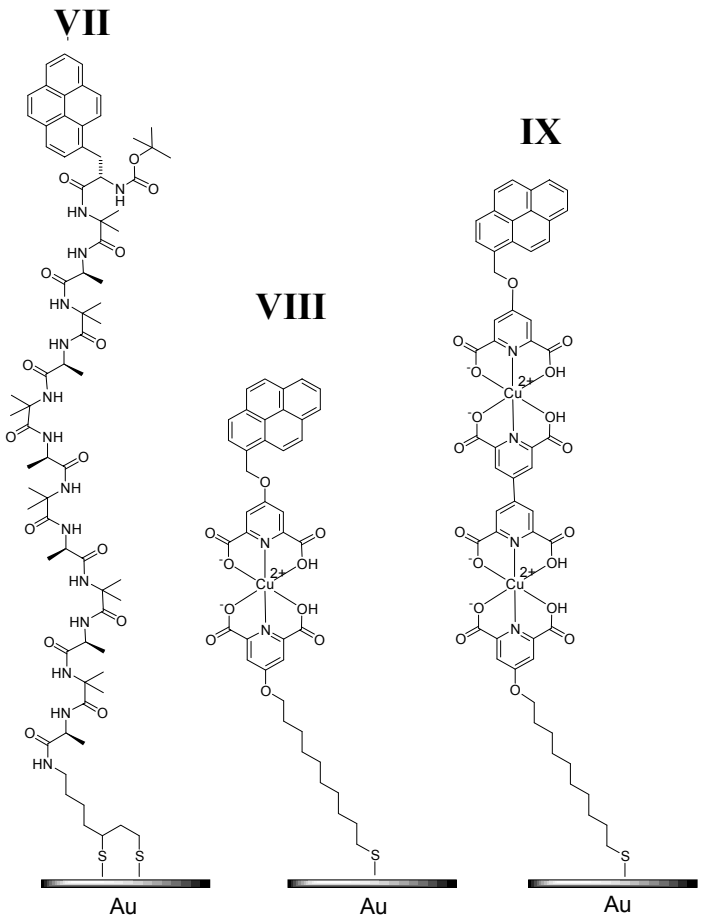

Film **VIII** consists of the multilayer: SAM + Cu(II) ions + pyrenyl capping unit. Film **IX** extends the thickness of the film by incorporating an additional linker unit between the monolayer and photosensitive head group.

Conductivity, impedance, contact angle, and IR experiments were carried out for SAM **VII** and for films **VIII** and **IX** (after the addition of each component). The conductivity (CV) results obtained for SAM **VII** in an aqueous solution of potassium ferricyanide showed that following deposition of **VII**, the conductivity of gold is significantly reduced in the range from -0.5 to 0.6 V versus SCE. (For a similar effect, see Figure 19) This

result as well as high impedance values indicate the formation of an ordered monolayer with few major defects.[35,36]

Conductivity and impedance values for **VIII** change as the individual components are deposited sequentially onto the gold surface. The CV of the bare gold surface shows the redox peaks of the ferricyanide,[52] whereas deposition of the pyridine-capped decanethiol again yields conductivity and impedance values (measured in the range from -0.5 to 0.6 V versus SCE) that suggest the formation of an ordered insulating monolayer.

After the monolayer is exposed to a solution of Cu(II) ions, the intensity of the CV redox wave returns to that which was observed for gold. Along with this result, there is the expected corresponding decrease in impedance values. Deposition of the pyrene containing ligand again results in attenuated conductivity and elevated impedance values. Film **IX** exhibited similar electrochemical behavior to Film **VIII** upon final construction.

Contact angle measurements confirm that substantial changes in the gold surface occurs following the addition of each layer. A summary of the contact angle results are shown in Table 3. Upon deposition of systems **VII**-**IX**, large changes in contact angle are observed for each layer. As expected, layers with exposed Cu(II) ions exhibit lower contact angles than layers with exposed alkyl groups, suggesting higher hydrophilicity and binding with water.

Table 3. Contact angle measurements for gold, dodecantethiol, SAM **VII**, and for films **VIII** and **IX**. Dodecanethiol is included as a hydrophobic model system that is known to form ordered SAMs on gold.

Sample	**Contact Angle (degrees)**
Gold	76
Dodecanethiol	75.6 +/- 0.6
SAM **VII**	48 +/- 2.4
VIII	
Component 1 (dicarboxypyridine SAM)	63.5 +/- 0.5
Component 2 (Cu(II) ions)	51.5 +/- 1.0
Component 3 (pyrene cap)	75.7 +/- 1.1
IX	
Component 1 (dicarboxypyridine SAM)	63.5 +/- 0.5
Component 2 (Cu(II) ions)	52.5 +/- 1.5
Component 3 (tetracarboxydipyridyl linker)	60.5 +/- 1.0
Component 4 (Cu(II) ions)	48 +/- 0.5
Component 5 (pyrene cap)	68 +/- 0.5

Grazing angle IR spectra were also collected for SAM **VII** and all of the component layers for films **VIII** and **IX**. For system **VII**, the IR spectrum of the SAM and the peptide were compared and showed the same major absorption bands. The most intense bands in the SAM spectrum are for the amide I and amide II absorptions at 1665 and 1545 cm^{-1}, respectively. Using the amide I/amide II absorbance ratio, the tilt angle of the helix from the surface normal was calculated to be 53°.[52] This is within an acceptable range, as peptidic SAMs have been shown in the literature to have cant angles from 32-66º.[52,57]

For thin films **VIII** and **IX**, IR spectra were obtained after the deposition of each layer. After formation of the initial SAM, the CH_2 symmetric and asymmetric vibration bands have similar frequencies to those observed in the spectrum of dodecanethiol.[58] This

suggests that the packing arrangement for films **VIII** and **IX** is similar to that of dodecanethiol. A broad, structureless band is observed for the carboxylic acid group above 3000 cm^{-1} and the characteristic carbonyl band is observed at 1726 cm^{-1}. With deposition of Cu(II) ions, two resolved peaks appear between 3300 – 3500 cm^{-1} and another band at 2088. As mentioned previously, these bands are related to carboxylic acid/carboxylate anion units in the complex. Upon capping **VIII** with pyrene, a significant increase in intensity for the aromatic C-C stretch at 1600 cm^{-1} is also observed. Film **IX** shows similar IR behavior to **VIII**, although a decrease in the CH_2 stretching at 3000 cm^{-1} is observed. In addition, there is an increase in the intensity of the aromatic stretching bands at 1600 cm^{-1} due to the presence of the aromatic linker group.

Photoexcitation of SAM **VII** and multilayer films **VIII** and **IX** in the presence of methyl viologen by an unfocused, unfiltered, omnidirectional, 20 W, 350 nm Rayonet lamp (power incident on sample approx 0.1 mW) causes generation of a cathodic photocurrent in the range of 5-30 nA/cm^2 with **VIII** and **IX** consistently exhibiting higher values than SAM **VII** (5-10 nA/cm^2 for SAM **VII**; 10-30 nA/cm^2 for **VIII** and **IX**). Figure 24 shows the change in photocurrent for **IX** as a result of alternately shuttering and unshuttering the light source.

A photocurrent of 30 nA/cm^2 is comparable to, although somewhat smaller than that reported by Imahori and co-workers (~ 50-100 nA/cm^2) and represents a quantum efficiency of ~1%. In addition to enhanced current generation, **VIII** and **IX** also appear to possess greater stability than SAM **VII**. While repeated photoexcitation of SAM **VII** eventually results in degradation of the film and loss of photocurrent after approximately

10 cycles, **VIII** and **IX** did not show any decrease in current over several hours of alternating light/dark cycles.

Figure 24. Photocurrent generated following exposure of **IX** to ~0.1 mW at 350 nm at constant applied voltage = 0V vs. SCE. Photocurrent is expressed as nA/cm^2.

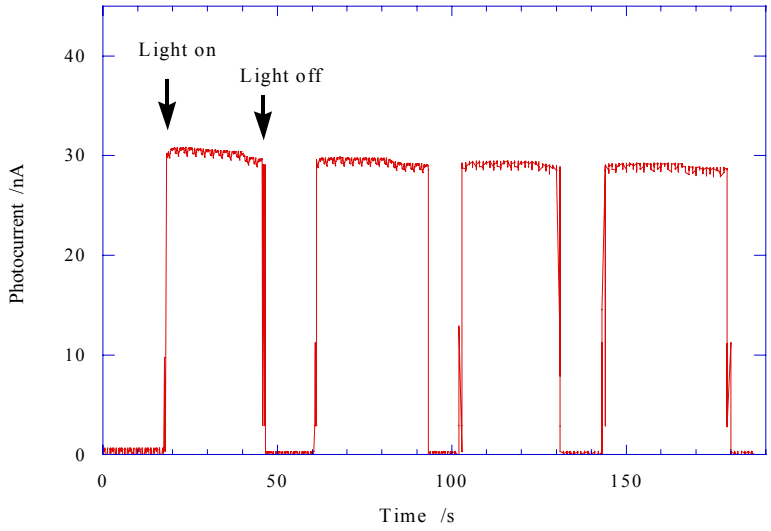

We note that neither **VIII** nor **IX** is an optimized system because there is a mismatch between the spectral output of the excitation lamp and the absorption spectrum of the pyrene chromophores. Factors that may influence the overall output of our system may include the type of metal ions used and the distance that the chromophore is from the gold surface. In addition, choosing a chromophores with a greater extinction coefficient, such as a rhodamine or porphyrin will also increase the efficiency of light harvesting. While neither **VIII** nor **IX** is an optimized system, they illustrate that a non-covalent

approach can be successful in the construction of systems that function as well as their covalently assembled analogues.

(iii) Multilayer Thin Films with Photoswitchable Wettability

McGimpsey, W.G.; MacDonald, J.C.; Soto, E.R.; Cooper, C.G.F. *J. Am. Chem. Soc. (Comm. Ed.)*, **2004**, *126*, 1030

-Materials and Methods and Experimental Data are provided in Section II-3 and II-4-

Control of surface wettability is currently of interest due to its importance in the fields of micro-and nanofluidics. Whitesides et al. and others have devoted considerable effort to the creation of multifunctional surfaces with variable wettability using microcontact printing techniques.[27,33,59,60] More recently, several groups have shown that wettability can be controlled by externally applied stimuli such as light or an electric field.[61,62,63,64]

In previous sections, we have demonstrated that a modular, non-covalent approach towards thin film construction can be used to build surfaces that act as molecular scale wires and as light-harvesting thin films. Both studies, besides offering interesting results from a materials point of view, have illustrated that the dimensions and function of a multilayer can be custom-tailored using a modular, non-covalent assembly method. Building on our previous work, we have employed non-covalent synthesis for the design of a modularly constructed multilayer system with photoswitchable wettability. Here we report a study in which the wettability of a multilayer surface capped with 2,2'-dipyridylethylene ligands can be switched permanently by photoinduced *cis-trans* isomerization of the ethylene. Besides its potential utility in the field of interfacial engineering, this system demonstrates that photoactive chelating molecules can be effectively incorporated into a multilayer film and drastically change the physical properties of that film.

For this work, we have assembled multilayer thin films **X** and **XI**. (Figure 25) Each film consists of a 2,2'-dipyridyl ethylene light absorbing group coupled to a gold surface via metal-ligand interactions. These films were fabricated by self-assembly of 4-[(10-mercaptodecyl)pyridine-2,6-dicarboxylic acid on a clean gold surface, followed by the deposition of Cu(II) ions that complex with the head group of the previous layer, and finally, deposition of the 2,2'-dipyridylethylene ligand in either the *cis* (film **X**) of *trans* (film **XI**) form, which serves to cap the Cu(II) ions.

Figure 25. Structure of thin films **X** and **XI**. **X** can be converted to **XI** by irradiation with 300 nm light.

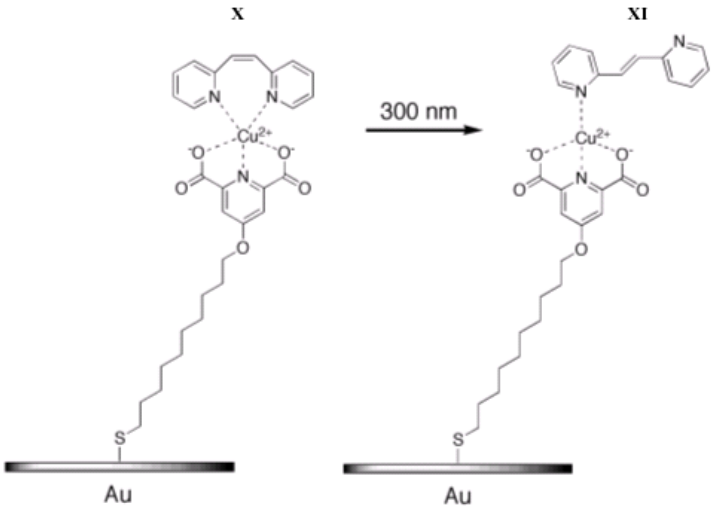

Conductivity, impedance, contact angle, and grazing incidence IR experiments were carried out on films **X** and **XI** after the addition of each layer, and confirmed the ordered deposition of each component. Conductivity (CV) values for both **X** and **XI** obtained in an aqueous solution of potassium ferricyanide change as the individual components are deposited sequentially onto the gold surface, as has been previously described. The CV of the bare gold surface shows the Fe^{3+}/Fe^{2+} redox peaks for oxidation and reduction of

ferricyanide, whereas deposition of the pyridine-capped decanethiol yields conductivity values (measured in the range -0.5V - +0.6V versus SCE) that indicate the formation of an insulating monolayer with few defects. After the monolayer is exposed to a solution of Cu(II) ions**,** the CV of the film is nearly identical to that of bare gold with only a small decrease in peak current. This result indicates that the Cu(II) ions promote tunneling of electrons between the gold surface and the solution. Deposition of the dipyridylethylene ligands again results in attenuated conductivity consistent with formation of an insulating layer on the surface.

These results, in addition to impedance observations are consistent with our previous studies of multilayer films. Contact angle measurements shown in Table 4 and IR spectra (not shown) also confirm that substantial changes in the surface occur following addition of each layer. In particular the IR measurements show conclusively the presence of each of the added layers.

Table 4. Contact angle measurements for Films **X** and **XI**.

Film	**Contact Angle (degrees)**
Gold	76 +/- 1.0
Film **X**	
Component 1 (pyridyl-capped decanthiol)	76.0+/- 1.5
Component 2 (Cu(II) ions)	58.0 +/- 2.0
Component 3 (*cis*-2,2'-dipyridylethylene)	76.5 +/- 2.5
Film **XI**	
Component 3 (*trans*-2,2'-dipyridylethylene)	63.5 +/- 0.5
Film **X** irradiated	57.0 +/- 2.0
Film **XI** irradiated	64.0 +/- 2.0

Deposition of *cis* and *trans*-dipyridylethylene leads to differences in the surface wettability with the *cis*-isomer providing a more hydrophobic surface as determined from contact angle measurements. The difference in contact angle of ~13º between **X** and **XI** is greater than that reported for a variety of photo-isomerizable thin films that typically exhibit changes of ca. 9º.[61] In addition, the CV results indicate that the *cis*-capped surface is less conductive than the *trans*-capped surface. Recalling that impedance measurements indicate well ordered films in each case and that IR studies confirm the presence of the dipyridylethylene in each film, the difference in surface hydrophobicity can be attributed to differences in the electrostatics of the two surfaces that arise from different orientations of the two isomers. Molecular modeling by our group and previous studies by others[65] of nickel–dipyridylethylene complexes indicate that the *cis*-isomer likely forms a symmetrical bidentate Cu(II) complex (Figure 25) that efficiently 'caps' the metal ion, producing a hydrophobic packing arrangement on the surface. The *trans*-isomer, however, is not able to form a stable bidentate complex due to its elongated structure. Although we have not yet determined the mode of binding, the trans isomer is likely monodentate, as shown in Figure 25. The structure shown in Figure 25 helps explain the enhanced wettability provided by this isomer, because the Cu(II) ion in this case is not completely coordinated and, therefore, is free to complex with water. The uncoordinated pyridine ring also is free to bind with water via hydrogen bonding at the ring nitrogen. Impedance measurements on **XI** in fact show elevated capacitance values for the *trans*-capped system, which indicates that diffusion occurs between the solution and the layer of metal ions.

The contact angle, CV, impedance and IR data also help to characterize the changes that occur following photoexcitation of the films. Exposure of film **X** to 300 nm irradiation in chloroform in the presence or the absence of oxygen results in a substantial decrease in the contact angle, from 76.5º to 57º, a change that is consistent with *cis*-*trans* isomerization. We note that the contact angle obtained is somewhat smaller than that of unirradiated film **XI**. The smaller angle is likely a result of different packing arrangements in the films. Also, the conductivity of film **X** increases following irradiation so as to be nearly identical to that of unirradiated film **XI**, while impedance measurements indicate that the irradiated film remains a well ordered system. The clearest confirmation of isomerization of film **X** is provided by IR measurements. Figure 26 shows the IR spectra of unirradiated films **X** and **XI** and film **X** following irradiation. While the IR absorption bands that are normally used to distinguish between *cis*- and *trans*-dipyridylethylenes lie at frequencies lower than 1000 cm^{-1}, the sensitivity of our grazing incidence IR instrument is low in this region. There are several aromatic stretching frequencies that absorb above 1000 cm^{-1}, however, that are found in the spectrum of unirradiated film **X** but are absent in the spectrum of film **XI**. In particular, film **X** absorbs strongly at 1511 cm^{-1} and less intensely at 1313, 1303, 1253, and 1186 cm^{-1}, while film **XI** does not. Following irradiation of film **X**, these bands are attenuated and the spectrum of the irradiated film resembles closely that of film **XI**.

Previous studies on the solution photochemistry of 2,2'-dipyridylethylenes report quantum yields for *cis*-*trans* and *trans*-*cis* photoisomerization equal to 0.84[66] and 0.12[67], respectively. Irradiation of film **XI**, however, does not yield any *cis* product as indicated

by the lack of change in the CV, IR and contact angle data. Failure of the *trans*-dipyridylethylene units to undergo photoisomerization back to the *cis* isomers likely is caused by ordered packing of the *trans*-dipyridylethylene units in films of **XI** that sterically inhibits the structural reorganization necessary for *trans-cis* isomerization to occur. The CV and impedance measurements of film **XI** indicate that the dipyridylethylene head groups in fact are well ordered in films of **XI**.

Figure 26. Grazing Angle IR Spectra of Films **X**, **XI**, and irradiated **X**.

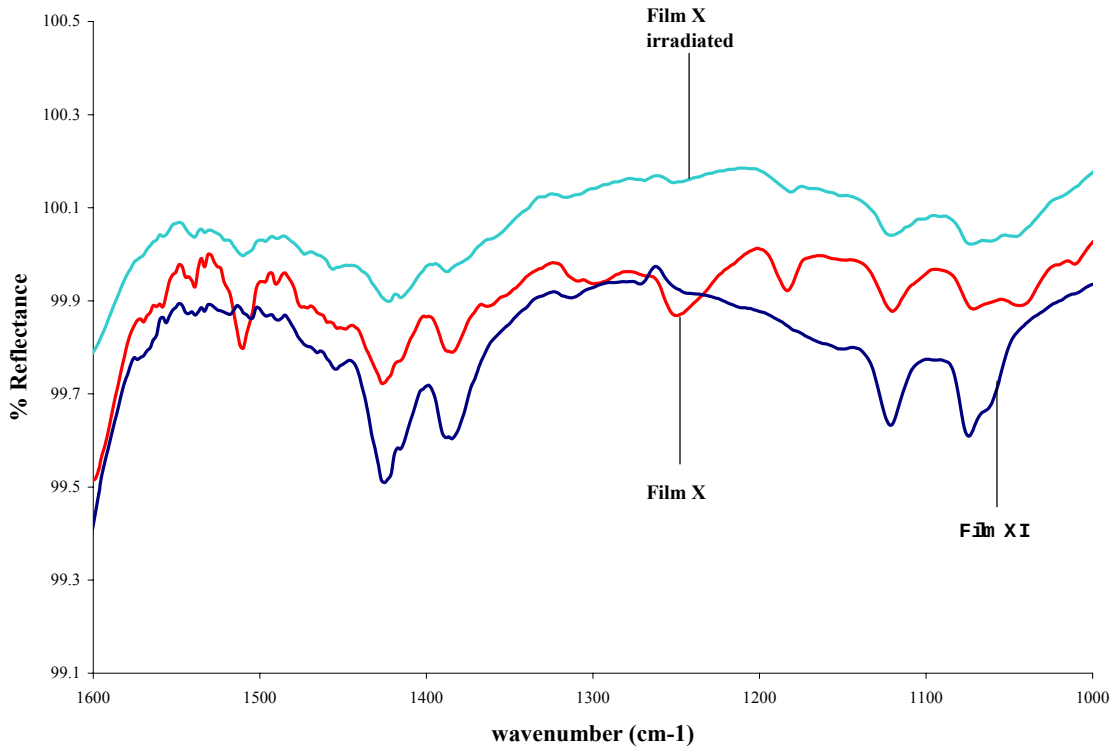

The system described here demonstrates that non-covalent multilayer assembly provides a convenient means to fabricate highly ordered thin films with wettability that can be switched. Although the wettability of surfaces functionalized with dipyridylethylene units

is not reversible, this work provides proof-of-concept that chromophores with photo-switchable molecular structures can be attached non-covalently to surfaces, that non-covalent multilayer films terminated with such chromophores have well-ordered surface structures, that the wettability of such surfaces can be controlled photolytically (applicable for microfluidic research), and that such multilayer thin films are stable before and after photoinduced changes in structure at the surface. We currently are using this methodology to incorporate photochromic molecules into similar non-covalent multilayer films to provide complete switchability while maintaining the substantial change in wettability that we have achieved in this system. This non-covalent approach also potentially provides a platform for the fabrication of other devices. Ongoing work is aimed at identifying methods for the selective replacement of ligands in order to provide spatially resolved regions of variable and switchable wettability.

3. Materials and Methods

Spectra for all compounds and synthetic schemes are provided in Appendix 1.

Materials. All materials were used as received from their respective vendors. Unless otherwise noted, reagents and solvents were purchased from Sigma-Aldrich. Amino acids, peptide resins, and coupling reagents were purchased from Nova Biochem. All solid-phase coupling reactions were carried out in technical grade DMF purchased from Pharmco.

General Methods.

Synthetic Procedures. NMR spectra were obtained in an Avance Bruker NMR spectrometer at 400 MHz for proton and 85 MHz for ^{13}C. Mass Spectra were measured by the SynPep Corporation in Dublin, CA. Samples were ionized by electrospray ionization, using acetonitrile as a carrier solvent with ultra-high purity nitrogen as a curtain gas. IR spectra were obtained using a Nexus FT-IR spectrometer equipped with either a transmission or ATR accessory, depending on the sample. Melting points were obtained on a Mel-Temp melting point apparatus and appear uncorrected.

A. Multilayer Films as Molecular Wires (Section II-A-2-i).

1. Preparation of 4-[(10-mercaptodecyl)oxy]pyridine-2,6-dicarboxylic acid.

(Starting Material for SAM **I** – Figure 16-I. The full reaction scheme is given in Scheme 5 in Appendix 1.)

(i) Diethyl 4-hydroxypyridine-2,6-dicarboxylate.

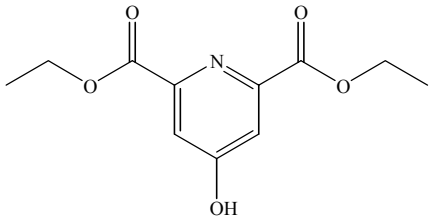

This compound was synthesized as described in refs.[68,69]. Thionyl chloride (6.2 mL, 85 mmol) was slowly added to 25 mL of absolute ethanol at 0º C. To this solution, 2.5 g (13.7 mmol) of chelidamic acid was added. The solution was stirred at room temperature for 18 h, and refluxed for 2 h to ensure completeness. Solvent was removed under reduced pressure, and 20 mL of distilled water was added to the crude product at 0º C. The mixture was neutralized with 5 mL of 10% aqueous sodium carbonate, and the product precipitated by addition of 5 mL 50% aqueous ethanol. The white precipitate was filtered and dried under vacuum to afford 3.26 g of product. Yield: 99%, R_f = 0.65 (normal phase, MeOH), m.p.: 115-116º; ^{1}H-NMR ($CDCl_3$) δ 1.45 (t, 6H, CH_3); 4.46 (q, 4H, CH_2); 7.31 (m, 2H, aromatic); 9.96 (bs, 1H, OH); ^{13}C-NMR ($CDCl_3$) δ 14.5 (CH_3); 63.5 (CH_2); 119.4 (Ar-C, broad due to tautomerism); 162.8-163.0 (C=O, broad due to tautomerism) ESI-MS *(m/z)* $[M+Na]^+$=262.3 (MW_{calcd} 262.2).

(ii) Diethyl 4-[(10-Bromodecyl)oxy]pyridine-2,6-dicarboxylate.

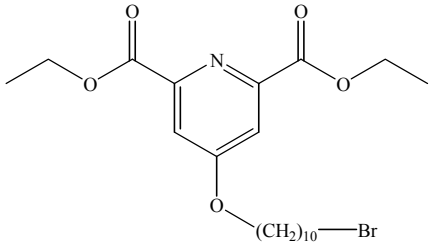

This new compound was made based on the synthesis described in ref.[30]. Diethyl 4-hydroxypyridine-2,6-dicarboxylate (2 g, 8.4 mmol) and 7.6 g (25.2 mmol) of 1, 10 dibromodecane were dissolved in 100 mL of dry acetone. To this solution, 2.32 g (16.8 mmol) of potassium carbonate was added, and the solution was heated to reflux for 40 h. The solvent was removed under reduced pressure, and the residue dissolved in a minimal amount of dichloromethane. The solution was filtered, and the filtrate was concentrated via evaporation. The resultant residue was purified on silica gel (R_f = 0.6) with 1:1 dichlormethane: hexane as the eluent to yield 2.89 g of product. Yield 75%; ^{1}H-NMR ($CDCl_3$) δ1.24-1.28 (m, 20 H, 14 from decyl CH_2, 6 from CH_3); 1.86 (m, 2H, CH_2CH_2Br); 3.41 (t, 2H, CH_2Br); 4.13 (t, 2H, $OCH_2(CH_2)_9Br$); 4.48 (q, 4H, O-CH_2CH_3); 7.74 (s, 2H, aromatic); ^{13}C-NMR ($CDCl_3$) δ14.6 (CH_3); 26.2, 28.5, 29.1, 29.6, 29.7, 29.8, 33.2, 34.5 (CH_2); 60.8, 69.4 (OCH_2); 114.7, 150.5, 165.2 (aromatic C); 167.4 (C=O).

(iii) Diethyl 4-[(10-Thioacetyldecyl)oxy]pyridine-2,6-dicarboxylate.

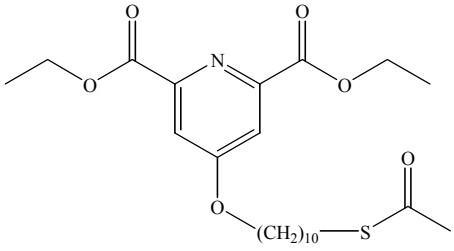

This new compound was made based on the synthesis of a similar compound described in ref.[30]. Diethyl 4-[(10-bromodecyl)oxy]-pyridine-2,6-dicarboxylate (1.20 g, 2.6 mmol) and 0.35 g (3.36 mmol) of potassium thioacetate were dissolved in 100 mL of ethanol and the solution brought to reflux for 24 h. The mixture was cooled, and the resulting white precipitate was filtered and dried under vacuum. The product was used in subsequent steps without further purification or characterization due to its low solubility in most organic solvents.

(iv) 4-[(10-mercaptodecyl)oxy]pyridine-2,6-dicarboxylic acid.

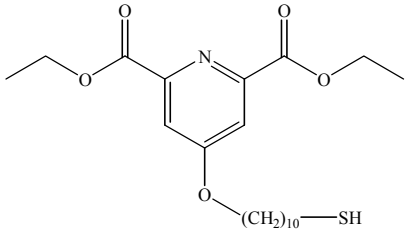

This compound was prepared by a similar method to the one described in ref.[30]. A 1.13 g sample of the product obtained in the previous step was suspended in 75 mL of 2 N KOH solution (in 70% aqueous ethanol). The solution was refluxed for 3 h, cooled, and the reaction quenched by acidifying with glacial acetic acid. The solvent was removed under reduced pressure, and the crude residue dissolved in dichloromethane. The organic fraction was washed with 1 N NaOH, and the organic phase discarded. The aqueous

phase was acidified with 3 N HCl, and extracted three times with 25 mL portions of dichloromethane. The organic fractions were combined, and the solvent removed under reduced pressure to yield 0.92 g of pure white powder. Yield: 94% ^{1}H-NMR ($CDCl_3$) δ1.24-1.44 (m, 16H, decyl CH_2); 1.85 (bs, 1H, SH); 2.51 (m, 2H, CH_2SH); 4.23 (m, 2H, O-CH_2); 6.49 (bs, 2H, COOH); 7.88 (s, 2H, aromatic); ESI-MS *(m/z)* $[M+H]^+$=356.2 (MW_{calcd} 356.4).

2. Preparation of 2,2',6,6'-Tetracarboxy-4,4'bipyridine.

(Linker ligand, SAM **III-VI** – Figure 16. The full reaction scheme is given in Scheme 6 in Appendix 1.)

(i) 2,2'-6,6'-Tetramethyl-4,4'-bipyridine.

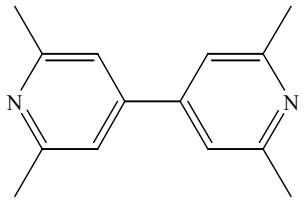

This compound was prepared based on the procedure described in ref.[70]. In a three-neck round bottom flask under nitrogen, 3.30 g (47.3 mmol) of a 33% Na dispersion in paraffin was suspended in 20 mL of dry toluene. The suspension was stirred with mild heating until all of the paraffin had dissolved. The solvent was then removed with a syringe and 4.50 g (43 mmol) of 2,6-lutidine in 40 mL dry THF was added. The reaction mixture was stirred until a precipitate formed and was left to react overnight. After 18 h, sulfur dioxide was passed over the sodium salt at such a rate as to prevent the solvent from rigorously boiling. After the reaction was finished, the flask was cooled with a

mixture of ice/NaCl and the reaction mixture quenched by the slow addition of 50 mL of ethanol. The reaction mixture was neutralized to pH 7-8 with 10 N NaOH, and diluted with 50 mL of H_2O. The mixture was then extracted three times with 60 mL portions of methyl t-butyl ether. The organic fractions were dried over anhydrous sodium sulfate, and the solvent removed under reduced pressure to yield 1.78 g of white product. Yield: 40%. ^{1}H-NMR (DMSO-d_6): δ 2.45 (s, br, 12H, CH_3); 7.43 (s, 4 H, pyridine); ^{13}C-NMR (DMSO-d_6): δ 24.4 (CH_3); 117.9, 145.7, 158.4 (pyridine).

(ii) 2,2',6,6'-Tetracarboxy-4,4'bipyridine.

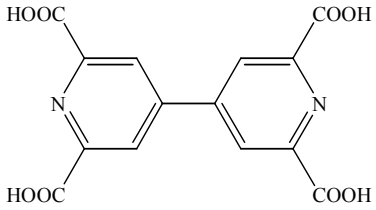

This compound was prepared based on the procedure described in ref.[70]. A 1 g (4.7 mmol) sample of 2,2'-6,6'-tetramethyl-4,4'-bipyridine was dissolved in 50 mL of concentrated sulfuric acid. The solution was cooled to 0°C and chromium trioxide (5.6 g, 0.055 mol) was added in small portions over a period of 2 hours. The reaction mixture was heated to 75°C for 2 hours, cooled to room temperature, and then transferred to a mixture of 150 mL of ice/water. The colorless product precipitated and was isolated via centrifugation to yield 1.1 g of product. Yield: 70%. ^{1}H-NMR (DMSO-d_6): δ 8.44 (s, 4 H, pyridine); 13.5 (s, br, 4 H, COOH); ESI-MS *(m/z)* $[M+Na]^+$=355.4 (MW_{calcd} 355.2).

B. Photocurrent Generation in Multilayer Thin Films (Section II-A-2-ii).

(Compounds used in the construction of **SAM VII** and films **VIII-IX.** (Figure 23) Synthetic Schemes and Spectra are documented in Appendix 1. (Schemes 7 and 8))

1. Synthesis of the compound used for the construction of SAM VII.[52,71,72,73,74]

The peptide backbone of **SAM VII**, $(Aib\text{-}Ala)_6$, was synthesized by an FMoc solid phase strategy on a Wang Resin using aminoisobutyric acid and L-alanine. The synthesis of L-pyrenyl alanine and general methods for solid phase peptide synthesis are described in detail in section II-B-3.

(i) N-t-butoxycarbonyl-L-1-pyrenyl alanine (preparation of tBoc protected pyrenyl alanine).

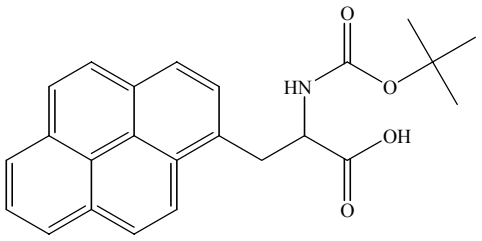

L-l-pyrenyl-alanine (1 g, 3.44 mmol) was suspended in 100 mL of a 1:1 water/dioxane mixture. A solution of 1 g (4.60 mmol) of di-tert-butoxycarbonyl (Boc_2O) and 0.5 g (0.66 mL, 5.00 mmol) of triethylamine in 20 mL of 1:1 dioxane:water was added to the L-1-pyrenylalanine suspension at 0°C. The solution was stirred at 0°C for 3 hours and then at room temperature for 24 hours. The solution was filtered to recover unreacted L-1-pyrenylalanine and the filtrate was concentrated under reduced pressure. A small amount of water (~ 5 mL) was added to the resulting brown residue, and the solution was acidified to pH 4 with 5% citric acid. The acidified solution was extracted 3 times with

25 mL portions of ethyl acetate. The organic fractions were washed with water and dried over anhydrous sodium sulfate. The solvent was removed and ether was added to the remaining oil until precipitation of the product occurred. The product was filtered, dried under vacuum, and recrystallized from chloroform/ether to afford 0.27 g of white powder. Yield: 20%. R_f = 0.45 (normal phase, $CHCl_3$/MeOH/AcOH 90:10:3); ^{1}H-NMR (DMSO-d_6): δ 1.49 (s, 9H, CH_3); 3.29, 3.60 (d of m, 2H, CH_2); 4.41 (d, 1H, CH); 7.47 (d, 1H, NH); 7.73-8.53 (m, 9H, CH pyrene); ^{13}C-NMR (DMSO-d_6): δ 22.2 (CH_3 from *t*-Boc); 34.5 (CH_2); 53.5 (CH); 122.9-132.0 (pyrene); 169.1, 173.1 (C=O); ESI-MS *(m/z)* $[M]^+$=389.2 (MW_{calcd} 389.4).

(ii) 1,2-dithia-3-(1-amino-n-pentyl)cyclopentane (lipoamine or LA).

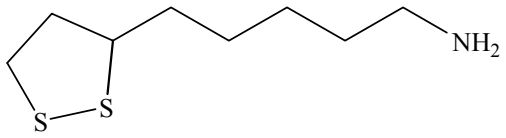

This compound was synthesized based on the procedure described in ref.[52]. D,L-α-lipoamide (1 g, 5.23 mmol) was dissolved in 100 mL THF and added to a dispersion of 0.826 g (21.76 mmol) of $LiAlH_4$ in 50 mL THF. The mixture was refluxed for 15 hours and was then cooled to 0°C. Distilled water (10 mL) was slowly added and the solution was stirred for 30 minutes. The solvent was evaporated, and 15 mL of methanol was added to the residue. The solution was filtered to remove insoluble material, and the methanol evaporated under reduced pressure. The resulting crude oil was diluted with 100 mL of water and the solution adjusted to pH 6.5 with 1 N HCl. The aqueous mixture was extracted 3 times with 20 mL portions of *n*-butanol, and the organic fractions washed twice with 10 mL portions of 1 N NaOH and 1 N HCl. The solvent was removed to

afford 0.233 g of pure yellow powder Yield: 25%. R_f = 0.2 (normal phase, $CHCl_3$/MeOHl/AcOH 90:10:3); ^{1}H-NMR ($CDCl_3$) δ 1.48 (m,4H,H_2N-CH_2CH_2*CH_2**CH_2**CH_2*CH_2), 1.71 (m, 4H, H_2N-CH_2*CH_2*CH_2CH_2*CH_2*), 1.89, 2.28 (m, 2H, CH*CH_2*CH_2SS); 2.40 (m. 2H, H_2N*CH_2*); 3.15 (2H, m, $CHCH_2$*CH_2*SS); 3.59 (m, 1H, *CH*CH_2CH_2SS); ^{13}C-NMR ($CDCl_3$) δ 26.4, 27.4, 28.7, 34.6, 38.5, 40.3, 42.8 (7 -CH_2); 56.8 (CH).

(iii) Coupling of Lipoamine (LA) to the Peptide C-terminus: (Aib-Ala)$_6$-LA.

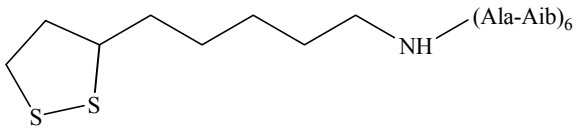

This coupling reaction was carried out with the procedure described in ref.[52]. The peptide (1 eq) was dissolved in DMF and was added dropwise to a solution of 5 equivalents each of lipoamine, HATU (coupling reagent) and DIPEA (diisopropyl ethyl amine) at 0°C over a period of 1 h. The solution was stirred at 0°C for an additional 30 minutes and then at room temperature for 24 hours. The solvent was removed under reduced pressure and the crude residue dissolved in chloroform. The organic layer was washed 3 times with 4% aqueous sodium bicarbonate. The organic fraction was dried over sodium sulfate, and the chloroform removed via rotary evaporation. The product was purified over silica gel using methanol as the eluent (R_f = 0.5). The crude product was further recrystallized from chloroform/hexane to yield a white powder. Yield: 25%. ^{1}H-NMR ($CDCl_3$) δ 1.26-1.71 (m, 63 H, CH_3 from Aib and Ala + 9 H from lipoamine fragment), 2.5-3.7 (m, 6 H from lipoamine + 6 CH from Ala); 7.5-8.5 (12 NH); ESI-MS *(m/z)* $[M+Na]^+$=1151.6 (MW_{calcd}1151.3)

(iv) Coupling of t-Boc Pya to (Aib-Ala)$_6$-LA: t-Boc Pya-(Aib-Ala)$_6$-LA (SAM VII).

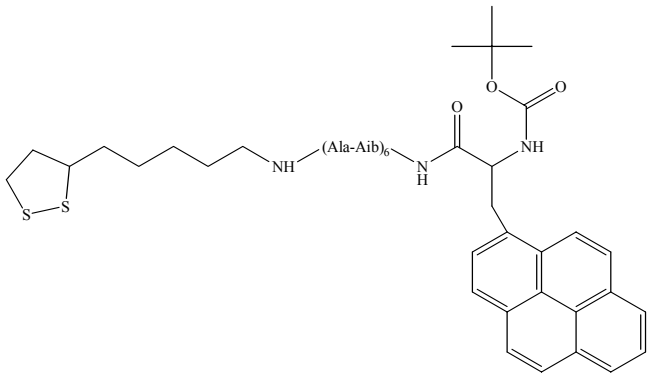

This coupling reaction was carried out under similar conditions to those described in ref.[52]. A 1 eq sample of (Aib-Ala)$_6$-LA was dissolved in DMF (2 mL DMF/mg peptide). The solution was cooled to 0°C and a solution containing 2.5 eq of Boc-pyrenyl-alanine, 2.5 eq of HATU and 5 eq of DIPEA in DMF was added. The solution was stirred at 0°C for 30 minutes and then at room temperature for 24 hours. The solvent was removed under reduced pressure and the crude residue was dissolved in chloroform. Insoluble materials were removed by filtration. The filtrate was washed twice with 4% sodium bicarbonate solution and the organic phase concentrated under reduced pressure. The crude product was recrystallized from chloroform/ether to yield a white powder. Yield: 80%. R_f = 0.40 (normal phase, 13:5:1 $CHCl_3$:MeOH:NH_4OH); ^{1}H-NMR ($CDCl_3$) δ 1.35-2.0 (broad band, 73 H, 54 H from CH_3 from Ala and Aib units, 9 from CH_3 t-Boc, 2 H from lipoamine ring CH_2*CH_2*CHSS and 8 CH_2 from lipoamine chain); 3.15-3.20 (m, 6H, 2 from CH_2 lipoamine ring, *CH_2*NH lipoamine chain and CH_2 Pya); 3.53 (m, 1H, CH lipoamine ring); 3.95-4.24 (m, 6H, CH Ala); 4.41 (CH Pya); 7.30-8.12 (21 H, 9 aromatic H from Pyrene + 12 NH); ^{13}C-NMR ($CDCl_3$) δ 14.2, 22.7, 23.3 (CH_3 from t-Boc, Aib and Ala respectively); 26.5, 29.4, 30.1, 32.0, 35.1, 38.8, 38.9, 40.2 (CH_2 from lipoamine

and from Pya at 32.0 and 35.1); 56.4 (CH from lipoamine ring); 53.5 (CH from Pya); 50.6 (CH from Ala); 123.1-131.3 (Aromatic C); 169.7-171.2 (carbonyl carbons).

Synthesis of the Components in Films VIII and IX.

4-[(10-mercaptodecyl)oxy]pyridine-2,6-dicarboxylic acid and 2,2',6,6'-tetracarboxy-4,4'bipyridine were prepared as previously described in this section.

1. 4-[(Methylpyrenyl)oxy]pyridine-2,6-dicarboxylic acid (Pyrenyl substituted chelidamic acid cap).

(i) Diethyl 4-[(methylpyrenyl)oxy]pyridine-2,6-dicarboxylate.

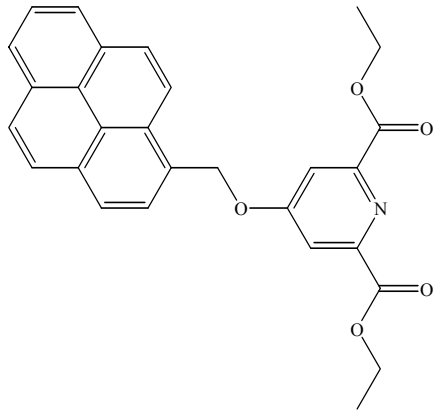

This compound was prepared based on the synthesis described in ref.[30]. A 0.98 g sample (3.75 mmol) of 1-bromomethylpyrene and diethyl 4-hydroxypyridine-2,6-dicarboxylate (1 g, 3.40 mmol) were separately dissolved in acetone. The clear solutions were mixed, 0.37 g (3.5 mmol) of sodium carbonate was added, and the mixture refluxed for 24h. The solution was filtered hot and the solvent was removed to afford a crude yellow product. The crude product was recrystallized from dichloromethane to yield 1.17 g of a light yellow powder. Yield: 77%. R_f = 0.40 (normal phase, 1:1 DCM:MeOH); m.p.: 154-156

°C. ^{1}H-NMR ($CDCl_3$) δ 1.46 (t,6H,CH_3); 4.47 (q,4H, CH_2); 5.90 (s, 2H, CH_2); 8.01-8.26 (m, 11H, aromatic H); ^{13}C-NMR ($CDCl_3$) δ 15.2 (CH_3); 30.2 (CH_2); 63.5 (CH_2); 115.7-131.6 (aromatic CH); 165.7 (C=O). ESI-MS *(m/z)* $[M+Na]^+$=476.8 (MW_{calcd} 476.5)

(ii) 4-[(Methylpyrenyl)oxy]pyridine-2,6-dicarboxylic acid.

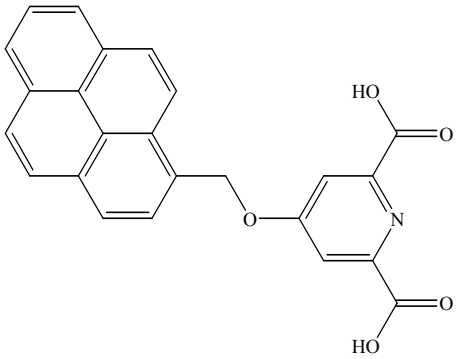

This compound was prepared based on the procedure described in ref.[30]. Diethyl 4-[(methylpyrenyl)oxy]pyridine-2,6-dicarboxylate (1.15 g, 2.5 mmol) was dissolved in 60 mL of ethanol. Potassium hydroxide (.504 g, 9.0 mmol) was added and the solution was heated to reflux for 6 hours. The solution was diluted with 50 mL of water and acidified to pH 2.5 with 6 N HCl. A white product precipitated and was isolated via filtration. The precipitate was washed with small portions of water, methanol and dichloromethane and dried under vacuum to yield 0.98 g of a white powder. Yield: 97%. R_f = 0.46 (normal phase, 1:1 DCM/MeOH); m.p.: decomposes above 225 °C. ^{1}H-NMR (DMSO-d_6) δ 6.10 (s, 2 H, CH_2); 7.92-8.41 (m, 11 H, Ar-H); ESI-MS *(m/z)* $[M+K]^+$=436.2 (MW_{calcd} 436.5)

C. Multilayer Thin-films as Photoswitchable Surfaces.

The preparation of 4-[(10-mercaptodecyl)oxy]pyridine-2,6-dicarboxylic acid has been described previously in this section. The compound described here is used as the cap to a copper terminated multilayer (Figure 25).

(i) Cis-(2,2'-dipyridyl)ethylene.

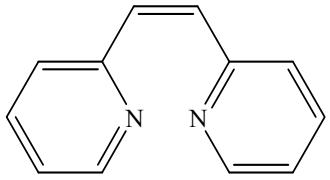

This compound was prepared based on the procedure provided in ref.[66]. A 2g sample (10.9 mmol) of trans-(2,2'-dipyridyl)ethylene was dissolved in 75 mL of spectroscopic grade chloroform, and placed in a pyrex tube. The tube was placed in a rotary photoreactor, and irradiated at 300 nm for a period of 1 h for isomerization. The chloroform was removed under reduced pressure, and the crude product purified over silica get using 15:1 Chloroform:Methanol as the mobile phase to yield 0.3 g of the yellow cis product. Yield: 15%, R_f 0.4 (15:1 $CHCl_3$:MeOH), GCMS r.t. = 10.63 min at 200°C, *(m/z)* $[M]^+$=155; ^{1}H-NMR ($CDCl_3$) δ 6.81 (s, 2H, ethylene CH_2); 7.05 (m, 1H, NCH*CH*CH); 7.20 (d, 1H, NC*CH*CH in ring); 7.42 (m, 1H, NCH*CH*CH in ring); 8.56 (d, 1H, N*CH*CH in ring); ^{13}C-NMR δ(ppm) 122.4 (ethylene CH); 124.2, 133.3, 136.4, 149.8, 155.9 (aromatic CH groups).

SAM and Multilayer Preparation.

Gold slides were purchased from Evaporated Metal Films (EMF). The slide dimensions were 25 mm x 75 mm x 1 mm of float glass with cut edges. Each slide was coated with 50 Å of Cr followed by 1000 Å of Au. The substrates were cut in different sizes according to experimental needs. Prior to use, the substrates were immersed in piranha solution (70% sulfuric acid, 30% hydrogen peroxide (30% aqueous)) at 90º C for 20 minutes to clean the surface. The slides were then washed with deionized water, dried with nitrogen, and used immediately. Monolayers were prepared by immersion of the clean gold slides in a 1-2 mM solution of the desired compound in ethanol. For 4-[(10-mercaptodecyl)oxy]pyridine-2,6-dicarboxylic acid solutions, full coverage of the surfaces was reached after 6 h, as evidenced by no further changes in the contact angle measurements. SAMs of dodecanethiol, and the peptidic SAM investigated were found to form complete monolayers between 4-6 h of exposure time. Copper (II) bromide was used as the source of Cu(II) ions (1 mM). Full Cu(II) complexation was reached after 3h of submersion. Capping of the copper ions was largely dependent on how many multilayers were assembled, and the type of capping unit being used. For the molecular wire work, Cu(II) was fully capped with the tetracarboxy dipyridyl linker (5 mM solution) unit after 4 h. However, capping of the Cu(II) ions by the pyrenyl substituted chelidamic acid unit (5 mM) took anywhere between 16-24 h. Capping of the copper ions with the cis and trans dipyridyl ethylenes was done with 5 mM solutions dissolved in either ethanol or acetone. Coverage was completed after 8 h of exposure. After every deposition, the films were rinsed with ethanol, and dried under nitrogen.

Thin Film Characterization: General Procedures.

Cyclic Voltammetry. All electrochemical experiments were carried out with an EG&G Princeton Applied Research Potentiostat/Galvanostat Model 273. A three-electrode setup was used with the SAM as the working electrode, a SCE as a the reference electrode, and platinum wire as the counter electrode. The monolayer was contacted with an alligator clamp with a working area of 1 cm^2. All solutions were freshly prepared and degassed with nitrogen before the experiments. The aqueous solution used for the experiments was 2mM potassium ferricyanide with 50 mM potassium chloride as a supporting electrolyte. To limit noise, the electrochemical cell was placed inside a Faraday cage. The cyclic voltammetry curves were obtained in the range of 0.0 to 0.7 V, with a scan rate of 50 mV/s and a scan increment of 1 V.

Contact Angle Measurements. Contact angle measurements were obtained with a Rame-Hart Model 100-00 Goniometer. 10 μL droplets of water were added to each surface using a calibrated Ependorff pipette.

Infrared spectroscopy. IR spectra were obtained on a Nexus FT-IR spectrometer equipped with a ThermoNicolet grazing angle accessory and a liquid-nitrogen cooled MCTA detector. The IR beam was incident at 75° on the gold substrates. The optical path was purged with nitrogen gas before and during data acquisition. Backgrounds were collected before every sample run. For each sample, 64 scans were collected with a 4 cm^{-1} resolution. The scan range was form 4000 to 600 cm^{-1}, although the detector cutoff occurs at just under 1000 cm^{-1}.

Impedance Spectroscopy. A 1255-HF frequency response analyzer was used in combination with a EG&G Princeton Applied Research Potentiostat/Galvanostat Model 273 for all impedance studies. Impedance experiments were performed using a three-electrode setup with the film as the working electrode, a SCE as the reference electrode, and platinum wire as the counter electrode. The electrolyte used was a 0.1 M solution of Na_2SO_4 in deionized water. The experimental conditions collected 20 points per decade, at a fixed potential of -0.5 V, with an amplitude of 20 mV, over a frequency range of 100000 to 0.01 Hz. The working electrode area was kept at 1 cm^2 for all experiments.

Photocurrent Measurements. Photocurrent experiments were performed using the three electrode setup described for cyclic voltammetry experiments. A 20 mM methyl viologen solution containing 50 mM sodium sulfate as a support was used. The samples were irradiated with a 350 nm Rayonet lamp through a slit in the Faraday cage. The cage itself was covered in order to prevent exposure of the cell to ambient light. The UV lamp was kept on continuously and a mechanical shutter was used to block exposure of the sample to the light. The sample was typically irradiated at intervals of 20-40 seconds. Individual experiments were performed at a fixed applied potential.

Photo-induced Isomerization of Films. The isomerization of dipyridyl ethylene capped films was attempted by submersing the substrate in chloroform in a pyrex flask, and irradiating with a 300 nm Rayonet lamp for periods between 30 min and 1 h. Samples irradiated less than 30 min showed incomplete conversion. Attempts to perform isomerizations in different solvents were unsuccessful, as were attempts performed in the

absence of any solvent. Samples placed in chloroform and left exposed to ambient light did not show any signs of isomerization.

4. Experimental Data

A. Multilayer Films as Molecular Wires.

All CV curves have been displayed within the main text of this chapter, along with IR spectra, impedance measurements, and contact angle measurements.

B. Photocurrent Generation From Multilayer Films.

Contact Angle Measurements.

Table 5. Contact angle measurements for gold, dodecanethiol, SAM **VII** and for films **VIII** and **IX** after deposition of each component. Dodecanthiol is included as a hydrophobic model system that is known to form ordered monolayers on gold.

Sample	**Contact Angle (degrees)**
Gold	76 +/- 1.0
Dodecanethiol	75.6 +/- 0.6
SAM VII	48 +/- 2.4
Film **VIII**	
Component 1 (pyridyl-capped decanethiol)	63.5 +/- 0.5
Component 2 (Cu(II) ions)	51.5 + /- 1.0
Component 3 (pyrenyl-capped pyridine)	75.7 +/- 1.1
Film **IX**	
Component 1 (pyridyl-capped decanethiol)	63.5 +/- 0.5
Component 2 (Cu(II) ions)	52.5 +/- 1.5
Component 3 (bipyridyl)	60.5 +/- 1.0
Component 4 (Cu(II) ions)	48 +/- 1.5
Component 5 (pyrenyl -capped pyridine)	68 +/- 0.5

CV Measurements.

Figure 27. Cyclic voltammograms obtained for bare gold and for **VIII** after the deposition of each component

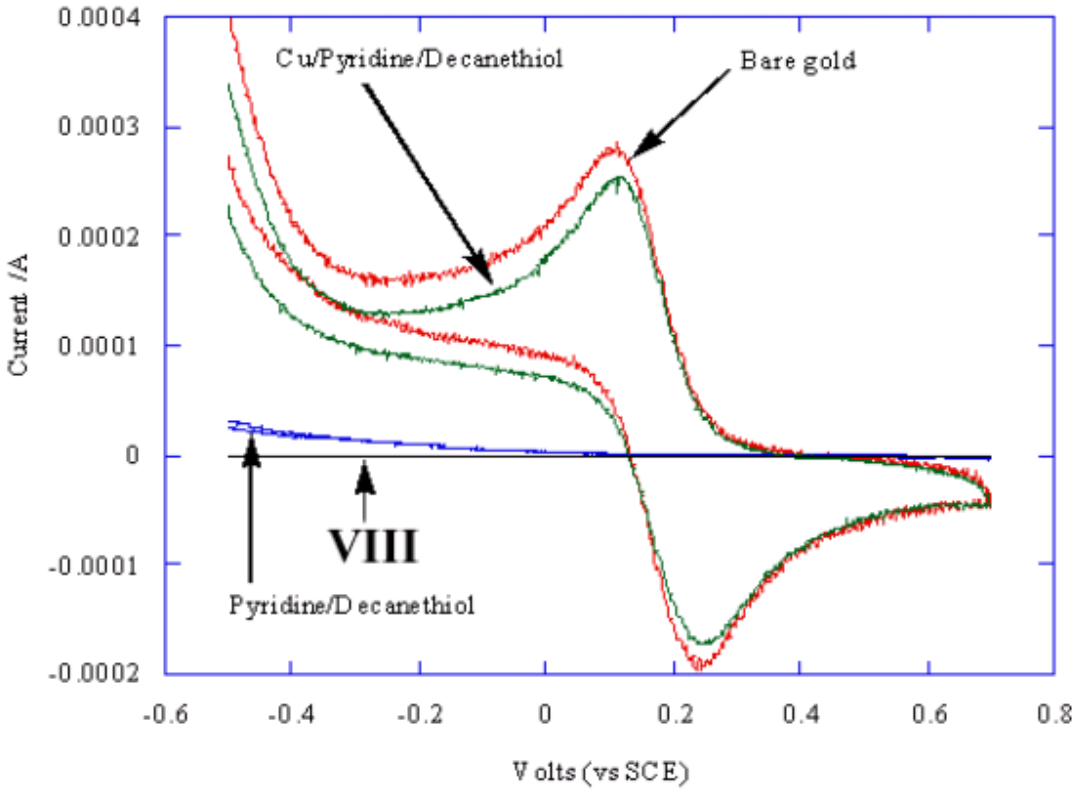

Grazing Angle IR Measurements.

Dodecanethiol: Assignment of the main absorption bands for a dodecanethiol SAM were based on the assignments observed in the literature.[47,75,76]

Table 6. IR assignments for dodecanethiol

Assignment	Peak frequency (cm^{-1})
$\nu_{a,\ ip}$ (CH_3)	2964.62
ν_a, FR (CH_3)	~~ very small shoulder
ν_a (CH_2)	2923.36
ν_s FR (CH_3)	2876.79
ν_s (CH_2)	2852.33
ν(CH_2) scissors deformation	1466.35
ν(CH_3) symmetric deformation	1380.16
CH_2 twisting and wagging	~1150-1350

a = asymmetric, s = symmetric, ip = in plane, FR = Fermi resonance

According to references 58 and 75, the positions of the CH_2 stretching modes are indicative of a crystalline-like packing of the sample. The weak CH_2 scissors deformation band is the result of a tilted orientation of the alkanethiol on the surface.

Table 7. IR assignments for **VIII**. (The individual layers are: (i) pyridine-decanethiol; (ii) Cu^{2+}; (iii) Pyrene-pyridine. The columns represent the peaks observed for the entire film following deposition of each component.)

Assignment	Peak frequency (cm^{-1})		
	Pyridine (Py)-decanethiol (dt)	Cu/Py-dt	Pyrene(Pyr)-Py/ Cu/Py-dt
COOH	3461.11 br (3232.06 sh)	3512.43 3415.16	***
ν(CH arom)	*** (3050 l)	***	3050.85 (3050)
ν_a (CH_2)	2924.56 (m) (2921.14 m)	2925.31	2924.13
ν_s (CH_2)	2852.88 (m) (2851.46 m)	2852.97	2853.04
COOH		2088.32	2099.97
ν(C=O)	1725.91 (s, br) (1750.15, 1725.52)	1739.17	1728.09 (1719.96)
	1683.6	1658.57	1688.07
ν(C-C aromatic)	1603.35 (1603.23)	1616.24	1601.01 (1599.62)
Ar ring	1423.41 (1417.77)	1415.22	1426.38
	1388.55 (1380?)	1378.51	1380.58
	1120.44 (1019.61)	1119.77	1112.22

***: not observed because of low intensity

Numbers in parenthesis are from IR spectra of the individual components, i.e., the pyridine-decanethiol and pyrene-pyridine units.

Table 8. IR assignments for **IX**. (The individual layers are: (i) pyridine-decanethiol; (ii) Cu^{2+}; (iii) Pyrene-pyridine. The columns represent the peaks observed for the entire film following deposition of each component.)

Assignment	Peak frequency (cm^{-1})				
	Py-dt	Cu/Py-dt	Bipyridyl (By)/ Cu/pyr-dt	Cu/By/Cu/py-dt	Pyr/Cu/By /Cu/Py-dt
COOH	3461.11 br	3512.43 3415.16	3273.92 br	3413.02 br	3483.94 br
ν(CH arom)	***	***	***	***	3010
ν_a (CH_2)	2924.56	2925.31	2924.90	***	***
ν_s (CH_2)	2852.88	2852.97	2853.24	***	***
COOH		2088.32	2103.94	2106.09	2105.13
ν(C=O)	1725.91	1739.17	1739.23	***	1728.33
	1683.6	1658.57	1669.68	1660.63	1684.61
ν(C-C arom)	1603.35 1423.41 1388.55 1120.44	1616.24 1415.22 1378.51 1119.77	1589.30 1377.05 1159.90	*** 1376.08	1601.10 1416.71 1370.73 1112.09

***: not observed because of low intensity

Grazing Angle IR Spectra.

Figure 28. The grazing angle IR spectrum of Dodecanethiol.

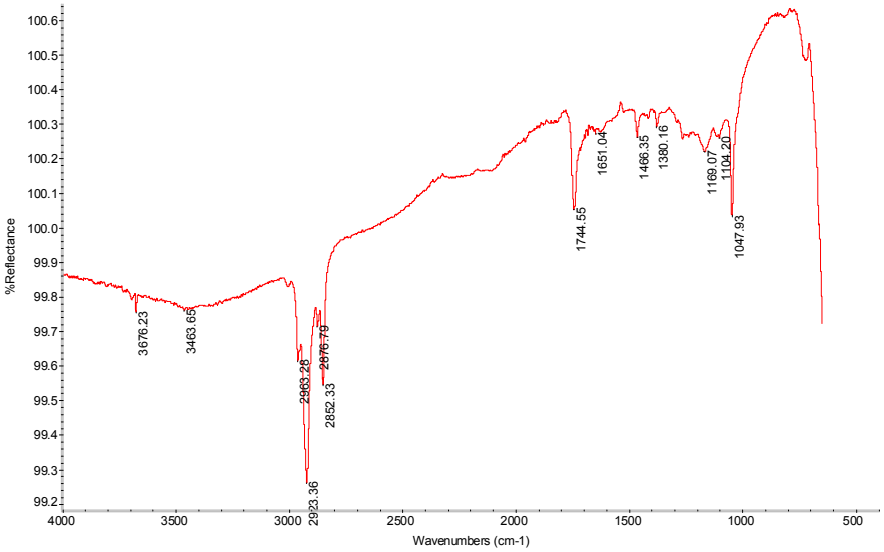

Figure 29. The grazing angle IR spectrum of peptidic SAM **VII** (top) with an expanded view of its amide I and II region (bottom).

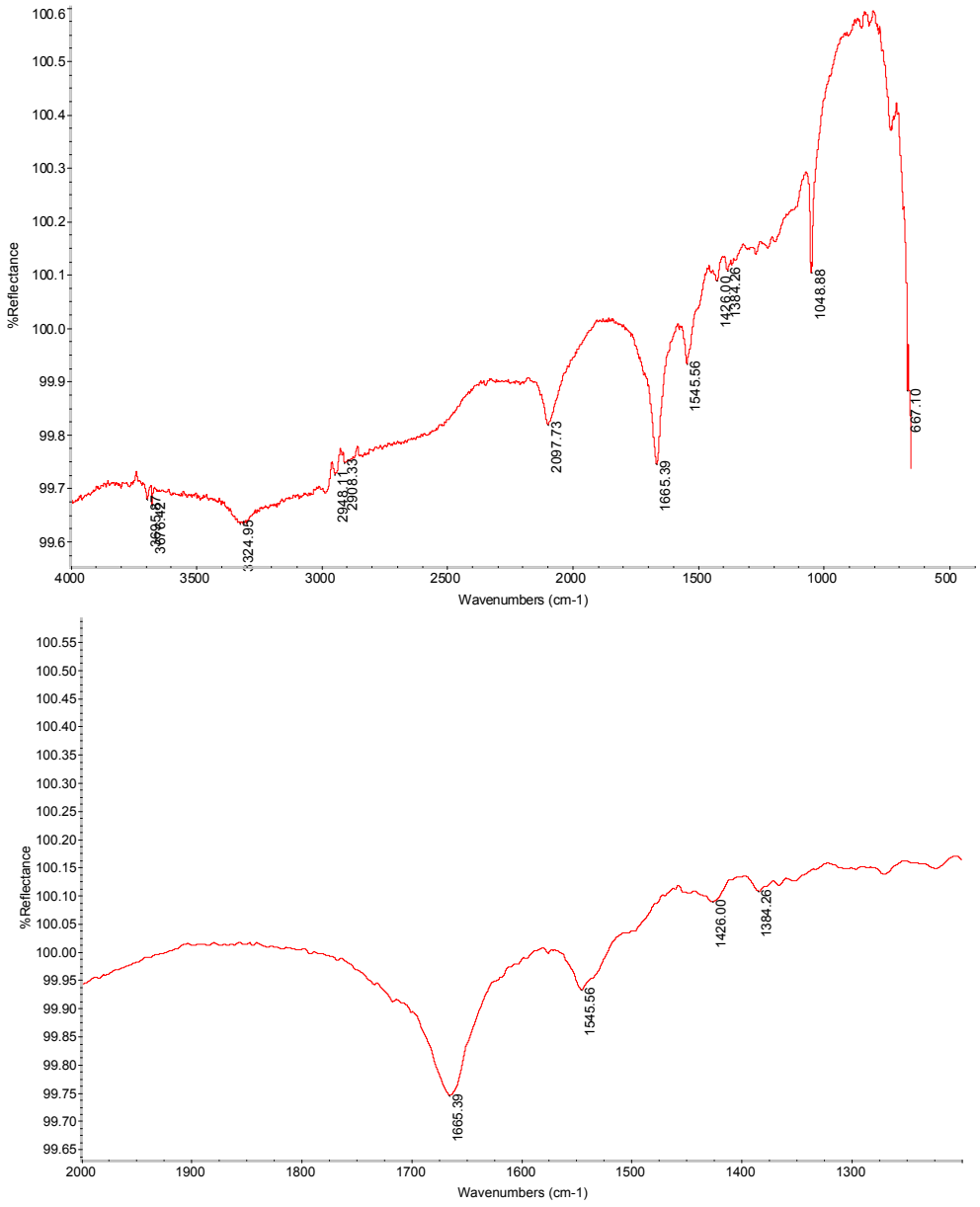

Figure 30. The grazing angle IR spectrum of a SAM of dicarboxypyridyl capped decane thiol.

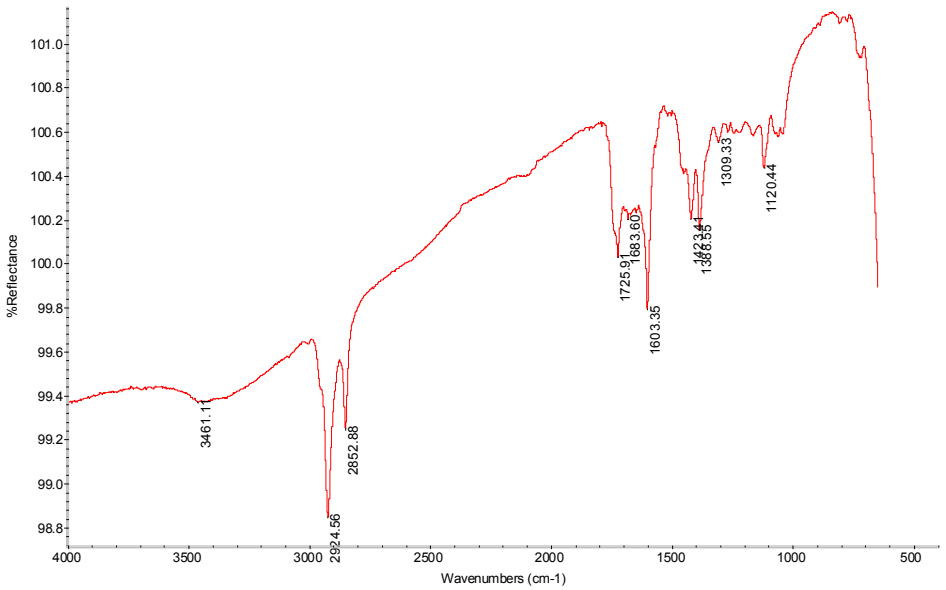

Figure 31. The grazing angle IR spectrum of the dicarboxy pyridyl SAM complexed with Cu(II) ions.

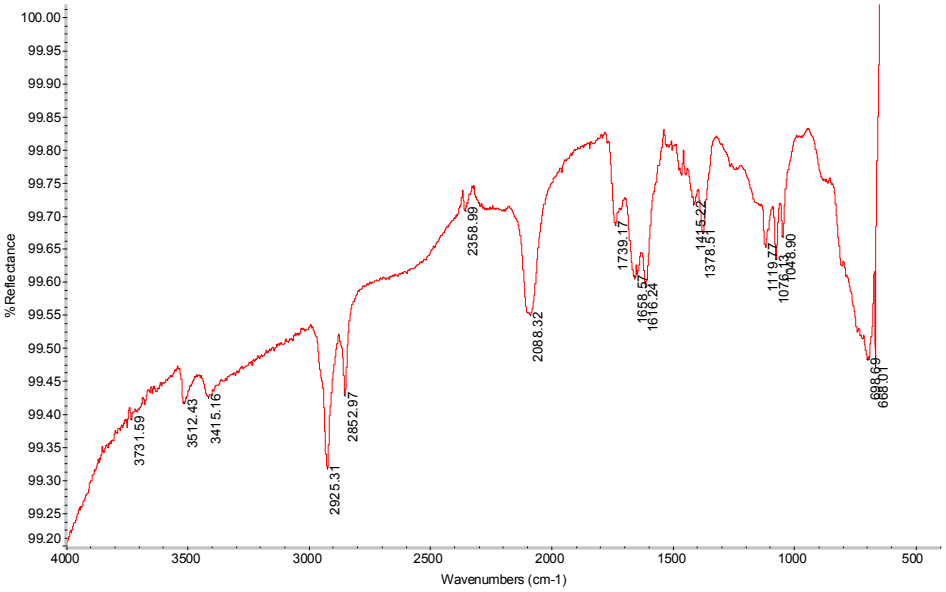

Figure 32. The grazing angle IR spectrum of SAM + Cu(II) ions + pyrene substituted cap.

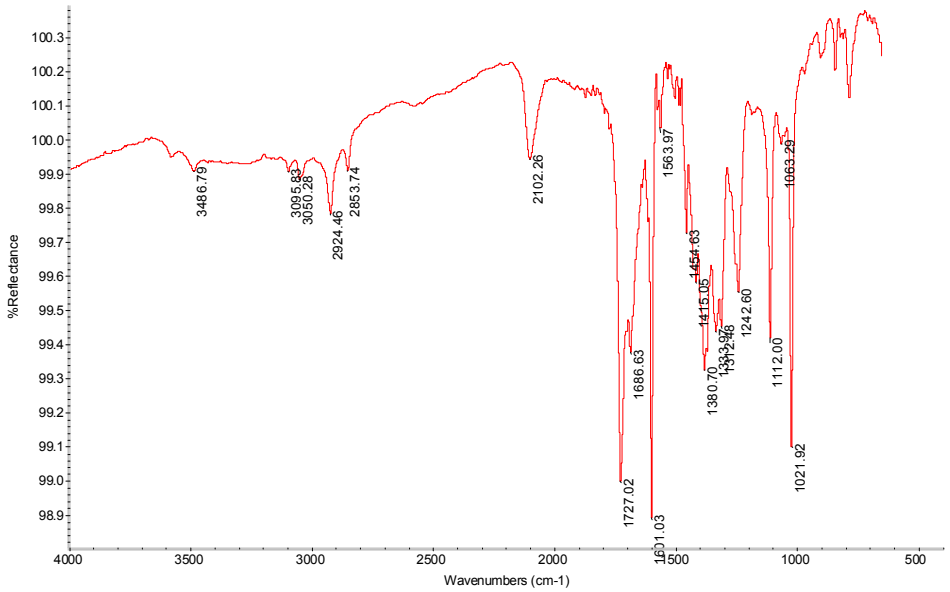

Figure 33. The grazing angle IR spectrum of SAM + Cu(II) ions + bipyridyl linker group.

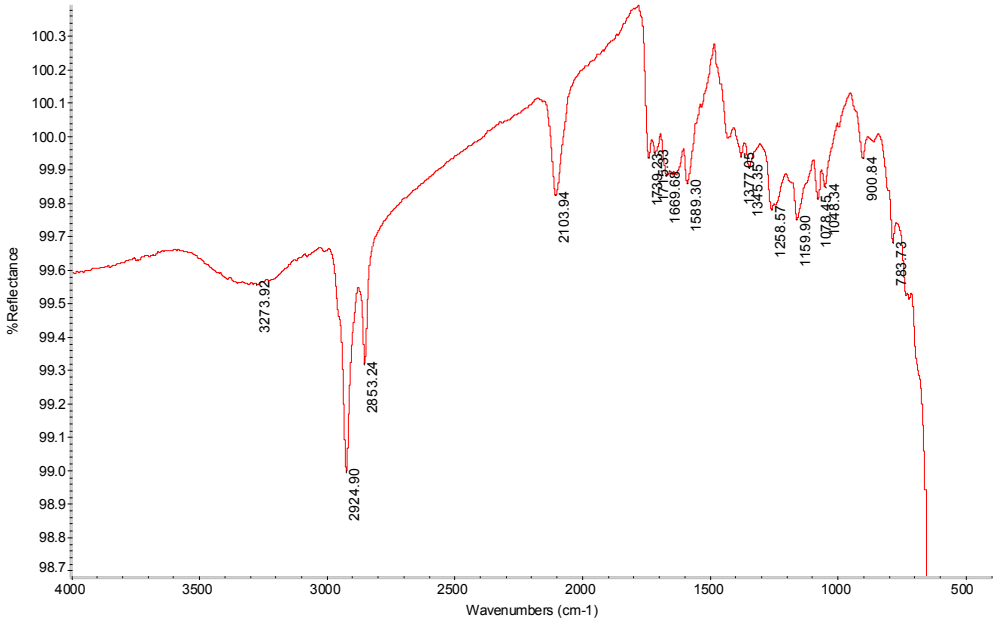

Figure 34. The grazing angle IR spectrum of SAM + Cu(II) ions + bipyridyl linker + Cu(II) ions.

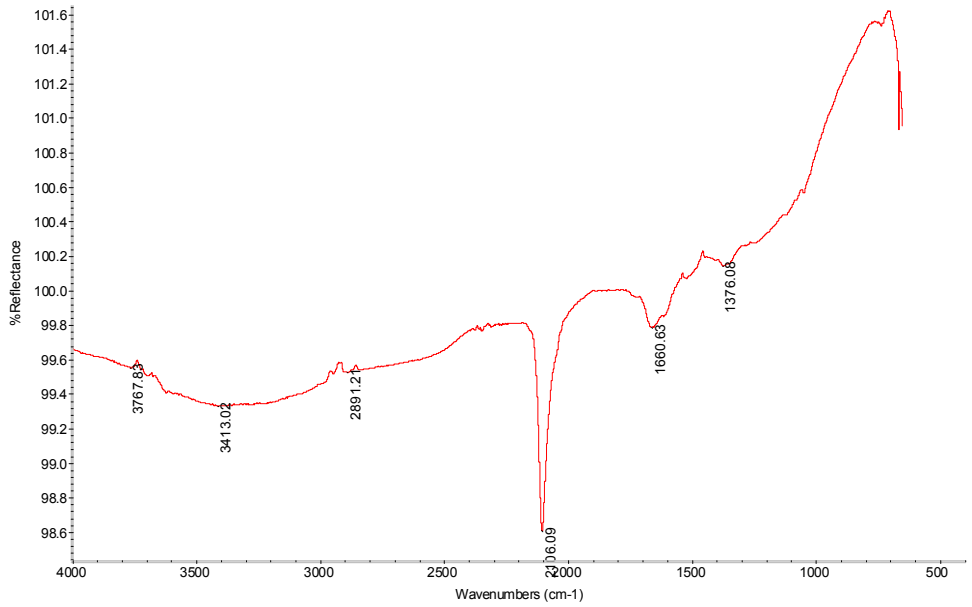

Figure 35. The grazing angle IR spectrum of SAM + Cu(II) ions + bipyridyl linker + Cu(II) ions + pyrene substituted cap.

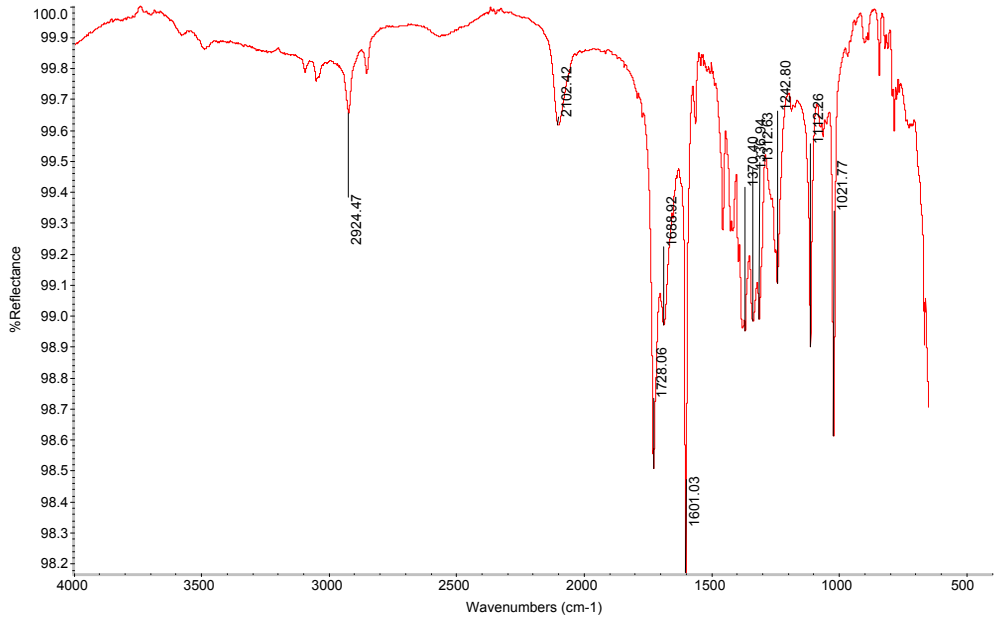

Impedance Measurements.

Figure 36. The impedance plot of a monolayer of pyridine decanethiol. The blue line represents a model circuit. The red dotted line represents experimental data.

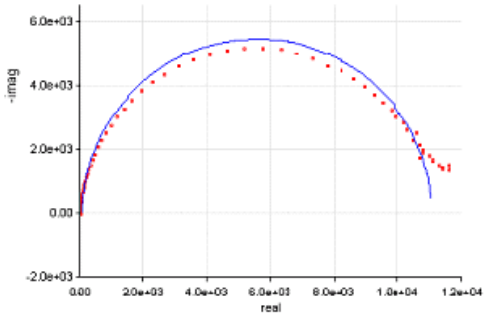

Figure 37. The impedance plot of a monolayer of pyridine decanethiol capped with Cu(II) ions. The blue line represents a model circuit. The red dotted line represents experimental data.

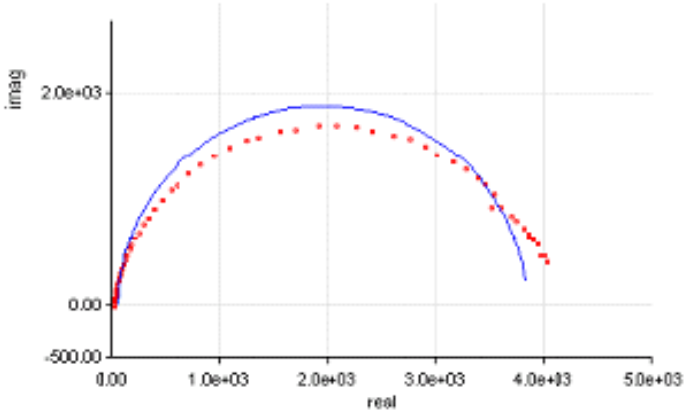

Figure 38. The impedance plot of a monolayer of pyridine decanethiol capped with Cu(II) ions and then with a pyrene substituted chelidamic acid moiety. The blue line represents a model circuit. The red dotted line represents experimental data.

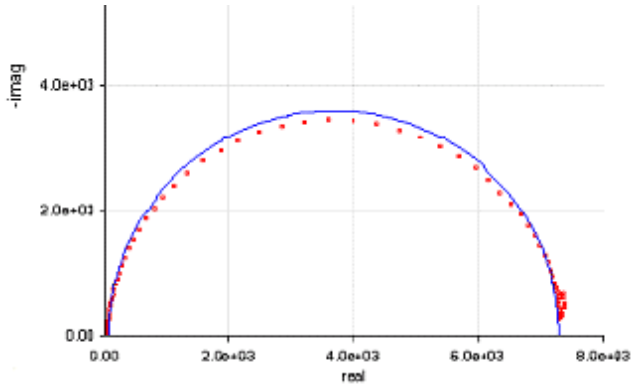

Table 9. Impedance measurements for the systems studied. The model circuit is displayed in Figure 11 .

Sample	R_{sol} (ohms)	R_{SAM} (ohms)	C_{dl} (μF)
Gold	37.4	*	37.4
Dodecanethiol	37.7	9040	2.29
SAM **VII**	37.7	11714	3.02
VIII			
Pyr-dt	34.1	7865	4.84
Cu-Pyr-dt	33.7	2138	16.1
Py-Cu-Pyrdt	39.2	6962	6.46
IX			
Pyr-dt	34.1	7865	4.84
Cu-Pyr-dt	33.7	2138	16.1
By-Cu-Pyrdt	37.7	6293	9.07
Cu-By-Cu-Pyr-dt	38.1	5884	9.37
Py-Cu-By-Cu-Pyr- dt	30.7	5468	9.79

Capacitance values in the range of 2 -10 μF are consistent with ordered monolayers with relatively few defects.[25,35,36]

C. Multilayer Thin Films as Photoswitchable Surfaces.

Contact angle results were presented in the main text.

Cyclic Voltammetry.

Figure 39. Cyclic votammograms obtained for bare gold, pyridine decane thiol on gold, and Cu/pyridine decanthiol on gold.

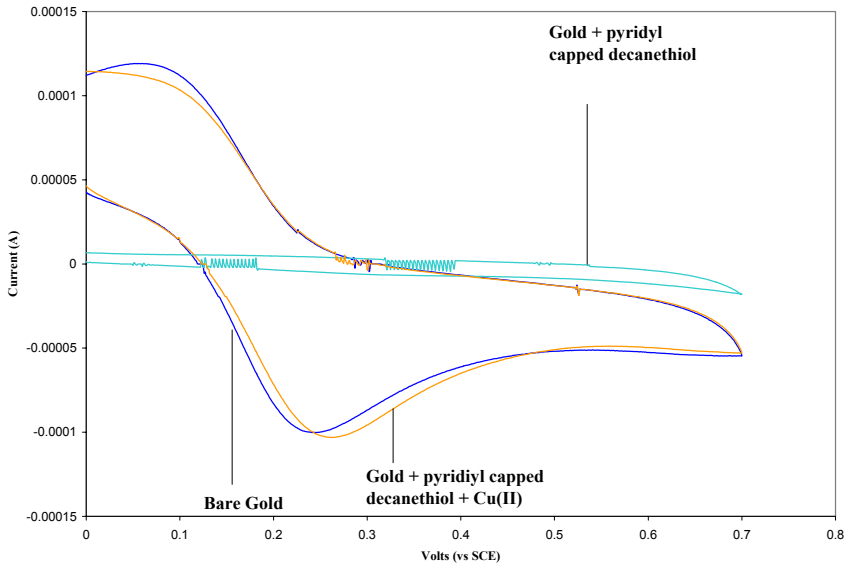

Figure 40. Cyclic Voltammagrams of Cu/pyridine decanethiol on gold, film **X**, film **XI**, and film **X** irradiated.

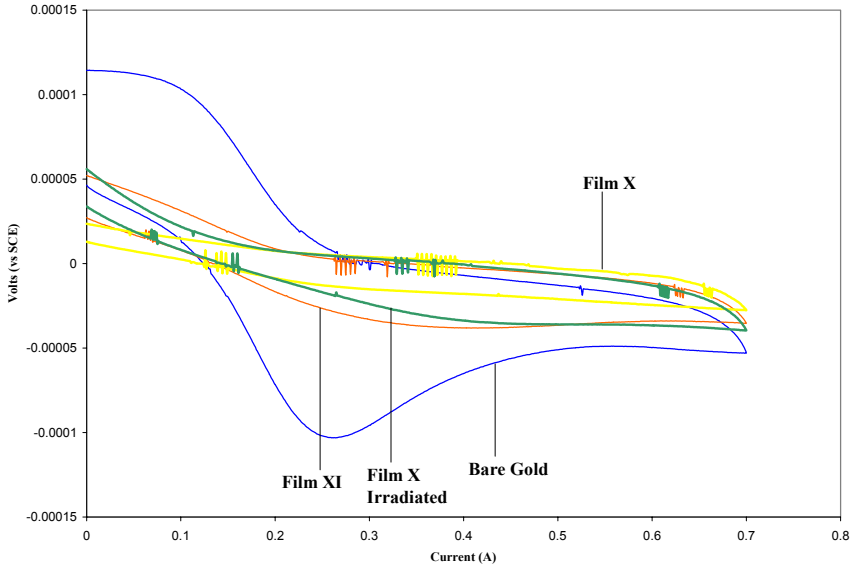

*Note that upon irradiation, the CV curve of film **X** resembles that of film **XI**.*

IR Measurements

The IR spectra, and absorbance assignments for the constituents in films **X** and **XI** have been described previously. Therefore, we will focus on the spectra of films **X**, **XI**, and irradiated **X** exclusively. The bands of interest for comparing these systems occur at 1511, 1313, 1303, 1253, and 1186 cm^{-1}.

Figure 41. IR spectra of film **X** vs. film **XI**.

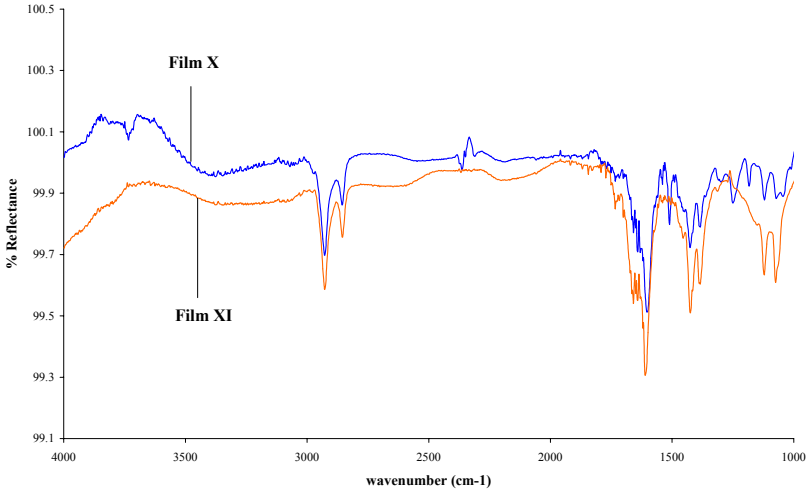

Figure 42. IR spectra of film **X** vs. film **XI** from 1650-1000 cm^{-1}.

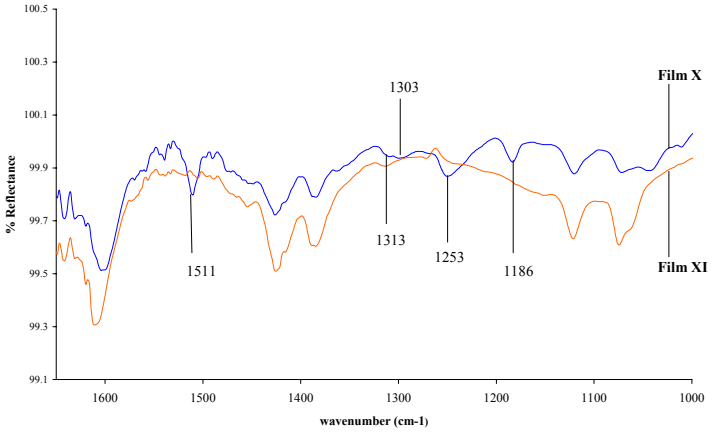

Figure 43. IR spectra of films **X**, **XI**, and **X** irradiated.

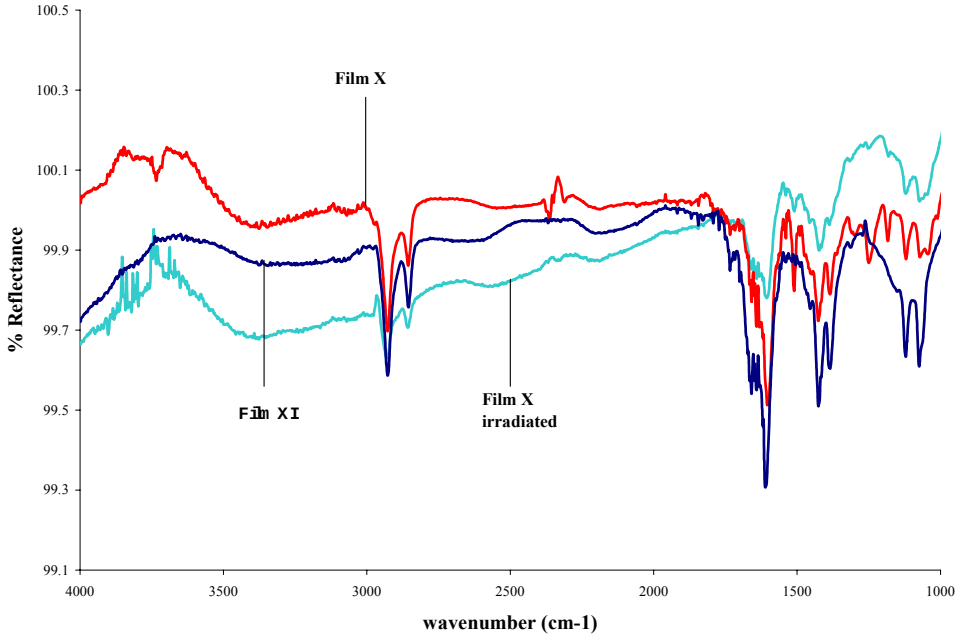

Figure 44. IR spectra of films **X**, **XI**, and **X** irradiated from 1600-1000 cm^{-1}.

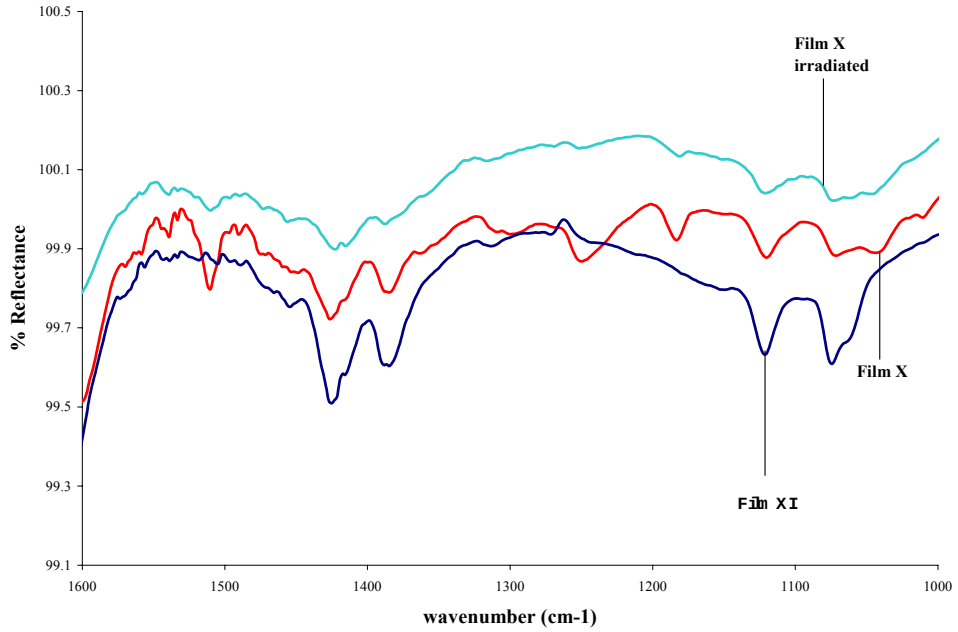

Figure 45. IR spectra of film **II** with and without irradiation in chloroform.

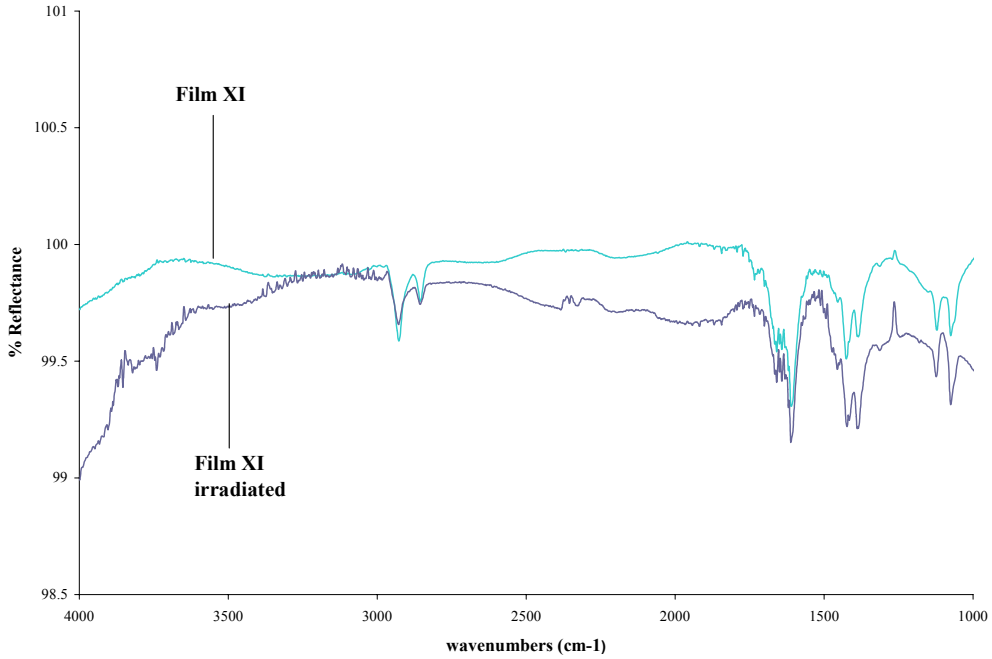

Figure 46. IR spectra of film **II** with and without irradiation in chloroform from 1650 – 1000 cm^{-1}.

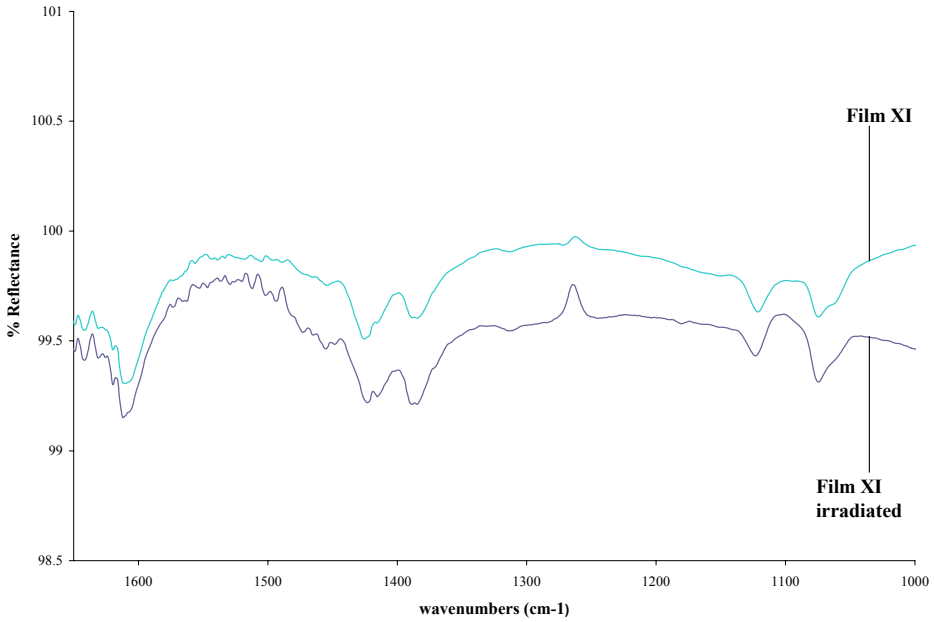

Figure 47. IR spectra of film **I** irradiated in a variety of solvents from 1650 – 1000 cm^{-1}.

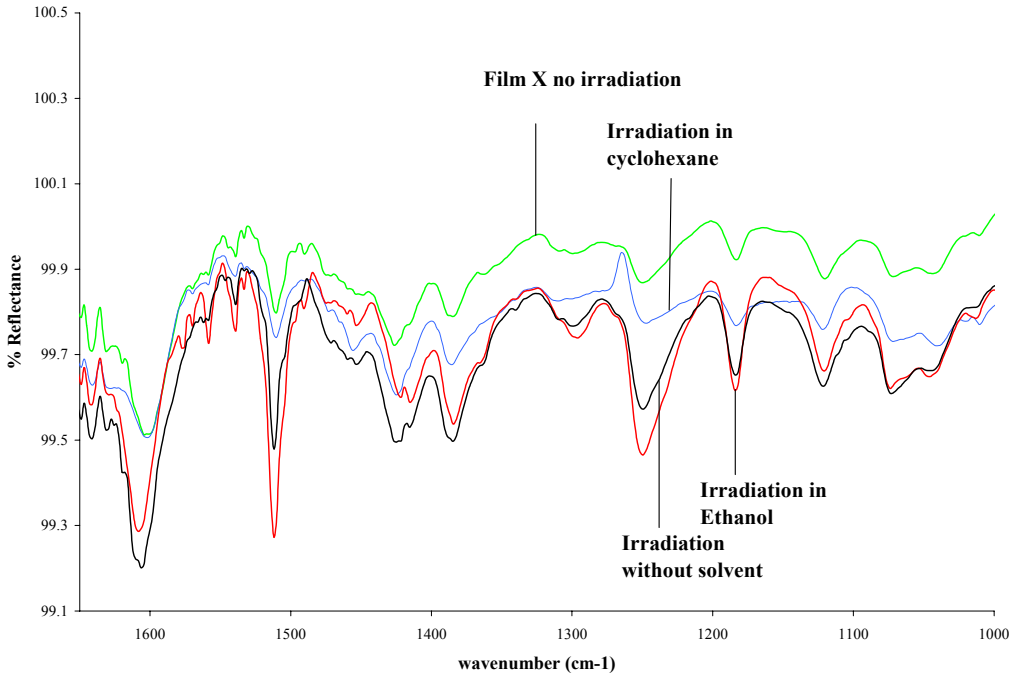

Impedance Measurements.

Table 10. Impedance values for the systems studied.

Sample	R_{sol} (ohms)	R_{SAM} (ohms)	C_{dl} (μF)
Pyridine decanethiol	146.8	12995.0	8.44
Pyridine decanthiol/Cu	79.7	6551.3	16.96
Film **X**	154.1	11076.0	10.13
Film **XI**	155.4	8742.7	13.70
Film **X** (irradiated)	135.9	7825.3	14.48

B. PYRENE CONTAINING CYCLIC PEPTIDE NANOTUBES

1. Background

As discussed previously, molecules that are able to self-assemble into predictable architectures are of considerable interest to the scientific community. The interest behind self-assembly is driven by the desire to create molecules that can spontaneously assemble into devices thereby eliminating the need for microfabrication, photolithography, and other top-down approaches.[77] Particular attention has been paid to systems that can predictably form nano-tubular or porous architectures. Such systems have potential applicability in areas including inclusion chemistry,[78] catalysis,[79] transmembrane channel transport,[80,81] and optical and electronic device fabrication.[82,83,84]

A variety of nano-constructs (e.g. carbon[85] and boron nitride nanotubes[86]) that facilitate energy or charge transfer have been reported and have been suggested as molecular scale electronic or photonic wires (Figure 48).

Figure 48. Computer representation of a single walled carbon nanotube. Boron Nitride nanotubes are structurally similar.

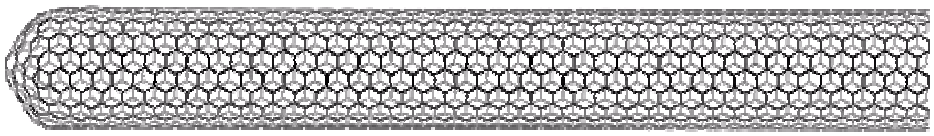

While these structures exhibit interesting properties, they require harsh synthetic conditions that often produce a low yield of the desired material, especially after the purification steps required.

Due to the problematic preparation of these tubular structures, past efforts have been focused in part on using biologically-inspired structures. Nature has already designed systems that are capable of transferring charge over long distances, similar to that observed in carbon and boron nitride nanotubes. DNA has been shown to perform this function, with charge conduction through the core of its double helix.[87,88,89,90] (Figure 49)

Figure 49. A view of the stacked heterocyclic base pairs present at DNA's core.

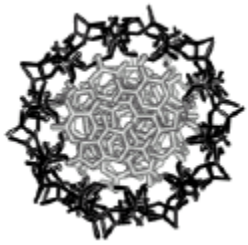

The observed electron transfer behavior of DNA has led to the suggestion that stacked aryl groups can provide a conduit for long range charge or energy transfer. Based on this suggestion, we became interested in constructing a self-assembling systems that promoted arene stacking. Further, we believe that the cyclic peptide architecture, through synthetic manipulation, can provide a scaffold for the assembly of stacked aromatic groups, similar to that which is observed in DNA's core.(Figure 50)

To this end, we have designed a series of cyclic peptides that are substituted with pyrene chromophores and that self-assemble into nanotubular structures. In the following sections we provide background on the known literature for cyclic peptide nanotubes, the phenomenon of long range charge conduction in ordered, stacked π-systems, and the photophysical behavior of pyrene. This information is provided as it serves as the basis for the work undertaken. We will then discuss our attempts at constructing pyrene substituted cyclic peptide nanotubes as conduits for long range electronic conduction.

(i) Peptide Nanotube Design Principles

Tubular structures based on peptide and protein constituents are well known, and are observed in a variety of natural systems. Both natural and synthetic polypeptides consisting of alternating D- and L-amino acids have been shown to adopt tubular structures when placed in membranes. Based on this known work, De Santis *et al.* first suggested that cylindrical tubular structures based on cyclic peptides could be formed.[91] However, early attempts to demonstrate this behavior proved to be unsuccessful because they did not take into account a variety of factors, besides a cyclic geometry, that need to be satisfied in order to undergo tube formation, including ring size and amino acid selection.

Ghadiri reported the first synthetic cyclic peptide capable of adopting a tubular secondary structure in 1993.[92] His work provided a descriptive set of design requirements that promote nanotube formation. It was observed that cyclic peptide structures comprised of an even number of alternating D- and L-amino acid residues minimized non-bonded intramolecular side chain interactions. This allowed the cyclic peptide monomer to adopt a flat plate-shaped conformation wherein all amide functionalities lie normal to the surface of the ring. Moreover, this allowed for all side chains to lie in the plane of the monomer ring, pointing outwards from the center. In this conformation, and only in this conformation, hydrogen bonding sites are arranged both above and below the plane of the monomer allowing cyclic peptides to spontaneously assemble (Figure 50).

Figure 50. The cyclic peptide architecture and assembly process. The R groups present "stack" during the assembly process.

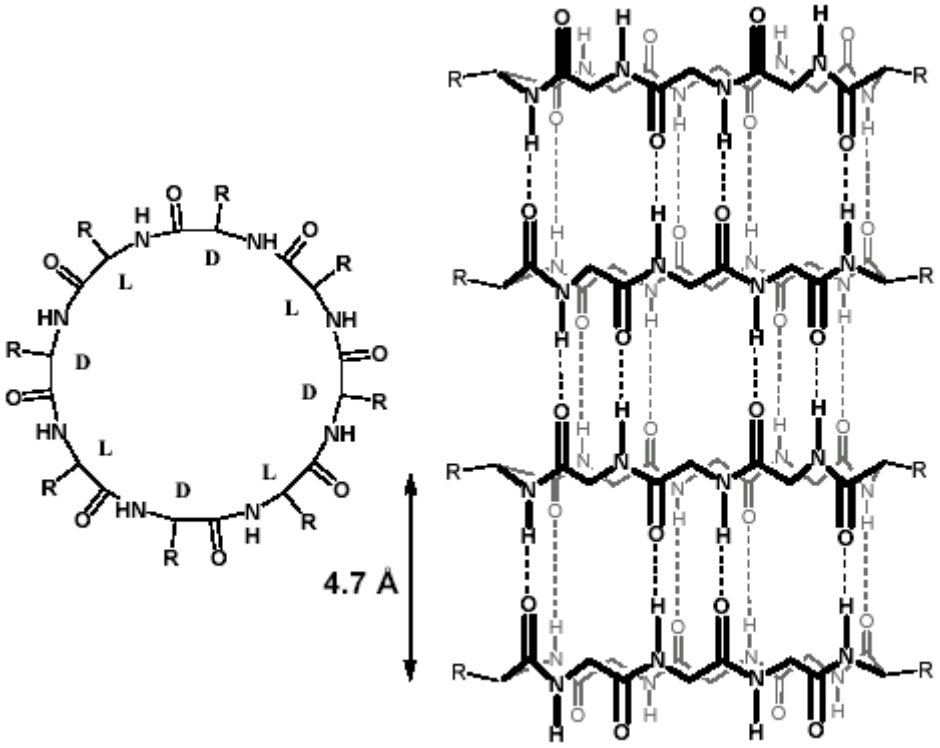

Ring size was also found to be a determining factor in cyclic peptide self-assembly, as it determines the stability of the monomer its flat conformation.[93] The plate-like conformation of cyclic peptides containing 6 or less amino acids possesses high ring strain. As a result, this conformation is less likely to occur, making spontaneous self-assembly difficult. Ghadiri has shown that the cyclic peptide cyclo[-D-^{Me}NAla-L-Phe-]$_4$ readily assembles into peptide dimers, while the corresponding six membered analogue, cyclo[-D-^{Me}NAla-L-Phe-]$_3$ does not.[93] Sun, *et al.*, have shown that tubular ensembles can be formed from cyclo[-D-Leu-L-^{Me}NAla-]$_3$, yet have also shown that cyclo[-L-Val-D-Leu-] and cyclo [-L-Phe-D-Phe-]$_3$ do not.[94] Based on this information, it appears that aggregation of cyclic hexapeptides cannot be regarded as a general trend, but rather as

something that occurs for very specific peptide sequences in the presence of the appropriate solvent and crystallization conditions.

Cyclic peptides containing more than eight amino acid residues have also been studied. While not hindered by ring strain, these systems possess a high degree of conformational freedom and numerous low-energy structures other than the plate structure necessary for assembly of nanotubes. Ghadiri and co-workers have successfully assembled nanotubes from cyclic peptides containing ten[95] and twelve[96] amino acid residues. However, formation of tubes from these larger cyclic peptides is highly residue-dependent, and occurs under very specific conditions. Based on the arguments of ring-strain and conformational freedom, cyclic octapeptides appear to be the most suitable for peptide nanotube formation and this has been demonstrated by experimental and computational studies.[97]

Self-assembly of cyclic peptides can lead to either parallel or anti-parallel stacking arrangements of the cyclic peptide rings (Figure 51).[93]

Figure 51. Anti-parallel (left) and parallel (right) stacking arrangements of cyclic peptide nanotubes.

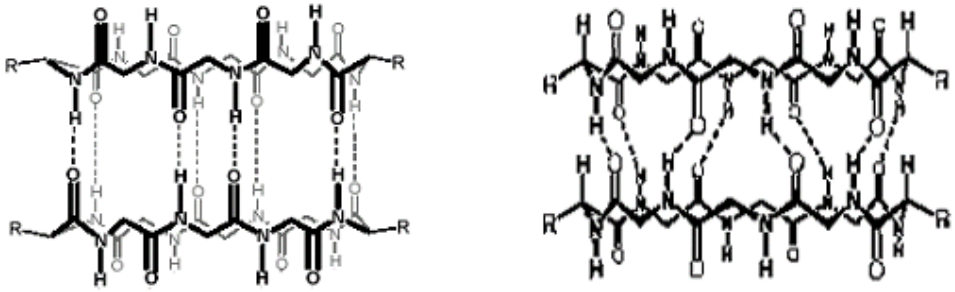

Here, parallel and anti-parallel are terms used to describe how the cyclic peptide backbones align with one another. In the anti-parallel arrangement, the cyclic peptide is aligned such that eight linear hydrogen bonds are formed from either face of the cyclic peptide. However, in a parallel alignment, the hydrogen bonds are no longer linear, and are therefore slightly elongated and, as a result, weaker (Figure 51). This causes the anti-parallel configuration to be exclusively favored over the parallel configuration, with a difference in free energy of 0.8 kCal/mole per bonded pair of cyclic peptide monomer units.[98] NMR and X-Ray Crystallography data have confirmed that it is hydrogen bonding, and not side chain interactions, that accounts for the difference in stability between anti-parallel and parallel arrangements.[98]

Cyclic peptide assembly can also be controlled by the choice of amino acids. As has been previously demonstrated, cyclic peptide formation is triggered by the formation of hydrogen bonds above and below the plane of the monomer ring. By selecting amino acids that block hydrogen bonding from occurring at either face, dimers, or monomers can be selectively formed. For example, in order to accurately measure the interactions between layers of cyclic peptides, Ghadiri constructed cyclo[-L-Phe-D-^{Me}NAla-]$_4$.[99] By incorporating four N-methyl alanine groups, hydrogen bonding was selectively prevented from one side of the ring, limiting the assembly strictly to dimers. By exclusively using N-methylated amino acids, monomers can also be constructed. An alternative for monomer construction is to alternate D- or L- amino acids with achiral disubstituted α-amino acids. The disubstitution, such as in α-aminoisobutyric acid, causes sufficient steric hindrance to prevent hydrogen bonding.

Once formed, peptide nanotubes exhibit remarkable mechanical and chemical stability, remaining intact under centrifugation, vortex mixing, and sonication. In addition, they can survive boiling water, as well as highly acidic (pH 1), and highly basic (pH 11) conditions.[100] Dissolution of cyclic peptides into monomeric subunits rarely occurs even in highly polar solvents such as DMSO and DMF.[41] Typically, the nanotubes can only be disassembled by exposure to extreme acids (i.e. neat TFA), which results in complete protonation of the cyclic peptide backbone.

Based on the design principles set forth in this section, it is reasonable to assume that we can construct cyclic peptides that will predictably assemble into peptide nanotubes. We can also make reasonable predictions as to how the peptide side chains will align based on the favored anti-parallel stacking arrangement. Finally, the properties of cyclic peptide nanotubes can be compared to those of cyclic peptide monomers by synthetically controlling whether or not the systems made will assemble.

(ii) Long Range Charge and Energy Transfer in Double Helical DNA

For the past 10 years, numerous research groups have demonstrated that DNA is capable of acting as a conduit for long range charge transfer[87.,101,102] The charge is believed to flow through the inner core of the DNA, which is comprised of a stacked array of aromatic, heterocyclic base pairs.

Many experiments have been conducted to probe charge transfer within DNA, the earliest of which involved a simple measure of charge flow through DNA fibers. These early results offered mixed opinions as to the ability of DNA to transport charge. Recently, however, Barton *et al*. showed that DNA systems of varying lengths with a photooxidizable group, $[Rh(phi)_2bpy']^{3+}$ (phi = phenanthrene quinine diimine; bpy' = 4'-methylbipyridine-4-butyricacid), tethered to the terminus of the strand, undergo long range charge transfer (Figure 52).[87]

Figure 52.[87] The DNA system used to test for long range charge-transfer. A chromophore (red) is excited at one end, causing oxidative damage of the guanine pairs (yellow).

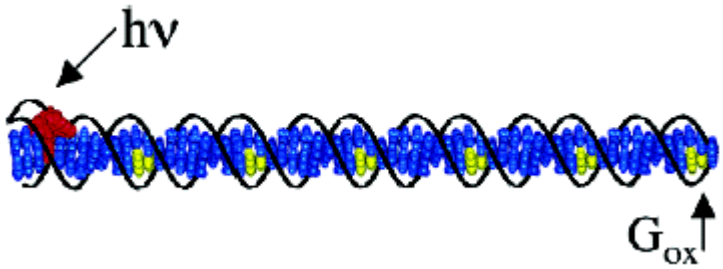

In this experiment, DNA strands were constructed with guanine doublets at specific sites along the DNA helix. Upon photooxidation of the rhodium complex, the guanine base pairs act as electron donors, and become oxidatively damaged. The distance between the damaged guanine units and the photooxidant gives an indication of the charge-transfer distance. This type of experiment has effectively shown that DNA base pairs can undergo charge transfer interactions over distances ranging from 17 to 197 Å.[87]

While the occurrence of long range charge transfer within DNA has been proven, there are still arguments as to how the transfer takes place. Currently, there are two accepted theories of the mechanism of DNA charge transfer; tunneling and charge hopping theory (Figure 53).[103]

In the tunneling theory, sometimes referred to as a "super exchange" mechanism, the DNA orbitals are energetically higher than the donor and acceptor orbitals, and charge passes through them without ever directly occupying them. If this mechanism were predominant, the efficiency of charge transfer would be exponentially dependent upon the distance between charge donor and acceptor. In the charge hopping mechanism, the orbitals of the DNA bridge are thought to be energetically similar to those of the acceptor and donor. This mechanism, as opposed to the tunneling mechanism, would be less distance dependant as the hopping steps are very small increments. While the predominant transfer mechanism has not been experimentally determined, both theories assume that the long range transfer occurs through the core of DNA, via its aggregated π-stack Without having this stack of heterocyclic aromatics, no empty π orbitals are available, and both theories fail.

Figure 53.[103] Pictorial representations of long range transfer: (a) tunneling (super exchange) mechanism, and (b) "hopping" mechanism.

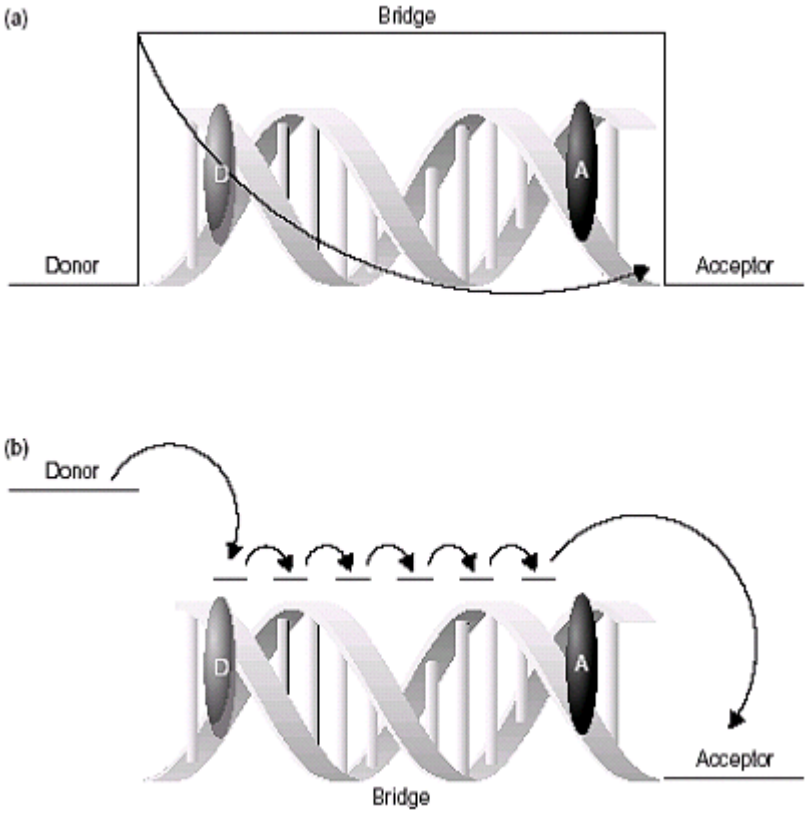

It is our belief that substituting a cyclic peptide at regular intervals with side chains containing aromatic groups will form an aggregated π stack similar to the one observed in DNA. Based on the work presented, it is reasonable to assume that such a system will be capable of long range charge transfer through the assembled π-stack.

(iii) The Photophysical Behavior of Pyrene

Pyrene, a flat disc shaped molecule, is composed of four fused benzene rings, and is known to aggregate with face to face π stacking interactions in its crystalline form.[104] The amount of pyrene aggregation can be conveniently measured in its fluorescence spectrum, as aggregated pyrene forms an emissive excimer. Excimer formation is of particular interest to our studies, as it has previously been shown to act as a probe for secondary structure.[105,106,107] Pyrene can serve then, as a conformational probe for cyclic peptide nanotube formation, as aggregated cyclic peptide monomers can allow for the stacking of pyrene. The amount to which this occurs can be measured by comparing monomer to excimer fluorescence. In addition, if stacking occurs, it is likely that the cyclic peptide system will conduct charge similar to that which is observed for DNA.

Complex formation between excited and ground state aromatic hydrocarbons in solution was first reported in 1955.[108] These complexes were called "excimers", a shortened notation for excited state dimers. Pyrene has long been known as a compound that readily undergoes excimer formation. In solution, excimer formation is a concentration dependent process, with observable formation beginning at a threshold concentration of roughly 10^{-5} M. The exact concentration at which excimer formation is initially observed is solvent dependent, with polar solvent leading to excimer formation at slightly lower concentrations. Excimer formation is evidenced in the fluorescence spectrum by a quenching of the monomer pyrene fluorescence, and a concomitant growth of a red-shifted, featureless emission band (Figure 54).

Figure 54.[109] Excimer formation with respect to pyrene concentration.

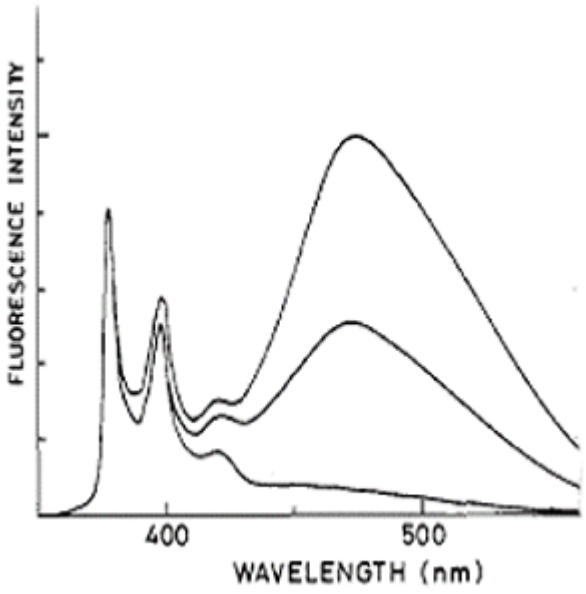

Excimer formation does not appear to lead to any permanent chemical change as the absorption and fluorescence spectra of oxygen-free pyrene solutions remain unchanged under prolonged irradiation.[110] The mechanism of pyrene excimer formation can be qualitatively explained by viewing the potential energy diagram in Figure 55.

Here, the energy of a pair of pyrene molecules depends directly upon their internuclear separation. In the ground state, the energy of the pair is constant until an abrupt increase at about 4 Å corresponding to repulsion between the π clouds of the two molecules. Excitation of one of the pyrene molecules leads to an electron deficiency of its π bonding orbitals, which can be stabilized by forming a face to face complex with the ground state pyrene at a separation of ~3.5 Å, shown in the diagram as a valley in the potential energy

surface. Emission from this state results in a structureless band, as the ground state complex is dissociative.

Figure 55.[111] Energy diagram of excimer formation.

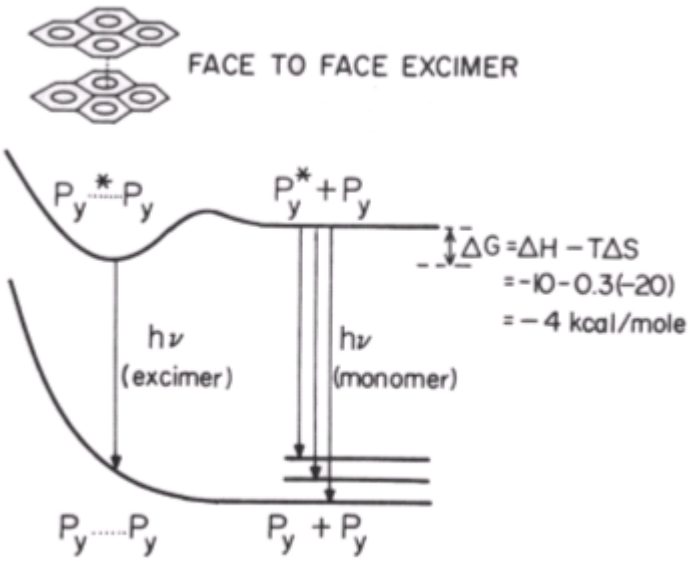

As excimer formation is dependent upon both diffusion and internuclear distance, we believe that incorporation of pyrene side-chains into cyclic peptide nanotubes, will promote concentration independent excimer fluorescence. Observation of such fluorescence will be indicative of assembly, and will lead to the formation of a delocalized π-stack, which can undergo long range transfer

Short range charge and energy transfer has been shown to occur in systems with pyrene molecules.[112,113,114] To date, there are few reports of long range charge transfer through pyrene systems, however, long range energy transfer in pyrene systems has been

reported. [115,116] Crystalline pyrene can undergo exciton formation and exciton hoping within the crystal, based on an analogous mechanism to the charge-hopping mechanism described for DNA. As cyclic peptides substituted with pyrene will present a quasi-crystalline environment, we believe these systems will be able to undergo long range energy transfer. Additionally, as the system is very similar to DNA's core, charge transfer should also be possible.

2. Results and Discussion

Two cyclic peptides, **CP1** and **CP2** (Figure 56) were constructed by solid phase peptide synthesis using an FMoc strategy.

Figure 56. The structures of **CP1** and **CP2**.

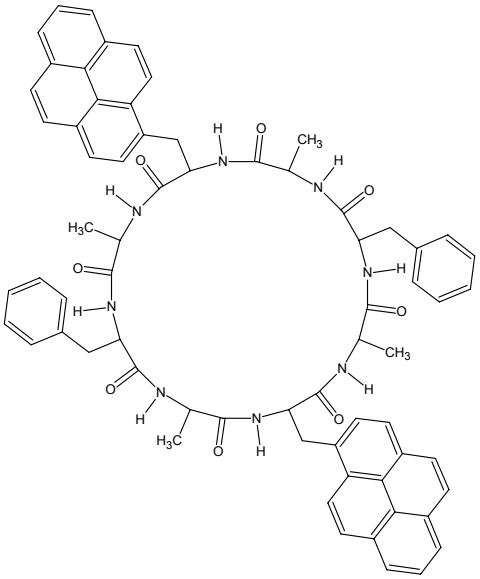

CP1

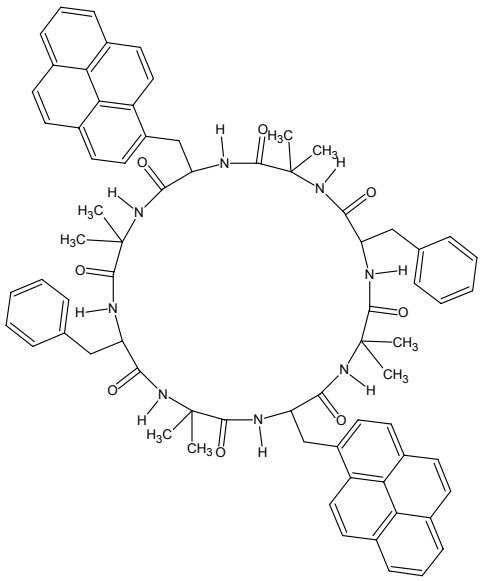

CP2

CP1, cyclo[-D-Ala-L-Pya-D-Ala-L-Phe-]$_2$, is based on analogous literature structures that are known to readily assemble into peptide nanotubes. In addition, molecular modeling calculations suggested that aggregation would occur in similar systems (Figure 57). Molecular modeling was performed using the MOE platform, with the peptide nanotube solvated by acetonitrile. An anti-parallel stacking arrangement was assumed when constructing peptide nanotubes, and energy minimization was performed using the AMBER forcefield. Dynamics calculations were also performed to study the tube stability. Dissociation of the tube did not occur over 1000 heating cycles from 298-500

K, using 1 second heating and cooling cycles. From this modeling, an interchromophore separation for pyrene molecules on adjacent cyclic peptides was calculated to be 4.68 Å.

Figure 57. Computational models of cyclo[-D-Ala-L-Glu-D-Ala-L-Pya-]$_2$. Modeling was performed using the MOE platform with an AMBER force field. The picture on the left shows the formed tube from the side, while the picture on the right looks down the core axis of the tube.

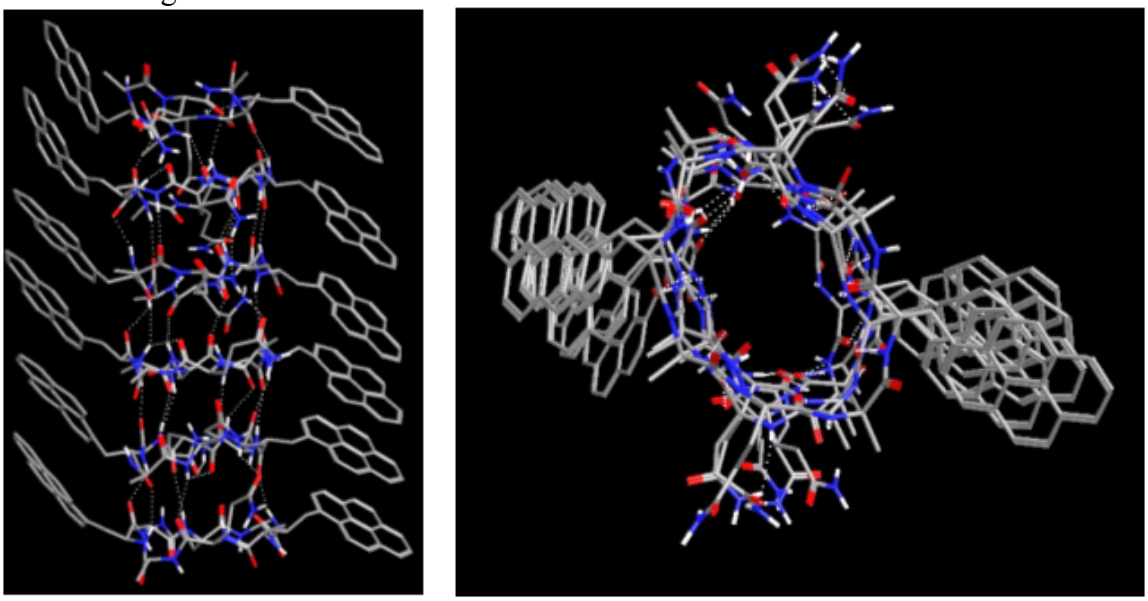

CP2, cyclo[-Aib-L-Pya-Aib-L-Phe-]$_2$, is not expected to form nanotubes, as incorporation of aminoisobutyric acid residues (Aib) has been shown to prevent aggregation due to the steric disruption of hydrogen bonding. Since the difference between these two systems is that **CP1** is expected to self-assemble into nanotubes while **CP2** is not, it was our expectation that **CP1** would exhibit excimer fluorescence but that the **CP2** fluorescence spectra would show only monomer fluorescence. If this is the case, it is likely that this architecture can be used to construct systems that undergo long range energy and charge transfer, similar to that which has been observed in DNA.

Fluorescence spectra were collected in a 1 cm^2 spectrasil quartz cuvette. Sample degassing with nitrogen showed no impact on the spectra obtained, and the spectra presented are for oxygen containing solutions. We have used as model systems the open chain (non-cyclized) linear peptides **LP1** and **LP2**. (Here **LP1** is the open chain analog analogue of **CPI** and **LP2** is the linear analogue of **CP2**.) The emission spectra of these peptides at varying concentrations in DMF are shown in Figures 58 and 59.

Figure 58. Normalized fluorescence spectra of **LP1** (open chain analogue of **CP1**). Solution concentrations (M) are given in the legend on the right

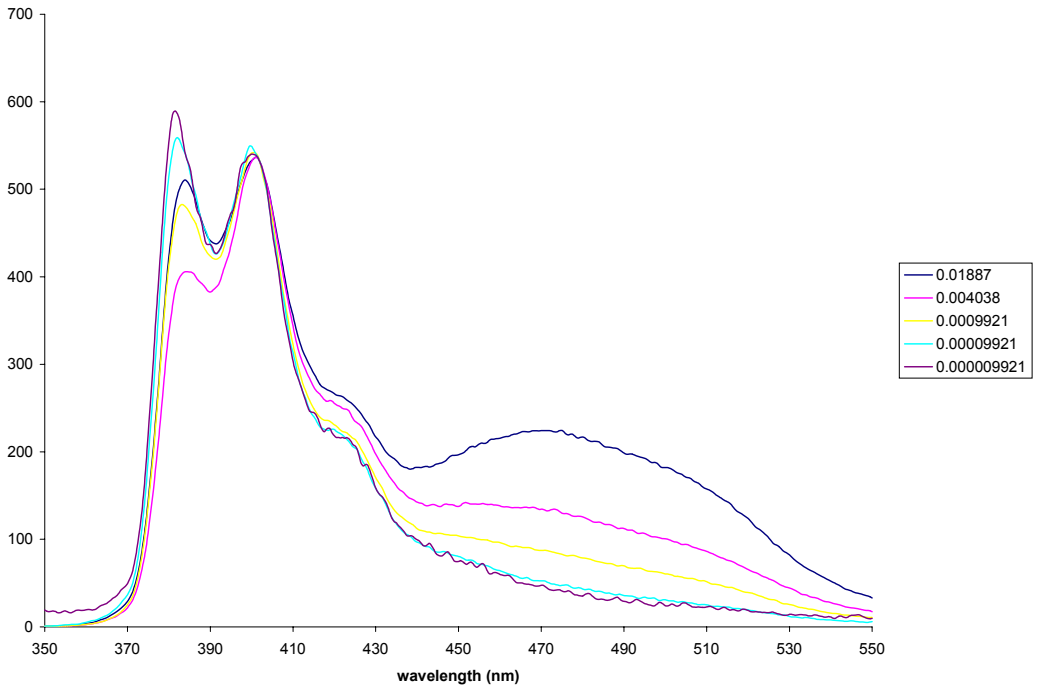

Figure 59. Normalized fluorescence spectra of **LP2** (open chain analogue of **CP2**). Solution concentrations (M) are given in the legend on the right.

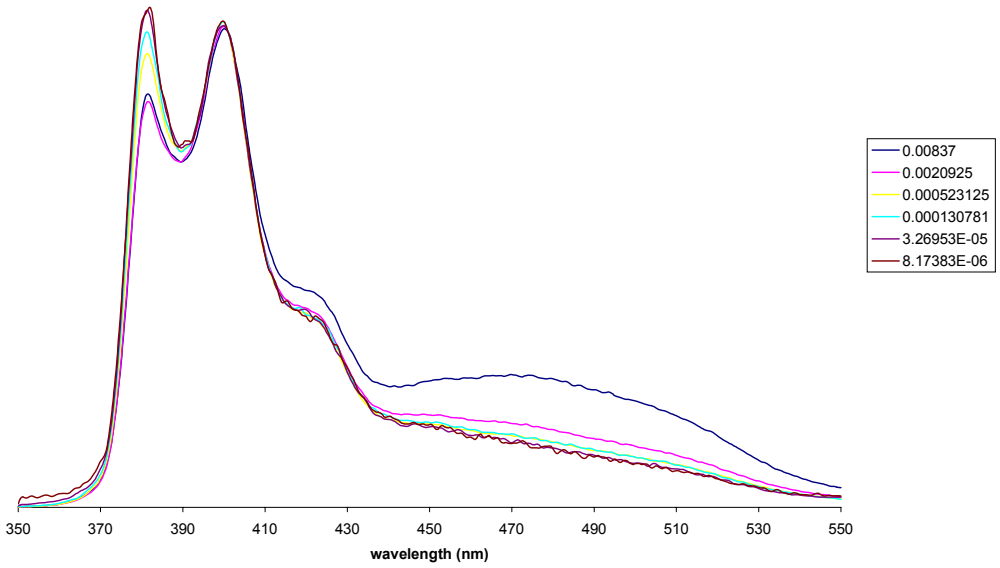

It is clear from these two sets of spectra that significant amounts of excimer are only formed for the linear peptides at millimolar concentrations.

Figures 61 and 61 display the emission spectra for solutions of **CP1** and **CP2** in DMF at various concentrations.

Figure 60. Normalized **CP1** fluorescence in DMF. Solution concentrations (M) are given in the legend on the right.

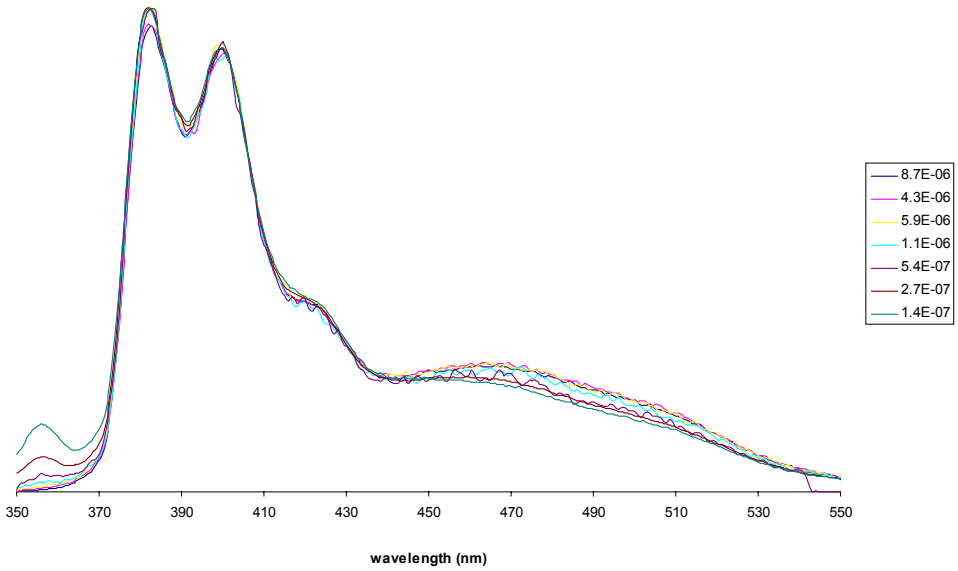

Figure 61. Excimer formation of **CP2** with respect to concentration. Concentrations (M) are given in the legend on the right.

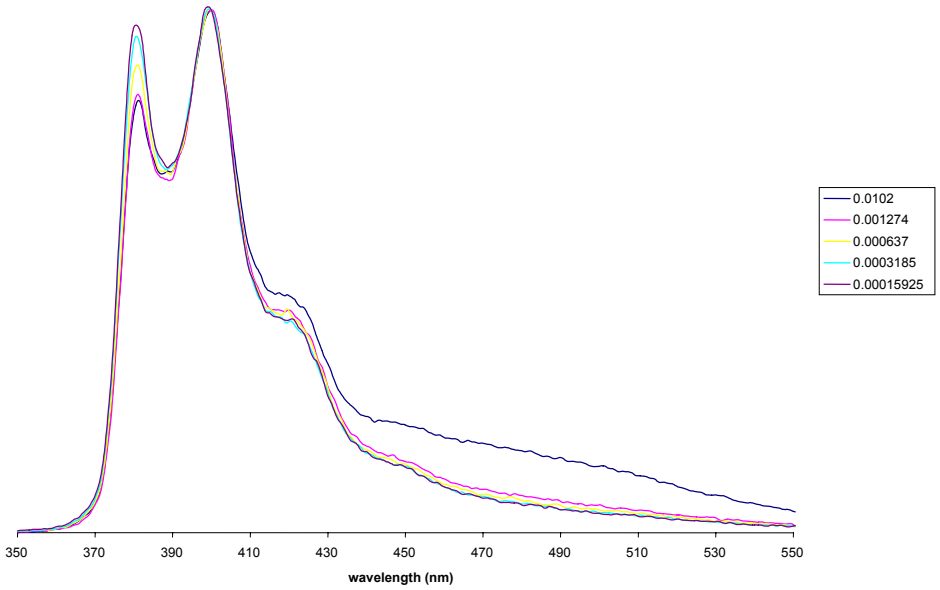

or **CP2**, there is a small amount of excimer emission at high concentration, although not as intense as for **LP1** or **LP2** at comparable concentrations. This behavior may be due to

the lower solubility of the linear peptide salt. For **CP1** however, excimer formation is completely independent of concentration and occurs at concentrations as low as 10^{-7} M, lending support to the suggestion that **CP1** assembles into tubes with pyrene stacking. In comparison to its linear analogue, more excimer was observed at a 10^{-7} M concentrations of **CP1** than at 10^{-3} M concentrations of **LP1**

The solvent DMF was chosen for these initial fluorescence studies, since all linear and cyclic peptides are soluble in it. Fluorescence studies were also performed in acetonitrile, although due to solubility problems, **LP1** and **LP2** were not measured (both the linear and cyclic pyrene-containing peptides were found to be insoluble in alcohols, halogenated solvents, and water). Figures 62 and 63 show the fluorescence spectra of **CP1** and **CP2** in acetonitrile.

Figure 62. Normalized fluorescence spectra of **CP1** in acetonitrile. Solution concentrations (M) are shown in the legend on the right.

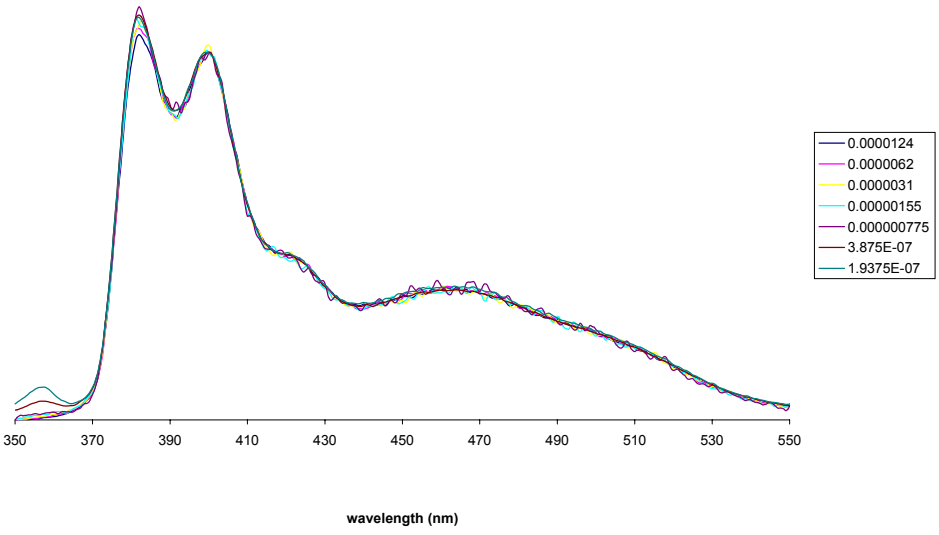

Figure 63. Fluorescence spectra of **CP2** in acetonitrile. Solution concentrations (M) are given in the legend on the right.

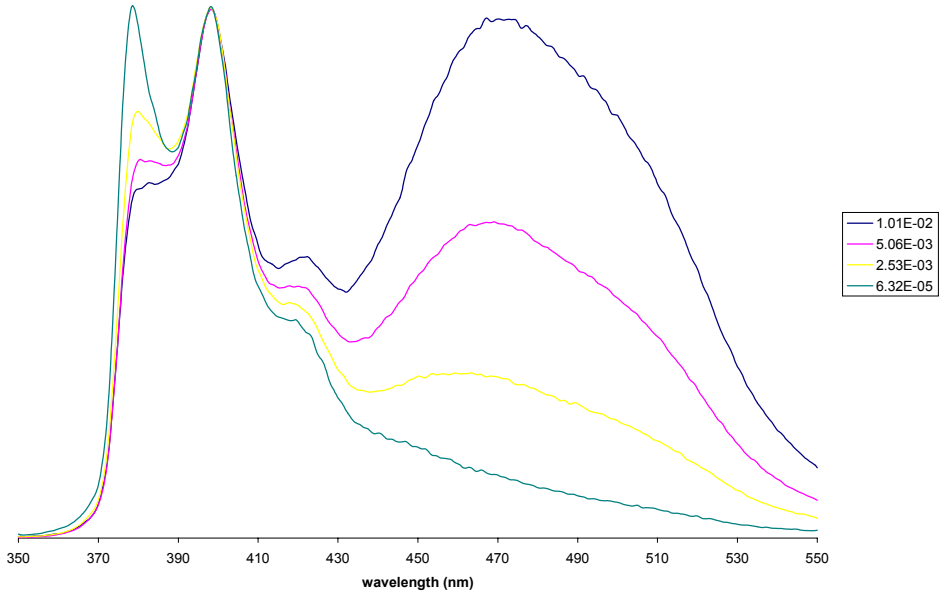

The results of changing solvent systems from DMF to acetonitrile serve to further accentuate the different behaviors of **CP1** and **CP2**. **CP2** again exhibits typical concentration dependence indicative of a diffusional interaction as the mechanism responsible for excimer formation. The more enhanced excimer formation observed in acetonitrile is likely due to the more polar nature of acetonitrile, which promotes excimer formation. However, **CP1** again shows no concentration dependence; the excimer was observable at concentrations as low as 2×10^{-7} M.

These spectra again support the conclusion that in **CP1** nanotube formation occurs and facilitates pyrene stacking. However, due to the structure of **CP2** it is not expected to form tubes, and there is no pyrene stacking other than that which is expected from a typical diffusional interaction.

It is important to note that despite the concentration independent excimer formation, indicating pre-association of cyclic peptide into nanotubes in CP1, a considerable amount of monomer emission is still observed. This is a different situation than for pyrene crystals in which only excimer emission is observed (Figure 64).

Figure 64. Fluorescence spectrum of crystalline pyrene.

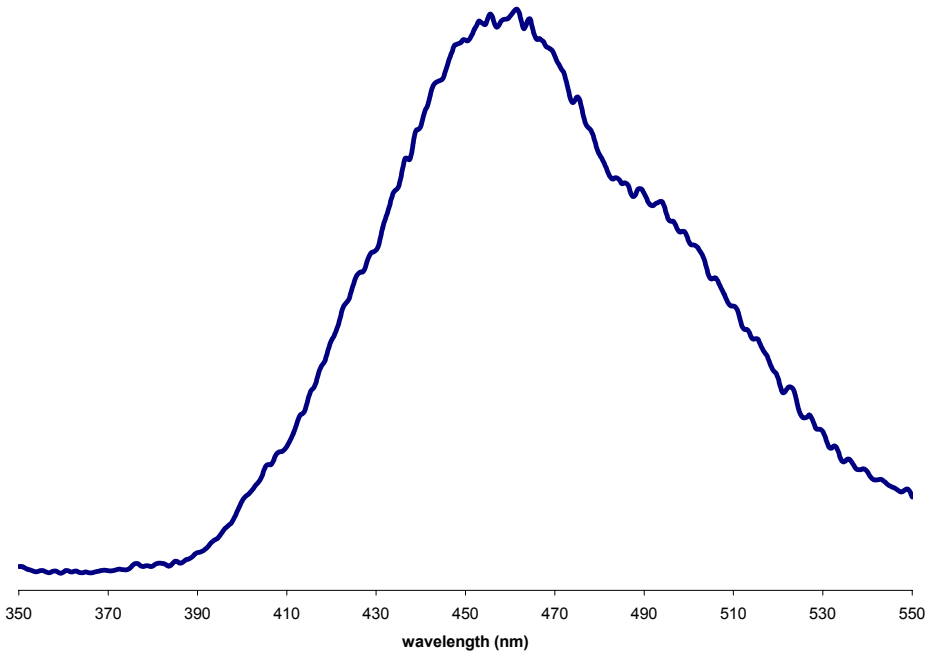

There are several potential explanations for this behavior. First, in nanotubes assembled from **CP1**, pyrene groups in adjacent peptide monomers can potentially take up eclipsed or staggered positions as shown in Figure 65.

Eclipsed positions will potentially lead to excimer formation. However, if the selection between eclipsed and staggered is random, then a mixture of monomer and excimer

emission would be expected. It is unclear at this time whether the pi-pi interaction of the pyrene groups in an eclipsed arrangement would be sufficient to bias nanotube formation into a predominantly eclipsed assembly. However, given the relative magnitudes of the interactions (H-bonding vs. π-π stacking) it is likely that a random assembly will be favored. Ghadiri has studied dimeric cyclic peptides systems where side chains can assemble in either an eclipsed or staggered arrangement and showed that side chain-side chain interactions are not sufficiently strong to favor one arrangement or the other. In fact, through 2D-NMR experiments, it was shown that regardless of the side chains employed, there is a statistical ratio of 1:1 of the staggered vs. eclipsed conformations formed. [98] (One caveat is that in none of Ghadiri's work were there large π-π interactions considered.)

Figure 65. The two possible antiparallel stacking arrangements for this system: pyrene groups eclipsed (left), staggered (right). For simplicity, all functionalities besides the side chains of interest have been omitted.

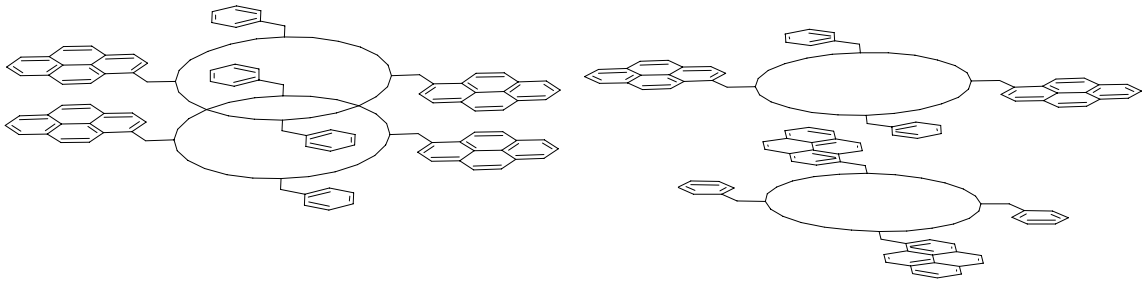

Alternatively, from modeling/dynamics studies (see above) the interchromophore pyrene distance in nanotubes formed from CP1 is ~ 4.7 Å. This is somewhat larger than the optimum inter pyrene distance for excimer formation (3.8 Å). Therefore, we envision a situation in which stacked pyrene units in a nanotube of **CP1** associate more closely with

one neighboring pyrene group in the stack than with its other neighbor in the stack, facilitated by vibrational motion of the pyrene groups. Such a situation would lead to a decrease in the efficiency of excimer formation, particularly when coupled with staggered conformations.

In conclusion, based on fluorescence results, there is some degree of preassociation of pyrene side chains in stacking cyclic peptides. We have offered a variety of possible reasons as to why excimer emission isn't exclusively observed. It's important note that these systems were designed such that even if assembly took place in a fashion where staggered conformations were formed, the pyrene units would still stack with phenyl rings, which would still lead to a delocalized π-cloud, and thus a system capable of long range charge transfer. Future work will focus on obtaining more detailed structural information on these peptides, including small angle neutron or x-ray data. In addition, we are still attempting to engineer an experiment that will allow us to accurately test charge flow through these cyclic peptide systems.

3. Materials and Methods

Spectra for all compounds as well as synthetic schemes are provided in Appendix A.

Materials. All materials were used as received from their respective companies. Unless otherwise noted, reagents and solvents were purchased from Sigma-Aldrich. Amino acids, peptide resins, and coupling reagents were purchased from Nova Biochem. All solid-phase coupling reactions were carried out in tech grade DMF purchased from Pharmco.

General Methods.

Photophysical Measurements. All fluorescence measurements were performed using a Perkin-Elmer LS-50B spectrophotometer, with the excitation and emission slit widths set to 5 nm. Absorption spectra were collected on a Shimadzu UV2100 spectrometer. All absorption and most fluorescence spectra were collected in 1 cm^2 spectrasil quartz fluorescence cuvettes. For highly concentrated samples of pyrene, fluorescence spectra were collected in a 2 mm narrow path length cell set at 45 degrees to the incident light, in order to avoid self-absorption by the sample.

Synthetic Procedures. NMR spectra were obtained in an Avance Bruker NMR spectrometer at 400 MHz for proton and 85 MHz for 13C. Mass Spectra were measured by the SynPep Corporation in Dublin, CA. Samples were ionized by electrospray ionization, using acetonitrile as a carrier solvent with ultra-high purity nitrogen as a

curtain gas. IR spectra were obtained using a Nexus FT-IR spectrometer equipped with either a transmission or ATR accessory, depending on the sample. Melting points were obtained on a Mel-Temp melting point apparatus and appear uncorrected.

A. Synthesis of N-fluorenylmethoxycarbonyl-L-1-pyrenyl alanine (Fmoc-Pya).[117,118,119]

(i) 1-(bromomethyl)pyrene.

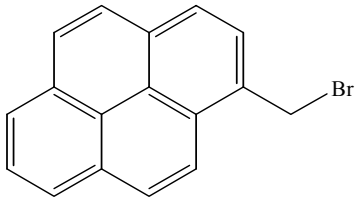

1-Pyrenemethanol (10 g, 43.1 mmol) was dissolved in 300 mL of benzene at 40º C. To this solution, 2.0 mL of phosphorous tribromide was added dropwise and the solution refluxed for 4 h. The mixture was allowed to return to room temperature, and was partitioned between 3:2 ethyl ether:water. The organic layer was rinsed 3 times with 50 mL portions of water, and then dried over anhydrous sodium sulfate. The solvent was removed under reduced pressure to yield 12.15 g of a yellow powder. Yield: 96%; R_f = 0.83 (CH_2Cl_2, normal phase), 0.95 (1:1 hexane:ethyl acetate, normal phase); mp 270 ºC (dec); ^{1}H-NMR ($CDCl_3$): δ 5.26 (s, 2H, CH_2), 7.98-8.85 (m, 9H, aromatic CH); ^{13}C-NMR: δ 32.65 (CH_2); 123.2-132.3 (aromatic C, pyrene).

(ii) Diethyl 2-(1-pyrenylmethyl)-2-acetamidomalonate.

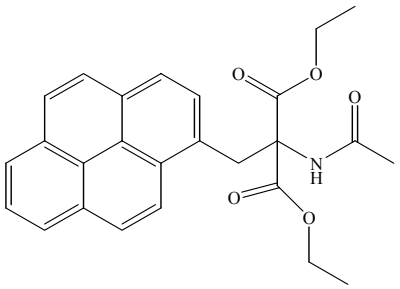

Diethyl acetamidomalonate (8.7 g, 40 mmol) and sodium hydride (1.2 g, 50 mmol) were placed in a two necked round bottom flask under nitrogen. The flask was placed in an ice bath, and 75 mL of anhydrous THF was introduced dropwise via syringe. The solution was allowed to stir for 5 min, and 2.5 mL of absolute ethanol was added to the flask to generate ethoxide. To this mixture, 11.8 g (40 mmol) of **(i)** dissolved in 200 mL of anhydrous THF was added, and the solution heated to reflux for 18 h. After reflux, the solvent was removed under reduced pressure, and the crude product partitioned between 200 mL of 1:1 dicloromethane:water in a separatory funnel. The organic fraction was washed 3 times with water, and dried over anhydrous sodium sulfate. The solvent was removed under reduced pressure to yield 14.32 g of pale yellow oil. Yield: 83%; Rf = 0.4 (4:1 EtOH:H_2O, reverse phase); ^{1}H-NMR ($CDCl_3$): δ 1.42 (t, 6H, CH_3), 1.95 (s, 3H, $COCH_3$); 3.75 (s, 2H, Py-CH_2); 4.35 (m, 4H, OCH_2); 6.42 (s, 1H, NH); 7.7-8.2 (m, 9H, pyrene); ^{13}C-NMR: 12.1 (CH_3); 23.7 ($COCH_3$); 32.7 (Py-CH_2); 51.6 (OCH_2); 121-129 (aromatic C, pyrene); 165.8, 167.8 (C=O).

(iii) N-Acetyl-DL-1-pyrenylalanine.

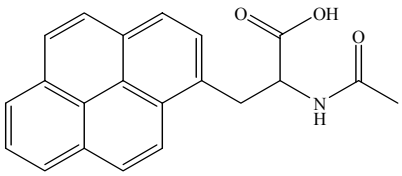

Diethyl 2-(1-pyrenylmethyl)-2-acetamidomalonate (12.5 g, 28.9 mmol) was dissolved in 350 mL of 80% aqueous ethanol. To this mixture, 4.87 g (86.7 mmol) of potassium hydroxide was added, and the solution heated to reflux for 18 h. The solution was allowed to return to room temperature, and the pH adjusted to 2 with 6M HCl and stirred for 20 min. The pH was then adjusted to 10 and the solution poured into a separatory funnel and washed 3 times with 75 mL portions of dichloromethane to remove organic impurities. The aqueous phase was again acidified to pH 2, and extracted three times with 100 mL portions of dichloromethane. The organic fractions were combined, dried over anhydrous sodium sulfate, and concentrated under reduced pressure to yield 9.41 g of white powder. Yield: 98%; R_f = 0.45 (8:1:0.5 CH_2Cl_2:MeOH:AcOH, normal phase). mp 215-218 ºC; ESI-MS *(m/z)* 332.2 $[M+H]^+$ (MW_{calcd} = 332.1).

(iv) L-1-pyrenylalanine.

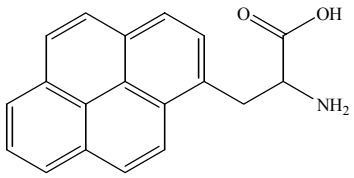

N-Acetyl-DL-1-pyrenylalanine (4 g, 13.8 mmol) was suspended in water and the pH adjusted to 7.8 with 2 M NaOH. Aspergillus Acylase (52 mg per mmol amino acid) was dissolved in a minimal amount of water, along with a catalytic amount of cobalt chloride hexahydrate (approx. 2 mg) as cofactor for the enzyme. The enzyme solution was added to the dissolved amino acid, and agitated on an orbital shaker for 72 h at 38 ºC. L-pyrenylalanine precipitated as a fine white powder, and was isolated from the solution by centrifugation. The precipitate was washed with water to remove excess salts, and dried via lyophilization to yield 1.67 g of off-white powder. Yield: 48%; R_f = 0.73 (8:1:0.5 CH_2Cl_2:MeOH:AcOH, normal phase); mp 205-210 ºC (dec); ESI-MS *(m/z)* $[M+H]^+$ 389.2 (MW_{calcd} 389.4).

(vi) N-Fmoc-L-1-pyrenylalanine.

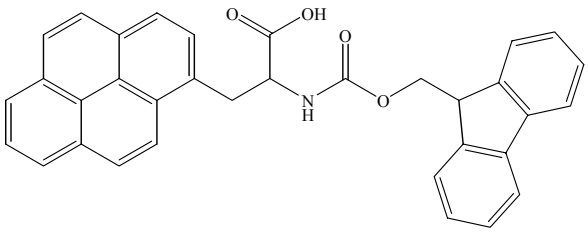

L-1-pyrenylalanine (1.0 g, 3.44 mmol) was suspended in 70 mL of dioxane, along with 1.28 g (3.8 mmol) of 9-Fluorenylmethyloxycarbonyl-N-hydroxysuccinimide (Fmoc-Osu), and 1.12 mL (0.83 g, 6.9 mmol) of diisopropylethylamine. The mixture was

agitated for 24 h, and filtered to remove unreacted starting material. The filtrate was acidified to a pH of 2 with 1N HCl, and the dioxane removed via rotarty evaporation. The resulting precipitate was filtered, and recrystallized from THF:Heptane to obtain N-Fmoc-L-1-pyrenylalanine as a tan powder. The product was further purified over normal phase silica gel with 10:1 CH_2Cl_2:MeOH as the mobile phase to give 0.85 g of the pure product. Yield: 48%; R_f = 0.23 (17:1 CH_2Cl_2:MeOH, normal phase); mp 186-190 ˚C; ^{1}H-NMR (DMSO-d_6): δ 3.50, 3.87 (d, 2H), 4.03 (m, 3H, overlap of chiral CH and Fmoc CH_2), 4.34 (m, 1H, fluorene bridgehead), 7.05-8.22 (m, 18H, pyrene and fluorene Ar-H); ESI-MS *(m/z)* $[M + Na]^+$ = 534.0 (MW_{calcd} 534.168), $[M + K]^+$ = 550.0 (MW_{calcd} 550.276).

Solid Phase Peptide Synthesis.[120,121]

General Procedures. The stepwise growth of peptide chains via solid phase synthesis has been extensively covered in the literature. Therefore, below we list the general procedures used for the construction of all peptides involved in this study. All were constructed using an F-Moc strategy on Wang resins. The completeness of each step was checked by colorimetric testing (either ninhydrin staining or the Kaiser test).

Common Solid Phase Peptide Synthesis Reagents.

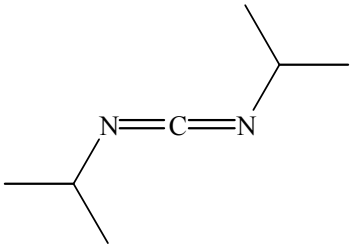

Diisopropyl Carbodiimide
(DIC)

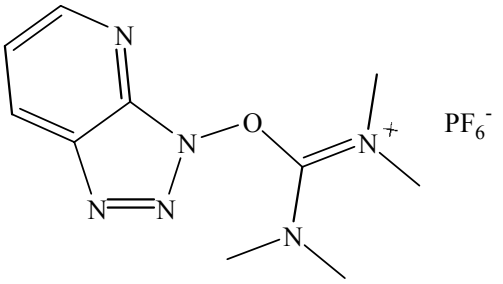

O-(7-Azabenzotriazol-1-yl)-N,N,N',N'-tetramethyluronium
hexafluorophosphate (HATU)

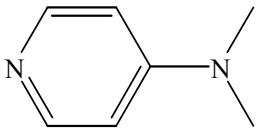

Dimethylamino pyridine
(DMAP

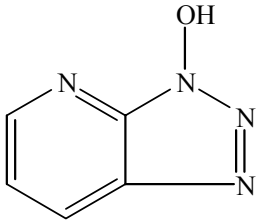

1-Hydroxy-7-azatriazole
(HOAT)

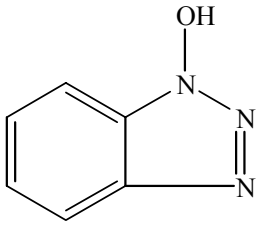

Hydroxybenzotriazole
(HOBT)

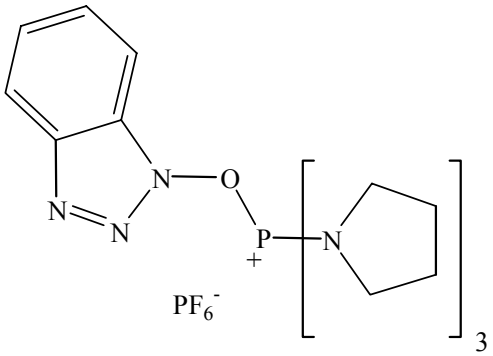

Benzotriazol-1-yloxy)tripyrrolidinophosphonium
hexafluorophosphate (PyBop)

The Kaiser Test for Primary Amines. The Kaiser test is a colorimetric test that will very accurately detect the presence of free amines. It is the test of choice for solid phase synthesis, because it is necessary to detect very low concentration of free amine on resin beads. Briefly, a few dried resin beads are placed into a small test tube. To the test tube, equal amounts (approx 0.1 mL) of 50 M phenol in EtOH, 10 μM potassium cyanide in

pyridine, and 0.3 M ninhydrin in ethanol are added. The solution should appear pale yellow. The tube is then placed into an oven at 120 ºC for 5 minutes. At the end of 5 minutes, if the beads and solution still appear either clear or pale yellow, the test is negative, and no free amine is present. However, if the solution and beads appear gray or blue, then the test is positive, and free amine is present.

Preparation an Activated Amino Acid for Wang Resin Loading. The amino acid of choice (5 equivalents relative to the resin loading) was dissolved in a minimal amount of dichloromethane. For some amino acids, small amounts of DMF had to be added to completely dissolve the sample. To this solution, 5 equivalents of 1,3-diisopropylcarbodiimide (DIC) were added, along with 10 equivalents of N,N-diisopropylethylamine (DIPEA). The solution was allowed to stir for 30 min, the solvent was removed, and the activated amino acid dried under vacuum. This product was used without further purification or characterization.

Loading of the Wang Resin. The Wang Resin (1 equivalent) was placed in a sintered glass solid phase peptide synthesizer, and swelled in DMF for 1 h using nitrogen as the agitating gas. After swelling, the DMF was drained from the resin, and the resin washed with DMF (or dichloromethane) 3 times. The activated amino acid for Wang resin loading was dissolved in DMF (approx 10 mL per mmol amino acid) and added to the peptide synthesizer along with 0.1 equivalent of dimethylaminopyridine (DMAP). The mixture was allowed to mix for 1.5 h, and the solution was drained from the resin. The

resin was washed 3 times with DMF, twice with methanol, once with ethanol, and was dried. A 20 mg sample of the dried resin was taken, and placed into 50 mL of 20% piperidine in DMF. The solution was stirred for 20 minutes, and 2 mL of the solution was taken so that an absorption spectrum could be obtained. The relative amount of amino acid loading was calculated using Beer's law by measuring the intensity of the fluorenyl absorption at 285 nm. If the loading was sufficiently high, the resin was swelled again in DMF, and the peptide synthesis begun. If not, the resin was loaded subsequent times, until a 90 % or greater loading was obtained.

Deprotection of the N-terminus of peptides. The N-termini of all peptides addressed in this study were protected by fluorenylmethoxycarbonyl groups (F-Moc). These groups are base labile and are removed as follows. The resin was washed 3 times with DMF, twice with ethanol, once with methanol, and again 3 times with DMF. The DMF was drained, and 50 mL of 20% piperidine in DMF were added and allowed to mix for 20 min. The piperidine solution was drained from the reaction vessel, and the resin again washed with DMF, methanol, and ethanol. After washing with ethanol, a few resin beads were taken and tested for the presence of primary amines. Once primary amines were observed, the resin was washed again with DMF, and was ready for addition of the next amino acid.

Coupling of Amino Acids to the Resin Bound Chain. The N-protected amino acid of choice (5.0 eq relative to the resin loading) was dissolved in DMF, along with 5 eq of

(benzotriazol-1-yloxy)tripyrrolidinophosphonium hexafluorophosphate (PyBOP), 5 eq of 1-hydroxybenzotriazole hydrate (HOBT) and 10 eq of N,N-diisopropylethylamine. This solution was added to the washed, deprotected resin, and allowed to mix for 2 h. At this point, the reaction mixture was drained from the resin, the resin washed as previously described, and the Kaiser test performed. A positive Kaiser test (blue solution) was indicative of coupling being incomplete. In such cases, the coupling procedure described above was repeated. A negative Kaiser test (clear/yellow solution) was indicative of completed coupling. In this case, the resin was again washed with DMF, and the N-terminus of the newly coupled amino acid deprotected as previously described.

Cleavage of the Linear Peptide from the Resin. After addition of the final desired amino acid, the N-terminus was deprotected, the resin washed with DMF, ethanol, and was dried under vacuum for 3 h. To the dry solution, a mixture of trifluoroacetic acid (TFA), triisopropyl silane (TIS) and water was added (9.5:0.25:0.25 respectively, 10 mL per mmol amino acid). The resin was stirred in the concentrated acid solution for 2.5 h, and was then filtered and concentrated in *vacuo*. The crude peptide was then precipitated by the addition absolute ether to the acidic medium.

Cyclization of the Linear Peptide. Linear peptide (1 eq) was dissolved in DMF (2 mL per mg linear peptide) at 0 ºC. To this solution, 2.5 eq O-(7-Azabenzotriazol-1-yl)-N,N,N',N'-tetramethyluronium hexafluorophosphate (HATU), 2.5 eq of 1-Hydroxy-7-azabenzotriazole (HOAT), and 10 eq of DIPEA were added. The solution was stirred at

0 ºC for 3 h, and then at r.t. for 8 h. The solvent was removed via rotary evaporation, and the crude residue dissolved in ethyl acetate. The residue was washed 3 times with saturate sodium bicarbonate, and twice with 2 M citric acid. The organic fraction was dried over sodium sulfate, and the solvent removed under reduced pressure.

Cyclic Peptide Synthesis.

Linear peptide lin[-aib-pya-aib-phe-]$_2$. Lin[-aib-pya-aib-phe-]$_2$ was synthesized via the described methods in a 65% overall yield relative to the resin loading. Crude linear peptide was purified by flash column chromatography on silica gel with 17:1 CH_2Cl_2:MeOH as the mobile phase. Peptide purity was assessed using reverse phase HPLC with 6:4 CH_3CN:0.1% TFA as the mobile phase. Mp = 158-162 ˚C ESI-MS *(m/z)* $[M+H]^+$=1195.4 (MW_{calcd} 1195.566).

Cyclic peptide cyclo[-aib-pya-aib-phe-]$_2$. Lin[-aib-pya-aib-phe-]$_2$ was cyclized via the described procedure, and was purified over silica gel with a 17:1 CH_2Cl_2 mobile phase. Peptide purity was assessed using reverse phase HPLC using the same conditions as for its linear analogue. Mp= 165-168 ˚C ESI-MS *(m/z)* $[M+H]^+$ = 1177.6 (MW_{calcd} 1177.556), $[M+Na]^+$ = 1199.8 (MW_{calcd} 1199.538).

Linear peptide lin[-ala-pya-ala-phe-]$_2$. Lin[-ala-pya-ala-phe-]$_2$ was synthesized by the methods described with an overall yield of 55% relative to the resin loading. The crude

linear peptide was purified over silica gel with a 17:1 CH_2Cl_2 mobile phase. Mp= 170-175 ˚C MS (ESI) *(m/z)* $[M+H]^+$ = 1139.6 (MW_{calcd} 1139.504) IR (ATR): Amide I band: 1629 cm^{-1}, Amide II band: 1529.27.

Cyclic Peptide cyclo[-ala-pya-ala-phe-]$_2$. Cyclo[-ala-pya-ala-phe-]$_2$ was produced by solution phase cyclization of its linear analogue by the method described earlier. Purification was performed using preparative TLC with 17:1 CH_2Cl_2 as the mobile phase. Before the TLC plate could be run, the sample had to be spotted onto the plate with DMF, due to solubility concerns. Mp= 178-180 ˚C MS (ESI) *(m/z)* $[M+K]^+$ = 1159.6 (MW_{calcd} 1159.583) IR (ATR): Amide I band 1626.25 cm^{-1}, Amide II band: 1512.39, 1504.36

Linear Peptide lin[-ala-pya-]$_4$. Lin[-ala-pya-]$_4$ was synthesized by the described methods in a 40% overall yield relative to the resin loading. The linear peptide exhibited exceptionally poor solubility, making purification very difficult. ESI-MS *(m/z)* $[M+H]^+$=1389.0 (MW_{calcd} 1388.6)

C. CONSIDERATIONS FOR FUTURE WORK

1. Cyclic Peptide Nanotubes

The cyclic studies presented are very preliminary since pyrene stacking is not yet optimized, and a definitive experiment for the measurement of charge and energy transfer in these systems has not yet been devised. In this section, suggestions will be presented as to how to maximize pyrene aggregation in these systems, and how to incorporate peptide nanotubes into systems that can be tested for charge and energy transfer.

Optimizing pyrene aggregation can be accomplished synthetically. It was suggested that the monomer fluorescence observed in the current systems is due to staggered conformations in the nanotubes. This situation could be eliminated by incorporating four pyrenyl side chains into the cyclic peptide. (Figure 66)

Figure 66. The structure and possible stacking arrangements of cyclo[-D-Ala-L-Pya-]$_4$.

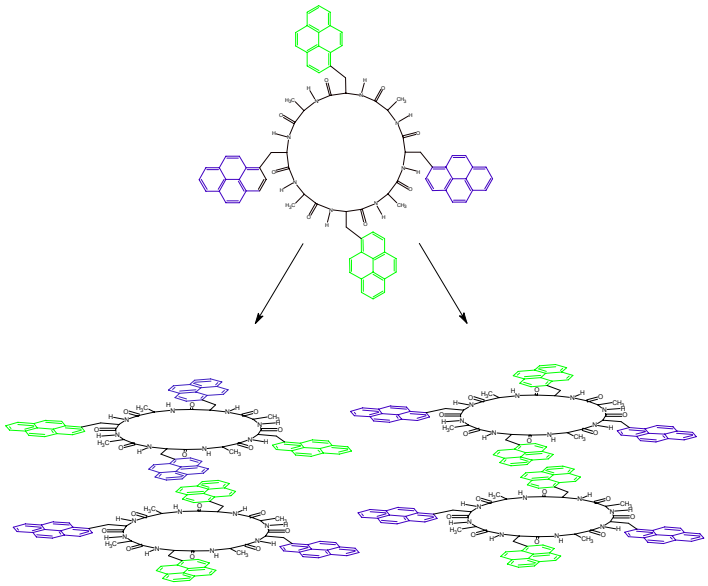

Unlike the possible stacking arrangements for the cyclic peptides already studied (Figure 65), this particular cyclic peptide can only adopt structures in which the pyrene side chains stack. Therefore, every pyrene group in the stack is capable of forming excimer. We would expect that fluorescence spectra of this system may contain proportionally more excimer emission than the systems already studied and discussed, thereby confirming that the less intense excimer emission observed for the latter were indeed due to the two different possible stacking arrangements shown in Figure 65.

To this end, the linear analogue of this peptide has already been synthesized and characterized. The cyclic form has not yet been completed due to characterization and purification problems encountered. Specifically, the tetrapyrenyl peptide is very insoluble in most organic solvents due to the very large non-polar character of its bulky side chains. Furthermore, the cyclization is a more sterically hindered process as either the C or N terminus of the linear peptide must contain a bulky pyrene group.

For a determination of the utility of these peptide nanotubes as conduits for energy or charge conduction characterization of their average length and state of intertube aggregation is desirable. To this end we suggest incorporating these assembled monolayer on gold as previously discussed by Ghadiri[122,123] and testing for photonic conduction as shown in Figure 67.

Figure 67. A pictorial representation of two small cyclic peptides on gold. The blue peptide tubes will each be substituted with a series of donor chromophores.

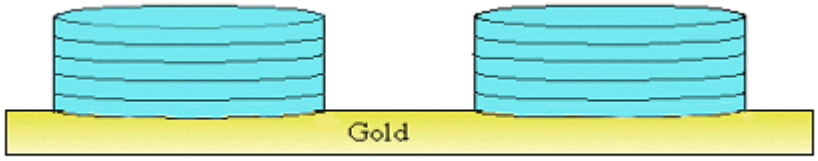

In Figure 67, the bare gold surface will be exposed to a solution containing cyclic peptide monomer units within a supporting matrix (typically an alkanethiol). Each of these monomer units would be substituted with chromophores that could be selectively excited to an excited state with a higher energy that that of pyrene. The amount of cyclic peptide deposited will be dependent initially upon the chain length of the supporting matrix, and therefore is controllable. The thickness of the deposited layer can be measured via ellipsometry. Once this layer is assembled, a second solution containing the tetrapyrenyl peptide (Figure 66) will be exposed to the surface allowing assembly on top of the donor layer. (Figure 68)

Figure 68. The donor layer (light blue) capped with the tetrapyrenyl cyclic peptide (light green).

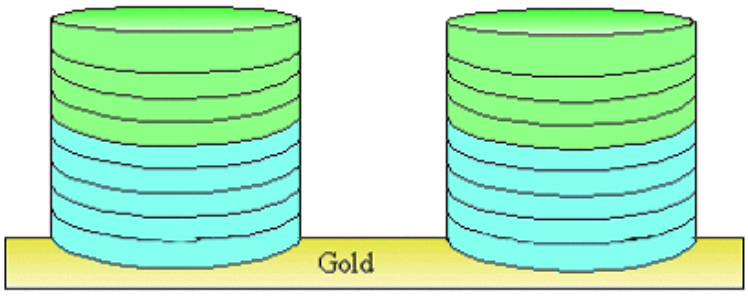

The deposited layer of tetrapyrenyl cyclic peptides should have a thickness dependent on the length of exposure to the solution. The thickness of this layer can again be measured via ellipsometry. A final capping unit will then be deposited. This cap will be a cyclic peptide that contains an energy accepting chromophore and four alternating N-methyl alanine units. (The N-methylated cyclic peptide can only bind from one face of the cyclic peptide ring, and therefore will form a cap that is exactly one molecule thick.) (Figure 69)

Figure 69. The fully assembled system for long range transfer studies including a capping layer (red).

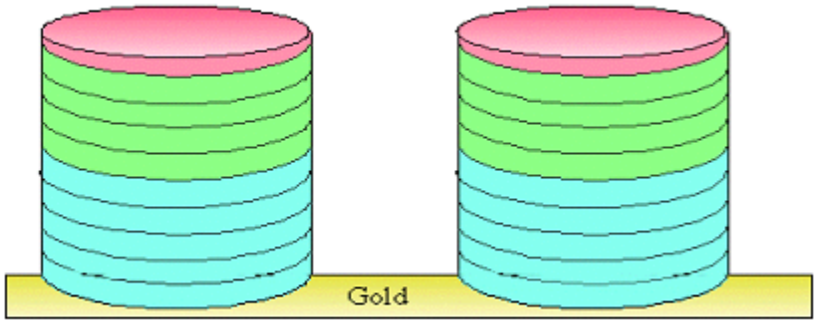

The identity of the acceptor chromophores has several restrictions. It cannot absorb at the same wavelength as the pyrene or donor groups, it must have a lower excited state energy than that of pyrene, and it must be emissive in either the singlet or triplet state. If all of these requirements are met, then the tetrapyrenyl cyclic peptide can potentially undergo long range energy transfer by exciting the donor layer, and monitoring acceptor emission. A control experiment would involve replacement of the pyrene layer with a

non-chromophore-containing cyclic peptide. Such an experiment should show no emission from the acceptor when the donor layer is excited.

It may be preferable to build a system similar to that described above, in which the initial donor layer is not assembled within the alkane thiol matrix. Using a matrix, raises potential difficulties if the cyclic peptides contain bulky or branched side chains. Also, a mixed monolayer can be difficult to characterize by contact angle and ellipsometry. These problems can likely be avoided by depositing the initial donor layer based on carboxylic acid dimer interactions with an appropriately functionalized gold surface. (Figure 70)

Figure 70. Peptide nanotube monolayers based on carboxylic acid dimers. Recall from above that the red layer is an acceptor layer, the green is the pyrenyl peptide layer, and the blue is a donor layer.

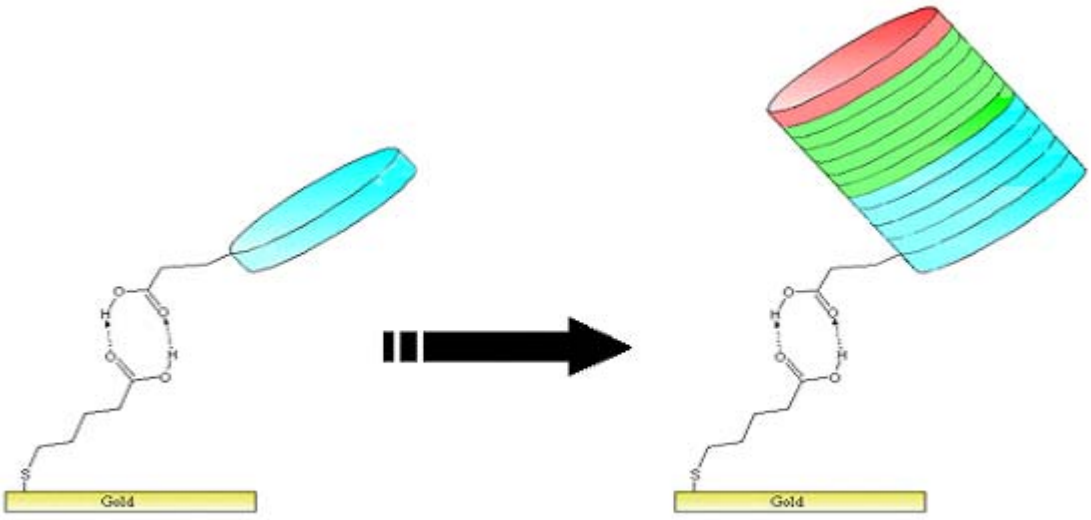

This system offers an additional advantage over the matrix-based systems in that the tubes will be deposited onto a SAM and therefore will possibly possess more order than in a matrix. The non-covalent interaction in this case, carboxylic acid dimers, is an

example only, and can be replaced by a variety of binding motifs including the metal-ligand systems described in previous sections.

A similar system can be envisioned for the testing of photocurrent generation. As demonstrated previously, photocurrent generation can occur through an alkyl thiolate monolayer so long as there is an appropriate photoactive cap. Therefore, it seems reasonable that a pyrenyl peptide nanotube tethered to the gold surface may undergo photocurrent generation upon irradiation in the presence of a suitable electron acceptor.

Finally, it is desirable to test the ability of cyclic peptides to conduct charge. We have suggested that charge will conduct through these systems if there exists a stacked array of aromatic molecules. There are multiple ways to test this. The first would involve the construction of the two cyclic peptides shown in Figure 71.

Figure 71. The two cyclic peptides proposed for the testing of charge transfer. The Glutamic Acid residues in each allow the peptides to be tethered to the surface via the interaction shown in Figure 70.

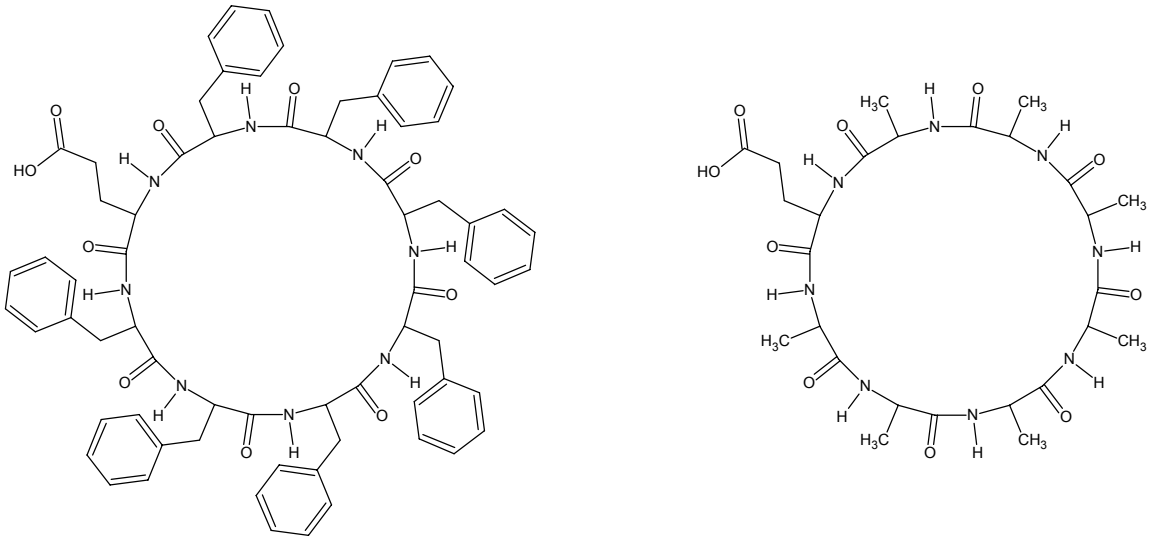

These peptides are chosen as targets because they differ only in the amount of pi-pi interactions they will experience upon assembly. Furthermore, these peptides are less demanding synthetically because large amounts of pyrenyl alanine are not required. (Since no optical absorption is needed, phenyl groups will be used. However, these should still provide π-π interactions). To test these systems for charge transfer, multilayers of each peptide will be constructed based on the assembly presented in Figure 70. At this point, there are several possible options for testing charge transfer capabilities. The simplest experiment will be to perform cyclic voltammetry and impedance measurements on them to determine if charge flows through either system. Ideally, conducting will be most efficient in the heptabenzyl cyclic peptide.

A second option for testing charge transfer ability will be to cap each multilayer with a single photoactive head group. Both systems will then be irradiated and the photocurrent produced measured with the expectation that the heptabenzyl system will produce more photocurrent than the alkyl cyclic peptide, due to the conduction facilitated by the aryl stacks.

An alternative approach for determining conducting ability would be an investigation of multilayer surfaces via STM. Initially, studying films of the cyclic peptide systems illustrated in Figure 71 could give an indication as to whether delocalized π systems will indeed enhance conduction in peptide nanotubes. A more interesting study would involve STM measurements of a surface consisting of tetrapyrenyl or octabenzyl

substituted cyclic peptides deposited within an alkane thiol supporting matrix. Probing these surfaces via STM should allow for a determination of whether the tubes are of higher conductivity than the surrounding insulating alkane thiol matrix

2. Pyrenyl Functionalized Diketopiperazines

The diketopiperazine architecture offers a second option for arranging pyrene in an aggregated fashion based on self-assembly. The diketopiperazine assembly motif is based on a two-dimensional hydrogen bonded network between amide functionalities (Figure 72).[124]

Figure 72. Self-Assembly of Diketopiperazines.

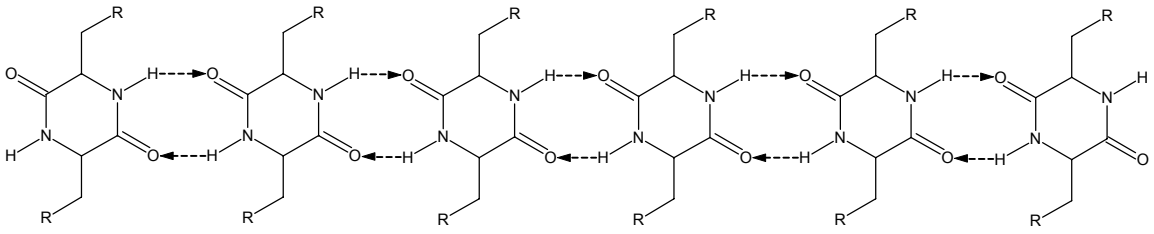

Based on this structural motif, an ordered array of pyrene molecules can be assembled by substituting the R group in Figure 72 with pyrene. This system may share similar characteristics to that which is expected for pyrene containing cyclic peptide nanotubes.

To this end, a cyclic diketopiperazine containing pyrene has been synthesized (see Appendix A). Unfortunately, crystallization of the diketopiperazine yielded small amounts of minute crystals which were unsuitable for obtaining structural information, and therefore additional testing was not carried out. Future work will focus on the

production of the aforementioned diketopiperazine on a larger scale, and the subsequent crystallization.

3. Multilayer Thin Films on Gold

(i) Creating Films with Increased Order

The construction of multilayer thin films on gold that function as molecular wires and photocurrent generators has been previously discussed. In both systems, it was observed that the behavior of the films begins to become unpredictable after the deposition of between six and ten layers. These variations likely arise from increasing disorder within the layers upon multiple depositions. It may be possible to prevent or lessen disorder by changing the linker molecule to one that imparts order within the linking layer, either through covalent or non-covalent interactions. A simple linker is shown in Figure 73.

Figure 73. Proposed linker molecule.

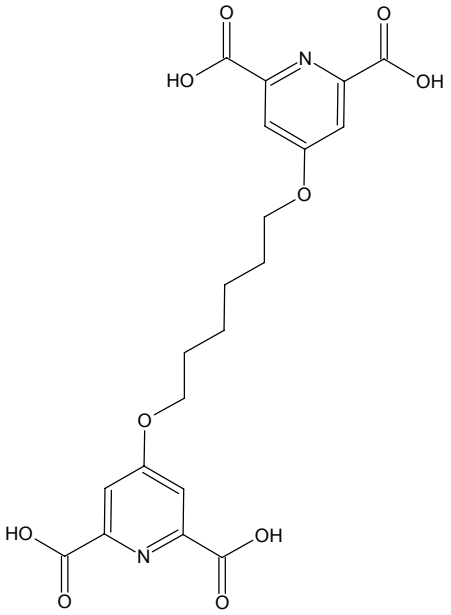

It is well documented that self-assembled monolayers on gold are extremely ordered for alkyl chains of six or more carbons due to van der Waals interactions between chains. The linker in Figure 73 seeks to take advantage of this ordering capability; i.e, increasing the alkyl chain length should maximize van der Waals interactions between linkers, thus giving each layer a greater amount of order. For both photocurrent and wire experiments, charge is believed to flow through these systems via a tunneling mechanism. Therefore the increased distance between layers may decrease tunneling efficiency (although we note that the initial tunneling event takes place through a distance of roughly 10 Å). A proposed synthesis of this linker is shown in Figure 74.

Figure 74. Proposed synthesis of linker.

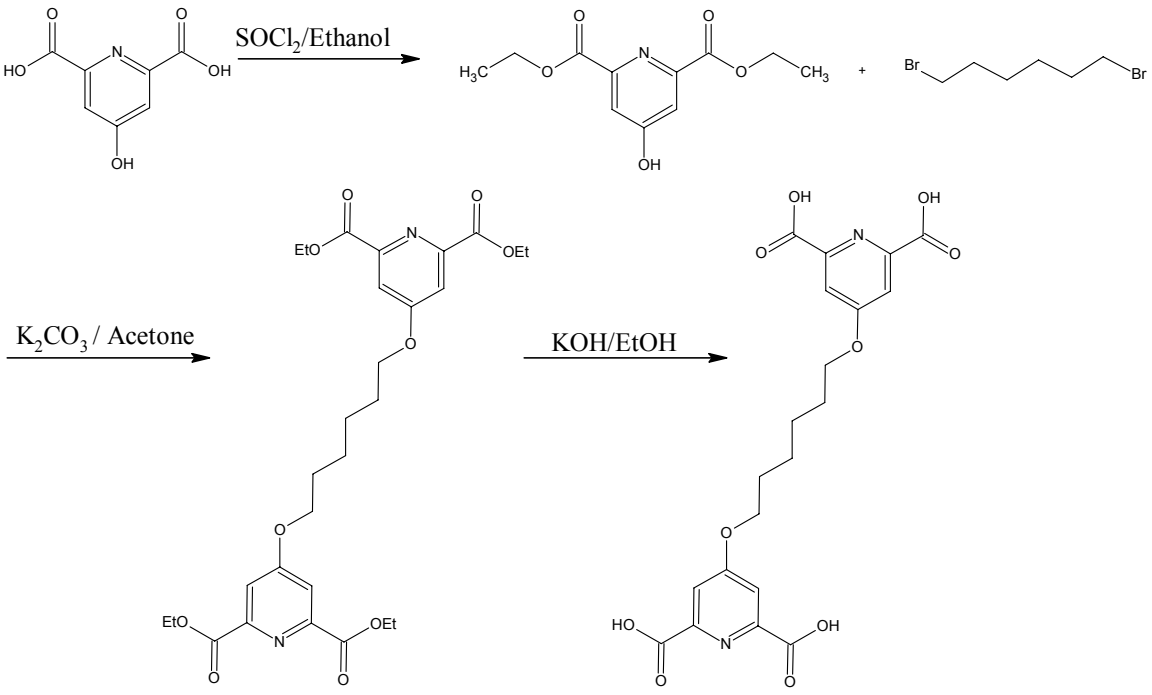

Varying the chain length incorporated into the linker molecule may also provide valuable information about how the length of the linker effects charge transfer efficiency.

With this in mind, we have already synthesized an acetylene containing analogue of the tetracarboxy dipyridine linker molecule, by coupling under Sonogashira conditions (Figure 75).

Figure 75. Synthesis of 4-[(2,6-dicarboxypyridin-4-yl)ethynyl]pyridine-2,6-dicarboxylic acid via a Sonogashira Coupling reaction.

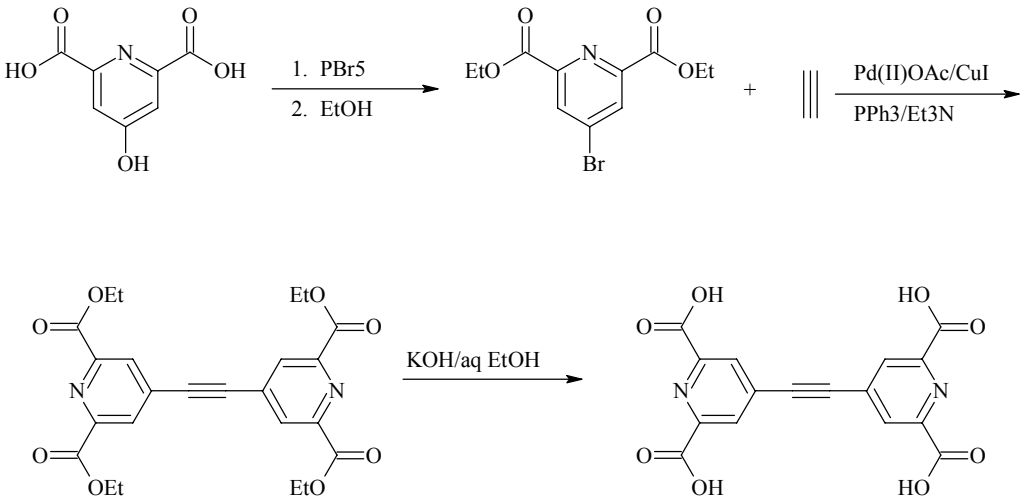

A drawback of this system is its insolubility in most organic solvents. Although it is sparingly soluble in DMSO, we have yet to form ordered multilayers incorporating this linker unit.

To impose more order within the linker layer, it may also be possible to construct a linker that can be crosslinked following assembly, by chemical or photochemical mechanisms. An example of a linker molecule that can be chemically crosslinked is shown in Figure 76, along with its proposed synthesis.

Figure 76. Proposed synthesis of 4-[2-(2,6-dicarboxypyridin-4-yl)-1-mercaptoethyl]pyridine-2,6-dicarboxylic acid.

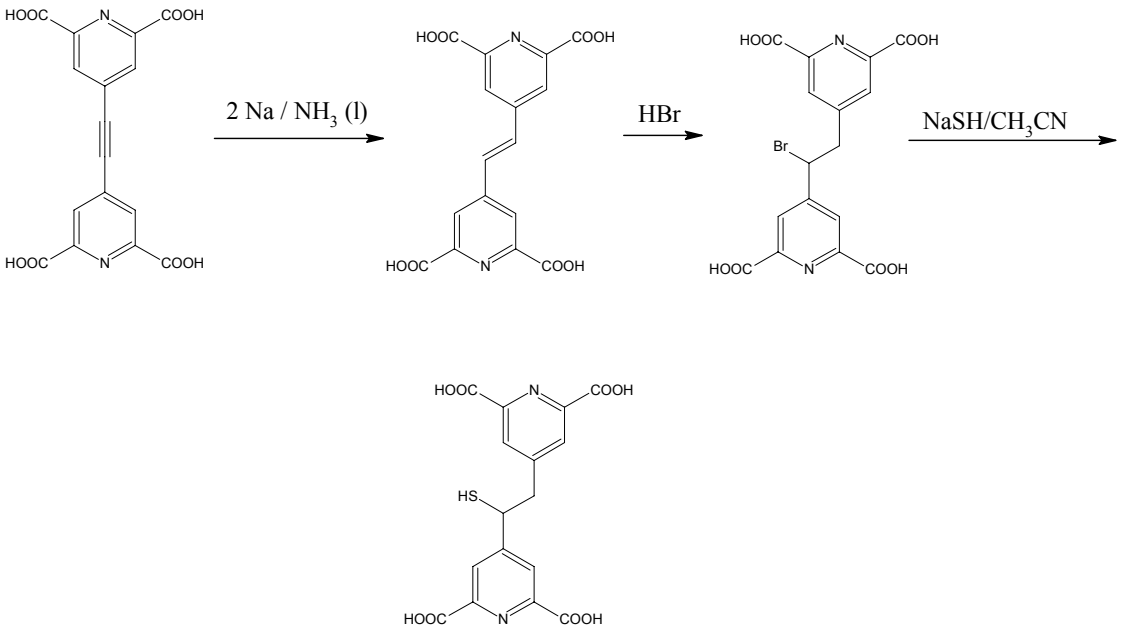

This linker unit can be used to assemble multilayers, similar to that which was discussed in previous sections. However, once the multilayer is assembled, exposure to either O_2 or I_2 will result in an oxidative coupling between thiol groups in adjacent molecules in the linker layer to yield bridges (Figure 77).

Figure 77. Chemical crosslinking of multilayers.

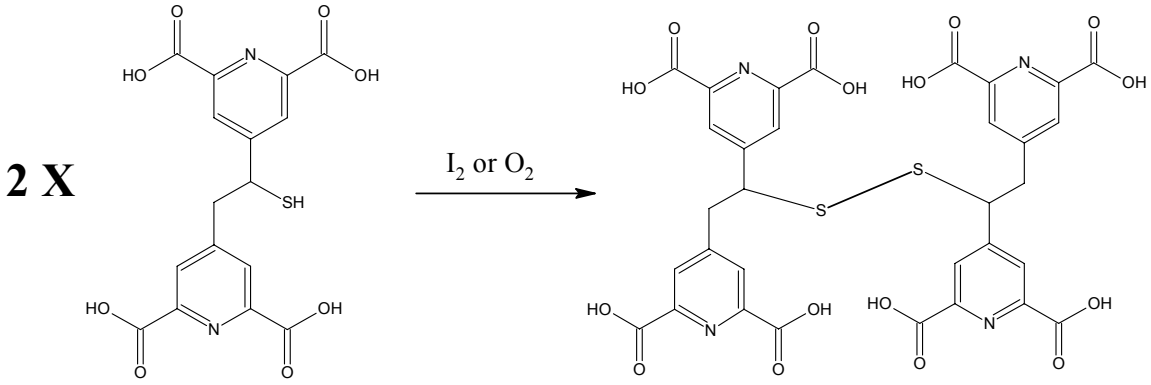

We note that while thiol functionalities may bind metal ions during multilayer assembly, the metal-dicarboxypyridine binding is expected to predominate, based on a higher binding constant.

Photochemical crosslinking is a second possible route to stabilization. There are numerous examples of photoreactive crosslinkers used in the polymer industry. One system that could be used in the application is shown in Figure 78.

Figure 78. Photochemical crosslinking of multilayers.

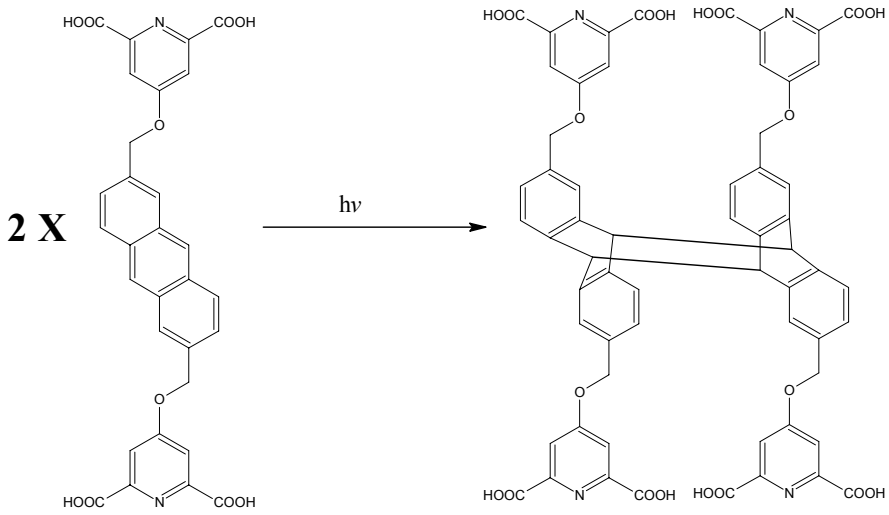

We have chosen this system as a possible target largely because the photochemistry of anthracene within self-assembled monolayers has been established previously.[125] The synthesis of this linker should be analogous to that illustrated in Figure 74. In addition to imparting order on the multilayers, the amount of crosslinking can be conveniently measured by either absorption or fluorescence spectroscopy.[29]

Whether additional order is imparted within multilayers non-covalently or covalently, it is clear that steps need to be taken that will allow for the construction of thin films that remain ordered at greater thicknesses. Greater thicknesses and ordering will allow for the construction of longer molecular wires, and will likely make the films considerably more robust.

(ii) Optimizing Photocurrent Generation From Thin Films

The photocurrent generation work carried out to date has served as a proof-of concept. The quantum efficiency of this system was roughly 1%, which is considerably less than the efficiencies seen in inorganic solar cells. Therefore, the system needs to be optimized in order to provide increased efficiency.

The obvious first step in this process is to substitute the chromophore used. While pyrene absorbs fairly strongly in the UV, chromophores with larger extinction coefficients and broader spectral coverage, particularly in the visible range will potentially yield higher efficiency. To this end, efforts have focused on incorporation of a porphyrin unit into the multi-layers.

In addition to changing the chromophores used, it may also be useful to determine if the alkyl chain length used in the formation of the initial monolayer has any effect on the overall efficiency of the system. Assuming that charge transfer takes place via tunneling, then the efficiency will be dependent on the distance between the gold surface and the acceptor. At shorter chain lengths (six carbon chain), a greater overall efficiency than that observed for a longer chain (10 or 12 carbon chain) may be observed.

(iii) Photoswitchable Surfaces

Our initial work in designing a photoswitchable surface has provided the foundation for a great deal of future work. In the immediate future, we will focus on identifying a ligand that is capable of reversible switchability on the surface, and which, as a result will have potential utility in microfluidics applications. With a transient or switchable ligand, irradiating a pattern on thin films will create microchannels. Theoretically, our initial work is capable of this to some degree. However, a reversible system will allow creation and erasure of microchannels at will.

There are several issues that need to be addressed in order for such a system to be realized. First, the ligand chosen must be able to bind metal(II) ions. For example, we have seen that cis-dipyridyl ethylene binds tightly to a multilayer capped with copper ions whereas cis-stilbene does not. The ligand chosen must also be photo-isomerizable with two thermally stable states that are non or weakly absorbing in the visible range, (so that a formed channel cannot be reversibly erased under normal laboratory conditions). The ligand must also undergo reversible photoisomerization. Finally, the ligand chosen must be of an appropriate size so that ordered packing can take place within the multilayer.

Keeping these design characteristics in mind, we have investigated spiropyrans as possible ligands (Figure 79).

Figure 79. The structure and conformations of spiropyran. The open ring form is called the "merrocyanine form", and is deeply colored unlike the colorless spiropyran conformation.

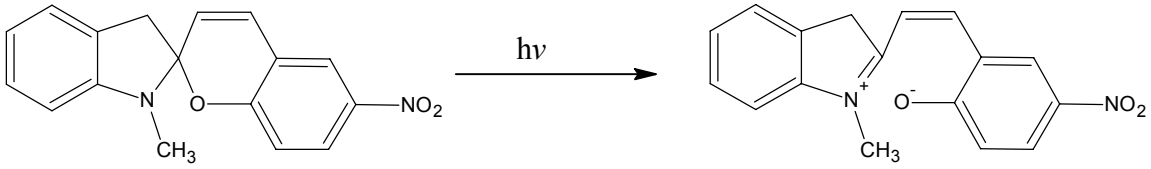

Spiropyrans are known to chelate metal ions and also have well established photophysical characteristics.[126] It is our belief that switching from the spiro to merrocyanine form could lead to a drastic change in wetting behavior because the latter is a zwitterion. However, to date, we have had little success in depositing multilayers containing these molecules, possibly due to their size, and/or their lack of ability to bind metal ions at the spiro bridge.

A potential alternative to spiropyrans can be found in the fulgide family of compounds. These compounds also have well established photochemistry due to their use as photochromics.[127] Also, fulgides possess a succinimidyl functionality that resembles the binding site in dicarboxypyridines (Figure 80). Besides possibly being able to bind metals and undergo photoisomerization, the fulgide geometry appears to be relatively small, thus making it plausible that it can be incorporated into ordered layers. Additionally, its ring-opened form should be more stable than the merrocyanine form of spiropyrans, as charge recombination isn't a driving force towards the closed form.

Figure 80. A typical fulgide: the succinimidyl group could take place in octahedral binding with a metal ion.

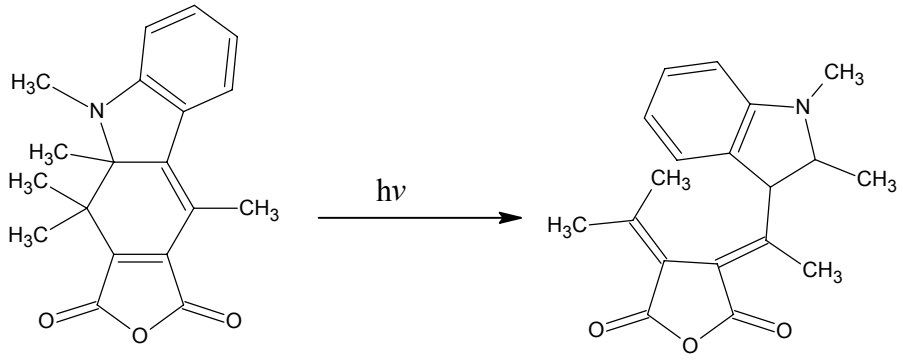

We are also very interested in identifying a photolabile ligand that can be selectively removed from the surface upon irradiation (Figure 81). This aspect of the work is particularly exciting, since the multilayer would essentially act as a photomask for templated growth of thin films. Thus, a multilayer could be constructed that is terminated with the photolabile surface group. A pattern can then be written into the surface by irradiating with a UV laser. By rinsing, the irradiated section can be removed leaving copper ions exposed to the surface. This by itself would be very useful for creating micro channels, however it could serve an additional purpose. Assuming the ability to selectively remove areas of the surface to expose copper, further deposition on the copper with different ligands will add different functionalities onto different areas of the surface. A potential application would be the incorporation of many different devices onto different areas of a single surface. In this sense, it may serve as a template for interfacing different devices with one another, as they can be deposited within close proximity to one another.

Figure 81. A non-covalent approach towards lithography. A photolabile ligand (green) is irradiated and washed off exposing a fresh surface of copper ions. Those copper ions can then be selectively capped with anything that binds metal (light blue).

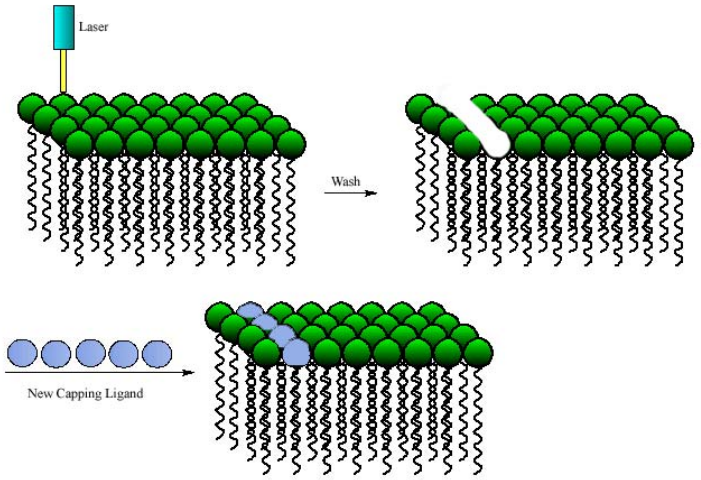

An excellent family of compounds that could possibly serve as photolabile ligands are azo compounds (Figure 82). Azo compounds are well known to undergo photocleavage upon n→ π* excitation. Once the cleavage takes place, molecular nitrogen is quickly evolved along with radical species.

Figure 82. Some commercially available azo compounds that could function as photolabile ligands.

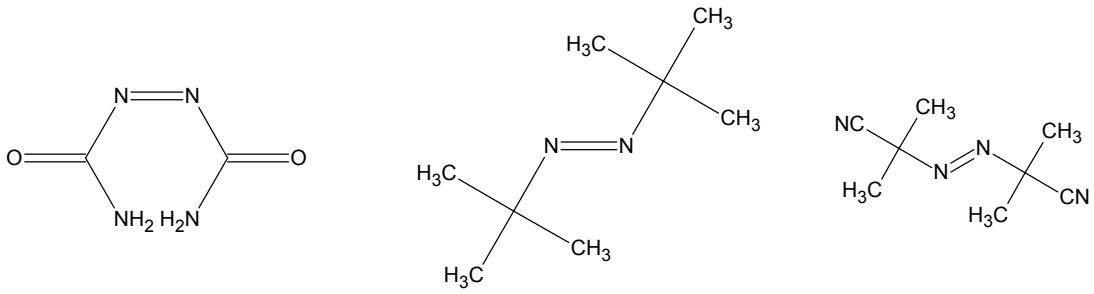

These compounds are especially desirable, as it is reasonable to assume that they will complex with metal ions through their azo functionalities based on the results from systems containing dipyridyl ethylene. Azobisformamide (Figure 82, left) is an especially attractive candidate, as it is highly likely that it will bind metal ions either through the azo or amide nitrogens. Industrially, it is used as a blowing agent and is well known for its complete decomposition both thermally (200º C) and photochemically.[128]

(iv) Gold Nanoparticles

In addition to the work we have presented on macroscopic surfaces, gold nanoparticles are also important surfaces to consider. We have previously noted that dipyridyl ethylene-capped thin films are photoswitchable. In addition, when the dipyridyl ethylene system is photochemically switched to the trans state, the underlaying copper ions become exposed to the solution as evidenced by impedance and cyclic voltammetry measurements. This behavior suggests the use of such surfaces as catalysts since numerous chemical reactions involve copper (II) as catalysts. Assuming it is possible to selectively expose copper (II) to a solution via irradiation, then Cu(II) catalyzed reactions could potentially be switched on and off by exposure to light.

Work with gold nanoparticles is well established now, and as a general rule, assembly on nanoparticle surfaces is a facile as on macroscopic gold surfaces. Besides catalysis, nanoparticles may be useful in constructing photocurrent generating thin films. The photocurrent generation we observe is dependent upon diffusion, as the electron acceptor used (paraquat) is in solution. Nanoparticles provide a unique construct, as the photocurrent generator itself is actually suspended in solution as well, and more likely to be in contact with the electron acceptor. As with catalysis, the surface area of the nanoparticles will allow for a much greater amount of photocurrent to be generated per unit area.

4. Self Assembled Monolayers on Quartz

Our group has recently synthesized fluoroionophores for incorporation into bulk membranes for blood analyte measurements.[129,130,131]

It is our intention to incorporate fluoroionophores into quartz SAMs, as the surface can then function as an optical sensor. To start, we have constructed a disubstituted diaza18-crown-6 (Figure 83) that undergoes PET fluorescence quenching, but is a relatively non-specific ion binder. This work seeks to provide proof of concept that self-assembled monolayers on quartz can function as sensors. However, bulk membranes impede diffusion of the analyte from the solution to the fluoroionophore. For this reason it is desirable to create a surface bound array of fluoroionophores. While surface modification of gold is facile, both absorption and reflectivity of the gold substrate can interfere with optical measurements. For this reason we have started in investigate quartz surfaces as substrates for fluoroionophores. We have constructed anthryl diaza 18-crown-6 (Figure 83) that acts as an off-on fluorescence switch upon exposure to alkali metal ions (K^+, Na^+) although it is a relatively non-specific ion binder. This work seeks to provide proof of concept that self-assembled monolayers on quartz can function as sensors.

Figure 83. The disubstituted diaza crown used to form monolayers on quartz. The molecule can be tethered to a quartz surface via the trichloro silyl functionality.

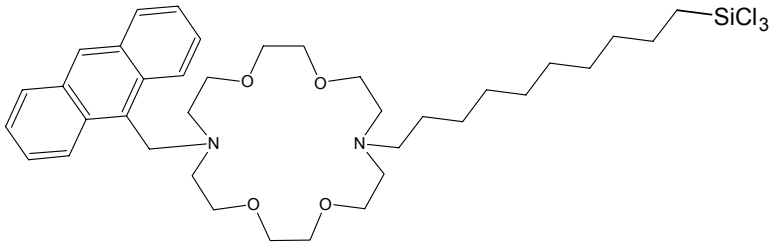

The diazacrown was first tested in solution for response to potassium ions. The resulting spectra are shown in Figure 84, and indicate a direct correlation between ion concentration and fluorescence intensity. Although diazacrowns are known to bind potassium ions, this study confirms that substituting the crown ether with a long alkyl chain does not alter the conformation or prohibit binding.

Monolayers of the disubstituted diaza crown were formed by exposing a clean quartz surface to a 10 mM solution of the crown in hexadecane for 20 h. Monolayer formation was monitored via changes in the contact angle. When no further change was evident in the contact angle, the slides were removed from the crown solution, and then sonicated in water and ethanol to clean any non-bound crown from the surface.

Figure 84. Fluorescence intensity of the disubstituted diaza crown in DCM with respect to K^+ concentration. The least intense fluorescence spectrum corresponds to 0 μM [K], with subsequent spectra increasing in 0.5 M increments. Each solution contains 0.01 μM Benzyl trimethyl ammonium hydroxide (BTMAH) to ensure deprotonation of the crown.

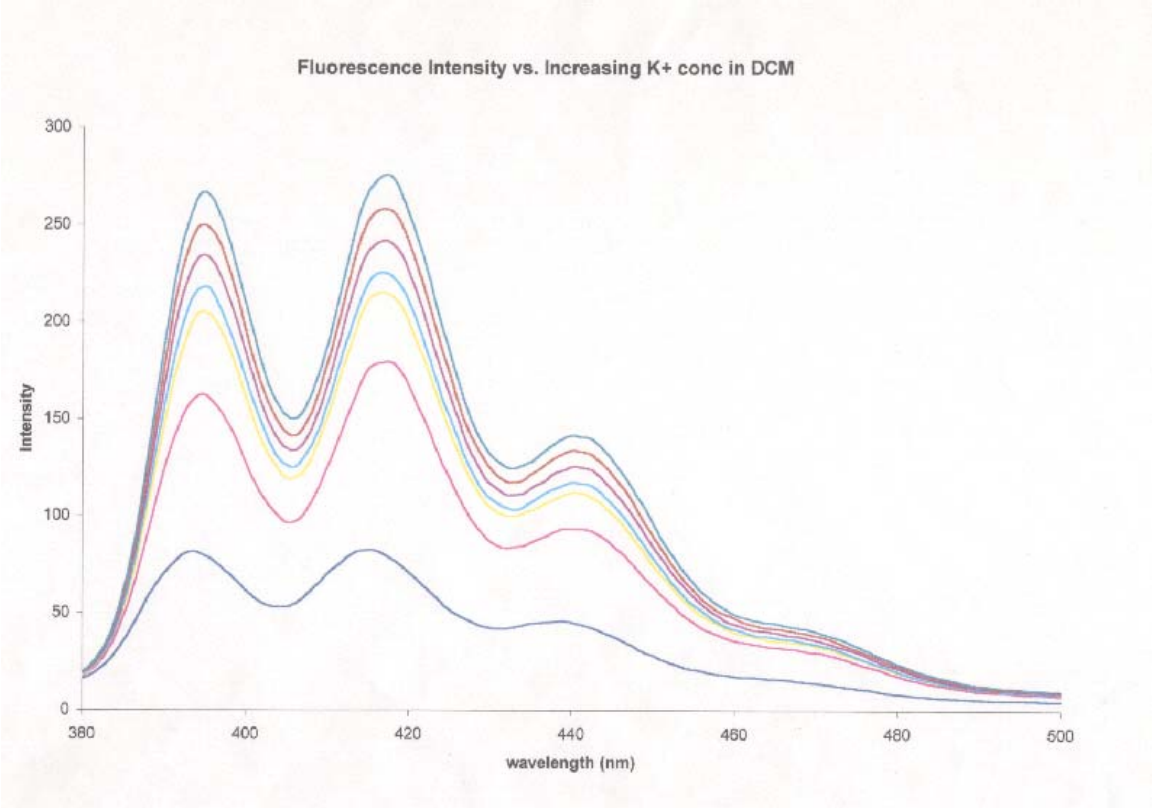

Initially, the monolayers were exposed to a solution of BTMAH to ensure deprotonation. Unfortunately, this led to the destruction of the monolayer. Therefore, fluorescence experiments were carried out in the absence of base for all monolayers. Currently, we are investigating other options for an organic base that will not harm the monolayers.

Fluorescence experiments were carried out via front face reflectance from the quartz slides. As this experiment sought to illustrate proof-of-concept, exposure to potassium ions was achieved by immersing the quartz in a concentrated solution of potassium acetate in carbon tetrachloride. After immersion, a fluorescence spectrum was collected,

the sample was washed and sonicated with water, and the fluorescence spectrum was obtained again. For two cycles of this process, the fluorescence output of the monolayers was well behaved (Figure 85).

Figure 85. Disubstituted Diaza crown monolayer on quartz fluorescence intensity with respect to K^+ exposure.

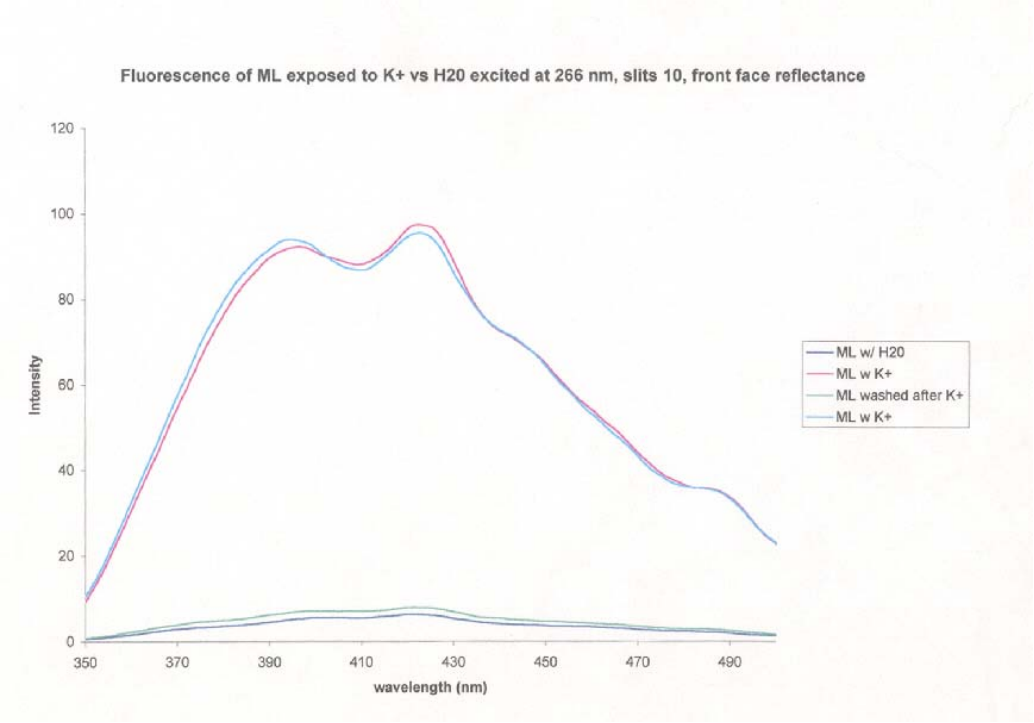

Upon exposure to a concentrated solution of potassium acetate, a 10 fold increase in the fluorescence output of the layer was observed. Upon continuous flushing with deionized water, the potassium ion could be washed out of the sensor, and the fluorescence returned to its baseline value. A second exposure to potassium ions again causes a 10 fold increase in the fluorescence output of the layer.

It is important to note that these experiments were not overly precise, with a great amount of fluctuation in the fluorescence measurements over the measurement of many samples.

Nevertheless, this work has demonstrated the ability to measure the optical properties of a monolayer, which in turn, leads us to believe that photochemical reactions will also be possible on quartz monolayers. It has also served to illustrate that fluoroionophores can be self-assembled on quartz substrates, and that they can possibly still perform as sensors. Future work will focus on increasing the consistency of the results obtained previously, and to incorporate ion specific fluoroionophores into a thin film.

5. Materials and Methods

The synthesis of linear peptide [-L-Pya-D-Ala-]$_4$ was previously described with the syntheses of all other cyclic peptides. Spectra for all compounds, as well as synthetic schemes, are included in Appendix A.

Materials. All materials were used as received from their respective companies. Unless otherwise noted, reagents and solvents were purchased from Sigma-Aldrich.

General Methods.

Monolayer Preparation on Quartz. Quartz monolayers were formed by first cleaning a 1 cm^2 piece of quartz in piranha solution followed by KOH. The surfaces were washed with distilled deionized water after treatment with each cleaning solution. A 0.1 M solution of 7N-Anthrylmethyl, 16N-decyl(10-trichlorosilyl), 1,4,10,13-tetraoxa-7,16-diazacyclooctadecane was prepared in DMSO. Although traditionally hexadecane is required, our disubstituted crown was not soluble in that medium. Monolayers were grown by exposing the clean quartz substrate to the 0.1 M DMSO solution, and heating at 40º C for 8 h. Completeness was monitored via contact angle measurements, and via fluorimetry.

Photophysical Measurements. All fluorescence measurements were performed using a Perkin-Elmer LS-50B spectrophotometer. Solution studies were performed in a 1 cm^2 quartz fluorescence cuvette with the emission and excitation slits set at 5 nm. The solutions were not degassed. Monolayer fluorescence was monitored via front face reflectance with excitation and emission slits set to 10 nm.

Synthetic Procedures. NMR spectra were obtained in an Avance Bruker NMR spectrometer at 400 MHz for proton and 85 MHz for 13C. Mass Spectra were measured by the SynPep Corporation in Dublin, CA. Samples were ionized by electrospray ionization, using acetonitrile as a carrier solvent with ultra-high purity nitrogen as a curtain gas. IR spectra were obtained using a Nexus FT-IR spectrometer equipped with either a transmission or ATR accessory, depending on the sample. Melting points were obtained on a Mel-Temp melting point apparatus and appear uncorrected.

A. Synthesis of 3,6-di(1-pyrenylmethyl)piperazine-2,5-dione (Diketopiperazine synthesis).

(i) L, 1-pyrenyl alanine methyl ester.

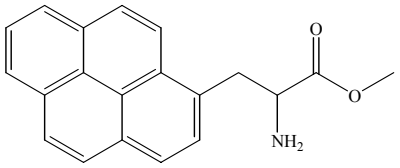

L, 1-pyrenyl alanine (2 g, 3.45 mmol) was dissolved in 250 mL of methanol in a three-necked flask. Hydrogen chloride gas was then bubbled through the flask for a period of 5 h. The solvent was removed under reduced pressure to yield 1.02 g of the off-white product. Yield: 97%; ^{1}H-NMR ($CDCl_3$) δ 2.03 (m, 2H, pyrene-*CH_2*); 3.55 (m, chiral CH), 3.78 (s, CH_3), 7.5-8 (m, pyrene H's).

(ii) Methyl 2-{[2-(Fluorenemethoxycarbonylamino)-3-pyrenylpropyl]amino}3-pyrenylpropanoate (FMoc-Pya-Pya-OMe Dipeptide).

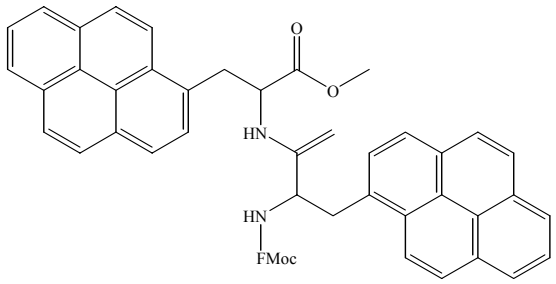

N-Fmoc 1-pyrenyl alanine (1.7 g, 3.32 mmol) was dissolved in a 100 mL of 9:1 DCM:DMF. To this mixture, 1 g (3.30 mmol) of L, 1-pyrenyl alanine methyl ester was added, along with 3.44 g PyBop (6.60 mmol), 0.792 g HOBT (6.60 mmol), and 3.20 mL of DIPEA (19.8 mmol). The solution was stirred at room temperature for 18 h, at which point the solvent was removed via rotary evaporation. The crude residue was dissolved in ethyl acetate, and washed 3 times with 25 mL portions of 2.5% Citric Acid, and 3 times with saturated sodium bicarbonate. The organic phase was dried over anhydrous sodium sulfate, and the solvent removed to yield 1.99 g of a yellowish oil. Yield: 76%. No spectral data was obtained due to problems with solubility.

(iii) 3,6-di(1-pyrenylmethyl)piperazine-2,5-dione (Dipyrenyl diketopiperazine).

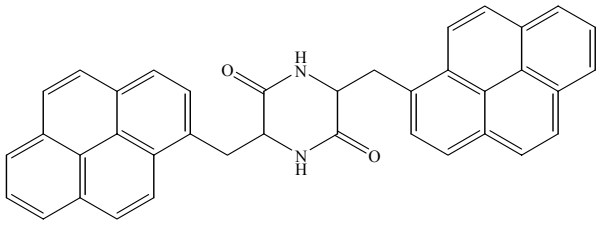

A 1.5 g sample (.00188 mmol) of the product obtained in the previous step was dissolved in 50 mL of 20% piperidine in DCM and stirred for 20 minutes at r.t. to deprotect the N-terminus. The solvent was then removed via rotary evaporation, which resulted in a

majority of the crude free amine product cyclizing due to the elevated temperature. The crude product was then dissolved in n-butanol, and refluxed for an additional 1.5 h to drive the cyclization reaction to completion. The crude product precipitated out of solution as it was formed, and was collected via vacuum filtration to yield 326 mg of yellow product. Yield: 32.6%; ESI-MS (Negative Mode) $(M-1)^-$ = 541.3 (calc.541.6).

B. Synthesis of 7N-Anthrylmethyl, 16N-decyl(10-trichlorosilyl), 1,4,10,13-tetraoxa-7,16-diazacyclooctadecane (Disubstitued Diaza 18-crown-6)

(i) 10-bromo-1-decene.

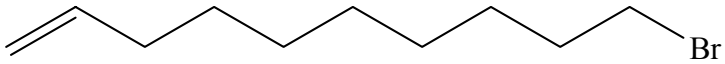

In a dry flask, 5 g (32.1 mmol) of 9-decen-1-ol was dissolved in 150 mL of benzene. To this mixture, 2.06 mL (11.4 mmol) of PBr_3 was slowly added, and the reaction heated to reflux for a period of 2 h. The resulting mixture was poured into a separatory funnel containing 450 mL of 3:2 ethyl ether:water. The organic phase was washed three times with saturated sodium carbonate, and was dried over anhydrous sodium sulfate. The product was concentrated via rotary evaporation to yield 6.85 g of a clear oil. Yield: 97 %; ^{1}H-NMR ($CDCl_3$) δ 1.357 (m, 8H, alkyl CH_2); 1.714 (m, 2H, *CH_2*CH); 1.818 (m, 2H, *CH_2*CH_2CH_2Br); 2.032 (m, 2H, *CH_2*CH_2Br); 3.39 (t, 2H, CH_2Br); 4.944 (d of d, 2H, *CH_2*=CH); 5.816 (m, 1H, CH_2=*CH*); ^{13}C-NMR δ 25.836; 28.116; 29.402; 29.449; 30.618; 30.684; 41.518; 52.361; 114.591; 139.523; GCMS retention time 3.5 min at 200º C; *(m/z)* $[M]^+$ = 220.0 (MW_{calcd} 220).

(ii) 7N-Anthrylmethyl, 1,4,10,13-tetraoxa-7,16-diazacyclooctadecane.

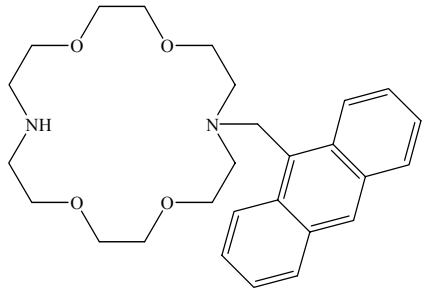

A 2g (7.63 mmol) sample of 1,4,10,13-tetraoxa-7,16-diazacyclooctadecane was dissolved in 200 mL of acetone along with 2.94 g (15.26 mmol) of cesium iodide, and 0.198 g (.763 mmol) of cesium iodide. The solution was heated to reflux, and 1.72 g (7.63 mmol) of anthryl chloride dissolved in 50 mL of acetone was added drop wise via an addition funnel over a period of 3 h. The reaction mixture was refluxed for an additional 4 h, and the mixture filtered hot to remove cesium carbonate. The acetone was removed via rotary evaporation, and the crude mixture dissolved in ethyl acetate. The organic phase was washed three times was 2.5% citric acid, and dried over anhydrous magnesium sulfate. The crude product was concentrated by rotary evaporation, and recrystallized from methanol to yield 1.6 g of a fine yellow powder. Yield: 46.3%; ^{1}H-NMR ($CDCl_3$) δ 2.902 (m, 8H, CH_2N crown); 3.62 (m, 16H, CH_2O crown); 4.613 (s, 2H, NCH_2-anthracene); 6.98-8.53 (m, 9H, anthracene); ^{13}C-NMR δ 49.271; 49.371; 53.678; 70.155; 70.266; 70.413; 70.932; 124.803-131.36 (anthracene); ESI-MS *(m/z)* $[M+Cs]^+$ = 585.1; $[M+1]^+$ = 453.2 (MW_{calcd} 585.5 and 453.6 respectively)

(iii) 7N-Anthrylmethyl, 16N-dec-10-enyl, 1,4,10,13-tetraoxa-7,16-diazacyclooctadecane.

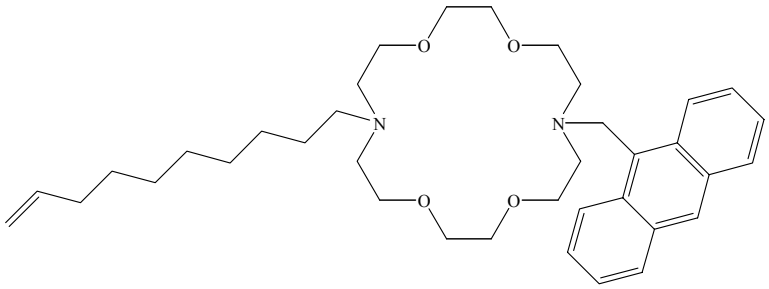

A 1.5 g (3.30 mmol) sample of 7N-Anthrylmethyl, 1,4,10,13-tetraoxa-7,16-diazacyclooctadecane was dissolved in acetone along with 1.39 g (6.60 mmol) of cesium carbonate, .094 g of cesium iodide, and 0.798 g of 10-bromo-1-decene. The reaction mixture was heated to reflux for a period of 4 h, and the solution filtered hot to remove excess cesium salts. The filtrate was concentrated by rotary evaporation, and the crude mixture recrystallized from chloroform and hexane to yield 1.05 g of light yellow powder. Yield: 54%; ^{1}H-NMR δ 1.346 (m, 14H, alkyl chain CH_2); 2.047 (t, 2H, CH_2-CH_2-*CH_2*-N); 2.902 (m, 8H, CH_2N crown); 3.602 (m, 16H, CH_2O crown); 4.569 (s, 2H, N-*CH_2*-anthracene); 4.942 (m, 2H, CH_2=CH); 5.818 (m, 1H, CH=CH_2); 7.420-8.561 (m, 9H, anthracene); ^{13}C-NMR δ 21.886; 26.128; 29.775; 29.944; 33.023; 33.188; 49.505; 52.338; 54.228; 70.532; 70.072; 70.831; 76.955; 114.543; 125.215; 143.584; ESI-MS *(m/z)* $[M+Cs]^+$ = 723.2; $[M+1]^+$ = 591.3 (MW_{calcd} = 723.7 and 590.836 respectively)

(iv) 7N-Anthrylmethyl, 16N-decyl(10-trichlorosilyl), 1,4,10,13-tetraoxa-7,16-diazacyclooctadecane.

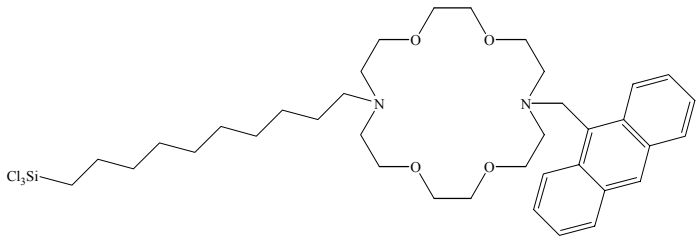

A 0.5 g (0.85 mmol) sample of 7N-Anthrylmethyl, 16N-dec-10-enyl, 1,4,10,13-tetraoxa-7,16-diazacyclooctadecane was dissolved in 50 mL of carbon tetrachloride. To the solution, 0.313 mL (2.55 mmol) of trichlorosilane was added, and the reaction mixed at room temperature for a period of 6 h. Excess trichlorosilane and carbon tetrachloride were removed under reduced pressure to yield 610 mg of crude product, which was then recrystallized in small amounts from chloroform. The product was not spectroscopically examined to any degree due to literature reports that the product was highly unstable, and need not be characterized.

E. APPENDICES

1. Reaction Schemes and Spectroscopic Data

Scheme 1. Synthesis of N-FMoc L, Pyrenyl Alanine

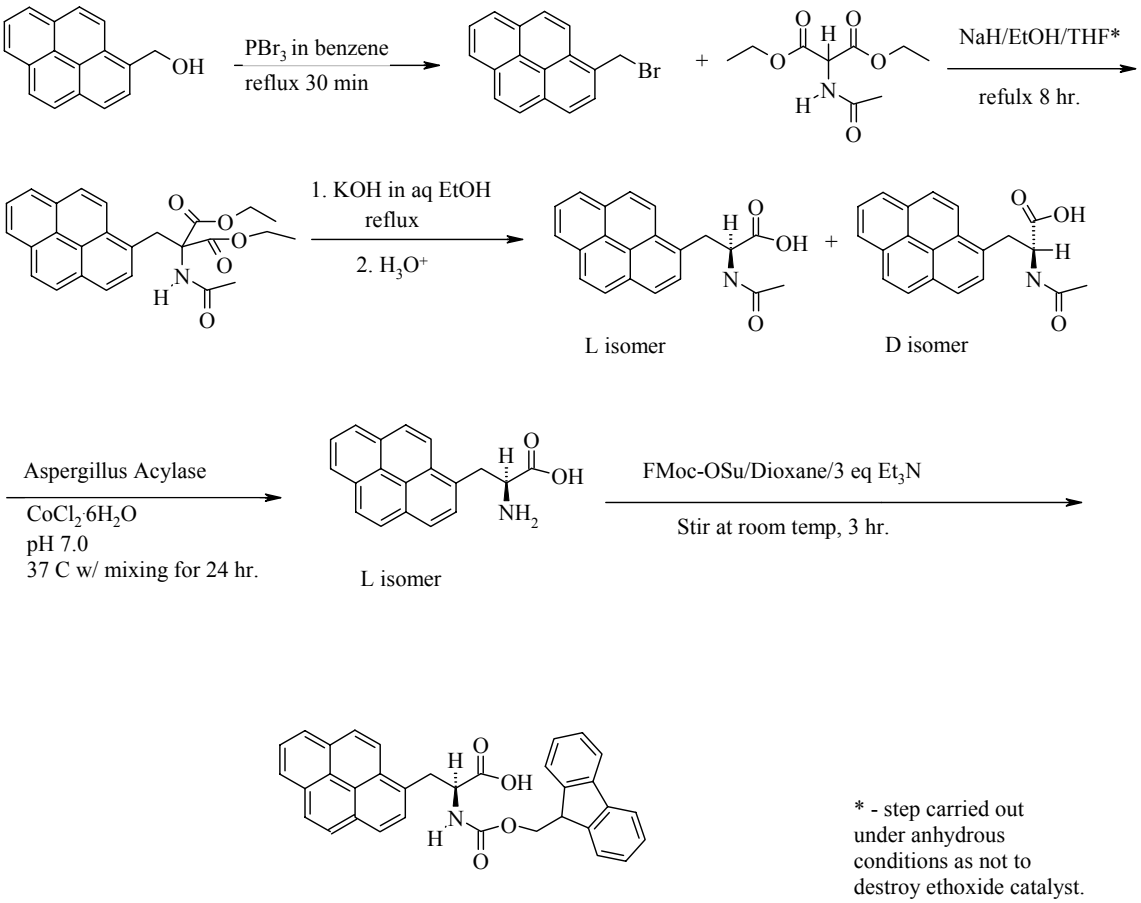

* - step carried out under anhydrous conditions as not to destroy ethoxide catalyst.

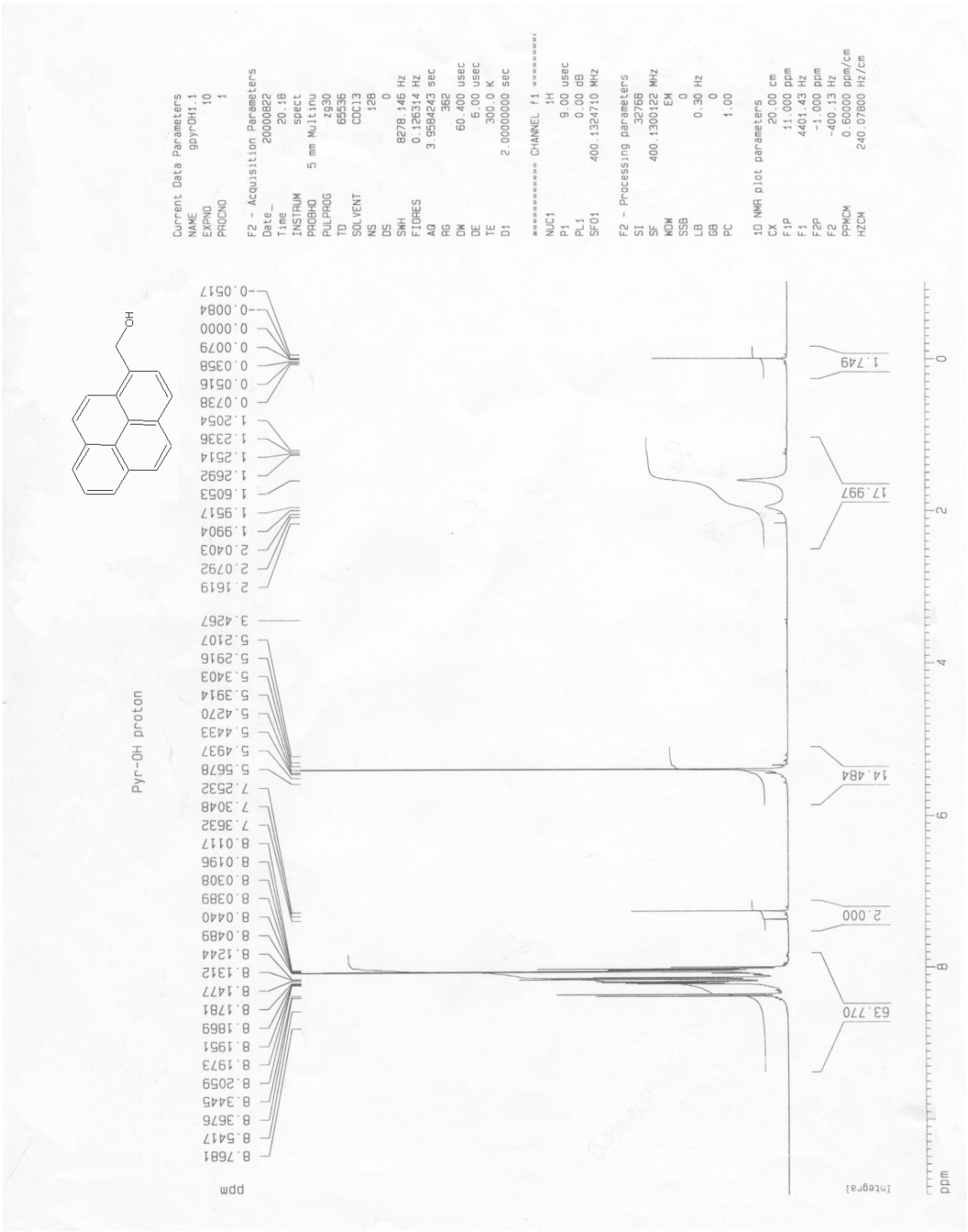
Current Data Parameters
NAME gpyrOH1.1
EXPNO 10
PROCNO 1
F2 - Acquisition Parameters
Date_ 20000822
Time 20.18
INSTRUM spect
PROBHD 5 mm Multinu
PULPROG zg30
TD 65536
SOLVENT CDCl3
NS 128
DS 0
SWH 8278.146 Hz
FIDRES 0.126314 Hz
AQ 3.9584243 sec
RG 362
DW 60.400 usec
DE 6.00 usec
TE 300.0 K
D1 2.00000000 sec
======== CHANNEL f1 ========
NUC1 1H
P1 9.00 usec
PL1 0.00 dB
SFO1 400.1324710 MHz
F2 - Processing parameters
SI 32768
SF 400.1300122 MHz
WDW EM
SSB 0
LB 0.30 Hz
GB 0
PC 1.00
1D NMR plot parameters
CX 20.00 cm
F1P 11.000 ppm
F1 4401.43 Hz
F2P -1.000 ppm
F2 -400.13 Hz
PPMCM 0.60000 ppm/cm
HZCM 240.07800 Hz/cm
Pyr-OH proton
ppm
Integral
63.770
2.000
14.484
17.997
1.749

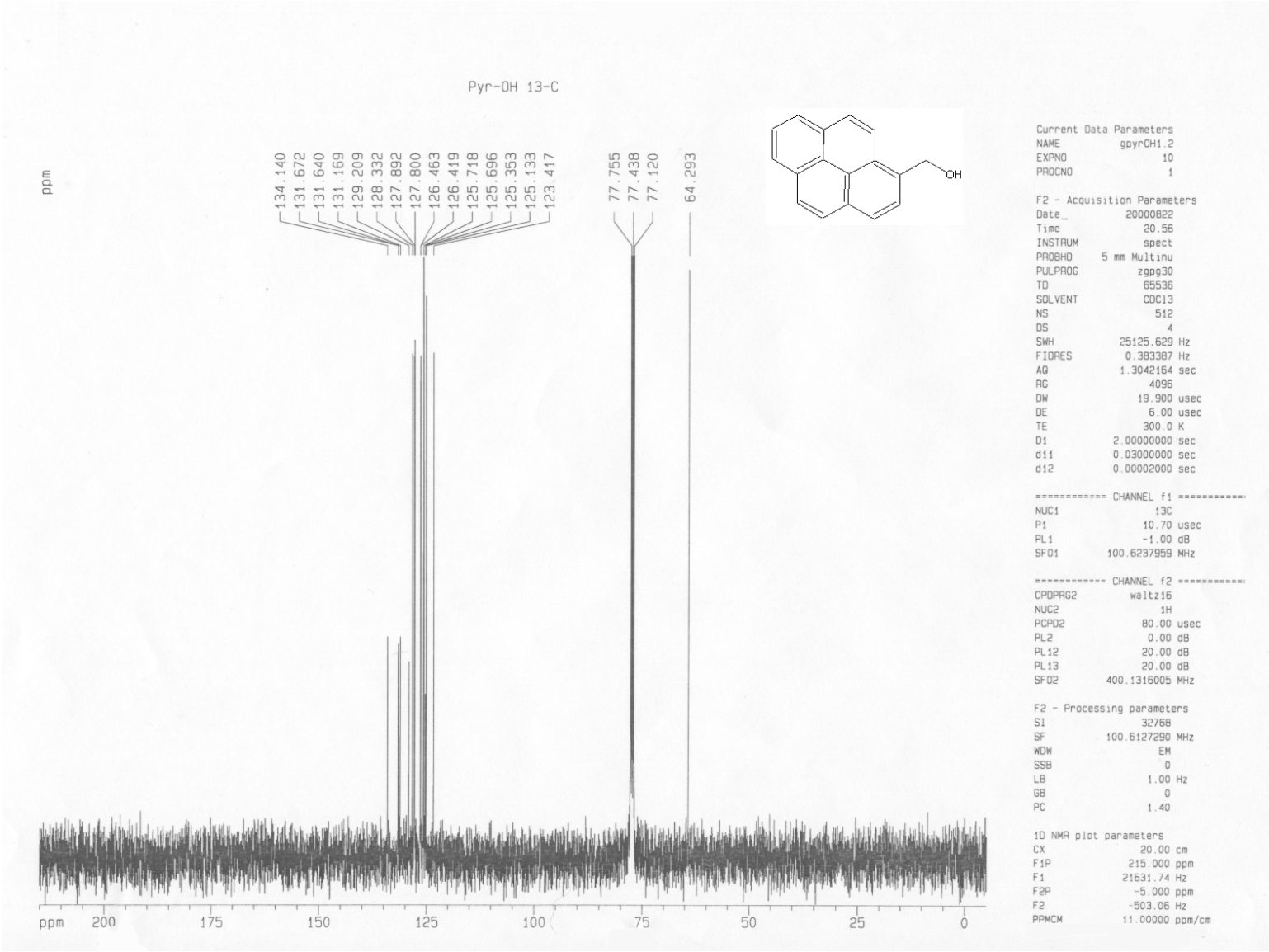
Pyr-OH 13-C
ppm
134.140
131.672
131.640
131.169
129.209
128.332
127.892
127.800
126.463
126.419
125.718
125.696
125.353
125.133
123.417
77.755
77.438
77.120
64.293
OH
ppm 200 175 150 125 100 75 50 25 0
Current Data Parameters
NAME gpyrOH1.2
EXPNO 10
PROCNO 1
F2 - Acquisition Parameters
Date_ 20000822
Time 20.56
INSTRUM spect
PROBHD 5 mm Multinu
PULPROG zgpg30
TD 65536
SOLVENT CDCl3
NS 512
DS 4
SWH 25125.629 Hz
FIDRES 0.383387 Hz
AQ 1.3042164 sec
RG 4096
DW 19.900 usec
DE 6.00 usec
TE 300.0 K
D1 2.00000000 sec
d11 0.03000000 sec
d12 0.00002000 sec
CHANNEL f1
NUC1 13C
P1 10.70 usec
PL1 -1.00 dB
SFO1 100.6237959 MHz
CHANNEL f2
CPDPRG2 waltz16
NUC2 1H
PCPD2 80.00 usec
PL2 0.00 dB
PL12 20.00 dB
PL13 20.00 dB
SFO2 400.1316005 MHz
F2 - Processing parameters
SI 32768
SF 100.6127290 MHz
WDW EM
SSB 0
LB 1.00 Hz
GB 0
PC 1.40
1D NMR plot parameters
CX 20.00 cm
F1P 215.000 ppm
F1 21631.74 Hz
F2P -5.000 ppm
F2 -503.06 Hz
PPMCM 11.00000 ppm/cm

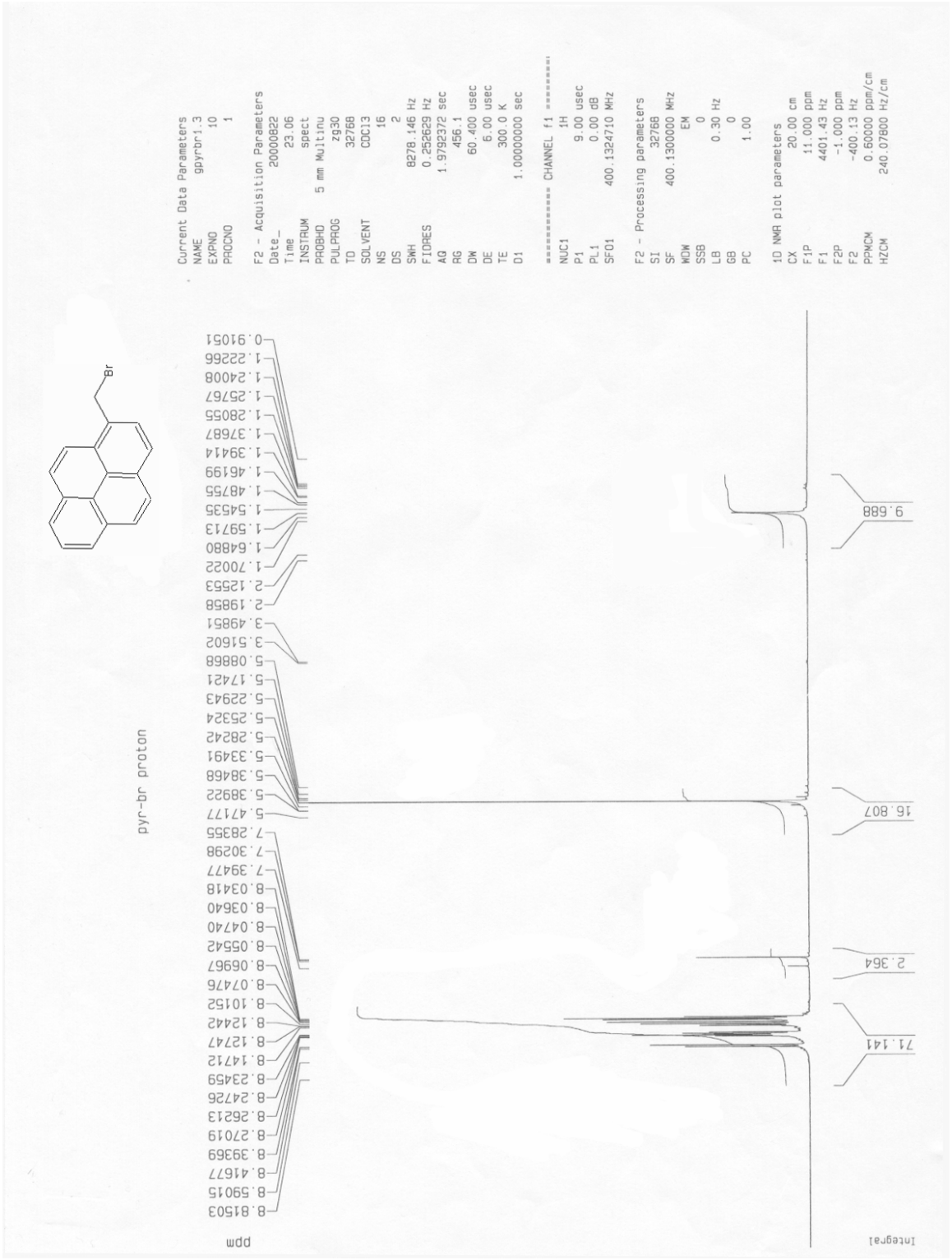
Current Data Parameters
NAME gpyrbr1.3
EXPNO 10
PROCNO 1
F2 - Acquisition Parameters
Date_ 20000822
Time 23.06
INSTRUM spect
PROBHD 5 mm Multinu
PULPROG zg30
TD 32768
SOLVENT CDCl3
NS 16
DS 2
SWH 8278.146 Hz
FIDRES 0.252629 Hz
AQ 1.9792372 sec
RG 456.1
DW 60.400 usec
DE 6.00 usec
TE 300.0 K
D1 1.00000000 sec
======== CHANNEL f1 ========
NUC1 1H
P1 9.00 usec
PL1 0.00 dB
SF01 400.1324710 MHz
F2 - Processing parameters
SI 32768
SF 400.1300000 MHz
WDW EM
SSB 0
LB 0.30 Hz
GB 0
PC 1.00
1D NMR plot parameters
CX 20.00 cm
F1P 11.000 ppm
F1 4401.43 Hz
F2P -1.000 ppm
F2 -400.13 Hz
PPMCM 0.60000 ppm/cm
HZCM 240.07800 Hz/cm
Br
pyr-br proton
ppm
Integral
9.688
16.807
2.364
71.141

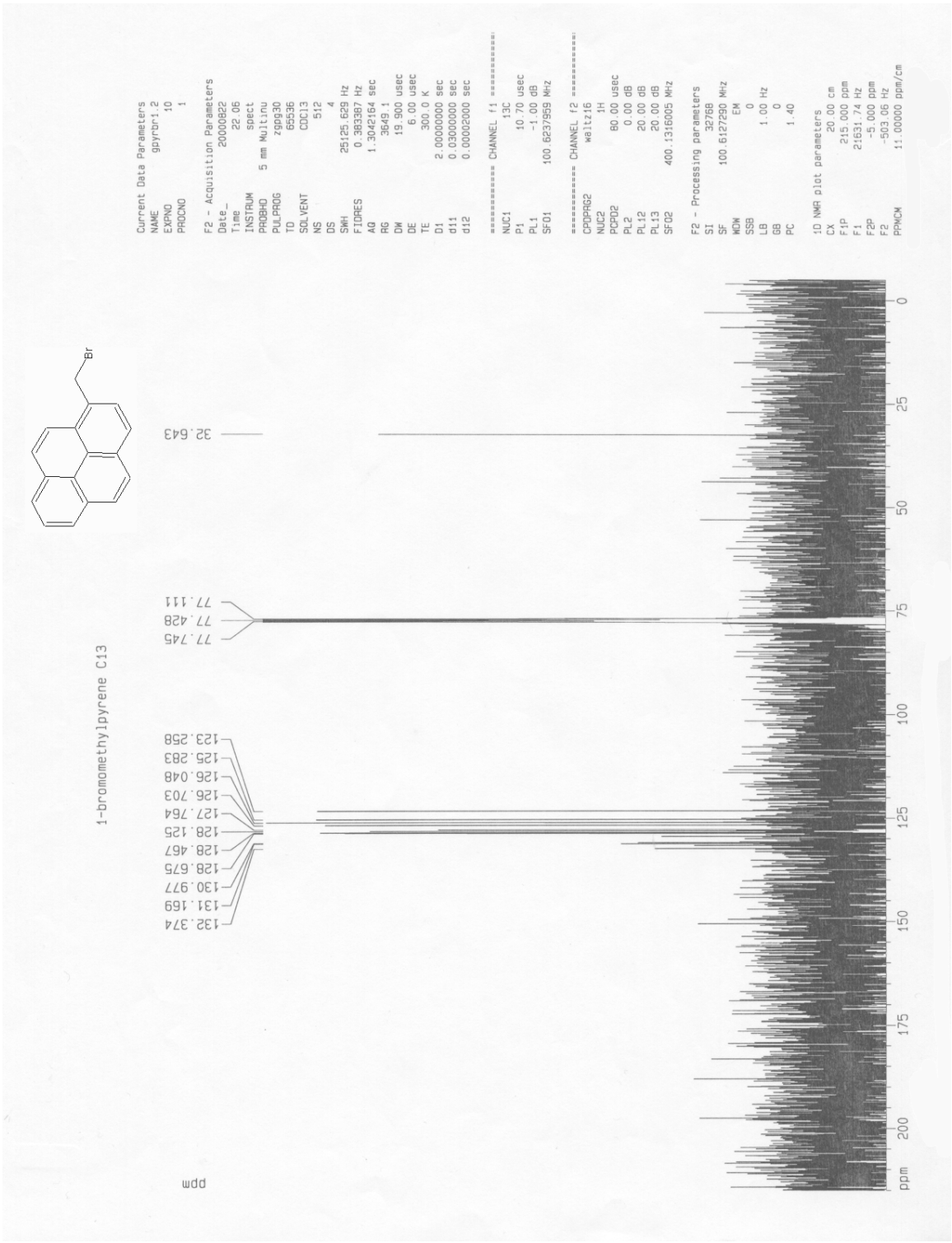
1-bromomethylpyrene C13
Br
32.643
77.111
77.428
77.745
123.258
125.283
126.048
126.703
127.764
128.125
128.467
128.675
130.977
131.169
132.374
Current Data Parameters
NAME gpyrbr1.2
EXPNO 10
PROCNO 1
F2 - Acquisition Parameters
Date_ 20000822
Time 22.06
INSTRUM spect
PROBHD 5 mm Multinu
PULPROG zgpg30
TD 65536
SOLVENT CDCl3
NS 512
DS 4
SWH 25125.629 Hz
FIDRES 0.383307 Hz
AQ 1.3042164 sec
RG 3649.1
DW 19.900 usec
DE 6.00 usec
TE 300.0 K
D1 2.00000000 sec
d11 0.03000000 sec
d12 0.00002000 sec
======== CHANNEL f1 ========
NUC1 13C
P1 10.70 usec
PL1 -1.00 dB
SFO1 100.6237959 MHz
======== CHANNEL f2 ========
CPDPRG2 waltz16
NUC2 1H
PCPD2 80.00 usec
PL2 0.00 dB
PL12 20.00 dB
PL13 20.00 dB
SFO2 400.1316005 MHz
F2 - Processing parameters
SI 32768
SF 100.6127290 MHz
WDW EM
SSB 0
LB 1.00 Hz
GB 0
PC 1.40
1D NMR plot parameters
CX 20.00 cm
F1P 215.000 ppm
F1 21631.74 Hz
F2P -5.000 ppm
F2 -503.06 Hz
PPMCM 11.00000 ppm/cm
ppm
0
25
50
75
100
125
150
175
200

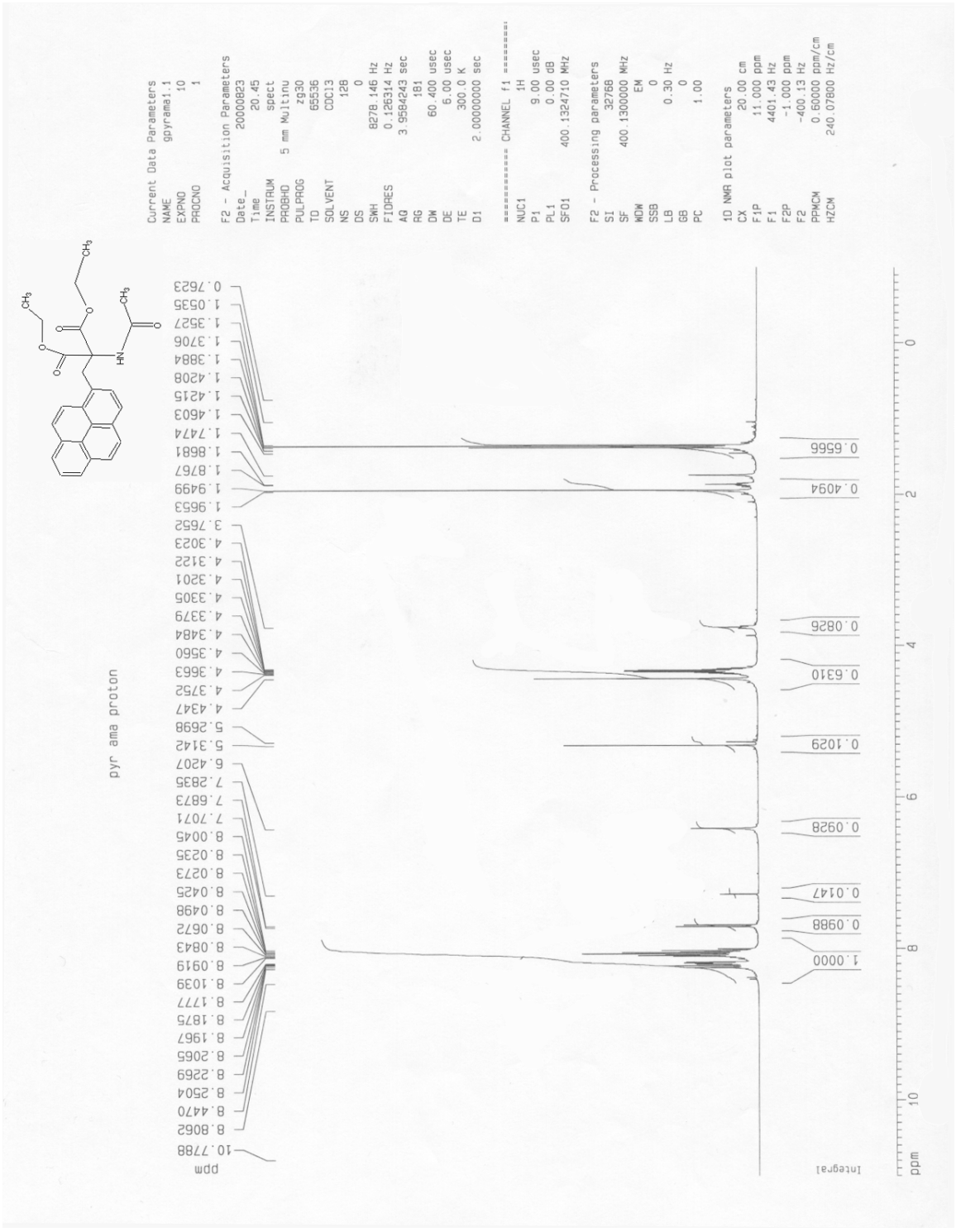
pyr ama proton
ppm
Integral
Current Data Parameters
NAME gpyrama1.1
EXPNO 10
PROCNO 1
F2 - Acquisition Parameters
Date_ 20000823
Time 20.45
INSTRUM spect
PROBHD 5 mm Multinu
PULPROG zg30
TD 65536
SOLVENT CDCl3
NS 128
DS 0
SWH 8278.146 Hz
FIDRES 0.126314 Hz
AQ 3.9584243 sec
RG 181
DW 60.400 usec
DE 6.00 usec
TE 300.0 K
D1 2.00000000 sec
======== CHANNEL f1 ========
NUC1 1H
P1 9.00 usec
PL1 0.00 dB
SFO1 400.1324710 MHz
F2 - Processing parameters
SI 32768
SF 400.1300000 MHz
WDW EM
SSB 0
LB 0.30 Hz
GB 0
PC 1.00
1D NMR plot parameters
CX 20.00 cm
F1P 11.000 ppm
F1 4401.43 Hz
F2P -1.000 ppm
F2 -400.13 Hz
PPMCM 0.60000 ppm/cm
HZCM 240.07800 Hz/cm
10.7788
8.8062
8.4470
8.2504
8.2269
8.2065
8.1967
8.1875
8.1777
8.1039
8.0919
8.0843
8.0672
8.0498
8.0425
8.0273
8.0235
8.0045
7.7071
7.6873
7.2835
6.4207
5.3142
5.2698
4.4347
4.3752
4.3663
4.3560
4.3484
4.3379
4.3305
4.3201
4.3122
4.3023
3.7652
1.9653
1.9499
1.8767
1.8681
1.7474
1.4603
1.4215
1.4208
1.3884
1.3706
1.3527
1.0535
0.7623
0.6566
0.4094
0.0826
0.6310
0.1029
0.0928
0.0147
0.0988
1.0000

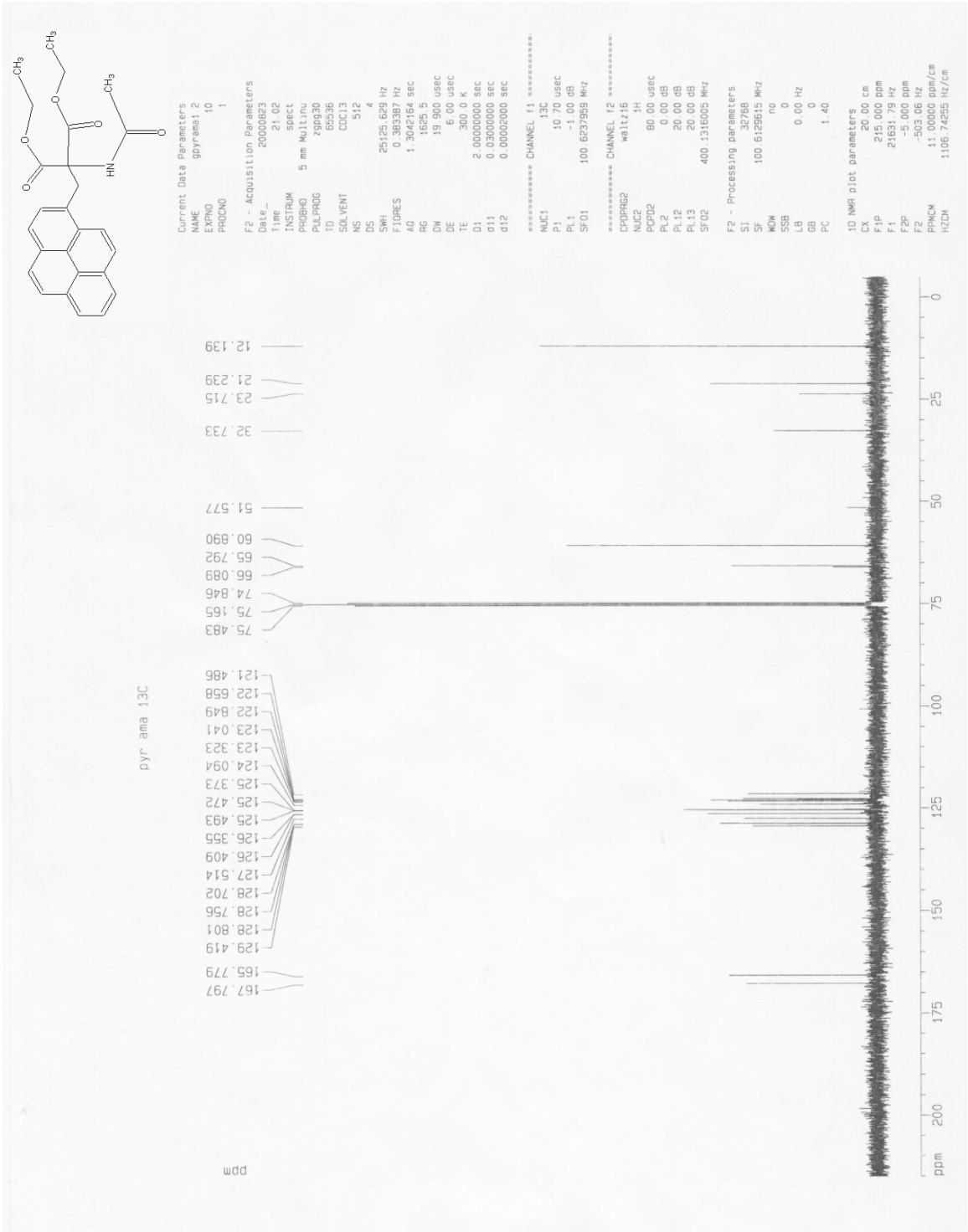
pyr ama 13C
ppm
Current Data Parameters
NAME gpyrama1.2
EXPNO 10
PROCNO 1
F2 - Acquisition Parameters
Date_ 20000823
Time_ 21.02
INSTRUM spect
PROBHD 5 mm Multinu
PULPROG zgpg30
TD 65536
SOLVENT CDCl3
NS 512
DS 4
SWH 25125.629 Hz
FIDRES 0.383387 Hz
AQ 1.3042164 sec
RG 1625.5
DW 19.900 usec
DE 6.00 usec
TE 300.0 K
D1 2.00000000 sec
d11 0.03000000 sec
d12 0.00002000 sec
CHANNEL f1
NUC1 13C
P1 10.70 usec
PL1 -1.00 dB
SFO1 100.6237959 MHz
CHANNEL f2
CPDPRG2 waltz16
NUC2 1H
PCPD2 80.00 usec
PL2 0.00 dB
PL12 20.00 dB
PL13 20.00 dB
SFO2 400.1316005 MHz
F2 - Processing parameters
SI 32768
SF 100.6128615 MHz
WDW no
SSB 0
LB 0.00 Hz
GB 0
PC 1.40
1D NMR plot parameters
CX 20.00 cm
F1P 215.000 ppm
F1 21631.79 Hz
F2P -5.000 ppm
F2 -503.06 Hz
PPMCM 11.00000 ppm/cm
HZCM 1106.74255 Hz/cm
12.139
21.239
23.715
32.733
51.577
60.890
65.792
66.089
74.846
75.165
75.483
121.486
122.658
122.849
123.041
123.323
124.094
125.373
125.472
125.493
126.355
126.409
127.514
128.702
128.756
128.801
129.419
165.779
167.797

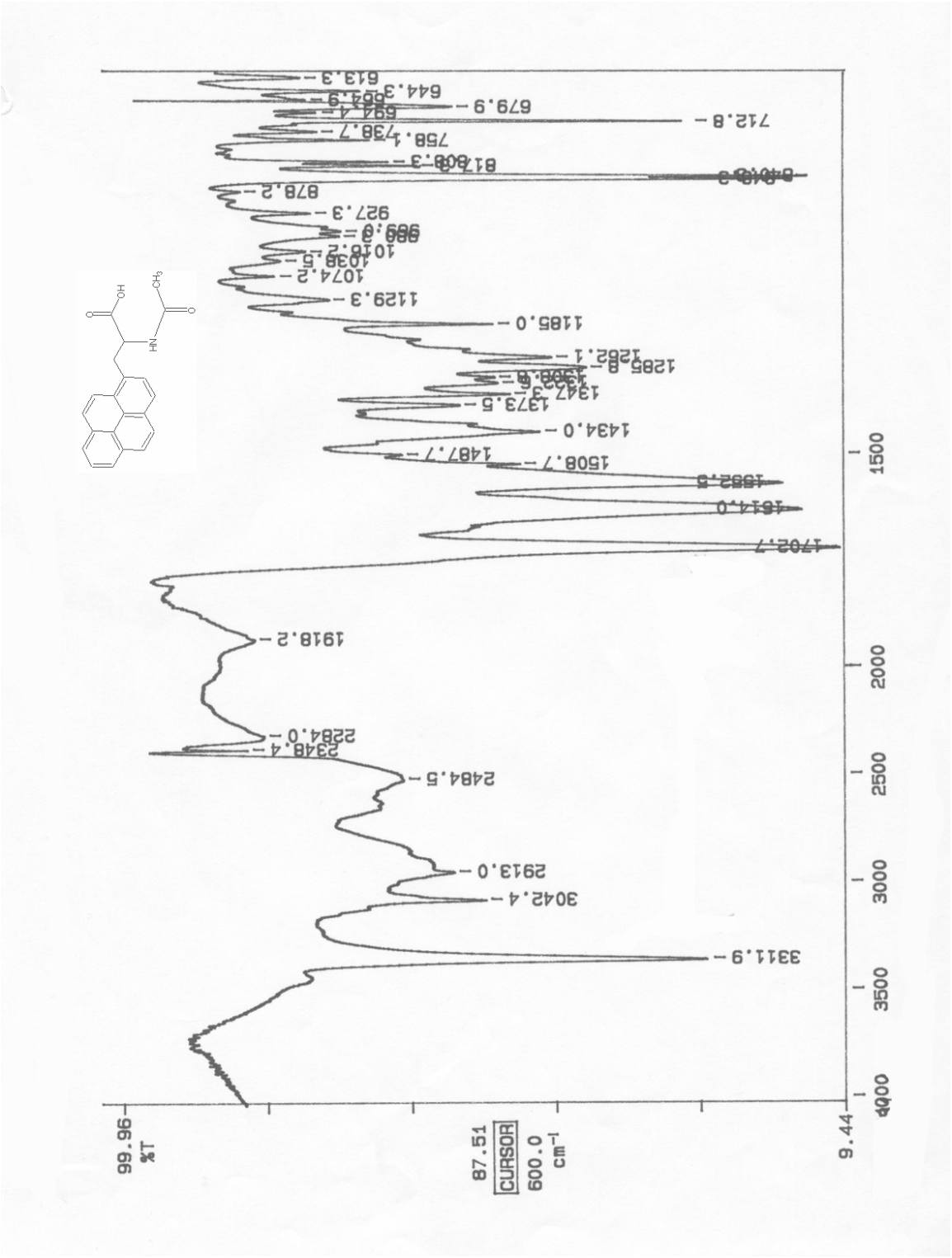
99.96
%T
87.51
CURSOR
600.0
cm-1
9.44
4000
3500
3000
2500
2000
1500
3311.9
3042.4
2913.0
2484.5
2348.4
2284.0
1918.2
1702.7
1614.0
1582.5
1508.7
1487.7
1434.0
1373.5
1347.3
1285.8
1262.1
1185.0
1129.3
1074.2
1038.5
1018.2
927.3
878.2
812.3
758.7
738.7
712.8
679.9
644.3
613.3

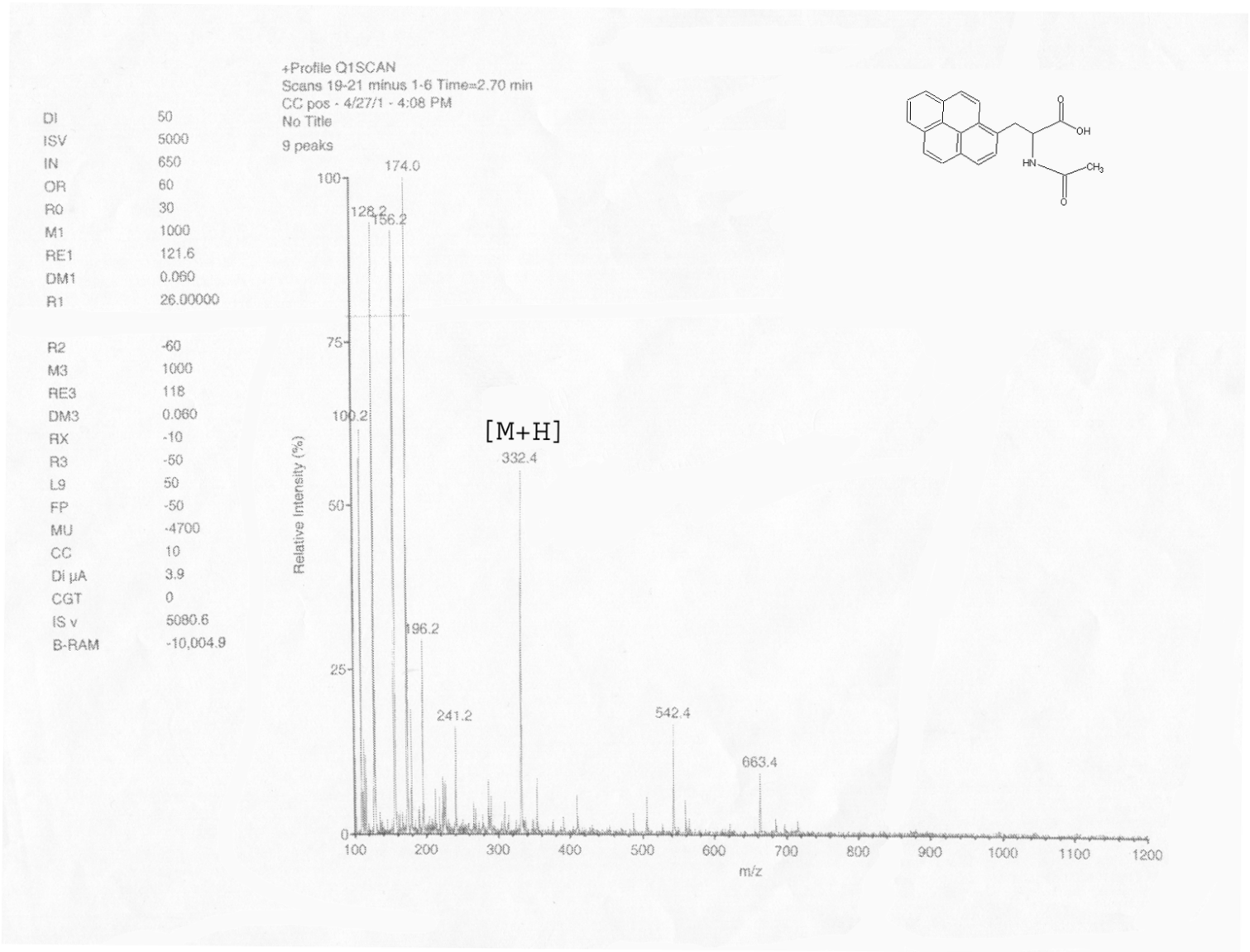
+Profile Q1SCAN
Scans 19-21 minus 1-6 Time=2.70 min
CC pos - 4/27/1 - 4:08 PM
No Title
9 peaks
DI 50
ISV 5000
IN 650
OR 60
R0 30
M1 1000
RE1 121.6
DM1 0.060
R1 26.00000
R2 -60
M3 1000
RE3 118
DM3 0.060
RX -10
R3 -50
L9 50
FP -50
MU -4700
CC 10
Di µA 3.9
CGT 0
IS v 5080.6
B-RAM -10,004.9
174.0
128.2
156.2
100.2
196.2
241.2
[M+H]
332.4
542.4
663.4
Relative Intensity (%)
m/z
OH
HN
CH3

+Profile Q1SCAN
Scans 37-38 minus 40-42 & 1-15 Time=4.25 min
290 pos-2 - 11/1/0 - 2:40 PM
No Title
4 peaks
[M+H]
290.2
273.2
227.1
1,156,222
OH
NH2
Relative Intensity (%)
m/z
0
11
22
32
43
150
200
250
300
350
400
450
DI 50
ISV 4800
IN 650
OR 80
R0 30
M1 1000
RE1 117.6
DM1 0.040
R1 27.8
L9 -100
FP -50
MU -4600
CC 10
DI µA 2.0
IS v 4924.3
UV -464.09
SYNPEP CORP
11/01/2000 14:03 9258039676
PAGE 02

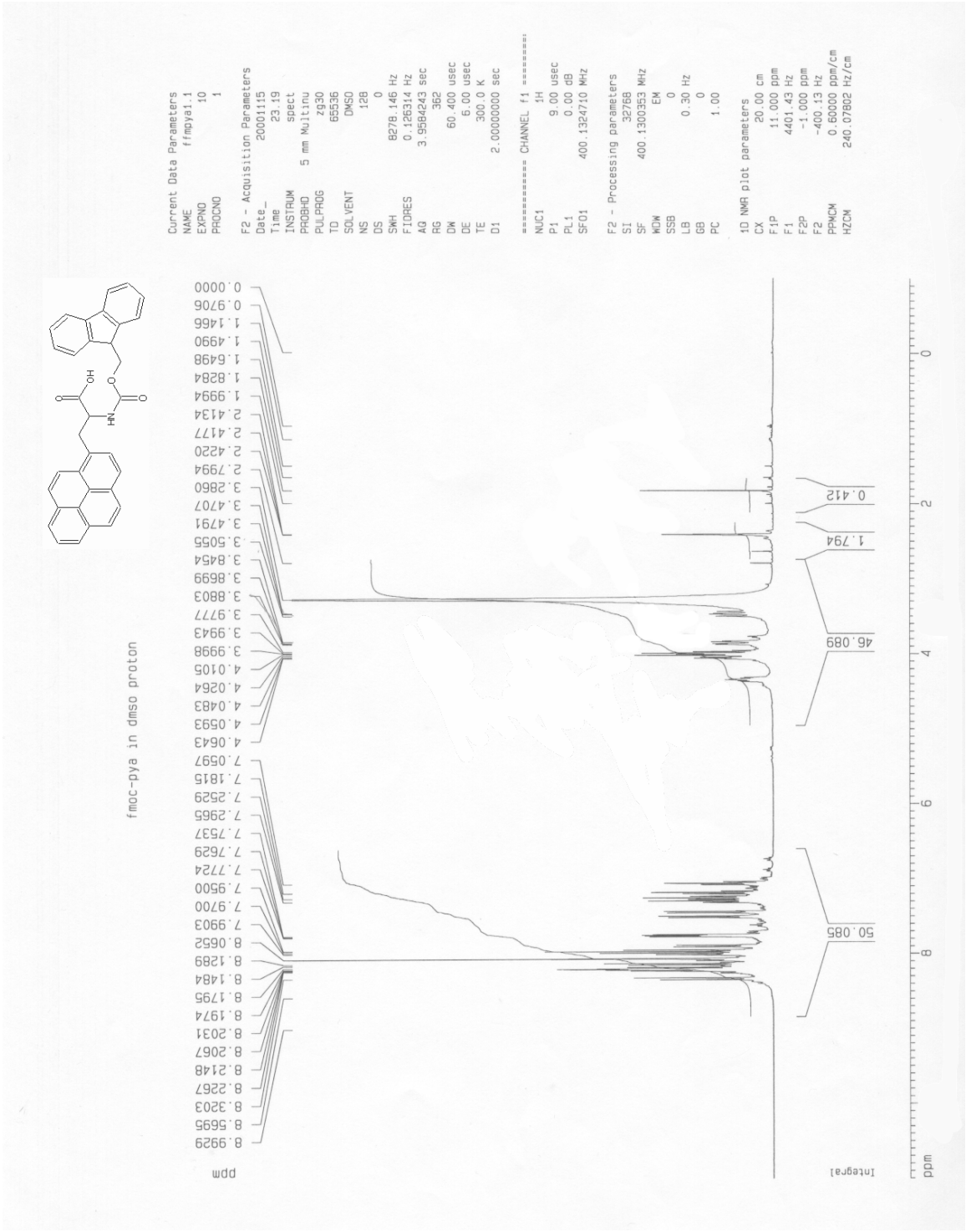
fmoc-pya in dmso proton
Current Data Parameters
NAME ffmoya1.1
EXPNO 10
PROCNO 1
F2 - Acquisition Parameters
Date_ 20001115
Time 23.19
INSTRUM spect
PROBHD 5 mm Multinu
PULPROG zg30
TD 65536
SOLVENT DMSO
NS 128
DS 0
SWH 8278.146 Hz
FIDRES 0.126314 Hz
AQ 3.9584243 sec
RG 362
DW 60.400 usec
DE 6.00 usec
TE 300.0 K
D1 2.00000000 sec
========== CHANNEL f1 ========
NUC1 1H
P1 9.00 usec
PL1 0.00 dB
SFO1 400.1324710 MHz
F2 - Processing parameters
SI 32768
SF 400.1300353 MHz
WDW EM
SSB 0
LB 0.30 Hz
GB 0
PC 1.00
1D NMR plot parameters
CX 20.00 cm
F1P 11.000 ppm
F1 4401.43 Hz
F2P -1.000 ppm
F2 -400.13 Hz
PPMCM 0.60000 ppm/cm
HZCM 240.07802 Hz/cm
ppm
Integral
50.085
46.089
1.794
0.412

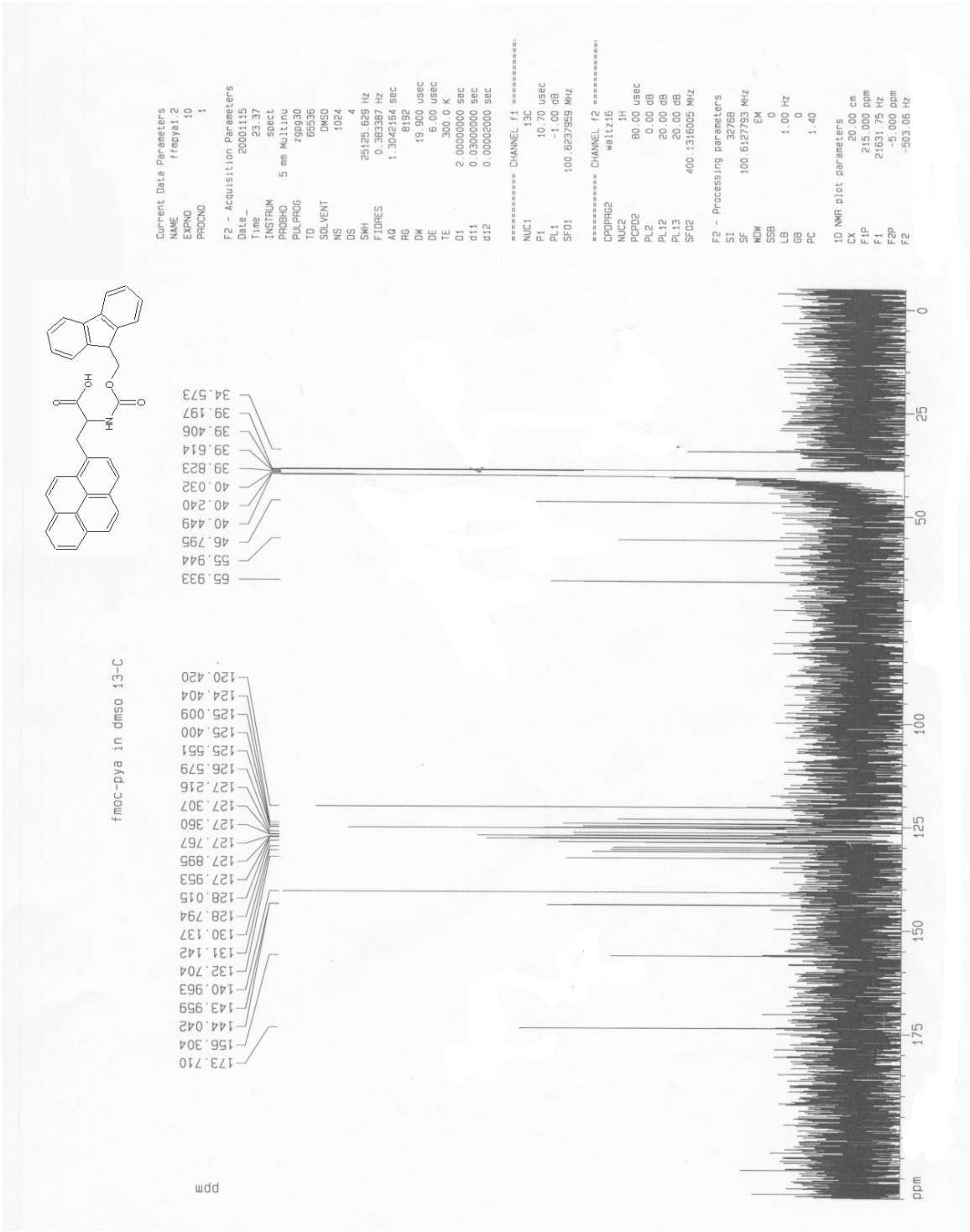
fmoc-pya in dmso 13-C
ppm
Current Data Parameters
NAME ffmpya1.2
EXPNO 10
PROCNO 1
F2 - Acquisition Parameters
Date_ 20001115
Time 23.37
INSTRUM spect
PROBHD 5 mm Multinu
PULPROG zgpg30
TD 65536
SOLVENT DMSO
NS 1024
DS 4
SWH 25125.629 Hz
FIDRES 0.383387 Hz
AQ 1.3042164 sec
RG 8192
DW 19.900 usec
DE 6.00 usec
TE 300.0 K
D1 2.00000000 sec
d11 0.03000000 sec
d12 0.00002000 sec
========== CHANNEL f1 ==========
NUC1 13C
P1 10.70 usec
PL1 -1.00 dB
SFO1 100.6237959 MHz
========== CHANNEL f2 ==========
CPDPRG2 waltz16
NUC2 1H
PCPD2 80.00 usec
PL2 0.00 dB
PL12 20.00 dB
PL13 20.00 dB
SFO2 400.1316005 MHz
F2 - Processing parameters
SI 32768
SF 100.6127793 MHz
WDW EM
SSB 0
LB 1.00 Hz
GB 0
PC 1.40
1D NMR plot parameters
CX 20.00 cm
F1P 215.000 ppm
F1 21631.75 Hz
F2P -5.000 ppm
F2 -503.06 Hz
34.573
39.197
39.406
39.614
39.823
40.032
40.240
40.449
46.795
55.944
65.933
120.420
124.404
125.009
125.400
125.551
126.579
127.216
127.307
127.360
127.767
127.895
127.953
128.015
128.794
130.137
131.142
132.704
140.963
143.959
144.042
156.304
173.710
0
25
50
100
125
150
175
ppm

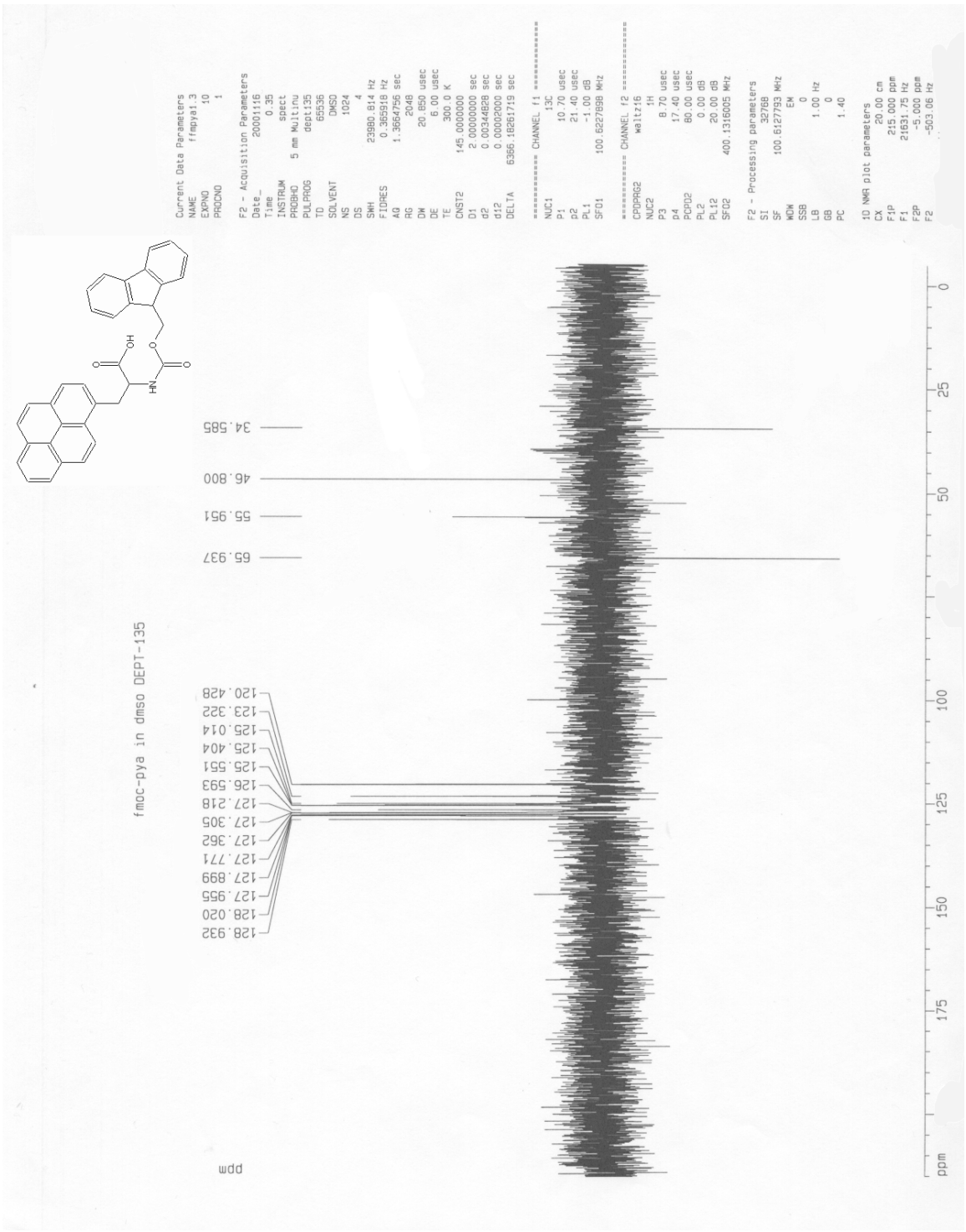
fmoc-pya in dmso DEPT-135
ppm
34.585
46.800
55.951
65.937
120.428
123.322
125.014
125.404
125.551
126.593
127.218
127.305
127.362
127.771
127.899
127.955
128.020
128.932
0
25
50
100
125
150
175
Current Data Parameters
NAME ffmpya1.3
EXPNO 10
PROCNO 1
F2 - Acquisition Parameters
Date_ 20001116
Time 0.35
INSTRUM spect
PROBHD 5 mm Multinu
PULPROG dept135
TD 65536
SOLVENT DMSO
NS 1024
DS 4
SWH 23980.814 Hz
FIDRES 0.365918 Hz
AQ 1.3654756 sec
RG 2048
DW 20.850 usec
DE 6.00 usec
TE 300.0 K
CNST2 145.0000000
D1 2.00000000 sec
d2 0.00344828 sec
d12 0.00002000 sec
DELTA 6366.18261719 sec
======== CHANNEL f1 ========
NUC1 13C
P1 10.70 usec
p2 21.40 usec
PL1 -1.00 dB
SFO1 100.6227898 MHz
======== CHANNEL f2 ========
CPDPRG2 waltz16
NUC2 1H
P3 8.70 usec
p4 17.40 usec
PCPD2 80.00 usec
PL2 0.00 dB
PL12 20.00 dB
SFO2 400.1316005 MHz
F2 - Processing parameters
SI 32768
SF 100.6127793 MHz
WDW EM
SSB 0
LB 1.00 Hz
GB 0
PC 1.40
1D NMR plot parameters
CX 20.00 cm
F1P 215.000 ppm
F1 21631.75 Hz
F2P -5.000 ppm
F2 -503.06 Hz

+Profile Q1SCAN
Scans 22-23 minus 1-4 Time=3.20 min
fmoc pos - 11/30/0 - 6:19 PM
No Title
2 peaks
DI 50
ISV 5000
IN 650
OR 130
R0 30
M1 1000
RE1 122.10
DM1 0.040
R1 26.5
L7 -50
R2 -50
M3 1000
RE3 118
DM3 0.060
RX -10
R3 -50
L9 50
FP -50
MU -4600
CC 10
Di µA 1.10
CGT 0
IS v 5124.6
B-RAM -10,004.9
273.334
[M+K]
550.2
[M+Na]
534.4
Relative Intensity (%)
m/z
100
75
50
25
0
200
300
400
500
600
700
800
900
OH
O
HN
O
O

Scheme 2. Synthesis of cyclo[L-Pya-D-Ala-L-Phe-D-Ala]$_2$

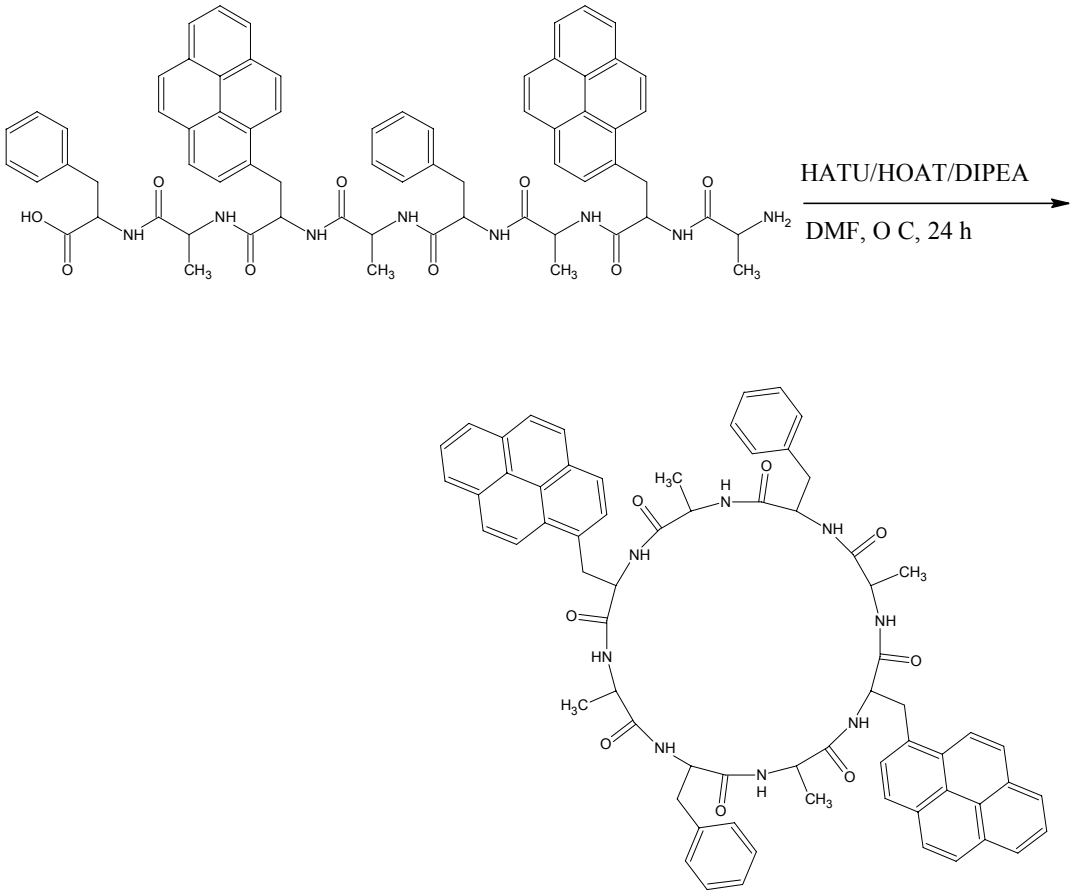

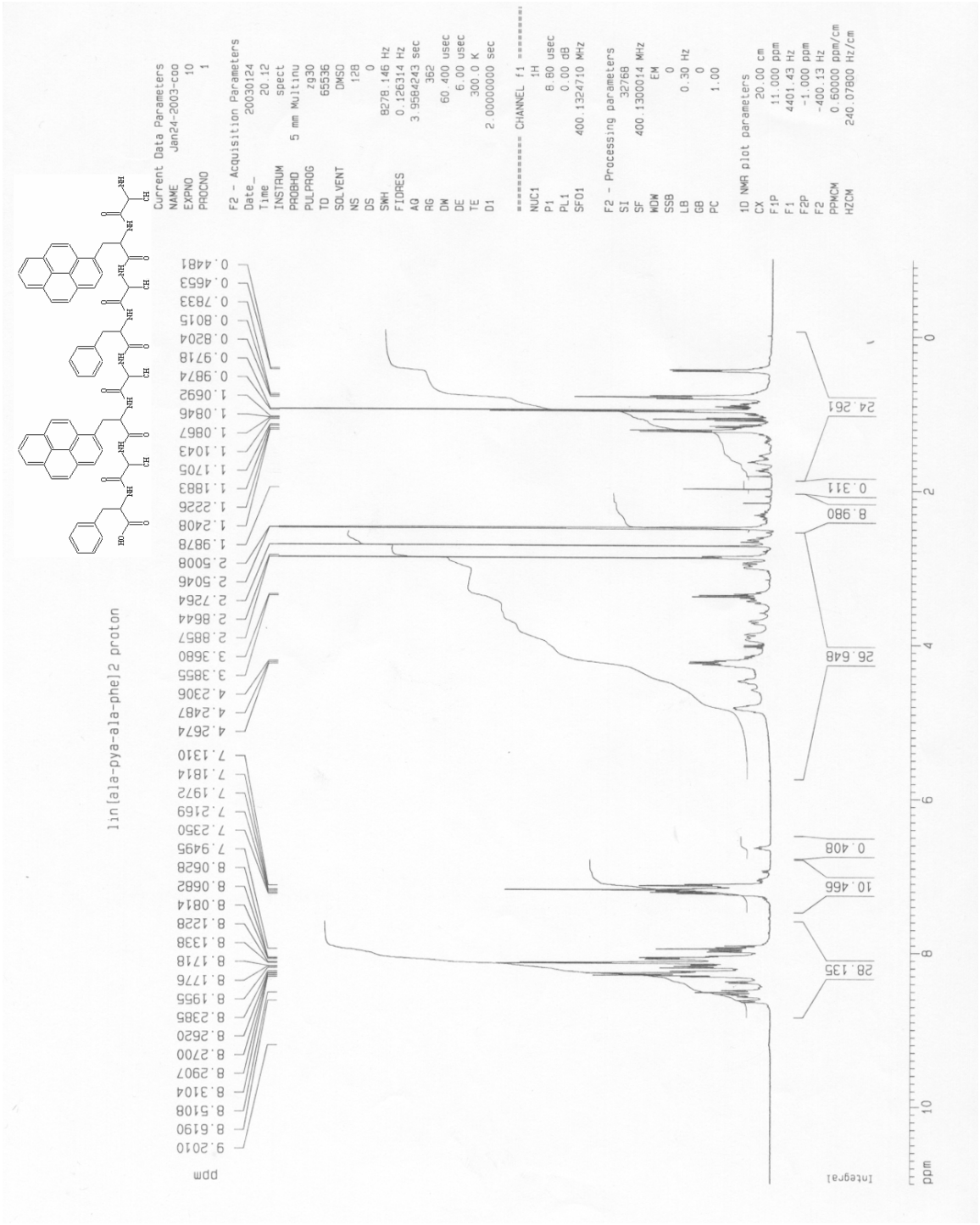
lin[ala-pya-ala-phe]2 proton
Current Data Parameters
NAME Jan24-2003-coo
EXPNO 10
PROCNO 1
F2 - Acquisition Parameters
Date_ 20030124
Time 20.12
INSTRUM spect
PROBHD 5 mm Multinu
PULPROG z930
TD 65536
SOLVENT DMSO
NS 128
DS 0
SWH 8278.146 Hz
FIDRES 0.126314 Hz
AQ 3.9584243 sec
RG 362
DW 60.400 usec
DE 6.00 usec
TE 300.0 K
D1 2.00000000 sec
======== CHANNEL f1 ========
NUC1 1H
P1 8.80 usec
PL1 0.00 dB
SFO1 400.1324710 MHz
F2 - Processing parameters
SI 32768
SF 400.1300014 MHz
WDW EM
SSB 0
LB 0.30 Hz
GB 0
PC 1.00
1D NMR plot parameters
CX 20.00 cm
F1P 11.000 ppm
F1 4401.43 Hz
F2P -1.000 ppm
F2 -400.13 Hz
PPMCM 0.60000 ppm/cm
HZCM 240.07800 Hz/cm
ppm
Integral
24.261
0.311
8.980
26.648
0.408
10.466
28.135

DI	50
ISV	5000
IN	650
OR	120
R0	30
M1	1000
RE1	122.4
DM1	0.060
R1	26.00000
R2	-60
M3	1000
RE3	118
DM3	0.060
RX	-10
R3	-50
L9	50
FP	-50
MU	-4700
CC	10
Di µA	1.8
CGT	-1.3
IS v	5163.7
B-RAM	-10,004.9

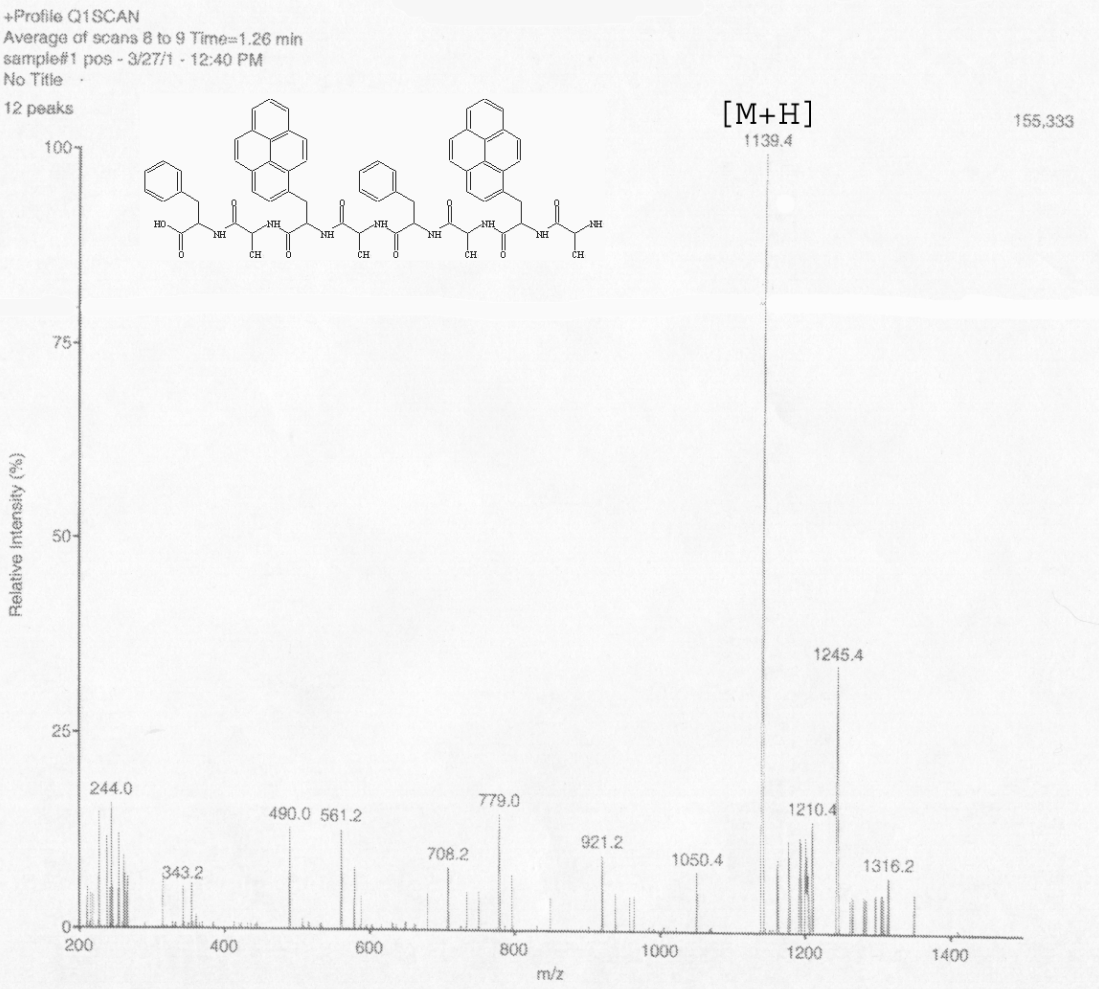

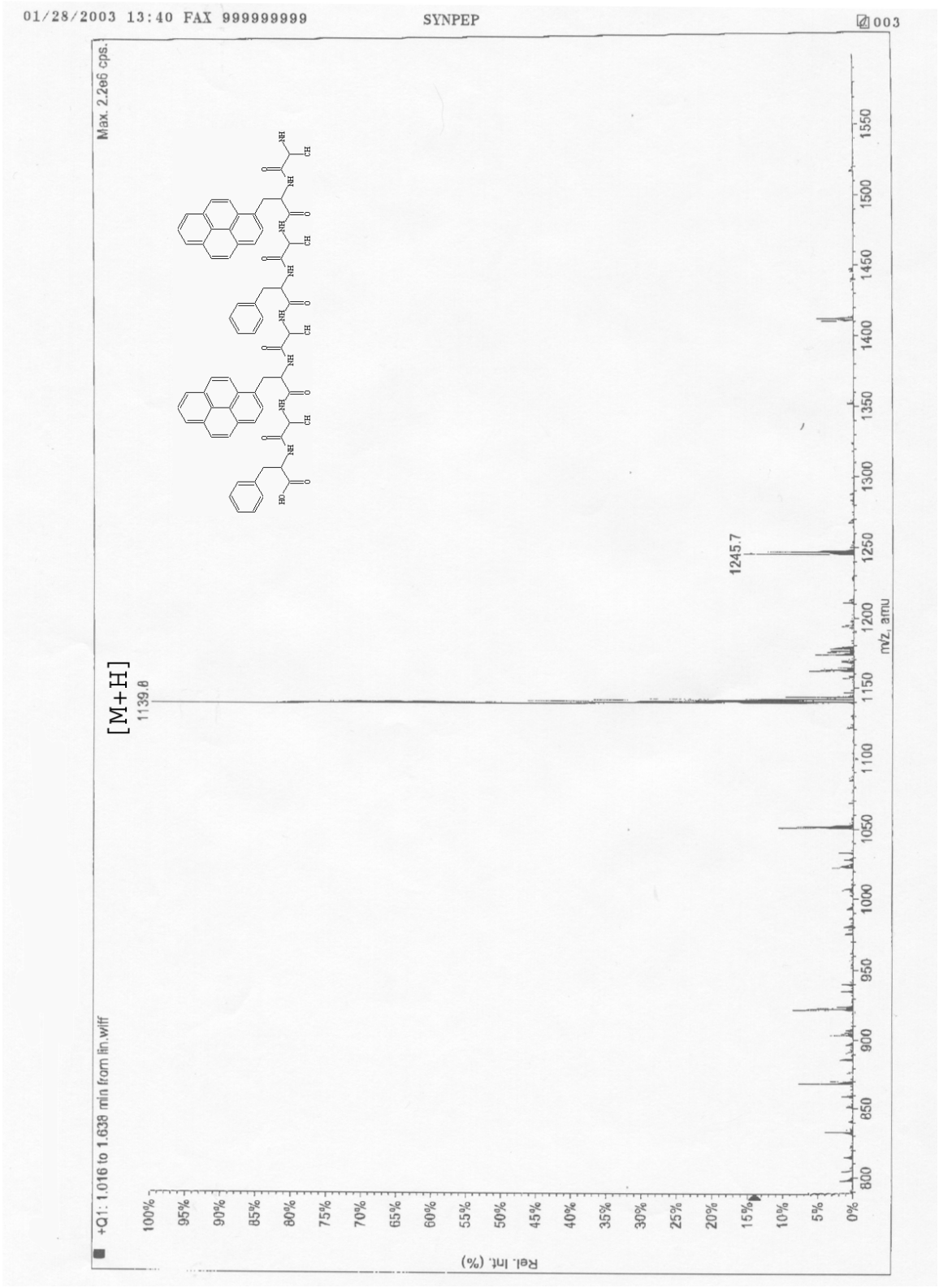
01/28/2003 13:40 FAX 999999999
SYNPEP
003
Max. 2.2e6 cps.
+Q1: 1.016 to 1.638 min from lin.wiff
[M+H]
1139.6
1245.7
Rel. Int. (%)
m/z, amu


cyclic proton
ppm
10.9619
8.6149
8.5109
8.2637
8.2414
8.1973
8.1804
8.1351
8.1250
8.1074
8.0862
8.0695
7.9922
7.9718
7.9506
7.9139
7.2188
7.1840
7.1359
4.2500
4.2313
4.2156
3.5375
3.4655
3.4477
3.4302
3.4128
3.3683
2.9864
2.9603
2.9479
2.8871
2.7284
2.6850
2.5031
1.2678
1.2527
1.2380
1.2221
1.0868
1.0717
1.0542
1.0367
1.0142
0.8923
0.8234
0.8059
0.7379
Integral
1.0000
0.4026
0.2494
1.0951
0.7557
ppm
10
8
6
4
2
0
-Current Data Parameters
NAME Jan25-2003
EXPNO 10
PROCNO 1
F2 - Acquisition Parameters
Date_ 20030125
Time_ 22.14
INSTRUM spect
PROBHD 5 mm Multinu
PULPROG zg30
TD 65536
SOLVENT DMSO
NS 128
DS 0
SWH 8278.146 Hz
FIDRES 0.126314 Hz
AQ 3.9584243 sec
RG 362
DW 60.400 usec
DE 6.00 usec
TE 300.0 K
D1 2.00000000 sec
======== CHANNEL f1 ========
NUC1 1H
P1 8.60 usec
PL1 0.00 dB
SFO1 400.1324710 MHz
F2 - Processing parameters
SI 32768
SF 400.1300000 MHz
WDW EM
SSB 0
LB 0.30 Hz
GB 0
PC 1.00
1D NMR plot parameters
CX 20.00 cm
F1P 11.000 ppm
F1 4401.43 Hz
F2P -1.000 ppm
F2 -400.13 Hz
PPMCM 0.60000 ppm/cm
HZCM 240.07800 Hz/cm

SYNPEP CORP

9258039676

02/23/2002 03:58

DI	50
ISV	5000
IN	650
OR	150
R0	30
M1	1000
RE1	119.2
DM1	0.050
R1	27.00000
L7	0
R2	10
M3	1000
RE3	120.0000
DM3	0.100
RX	-10
R3	-50
L9	-250
FP	200
MU	-3400
CC	1
Di µA	1.7
CGT	1.3
IS v	5129.5

+Profile Q1SCAN
Average of scans 8 to 10 Time=1.07 min
cp b2 pos. - 3/4/2 - 9:28 PM
No Title
12 peaks

cp b2 pos./Scans 8-10

67,275

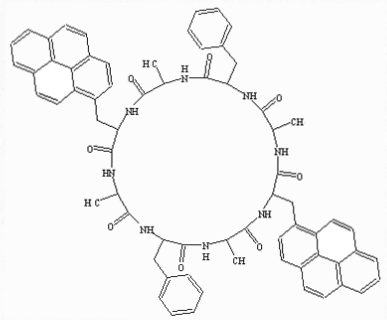

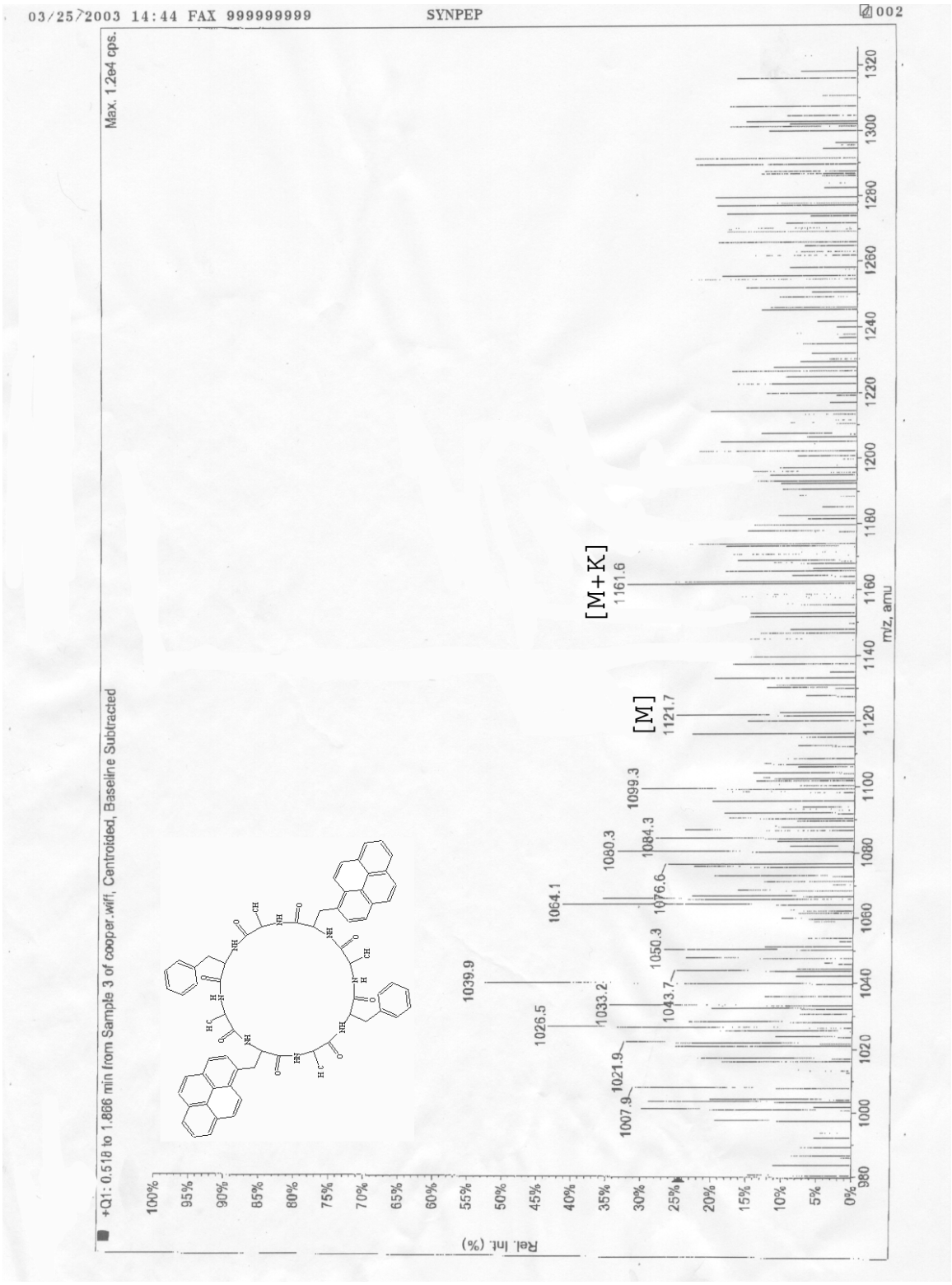
03/25/2003 14:44 FAX 999999999
SYNPEP
002
+Q1: 0.518 to 1.866 min from Sample 3 of cooper.wiff, Centroided, Baseline Subtracted
Max. 1.2e4 cps.
Rel. Int. (%)
m/z, amu
[M+K]
[M]
1161.6
1121.7
1099.3
1084.3
1080.3
1076.6
1064.1
1050.3
1043.7
1039.9
1033.2
1026.5
1021.9
1007.9

DSC Data for Cyclic and Linear Peptides

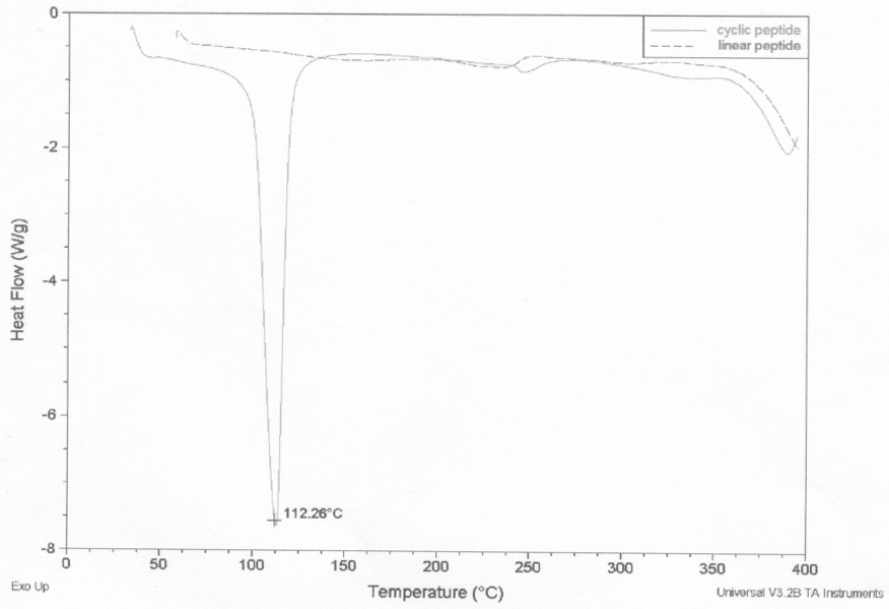

TGA DATA

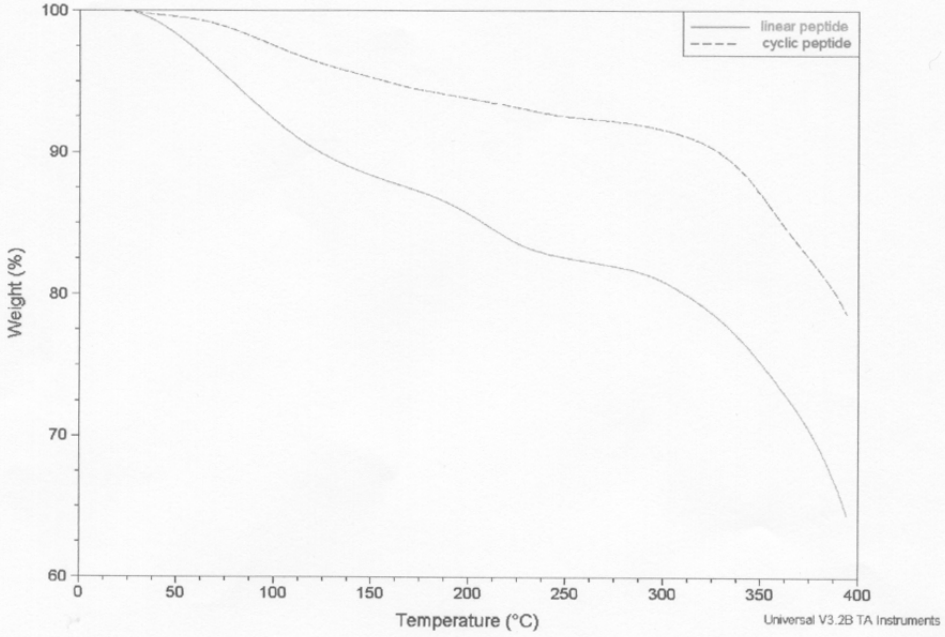
linear peptide
cyclic peptide
100
90
80
70
60
Weight (%)
0
50
100
150
200
250
300
350
400
Temperature (°C)
Universal V3.2B TA Instruments

Cyclic Peptide TGA and DSC Data

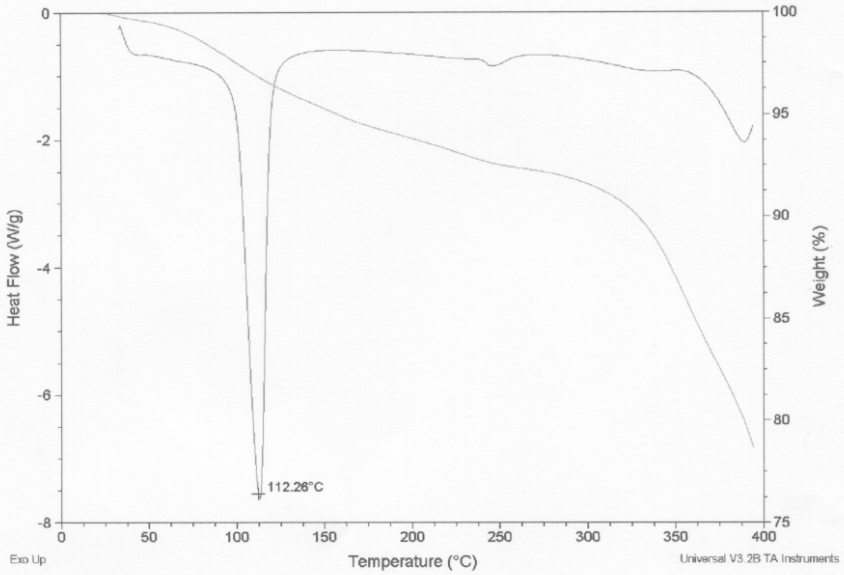

Scheme 3. Synthesis of cyclo[L-Phe-Aib-L-Pya-Aib]$_2$

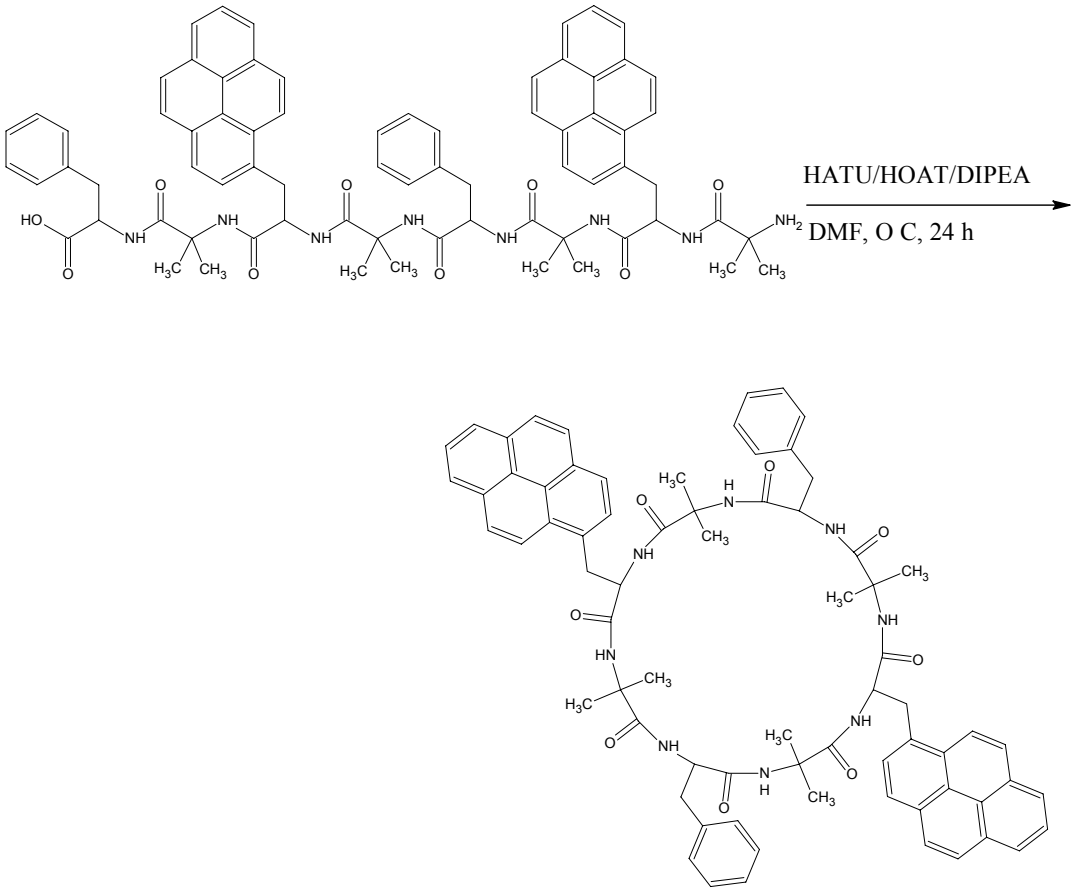

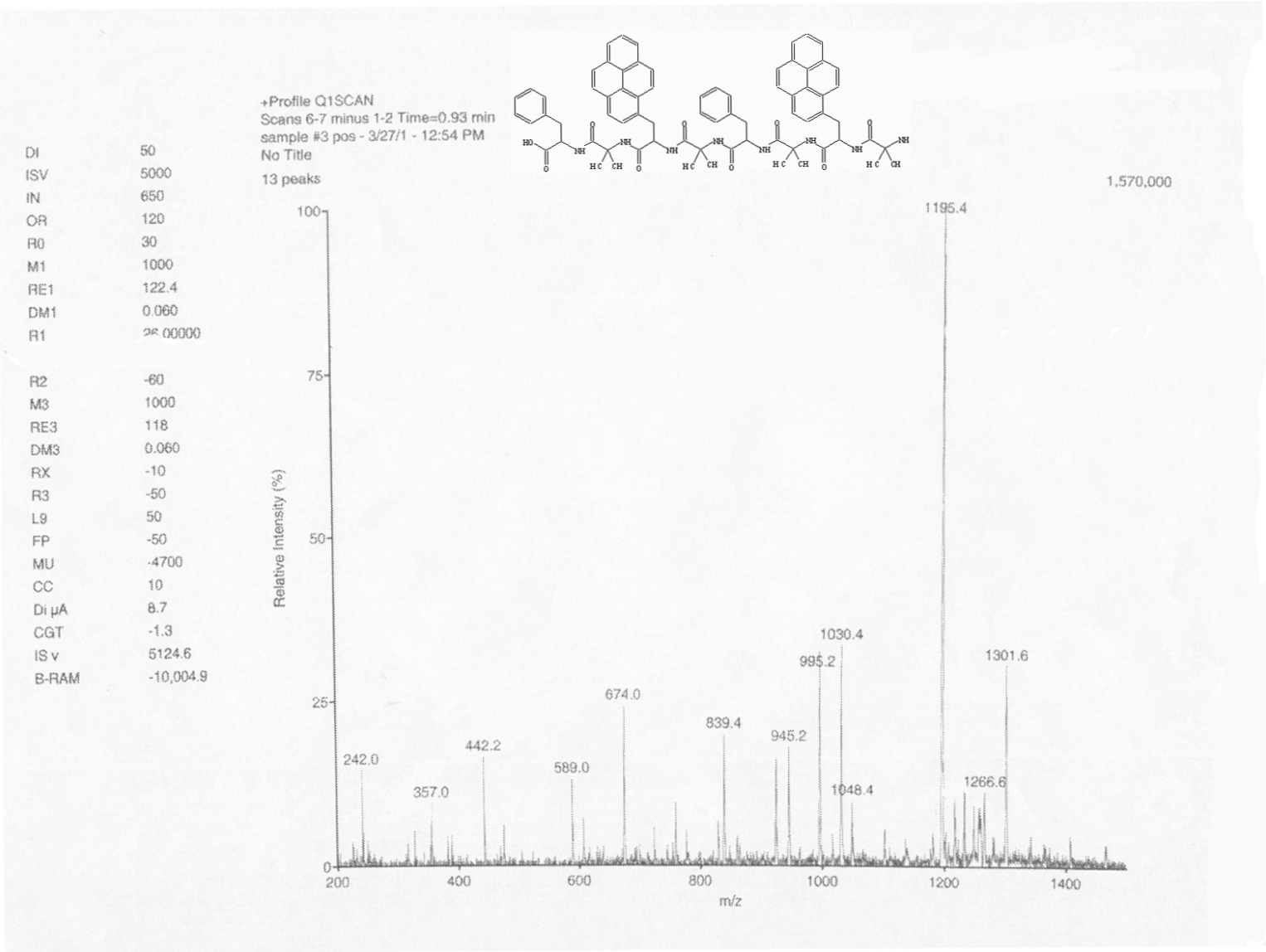
+Profile Q1SCAN
Scans 6-7 minus 1-2 Time=0.93 min
sample #3 pos - 3/27/1 - 12:54 PM
No Title
13 peaks
DI 50
ISV 5000
IN 650
OR 120
R0 30
M1 1000
RE1 122.4
DM1 0.060
R1
R2 -60
M3 1000
RE3 118
DM3 0.060
RX -10
R3 -50
L9 50
FP -50
MU -4700
CC 10
Di µA 8.7
CGT -1.3
IS v 5124.6
B-RAM -10,004.9
1,570,000
Relative Intensity (%)
m/z
1195.4
1030.4
995.2
1301.6
674.0
839.4
945.2
442.2
242.0
589.0
357.0
1048.4
1266.6

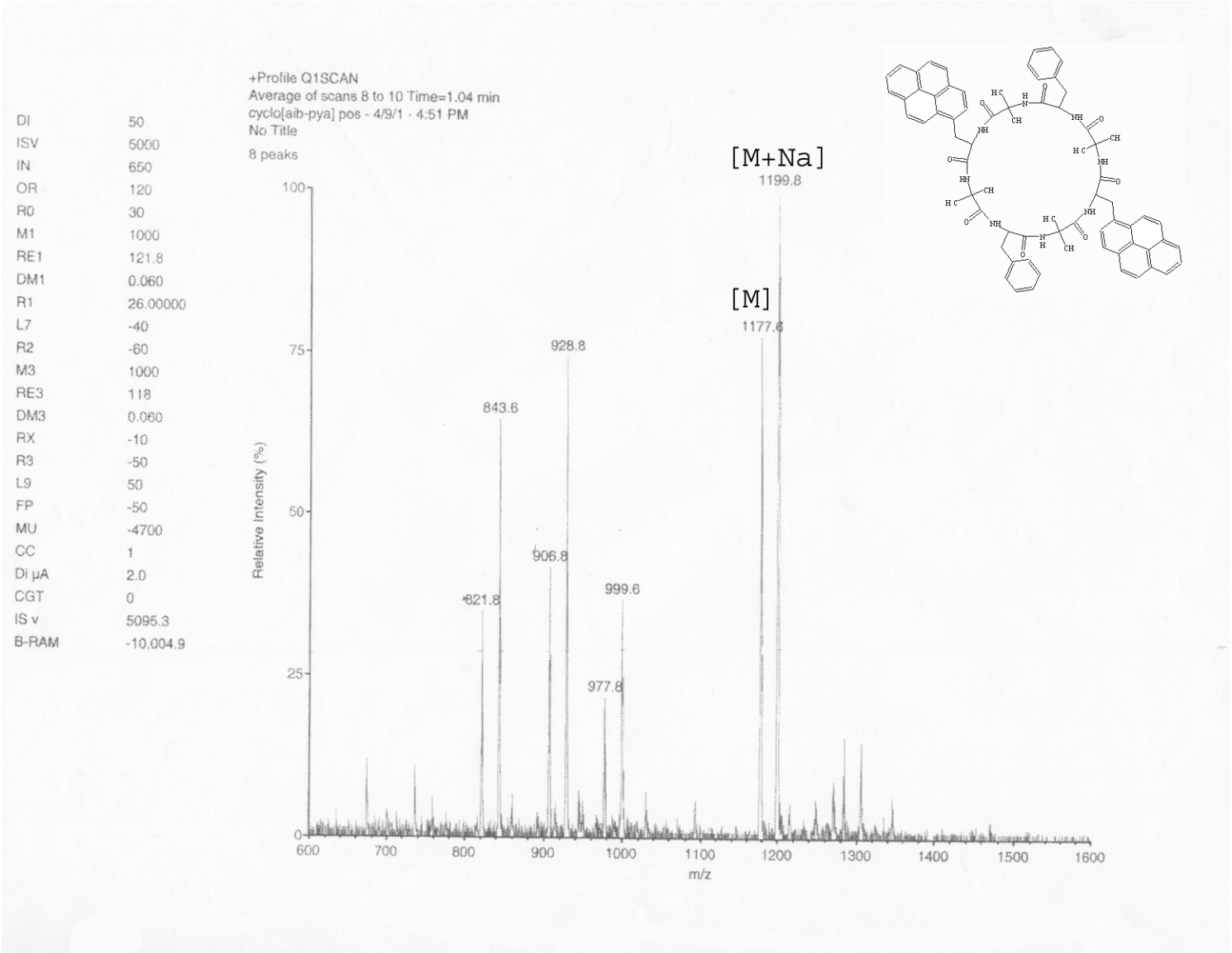
+Profile Q1SCAN
Average of scans 8 to 10 Time=1.04 min
cyclo[aib-pya] pos - 4/9/1 - 4:51 PM
No Title
8 peaks
DI 50
ISV 5000
IN 650
OR 120
R0 30
M1 1000
RE1 121.8
DM1 0.060
R1 26.00000
L7 -40
R2 -60
M3 1000
RE3 118
DM3 0.060
RX -10
R3 -50
L9 50
FP -50
MU -4700
CC 1
DI µA 2.0
CGT 0
IS v 5095.3
B-RAM -10,004.9
[M+Na]
1199.8
[M]
1177.6
928.8
843.6
906.8
999.6
821.8
977.8
Relative Intensity (%)
m/z
100
75
50
25
0
600
700
800
900
1000
1100
1200
1300
1400
1500
1600

Scheme 4. Synthesis of linear[L-Pya-D-Ala]$_4$

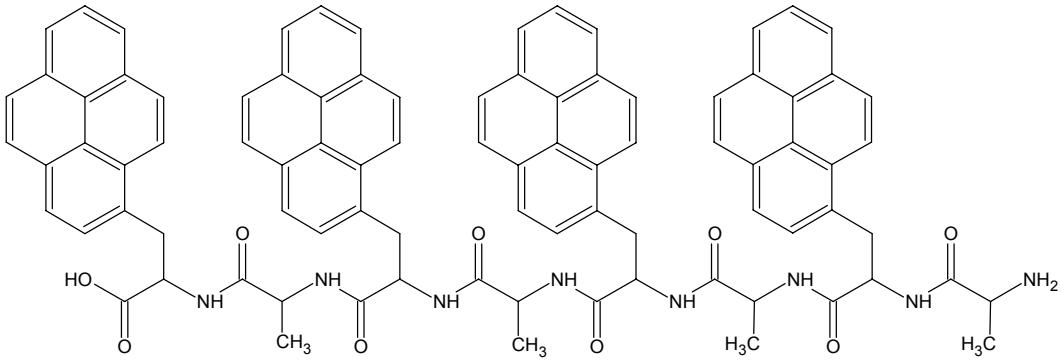

Note: The cyclic form of this compound has not yet been successfully isolated. Additionally, the linear form suffers from extremely poor solubility.

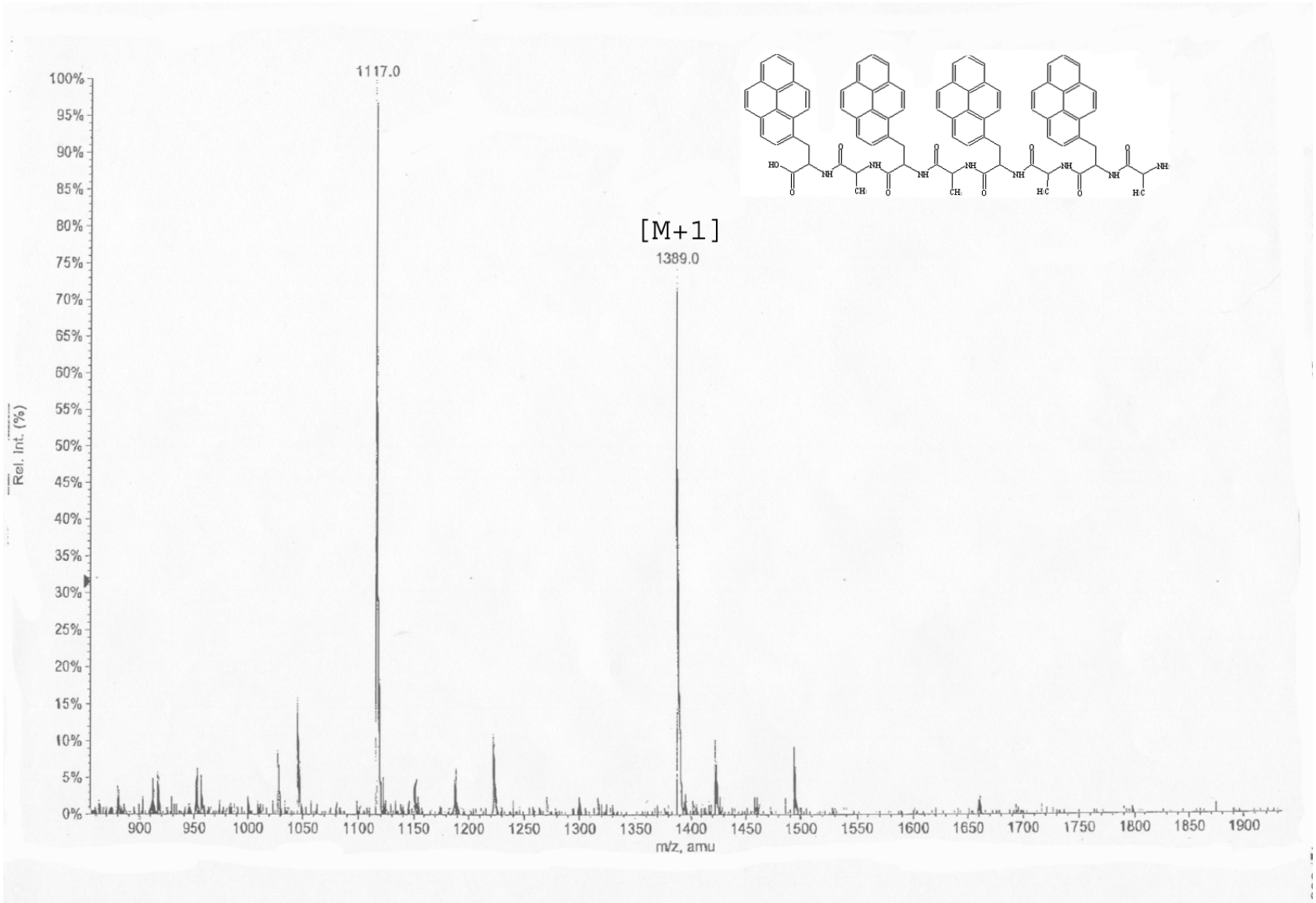
1117.0
[M+1]
1389.0
Rel. Int. (%)
m/z, amu
100%
95%
90%
85%
80%
75%
70%
65%
60%
55%
50%
45%
40%
35%
30%
25%
20%
15%
10%
5%
0%
900
950
1000
1050
1100
1150
1200
1250
1300
1350
1400
1450
1500
1550
1600
1650
1700
1750
1800
1850
1900

Scheme 5. Synthesis of 4-[(10-mercaptodecyl)oxy]pyridine-2,6-dicarboxylic acid

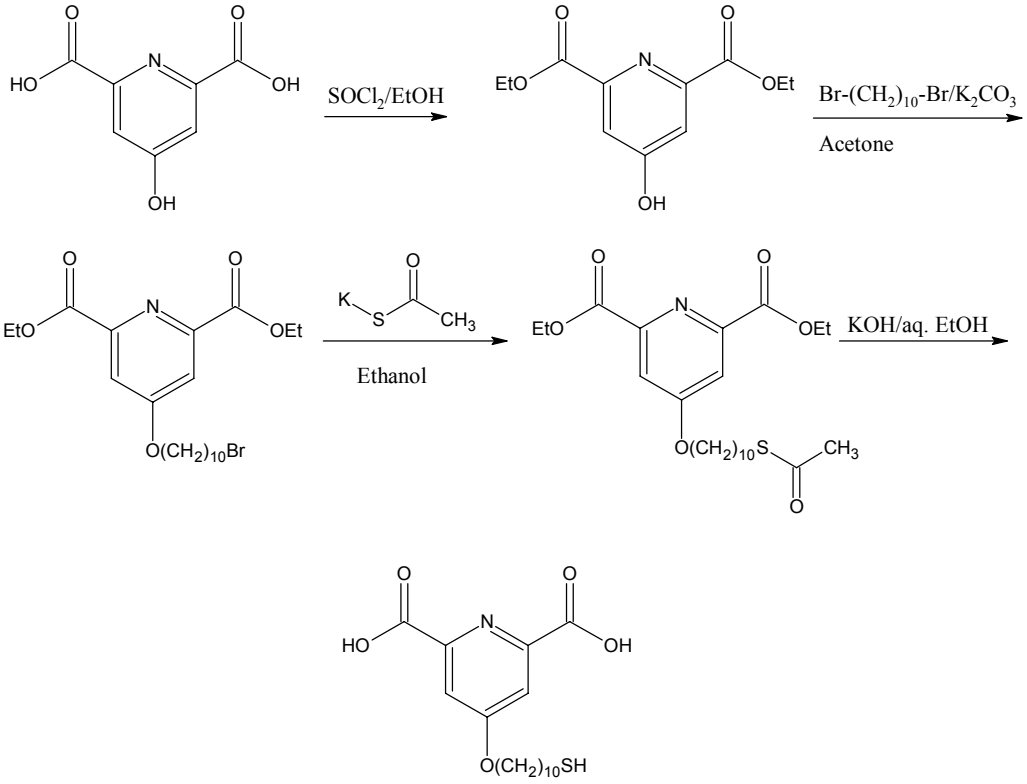

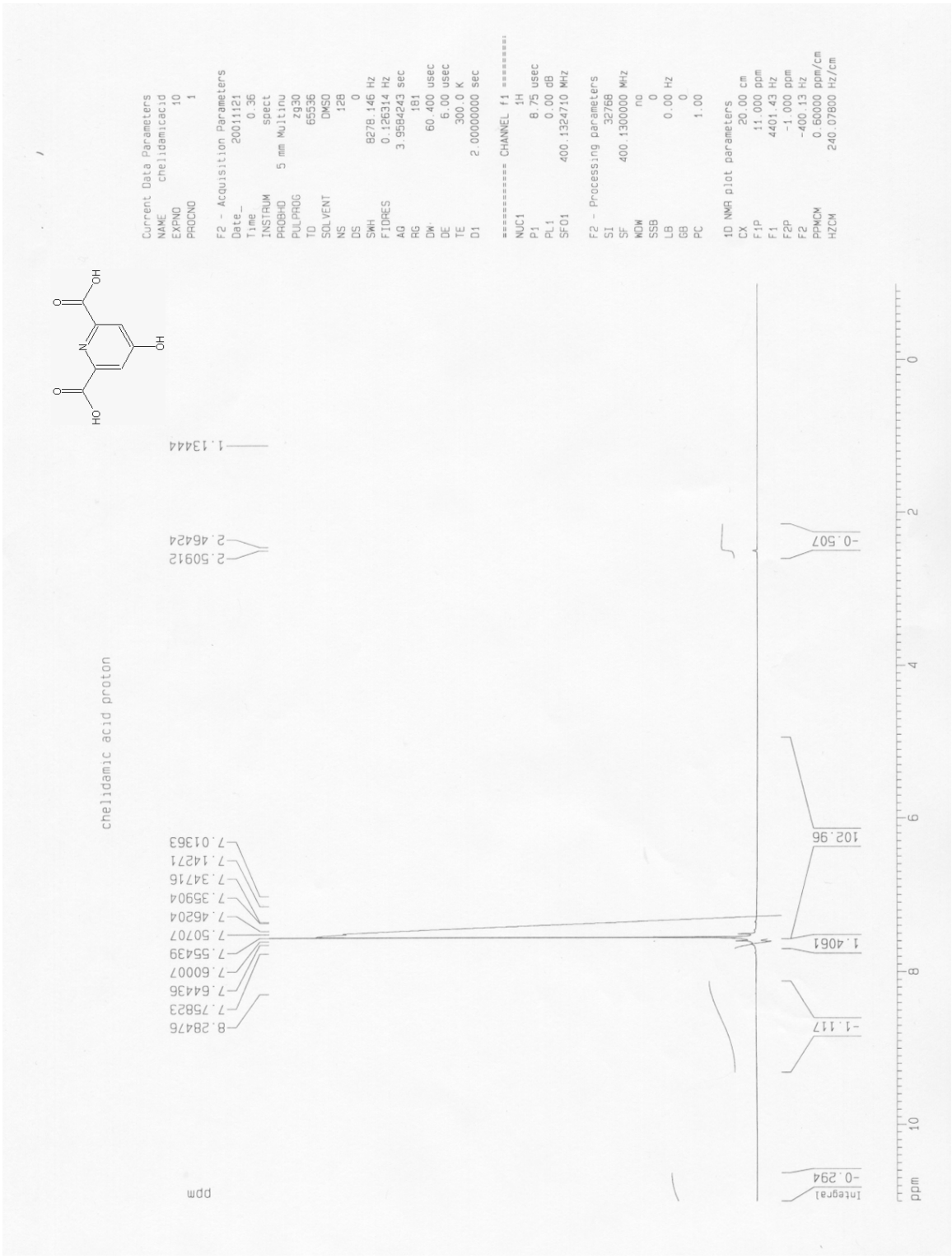
chelidamic acid proton
ppm
Integral
-0.294
-1.117
1.4061
102.96
-0.507
1.13444
2.46424
2.50912
7.01363
7.14271
7.34716
7.35904
7.46204
7.50707
7.55439
7.60007
7.64436
7.75823
8.28476
Current Data Parameters
NAME chelidamicacid
EXPNO 10
PROCNO 1
F2 - Acquisition Parameters
Date_ 20011121
Time 0.36
INSTRUM spect
PROBHD 5 mm Multinu
PULPROG zg30
TD 65536
SOLVENT DMSO
NS 128
DS 0
SWH 8278.146 Hz
FIDRES 0.126314 Hz
AQ 3.9584243 sec
RG 181
DW 60.400 usec
DE 6.00 usec
TE 300.0 K
D1 2.00000000 sec
========== CHANNEL f1 ========
NUC1 1H
P1 8.75 usec
PL1 0.00 dB
SFO1 400.1324710 MHz
F2 - Processing parameters
SI 32768
SF 400.1300000 MHz
WDW no
SSB 0
LB 0.00 Hz
GB 0
PC 1.00
1D NMR plot parameters
CX 20.00 cm
F1P 11.000 ppm
F1 4401.43 Hz
F2P -1.000 ppm
F2 -400.13 Hz
PPMCM 0.60000 ppm/cm
HZCM 240.07800 Hz/cm

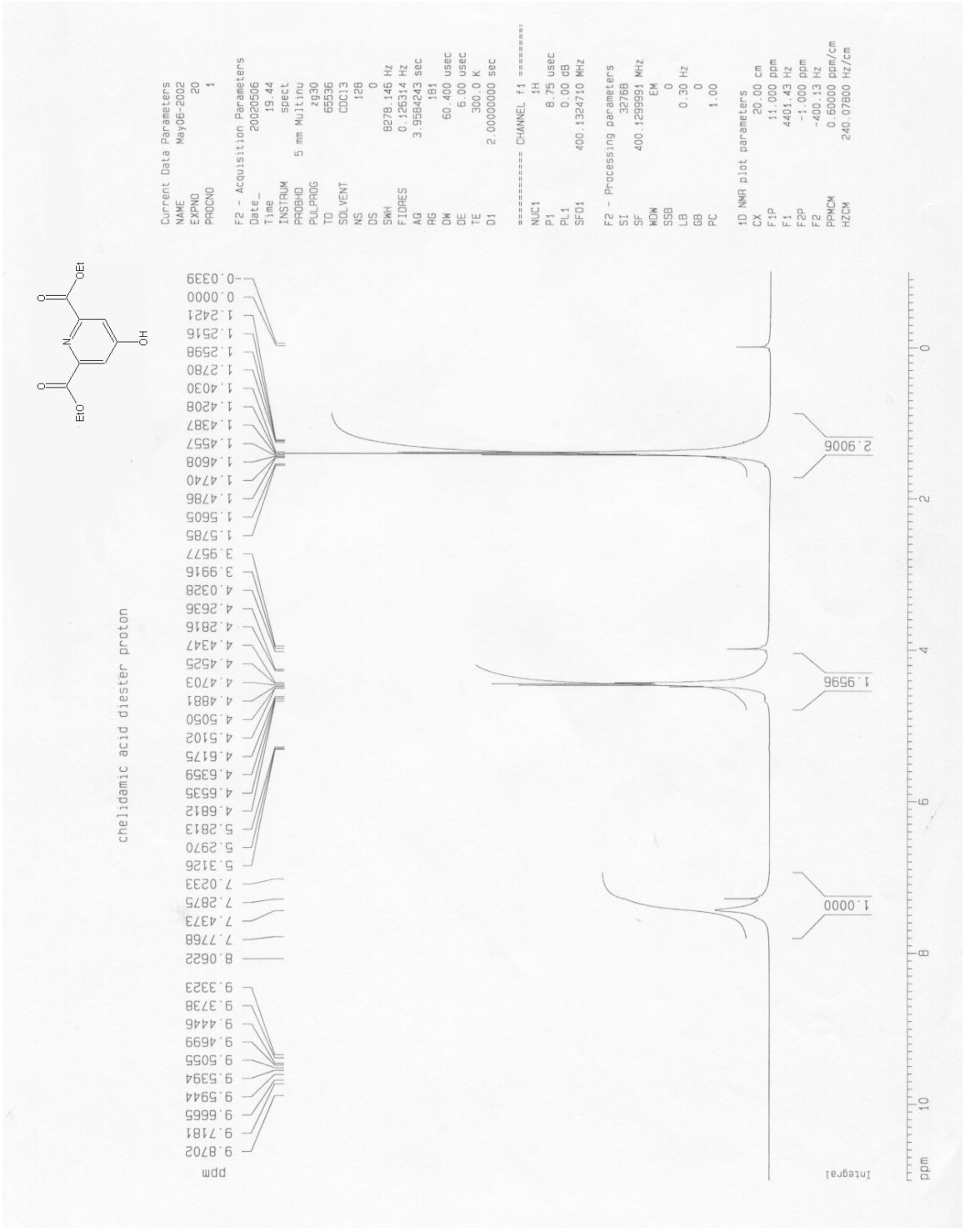
chelidamic acid diester proton
Current Data Parameters
NAME May06-2002
EXPNO 20
PROCNO 1
F2 - Acquisition Parameters
Date_ 20020506
Time 19.44
INSTRUM spect
PROBHD 5 mm Multinu
PULPROG zg30
TD 65536
SOLVENT CDCl3
NS 128
DS 0
SWH 8278.146 Hz
FIDRES 0.126314 Hz
AQ 3.9584243 sec
RG 181
DW 60.400 usec
DE 6.00 usec
TE 300.0 K
D1 2.00000000 sec
========== CHANNEL f1 ==========
NUC1 1H
P1 8.75 usec
PL1 0.00 dB
SFO1 400.1324710 MHz
F2 - Processing parameters
SI 32768
SF 400.1299991 MHz
WDW EM
SSB 0
LB 0.30 Hz
GB 0
PC 1.00
1D NMR plot parameters
CX 20.00 cm
F1P 11.000 ppm
F1 4401.43 Hz
F2P -1.000 ppm
F2 -400.13 Hz
PPMCM 0.60000 ppm/cm
HZCM 240.07800 Hz/cm
OEt
OH
EtO
ppm
Integral
1.0000
1.9596
2.9006

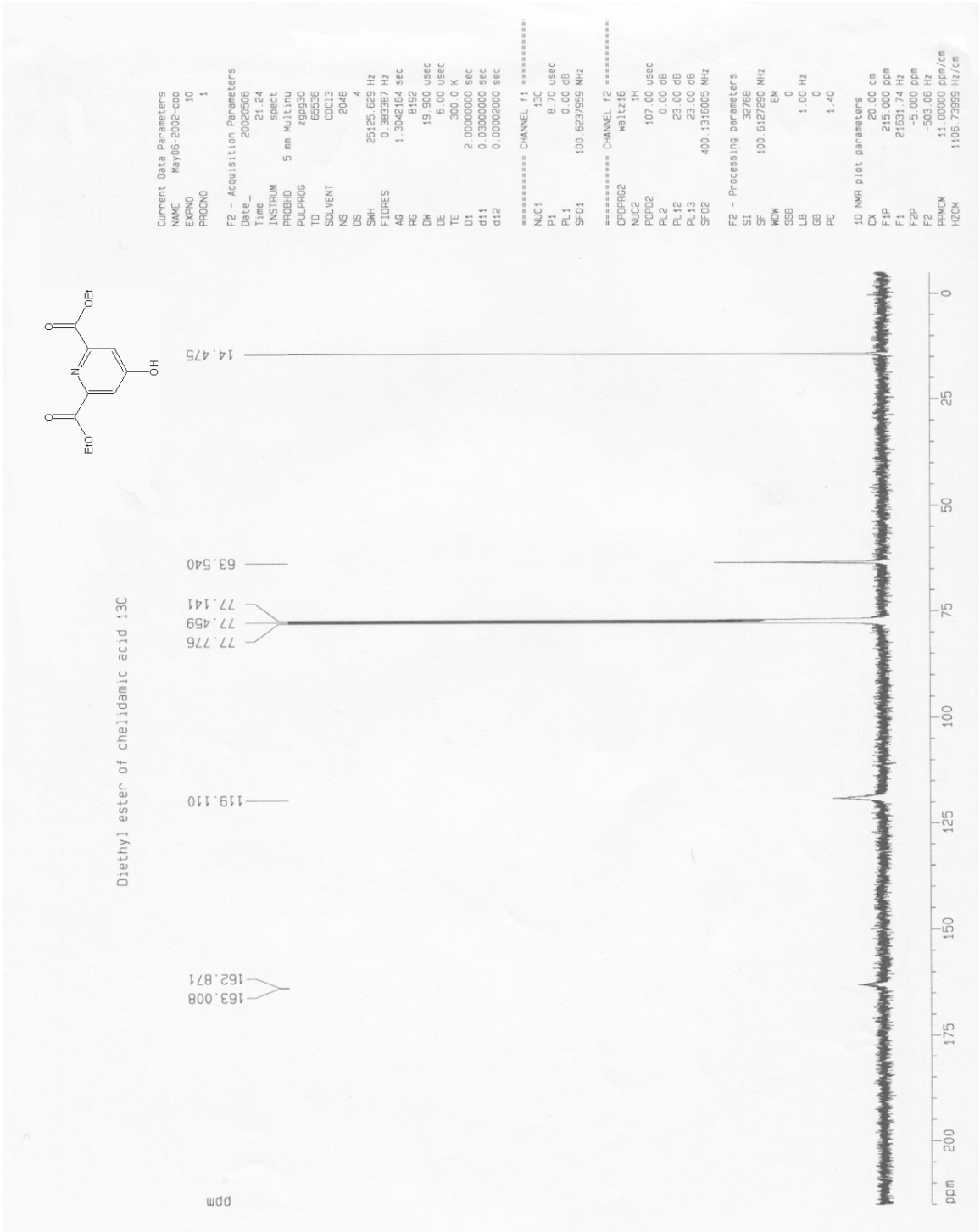
Diethyl ester of chelidamic acid 13C
ppm
14.475
63.540
77.141
77.459
77.776
119.110
162.871
163.008
Current Data Parameters
NAME MayO6-2002-coo
EXPNO 10
PROCNO 1
F2 - Acquisition Parameters
Date_ 20020506
Time 21.24
INSTRUM spect
PROBHD 5 mm Multinu
PULPROG zgpg30
TD 65536
SOLVENT CDCl3
NS 2048
DS 4
SWH 25125.629 Hz
FIDRES 0.383387 Hz
AQ 1.3042164 sec
RG 8192
DW 19.900 usec
DE 6.00 usec
TE 300.0 K
D1 2.00000000 sec
d11 0.03000000 sec
d12 0.00002000 sec
CHANNEL f1
NUC1 13C
P1 8.70 usec
PL1 0.00 dB
SFO1 100.6237959 MHz
CHANNEL f2
CPDPRG2 waltz16
NUC2 1H
PCPD2 107.00 usec
PL2 0.00 dB
PL12 23.00 dB
PL13 23.00 dB
SFO2 400.1316005 MHz
F2 - Processing parameters
SI 32768
SF 100.6127690 MHz
WDW EM
SSB 0
LB 1.00 Hz
GB 0
PC 1.40
1D NMR plot parameters
CX 20.00 cm
F1P 215.000 ppm
F1 21631.74 Hz
F2P -5.000 ppm
F2 -503.06 Hz
PPMCM 11.00000 ppm/cm
HZCM 1106.73999 Hz/cm
ppm
200
175
150
125
100
75
50
25
0

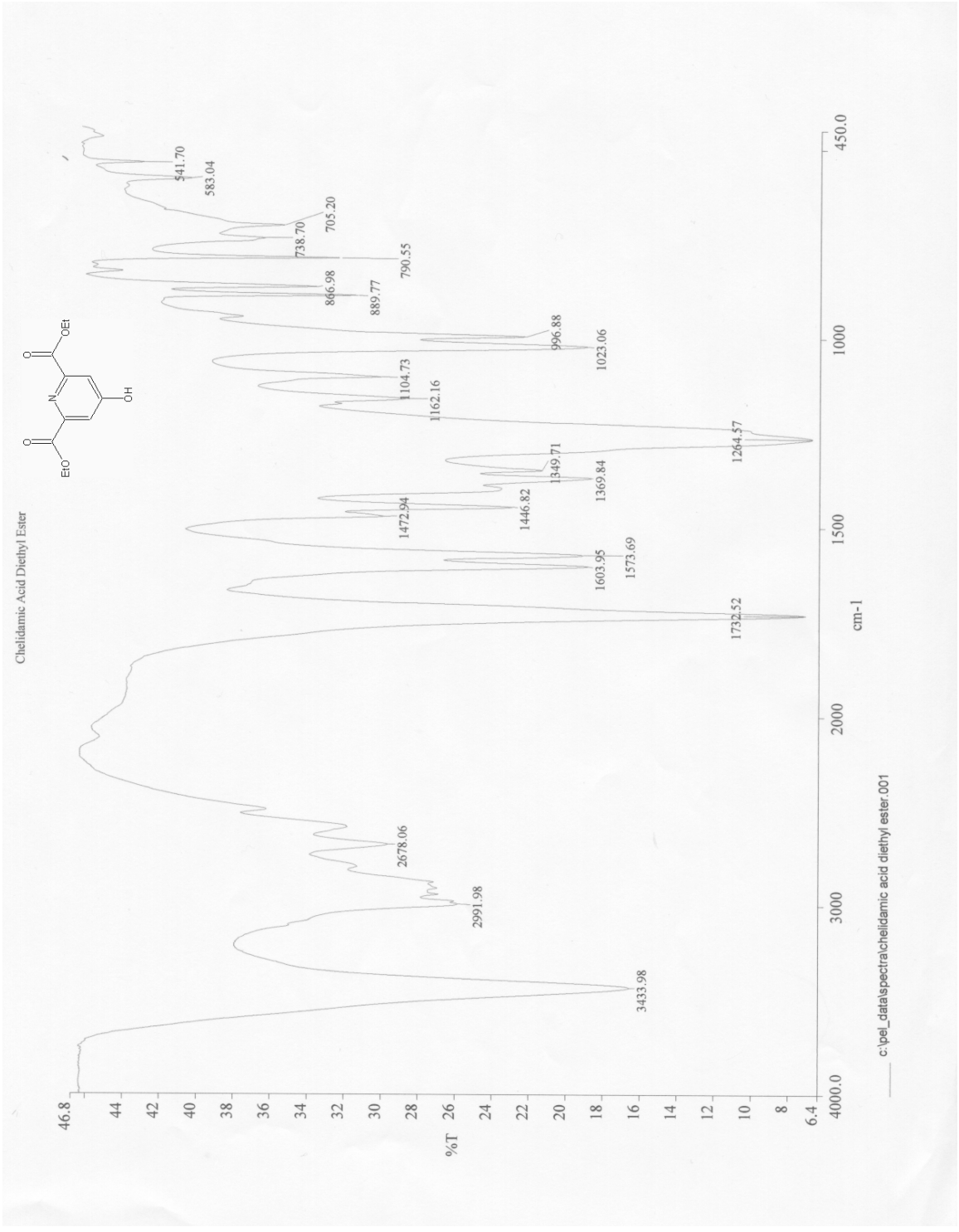
Chelidamic Acid Diethyl Ester
OEt
O
N
OH
EtO
O
%T
cm-1
4000.0
3000
2000
1500
1000
450.0
46.8
44
42
40
38
36
34
32
30
28
26
24
22
20
18
16
14
12
10
8
6.4
3433.98
2991.98
2678.06
1732.52
1603.95
1573.69
1472.94
1446.82
1369.84
1349.71
1264.57
1162.16
1104.73
1023.06
996.88
889.77
866.98
790.55
738.70
705.20
583.04
541.70
c:\pel_data\spectra\chelidamic acid diethyl ester.001

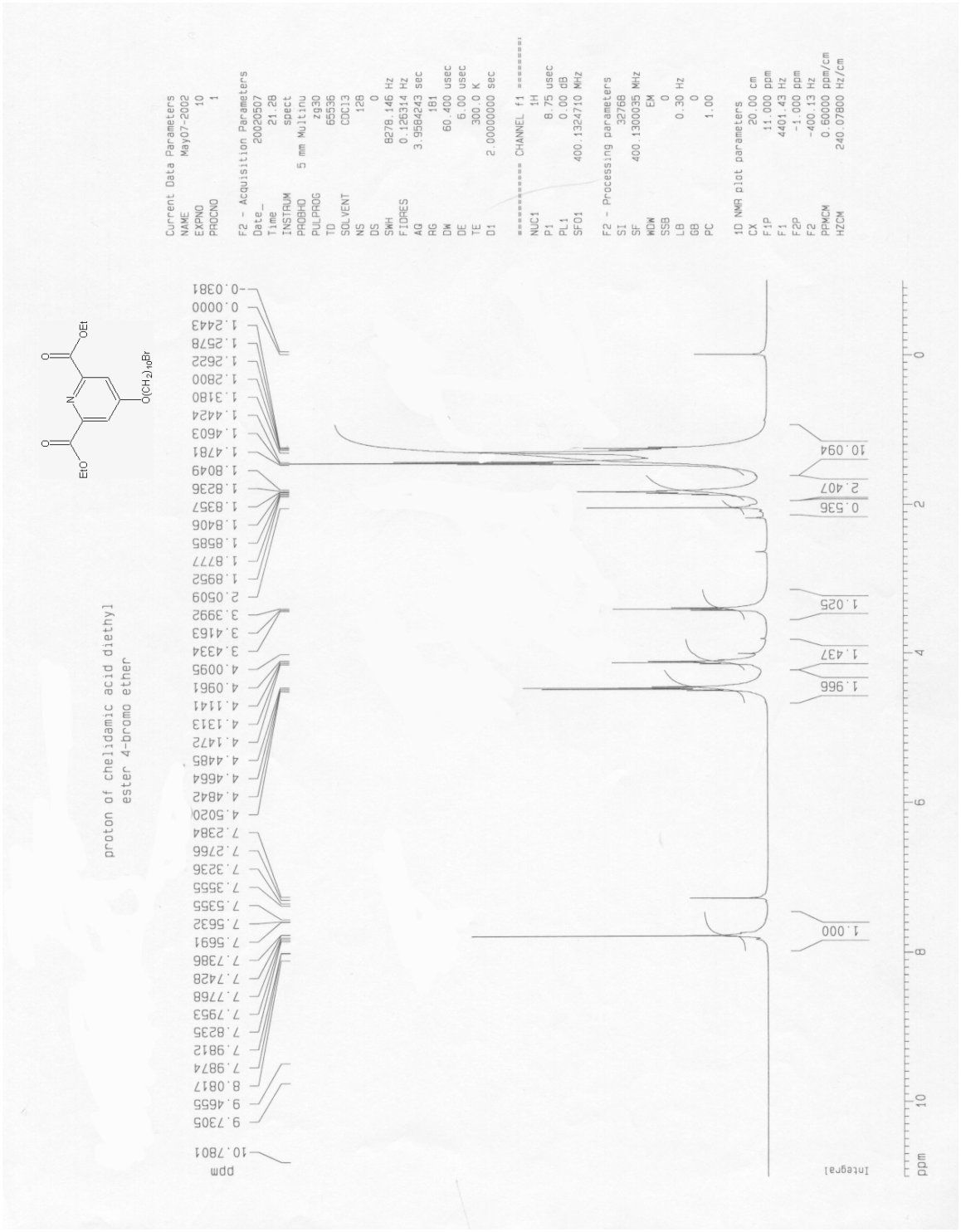
proton of chelidamic acid diethyl ester 4-bromo ether
OEt
O
N
O(CH2)10Br
EtO
Current Data Parameters
NAME May07-2002
EXPNO 10
PROCNO 1
F2 - Acquisition Parameters
Date_ 20020507
Time 21.28
INSTRUM spect
PROBHD 5 mm Multinu
PULPROG zg30
TD 65536
SOLVENT CDCl3
NS 128
DS 0
SWH 8278.146 Hz
FIDRES 0.126314 Hz
AQ 3.9584243 sec
RG 181
DW 60.400 usec
DE 6.00 usec
TE 300.0 K
D1 2.00000000 sec
========== CHANNEL f1 ==========
NUC1 1H
P1 8.75 usec
PL1 0.00 dB
SFO1 400.1324710 MHz
F2 - Processing parameters
SI 32768
SF 400.1300035 MHz
WDW EM
SSB 0
LB 0.30 Hz
GB 0
PC 1.00
1D NMR plot parameters
CX 20.00 cm
F1P 11.000 ppm
F1 4401.43 Hz
F2P -1.000 ppm
F2 -400.13 Hz
PPMCM 0.60000 ppm/cm
HZCM 240.07800 Hz/cm
ppm
-0.0381
0.0000
1.2443
1.2578
1.2622
1.2800
1.3180
1.4424
1.4603
1.4781
1.8049
1.8236
1.8357
1.8406
1.8585
1.8777
1.8952
2.0509
3.3992
3.4163
3.4334
4.0095
4.0961
4.1141
4.1313
4.1472
4.4485
4.4664
4.4842
4.5020
7.2384
7.2766
7.3236
7.3555
7.5355
7.5632
7.5691
7.7386
7.7428
7.7768
7.7953
7.8235
7.9812
7.9874
8.0817
9.4655
9.7305
10.7801
Integral
1.000
1.966
1.437
1.025
0.536
2.407
10.094
ppm

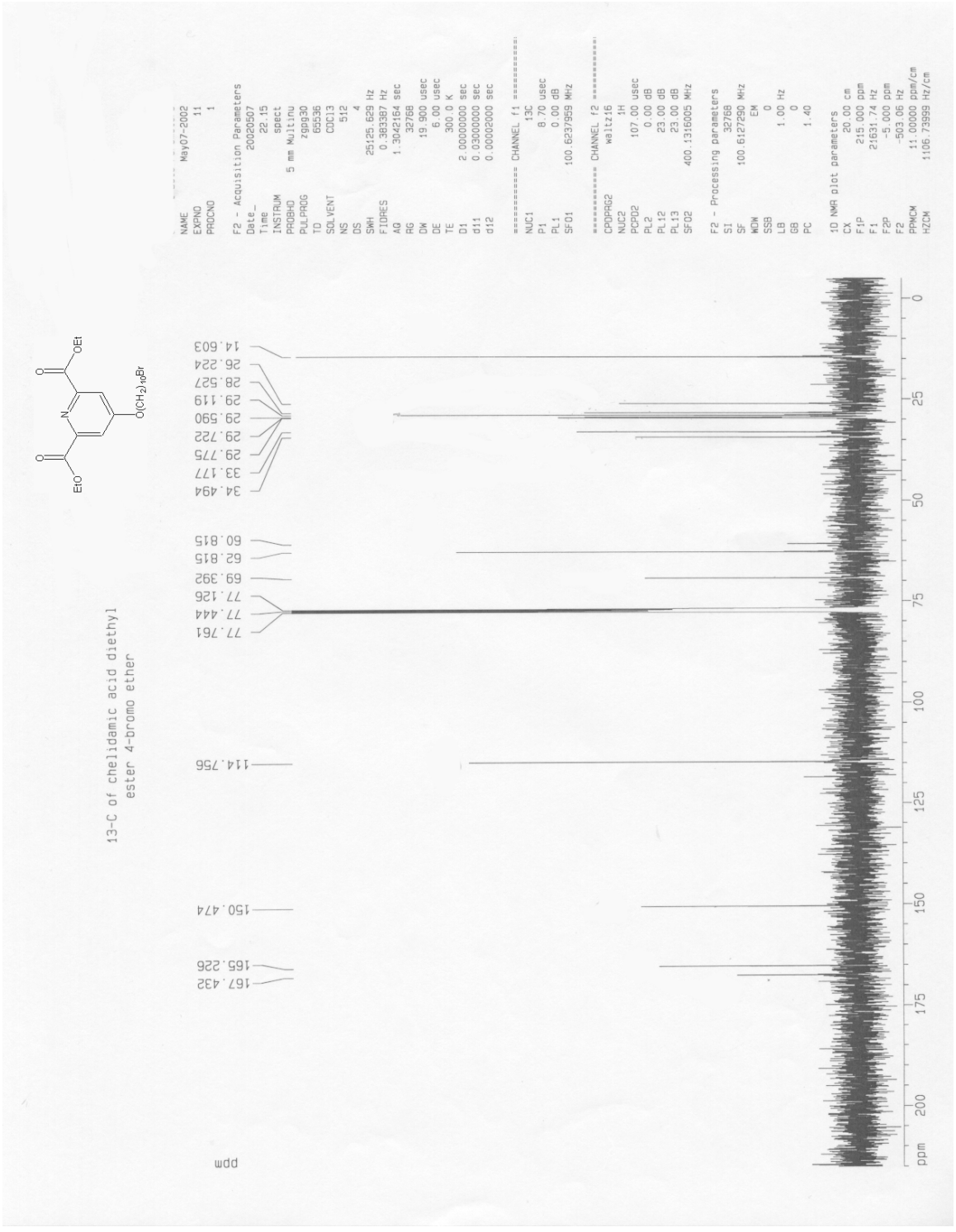
13-C of chelidamic acid diethyl
ester 4-bromo ether
OEt
O(CH2)10Br
EtO
14.603
26.224
28.527
29.119
29.590
29.722
29.775
33.177
34.494
60.815
62.815
69.392
77.126
77.444
77.761
114.756
150.474
165.226
167.432
ppm
0
25
50
75
100
125
150
175
200
NAME May07-2002
EXPNO 11
PROCNO 1
F2 - Acquisition Parameters
Date_ 20020507
Time 22.15
INSTRUM spect
PROBHD 5 mm Multinu
PULPROG zgpg30
TD 65536
SOLVENT CDCl3
NS 512
DS 4
SWH 25125.629 Hz
FIDRES 0.383387 Hz
AQ 1.304264 sec
RG 32768
DW 19.900 usec
DE 6.00 usec
TE 300.0 K
D1 2.00000000 sec
d11 0.03000000 sec
d12 0.00002000 sec
========== CHANNEL f1 ==========
NUC1 13C
P1 8.70 usec
PL1 0.00 dB
SFO1 100.6237959 MHz
========== CHANNEL f2 ==========
CPDPRG2 waltz16
NUC2 1H
PCPD2 107.00 usec
PL2 0.00 dB
PL12 23.00 dB
PL13 23.00 dB
SFO2 400.1316005 MHz
F2 - Processing parameters
SI 32768
SF 100.6127290 MHz
WDW EM
SSB 0
LB 1.00 Hz
GB 0
PC 1.40
1D NMR plot parameters
CX 20.00 cm
F1P 215.000 ppm
F1 21631.74 Hz
F2P -5.000 ppm
F2 -503.06 Hz
PPMCM 11.00000 ppm/cm
HZCM 1106.73999 Hz/cm

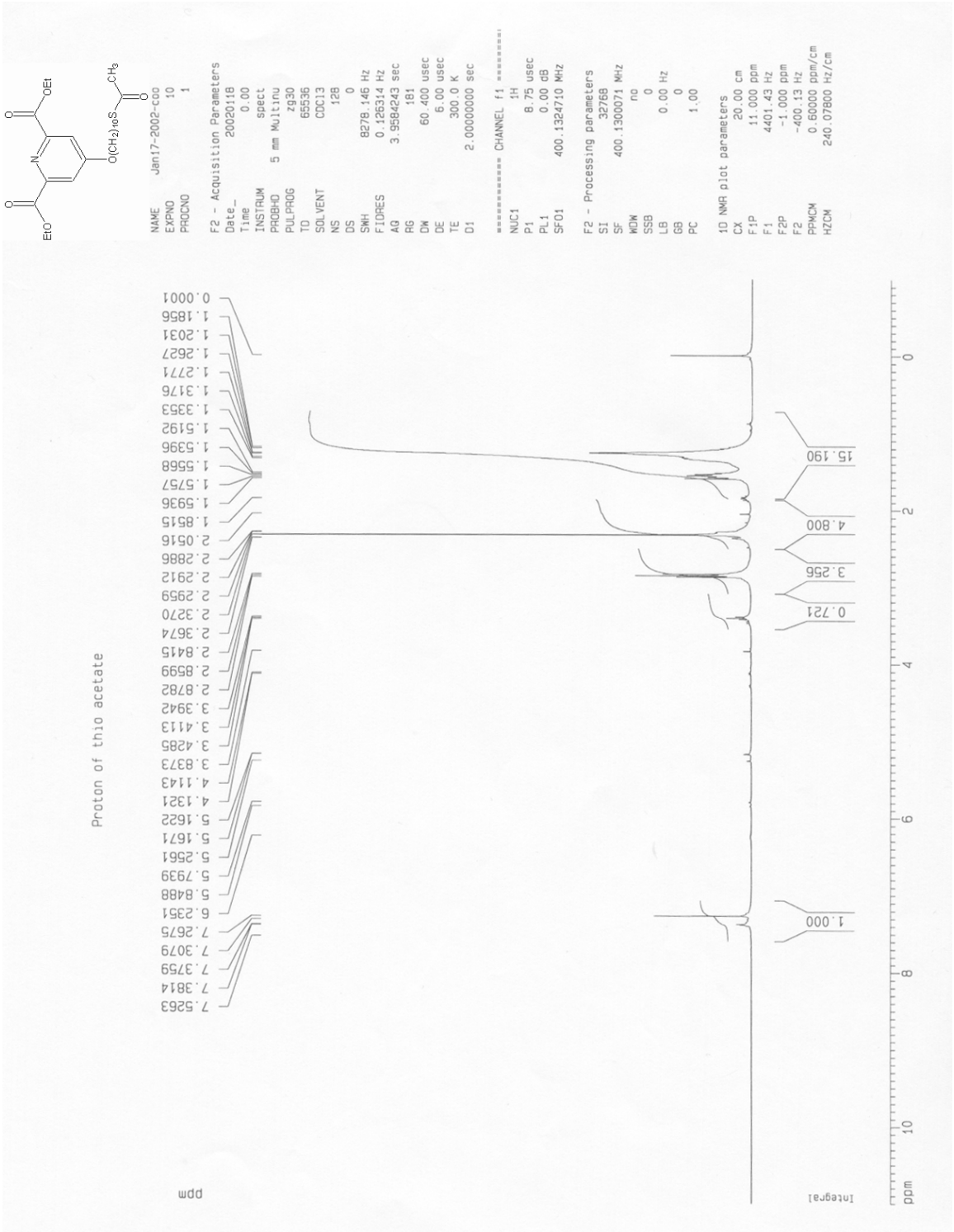
Proton of thio acetate
ppm
Integral
EtO
OEt
O(CH2)10S
CH3
NAME Jan17-2002-coo
EXPNO 10
PROCNO 1
F2 - Acquisition Parameters
Date_ 20020118
Time 0.00
INSTRUM spect
PROBHD 5 mm Multinu
PULPROG zg30
TD 65536
SOLVENT CDCl3
NS 128
DS 0
SWH 8278.146 Hz
FIDRES 0.126314 Hz
AQ 3.9584243 sec
RG 181
DW 60.400 usec
DE 6.00 usec
TE 300.0 K
D1 2.00000000 sec
======== CHANNEL f1 ========
NUC1 1H
P1 8.75 usec
PL1 0.00 dB
SFO1 400.1324710 MHz
F2 - Processing parameters
SI 32768
SF 400.1300071 MHz
WDW no
SSB 0
LB 0.00 Hz
GB 0
PC 1.00
1D NMR plot parameters
CX 20.00 cm
F1P 11.000 ppm
F1 4401.43 Hz
F2P -1.000 ppm
F2 -400.13 Hz
PPMCM 0.60000 ppm/cm
HZCM 240.07800 Hz/cm
7.5263
7.3814
7.3759
7.3079
7.2675
6.2351
5.8488
5.7939
5.2561
5.1671
5.1622
4.1321
4.1143
3.8373
3.4285
3.4113
3.3942
2.8782
2.8599
2.8415
2.3674
2.3270
2.2959
2.2912
2.2886
2.0516
1.8515
1.5936
1.5757
1.5568
1.5396
1.5192
1.3353
1.3176
1.2771
1.2627
1.2031
1.1856
0.0001
15.190
4.800
3.256
0.721
1.000
ppm

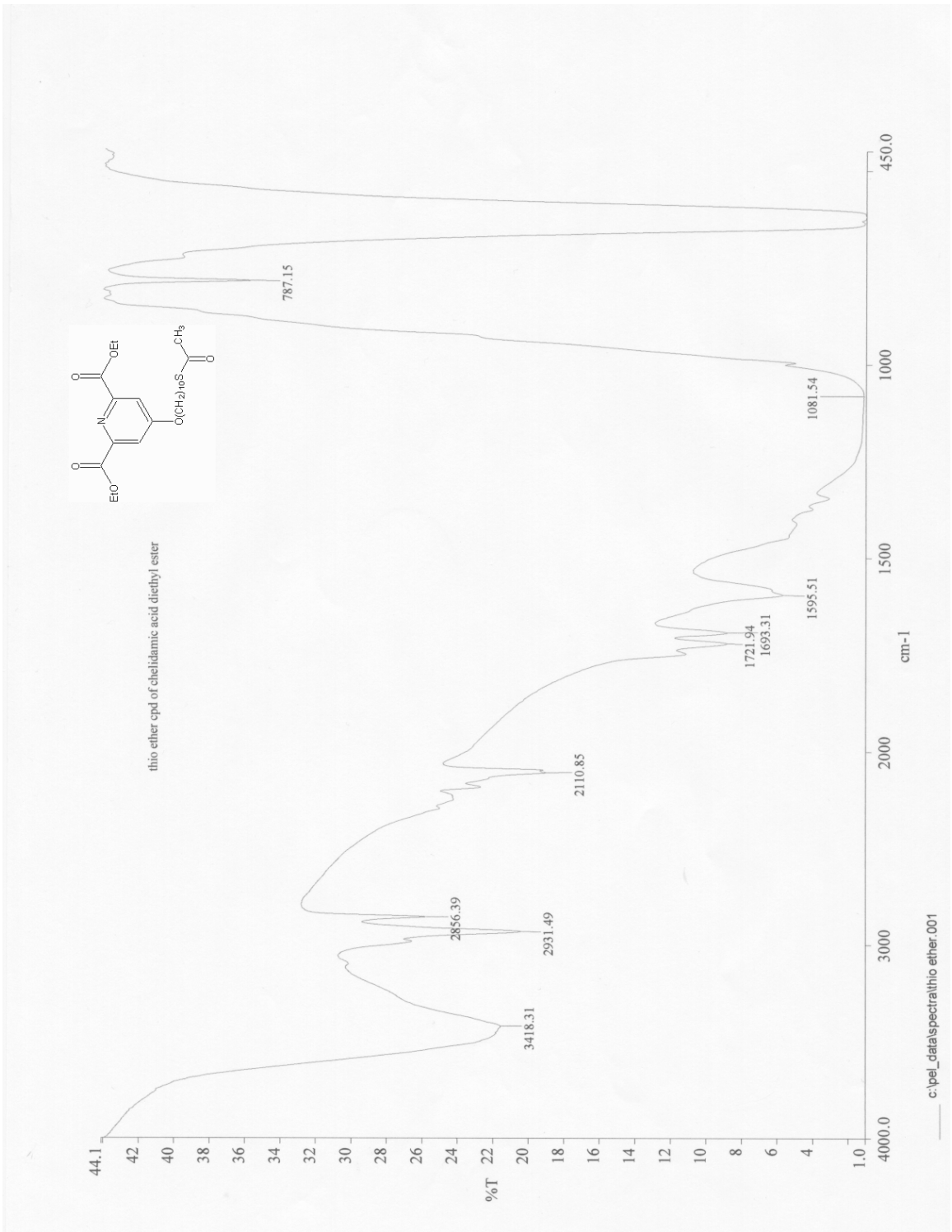
thio ether cpd of chelidamic acid diethyl ester
EtO
OEt
N
O(CH2)10S
CH3
%T
cm-1
44.1
42
40
38
36
34
32
30
28
26
24
22
20
18
16
14
12
10
8
6
4
1.0
4000.0
3000
2000
1500
1000
450.0
3418.31
2931.49
2856.39
2110.85
1721.94
1693.31
1595.51
1081.54
787.15
c:\pel_data\spectra\thio ether.001

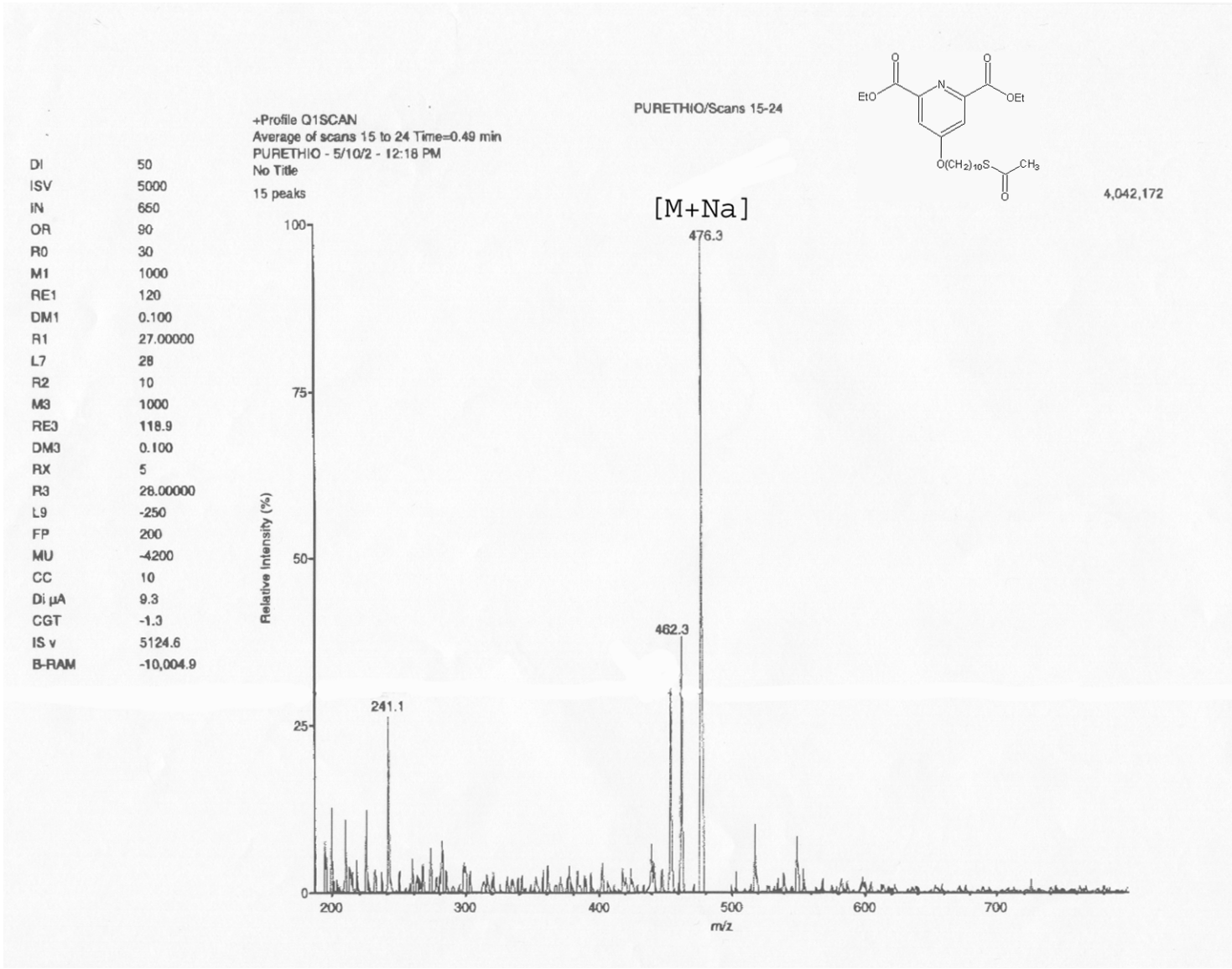
+Profile Q1SCAN
Average of scans 15 to 24 Time=0.49 min
PURETHIO - 5/10/2 - 12:18 PM
No Title
15 peaks
PURETHIO/Scans 15-24
4,042,172
[M+Na]
476.3
462.3
241.1
Relative Intensity (%)
m/z
DI 50
ISV 5000
IN 650
OR 90
R0 30
M1 1000
RE1 120
DM1 0.100
R1 27.00000
L7 28
R2 10
M3 1000
RE3 118.9
DM3 0.100
RX 5
R3 28.00000
L9 -250
FP 200
MU -4200
CC 10
Di µA 9.3
CGT -1.3
IS v 5124.6
B-RAM -10,004.9

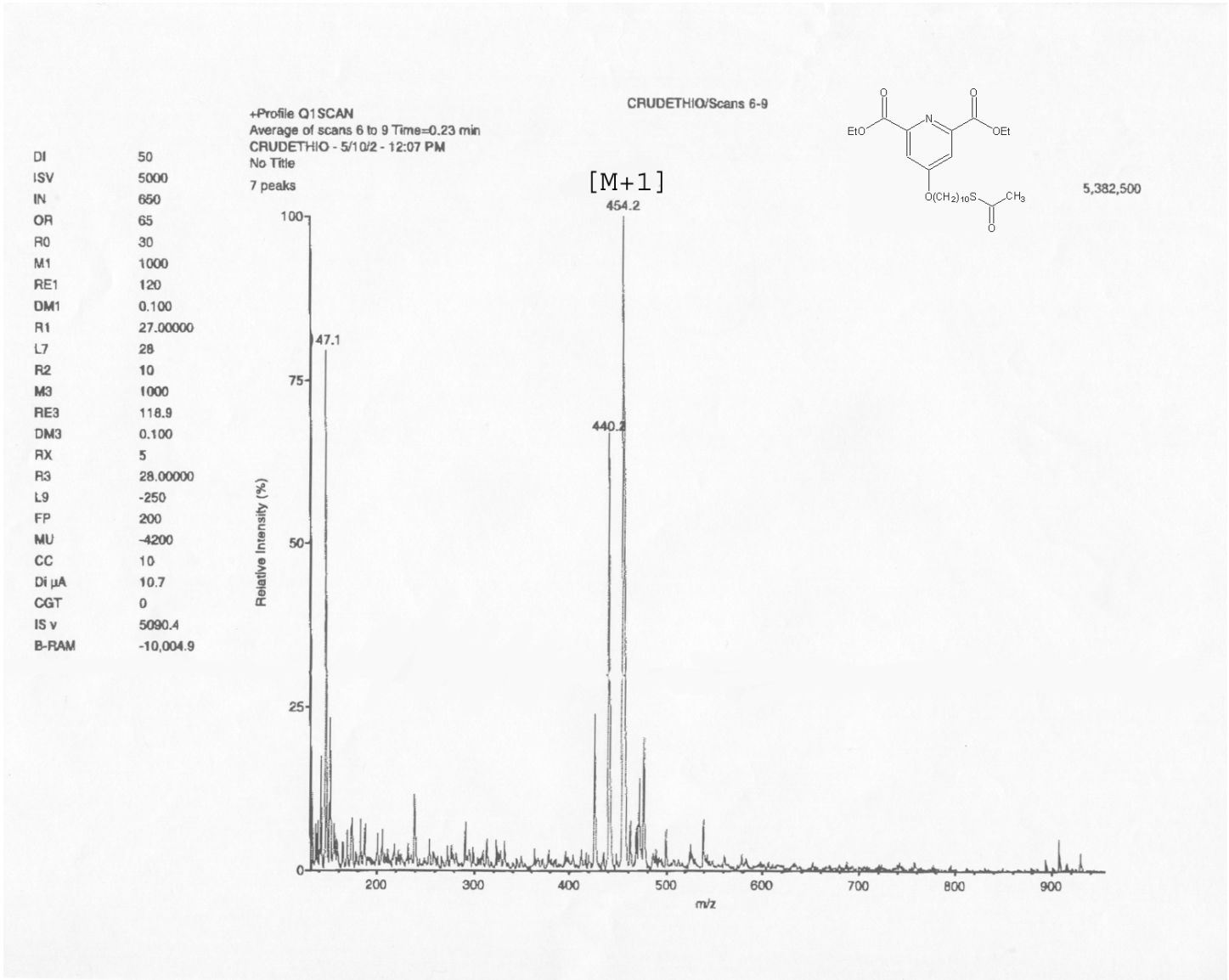
+Profile Q1 SCAN
Average of scans 6 to 9 Time=0.23 min
CRUDETHIO - 5/10/2 - 12:07 PM
No Title
7 peaks
CRUDETHIO/Scans 6-9
[M+1]
454.2
47.1
440.2
5,382,500
DI 50
ISV 5000
IN 650
OR 65
R0 30
M1 1000
RE1 120
DM1 0.100
R1 27.00000
L7 28
R2 10
M3 1000
RE3 118.9
DM3 0.100
RX 5
R3 28.00000
L9 -250
FP 200
MU -4200
CC 10
Di µA 10.7
CGT 0
IS v 5090.4
B-RAM -10,004.9
Relative Intensity (%)
100
75
50
25
0
200
300
400
500
600
700
800
900
m/z

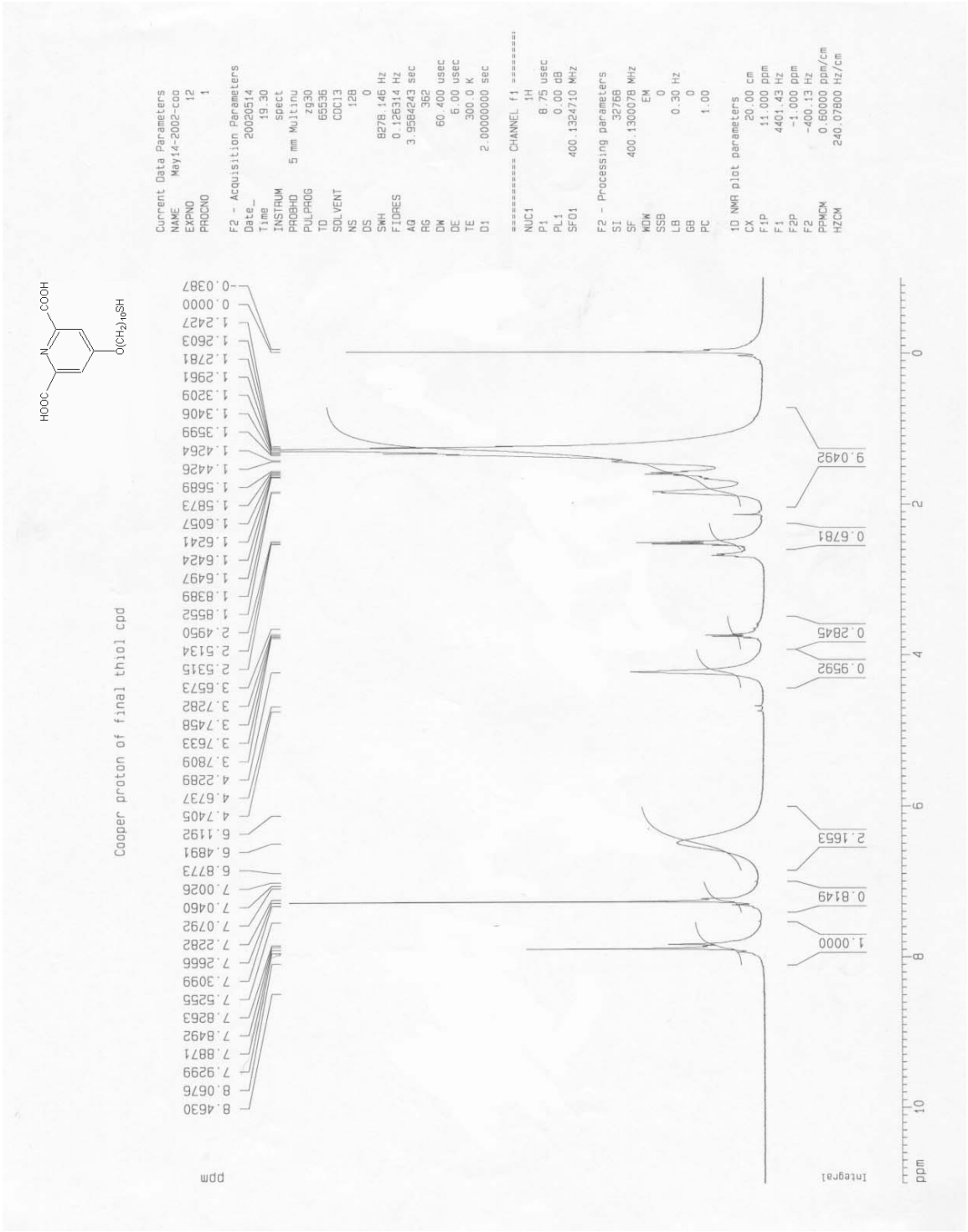
COOH
N
HOOC
O(CH2)10SH
Cooper proton of final thiol cpd
Current Data Parameters
NAME May14-2002-coo
EXPNO 12
PROCNO 1
F2 - Acquisition Parameters
Date_ 20020514
Time 19.30
INSTRUM spect
PROBHD 5 mm Multinu
PULPROG zg30
TD 65536
SOLVENT CDCl3
NS 128
DS 0
SWH 8278.146 Hz
FIDRES 0.126314 Hz
AQ 3.9584243 sec
RG 362
DW 60.400 usec
DE 6.00 usec
TE 300.0 K
D1 2.00000000 sec
========== CHANNEL f1 ========
NUC1 1H
P1 8.75 usec
PL1 0.00 dB
SFO1 400.1324710 MHz
F2 - Processing parameters
SI 32768
SF 400.1300078 MHz
WDW EM
SSB 0
LB 0.30 Hz
GB 0
PC 1.00
1D NMR plot parameters
CX 20.00 cm
F1P 11.000 ppm
F1 4401.43 Hz
F2P -1.000 ppm
F2 -400.13 Hz
PPMCM 0.60000 ppm/cm
HZCM 240.07800 Hz/cm
8.4630
8.0676
7.9299
7.8871
7.8492
7.8263
7.5255
7.3099
7.2666
7.2282
7.0792
7.0460
7.0026
6.8773
6.4891
6.1192
4.7405
4.6737
4.2289
3.7809
3.7633
3.7458
3.7282
3.6573
2.5315
2.5134
2.4950
1.8552
1.8389
1.6497
1.6424
1.6241
1.6057
1.5873
1.5689
1.4426
1.4264
1.3599
1.3406
1.3209
1.2961
1.2781
1.2603
1.2427
0.0000
0.0387
ppm
Integral
9.0492
0.6781
0.2845
0.9592
2.1653
0.8149
1.0000
ppm
10
8
6
4
2
0

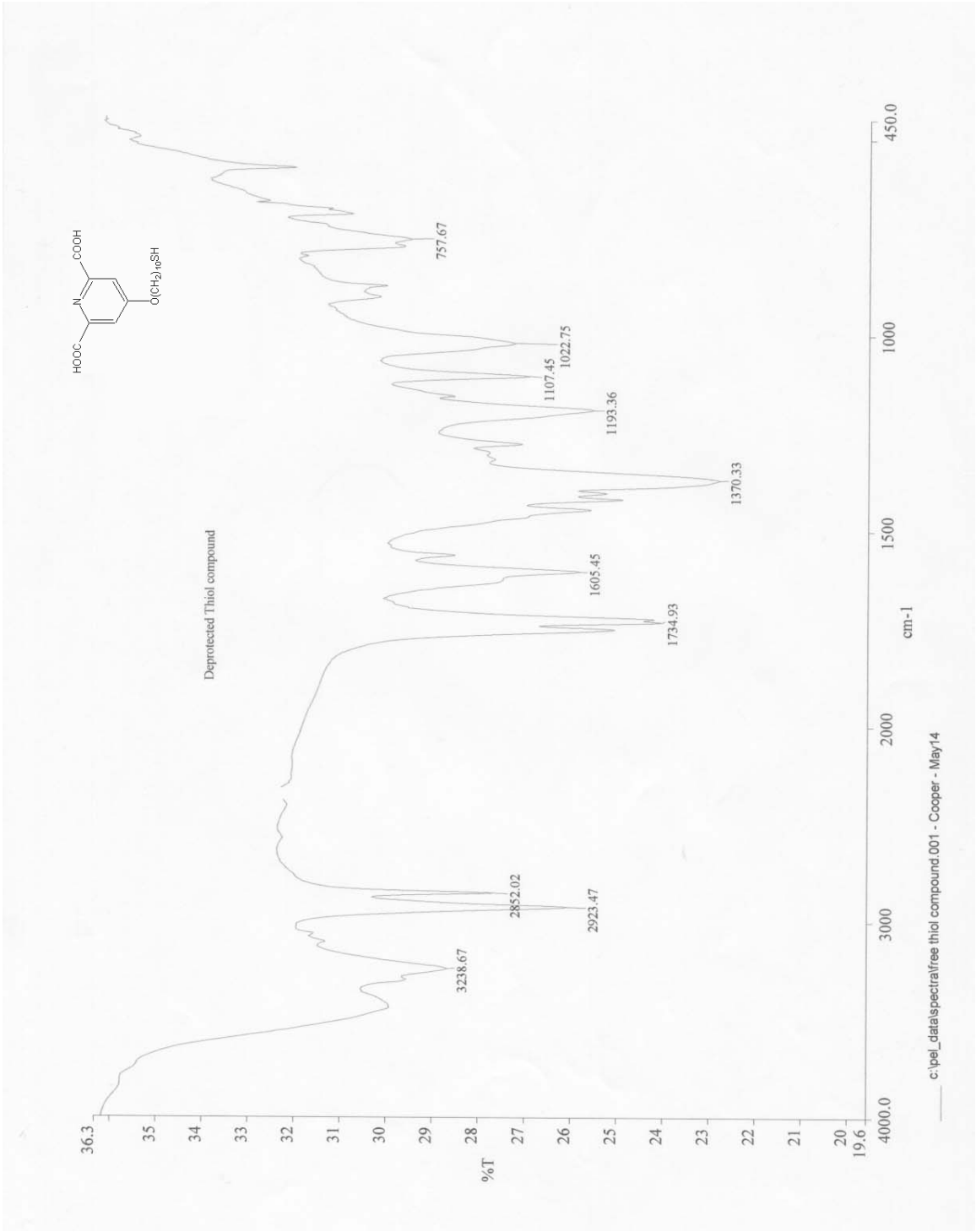
COOH
HOOC
N
O(CH2)10SH
Deprotected Thiol compound
%T
cm-1
36.3
35
34
33
32
31
30
29
28
27
26
25
24
23
22
21
20
19.6
4000.0
3000
2000
1500
1000
450.0
3238.67
2852.02
2923.47
1734.93
1605.45
1370.33
1193.36
1107.45
1022.75
757.67
c:\pel_data\spectra\free thiol compound.001 - Cooper - May14

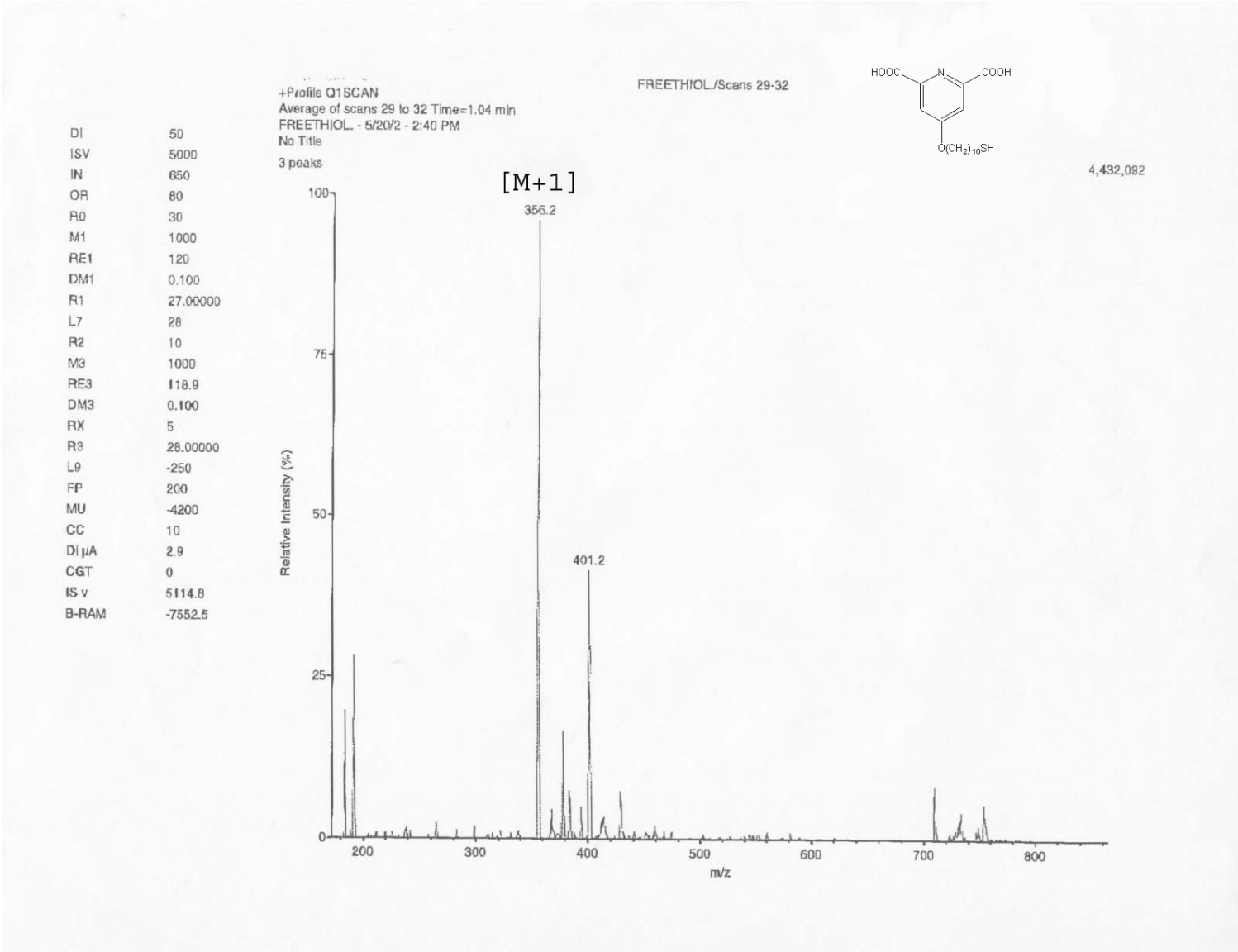
DI 50
ISV 5000
IN 650
OR 80
R0 30
M1 1000
RE1 120
DM1 0.100
R1 27.00000
L7 28
R2 10
M3 1000
RE3 118.9
DM3 0.100
RX 5
R3 28.00000
L9 -250
FP 200
MU -4200
CC 10
Di µA 2.9
CGT 0
IS v 5114.8
B-RAM -7552.5
+Profile Q1SCAN
Average of scans 29 to 32 Time=1.04 min
FREETHIOL. - 5/20/2 - 2:40 PM
No Title
3 peaks
FREETHIOL./Scans 29-32
HOOC
N
COOH
O(CH2)10SH
4,432,092
[M+1]
356.2
401.2
Relative Intensity (%)
100
75
50
25
0
200
300
400
500
600
700
800
m/z

Scheme 6. Synthesis of 2, 2', 5, 5'-tetracarboxy-4, 4'-dipyridine

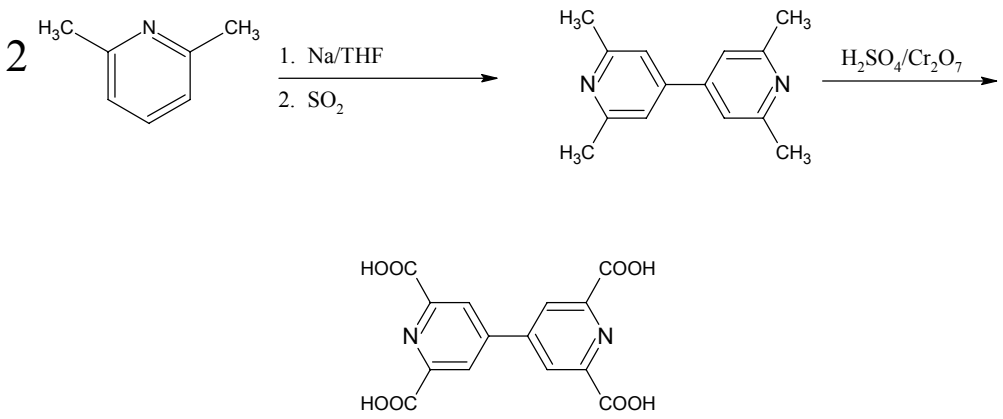

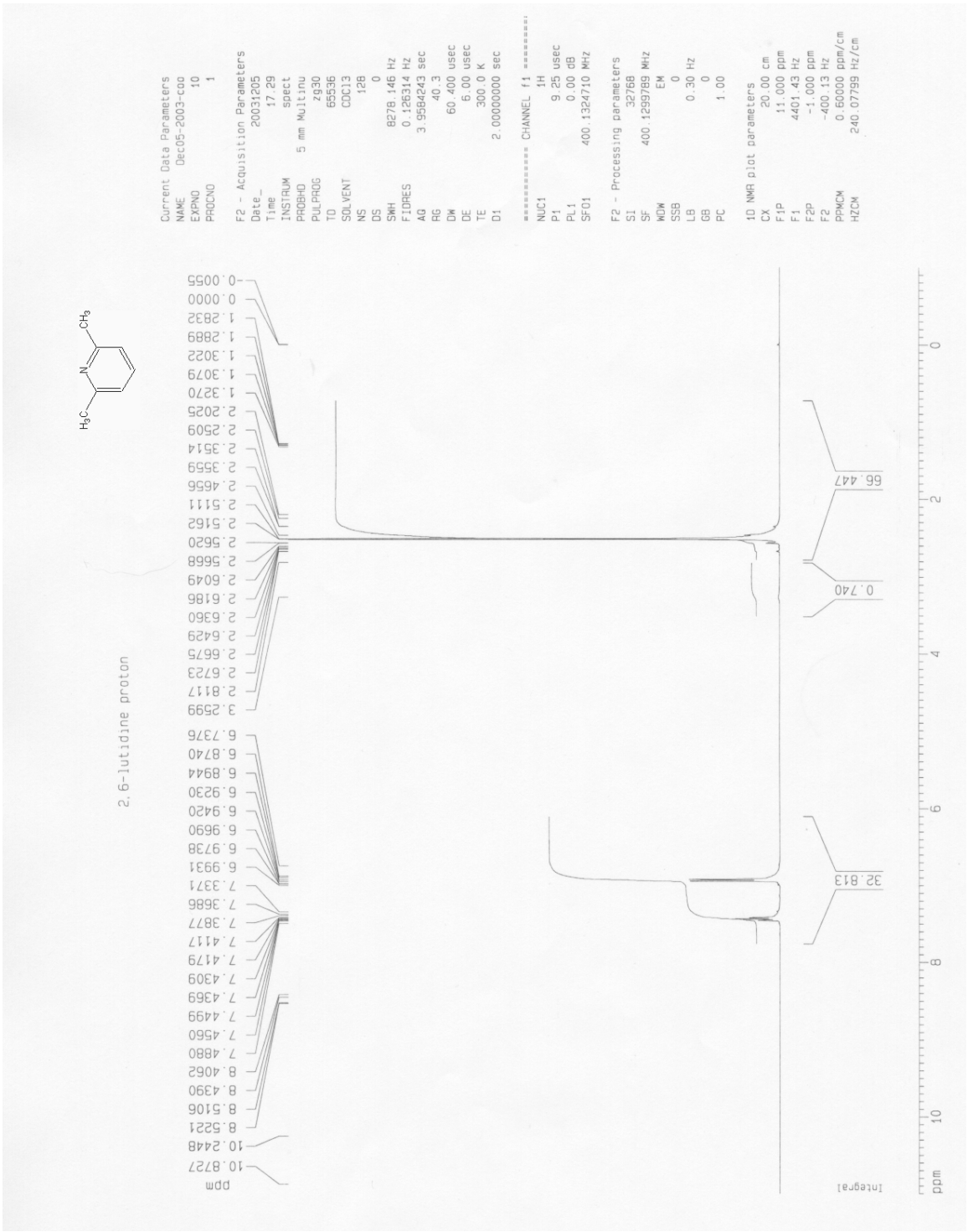
2,6-lutidine proton
Current Data Parameters
NAME Dec05-2003-coo
EXPNO 10
PROCNO 1
F2 - Acquisition Parameters
Date_ 20031205
Time 17.29
INSTRUM spect
PROBHD 5 mm Multinu
PULPROG zg30
TD 65536
SOLVENT CDCl3
NS 128
DS 0
SWH 8278.146 Hz
FIDRES 0.126314 Hz
AQ 3.9584243 sec
RG 40.3
DW 60.400 usec
DE 6.00 usec
TE 300.0 K
D1 2.00000000 sec
======== CHANNEL f1 ========
NUC1 1H
P1 9.25 usec
PL1 0.00 dB
SFO1 400.1324710 MHz
F2 - Processing parameters
SI 32768
SF 400.1299789 MHz
WDW EM
SSB 0
LB 0.30 Hz
GB 0
PC 1.00
1D NMR plot parameters
CX 20.00 cm
F1P 11.000 ppm
F1 4401.43 Hz
F2P -1.000 ppm
F2 -400.13 Hz
PPMCM 0.60000 ppm/cm
HZCM 240.07799 Hz/cm
ppm
10.872
10.244
8.522
8.510
8.439
8.406
7.488
7.456
7.449
7.436
7.430
7.417
7.411
7.387
7.368
7.337
6.993
6.973
6.969
6.942
6.923
6.894
6.874
6.737
3.259
2.811
2.672
2.667
2.642
2.636
2.618
2.604
2.566
2.562
2.511
2.465
2.355
2.350
2.250
2.202
1.327
1.307
1.302
1.288
1.283
0.000
0.005
Integral
66.447
0.740
32.813
10
8
6
4
2
0
ppm

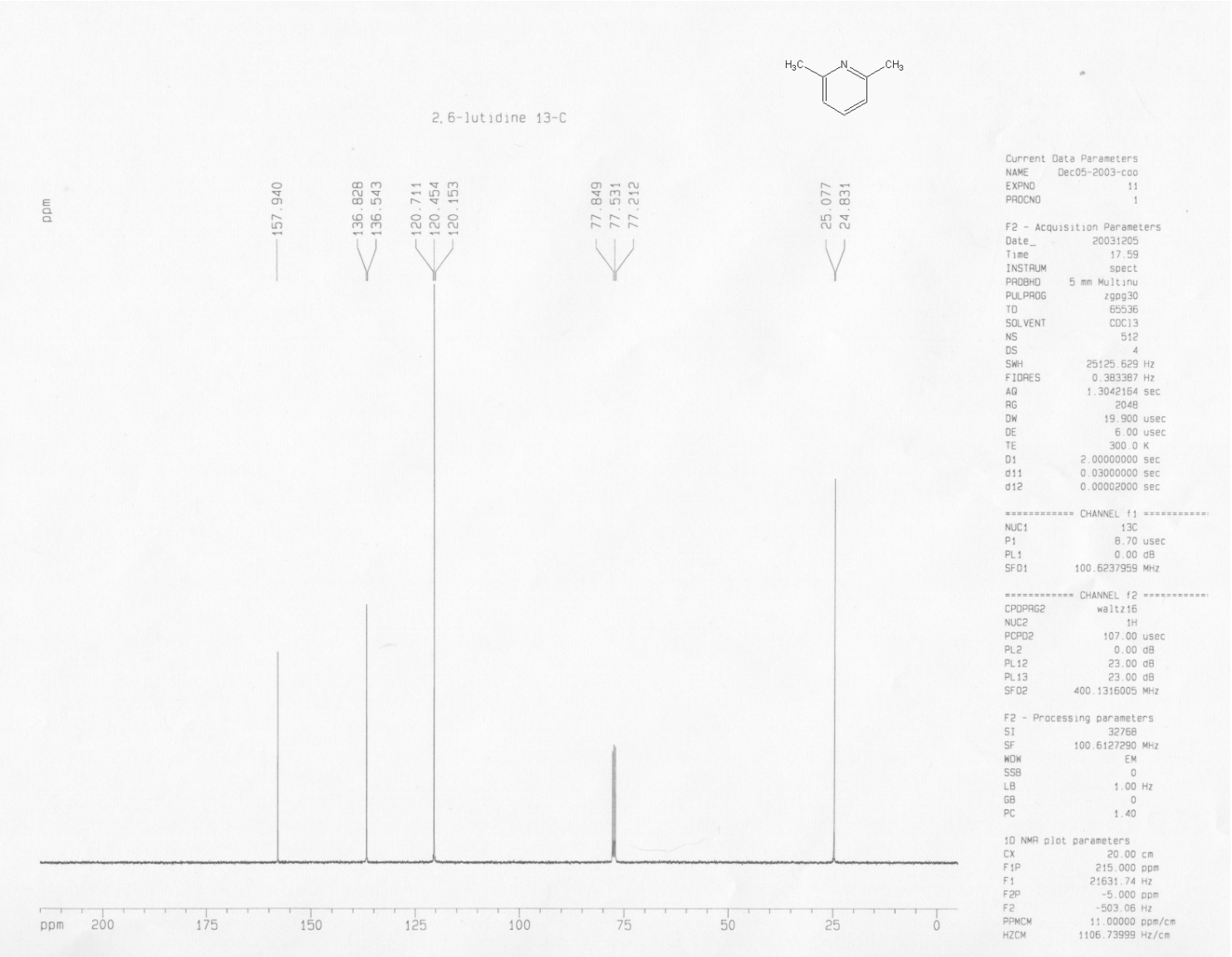
2,6-lutidine 13-C
ppm
157.940
136.828
136.543
120.711
120.454
120.153
77.849
77.531
77.212
25.077
24.831
ppm 200 175 150 125 100 75 50 25 0
Current Data Parameters
NAME Dec05-2003-coo
EXPNO 11
PROCNO 1
F2 - Acquisition Parameters
Date_ 20031205
Time 17.59
INSTRUM spect
PROBHD 5 mm Multinu
PULPROG zgpg30
TD 65536
SOLVENT CDCl3
NS 512
DS 4
SWH 25125.629 Hz
FIDRES 0.383387 Hz
AQ 1.3042164 sec
RG 2048
DW 19.900 usec
DE 6.00 usec
TE 300.0 K
D1 2.00000000 sec
d11 0.03000000 sec
d12 0.00002000 sec
CHANNEL f1
NUC1 13C
P1 8.70 usec
PL1 0.00 dB
SF01 100.6237959 MHz
CHANNEL f2
CPDPRG2 waltz16
NUC2 1H
PCPD2 107.00 usec
PL2 0.00 dB
PL12 23.00 dB
PL13 23.00 dB
SF02 400.1316005 MHz
F2 - Processing parameters
SI 32768
SF 100.6127290 MHz
WDW EM
SSB 0
LB 1.00 Hz
GB 0
PC 1.40
1D NMR plot parameters
CX 20.00 cm
F1P 215.000 ppm
F1 21631.74 Hz
F2P -5.000 ppm
F2 -503.06 Hz
PPMCM 11.00000 ppm/cm
HZCM 1106.73999 Hz/cm

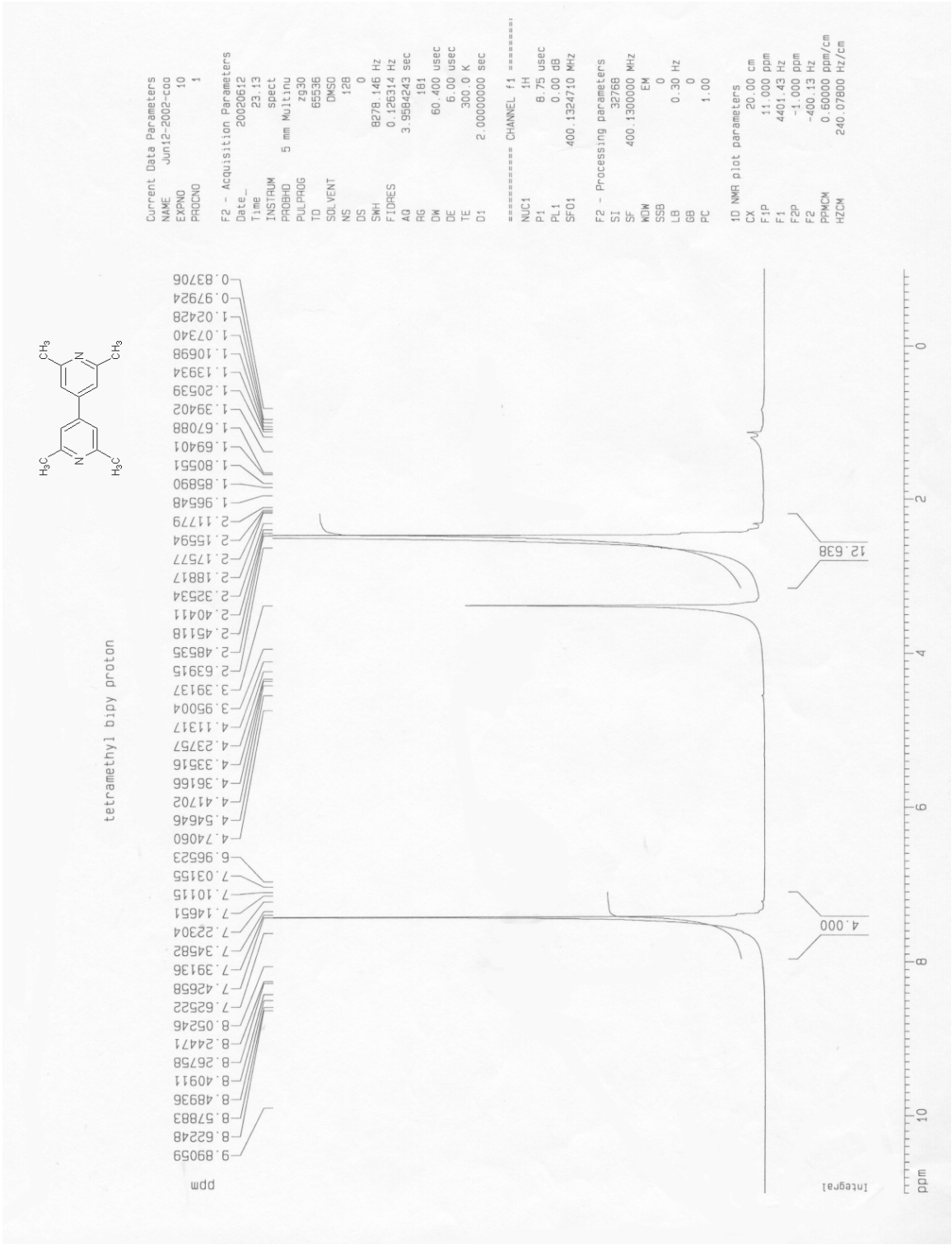
tetramethyl bipy proton
Current Data Parameters
NAME Jun12-2002-coo
EXPNO 10
PROCNO 1
F2 - Acquisition Parameters
Date_ 20020612
Time 23.13
INSTRUM spect
PROBHD 5 mm Multinu
PULPROG zg30
TD 65536
SOLVENT DMSO
NS 128
DS 0
SWH 8278.146 Hz
FIDRES 0.126314 Hz
AQ 3.9584243 sec
RG 181
DW 60.400 usec
DE 6.00 usec
TE 300.0 K
D1 2.00000000 sec
========== CHANNEL f1 ==========
NUC1 1H
P1 8.75 usec
PL1 0.00 dB
SFO1 400.1324710 MHz
F2 - Processing parameters
SI 32768
SF 400.1300000 MHz
WDW EM
SSB 0
LB 0.30 Hz
GB 0
PC 1.00
1D NMR plot parameters
CX 20.00 cm
F1P 11.000 ppm
F1 4401.43 Hz
F2P -1.000 ppm
F2 -400.13 Hz
PPMCM 0.60000 ppm/cm
HZCM 240.07800 Hz/cm
ppm
Integral
12.638
4.000

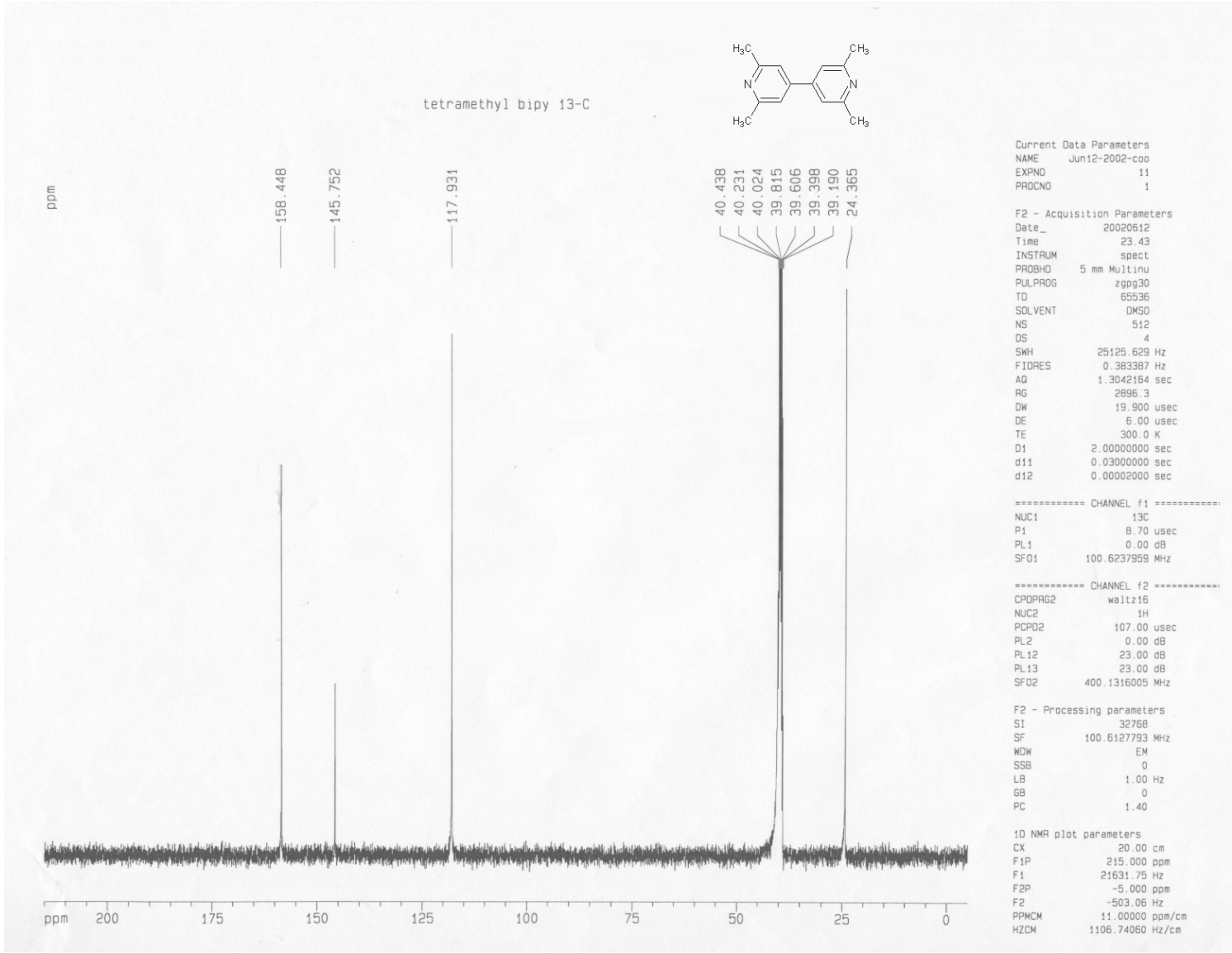
tetramethyl bipy 13-C
ppm
158.448
145.752
117.931
40.438
40.231
40.024
39.815
39.606
39.398
39.190
24.365
ppm 200 175 150 125 100 75 50 25 0
Current Data Parameters
NAME Jun12-2002-coo
EXPNO 11
PROCNO 1
F2 - Acquisition Parameters
Date_ 20020612
Time 23.43
INSTRUM spect
PROBHD 5 mm Multinu
PULPROG zgpg30
TD 65536
SOLVENT DMSO
NS 512
DS 4
SWH 25125.629 Hz
FIDRES 0.383387 Hz
AQ 1.3042164 sec
RG 2896.3
DW 19.900 usec
DE 6.00 usec
TE 300.0 K
D1 2.00000000 sec
d11 0.03000000 sec
d12 0.00002000 sec
CHANNEL f1
NUC1 13C
P1 8.70 usec
PL1 0.00 dB
SFO1 100.6237959 MHz
CHANNEL f2
CPDPRG2 waltz16
NUC2 1H
PCPD2 107.00 usec
PL2 0.00 dB
PL12 23.00 dB
PL13 23.00 dB
SFO2 400.1316005 MHz
F2 - Processing parameters
SI 32768
SF 100.6127793 MHz
WDW EM
SSB 0
LB 1.00 Hz
GB 0
PC 1.40
1D NMR plot parameters
CX 20.00 cm
F1P 215.000 ppm
F1 21631.75 Hz
F2P -5.000 ppm
F2 -503.06 Hz
PPMCM 11.00000 ppm/cm
HZCM 1106.74060 Hz/cm

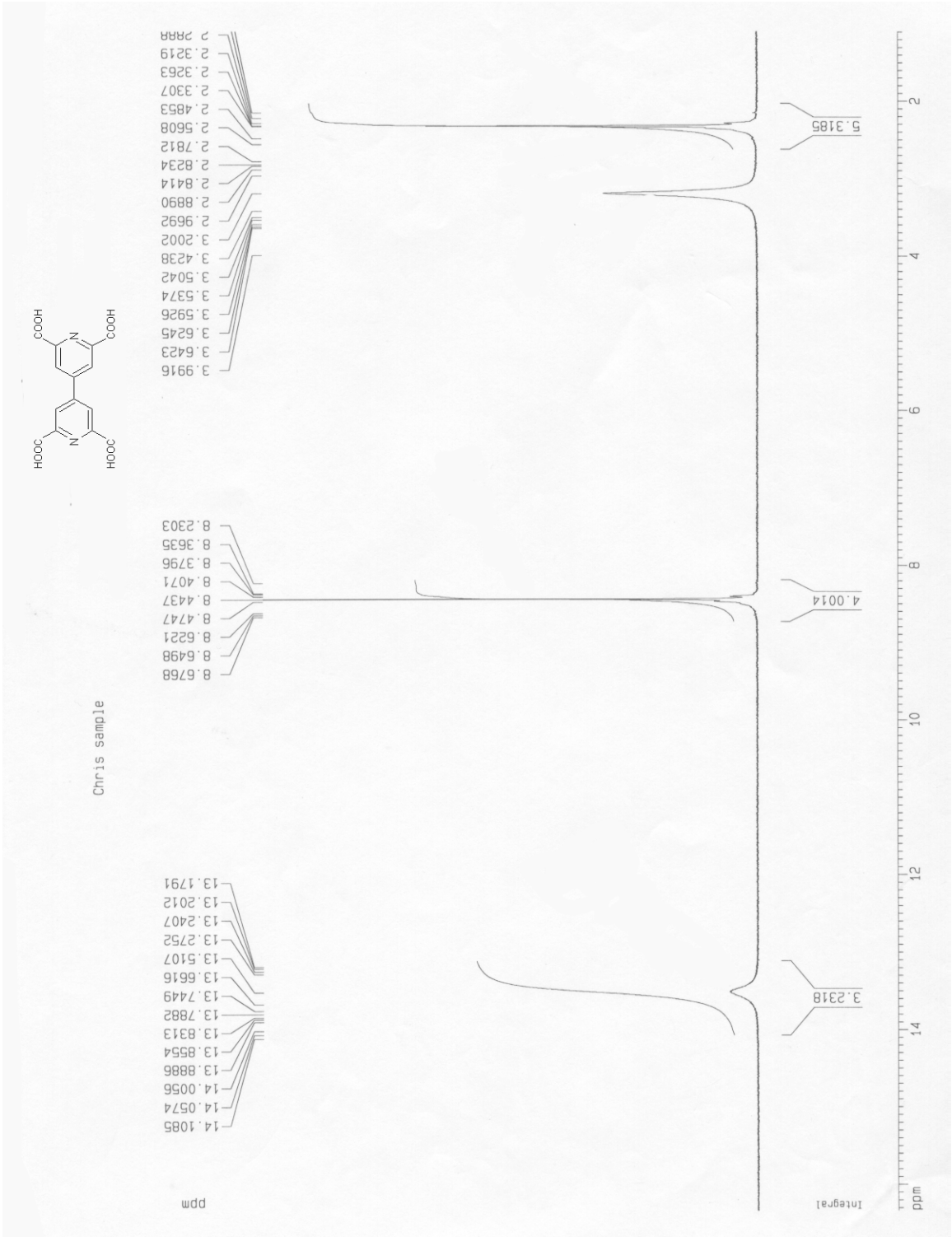
Chris sample
COOH
COOH
HOOC
HOOC
N
N
13.1791
13.2012
13.2407
13.2752
13.5107
13.6616
13.7449
13.7882
13.8313
13.8554
13.8886
14.0056
14.0574
14.1085
8.2303
8.3635
8.3796
8.4071
8.4437
8.4747
8.6221
8.6498
8.6768
3.9916
3.6423
3.6245
3.5926
3.5374
3.5042
3.4238
3.2002
2.9692
2.8890
2.8414
2.8234
2.7812
2.5608
2.4853
2.3307
2.3263
2.3219
2.2882
5.3185
4.0014
3.2318
ppm
Integral
2
4
6
8
10
12
14

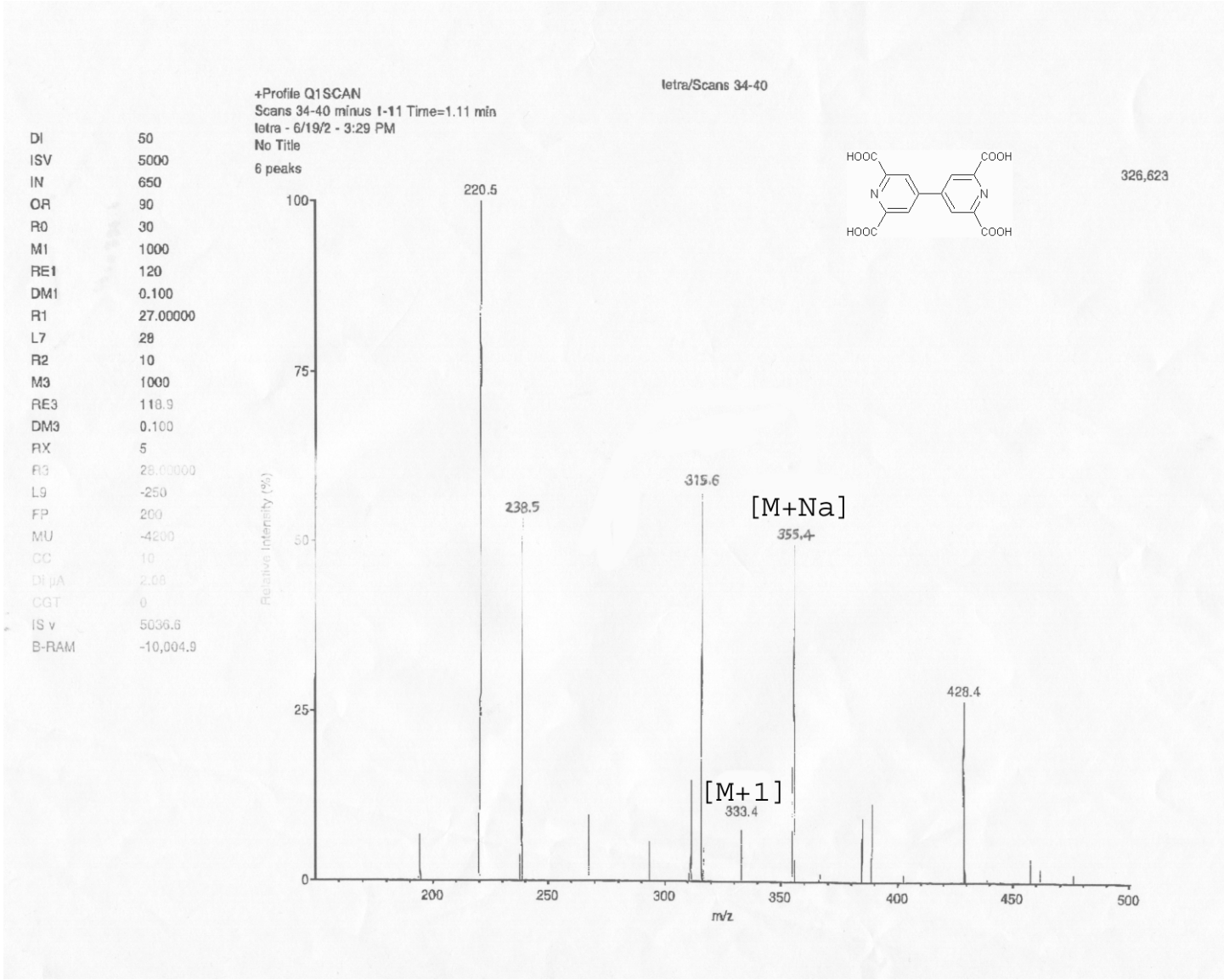
+Profile Q1SCAN
Scans 34-40 minus 1-11 Time=1.11 min
tetra - 6/19/2 - 3:29 PM
No Title
6 peaks
tetra/Scans 34-40
DI 50
ISV 5000
IN 650
OR 90
R0 30
M1 1000
RE1 120
DM1 0.100
R1 27.00000
L7 28
R2 10
M3 1000
RE3 118.9
DM3 0.100
RX 5
L9 -250
FP 200
MU -4200
IS v 5036.6
B-RAM -10,004.9
HOOC
COOH
N
N
HOOC
COOH
326,623
220.5
315.6
238.5
[M+Na]
355.4
428.4
[M+1]
333.4
Relative Intensity (%)
100
75
50
25
0
200
250
300
350
400
450
500
m/z

Scheme 7. Synthesis of 4-(Methylpyrenyl)oxypyridine-2,6-dicarboxylic acid

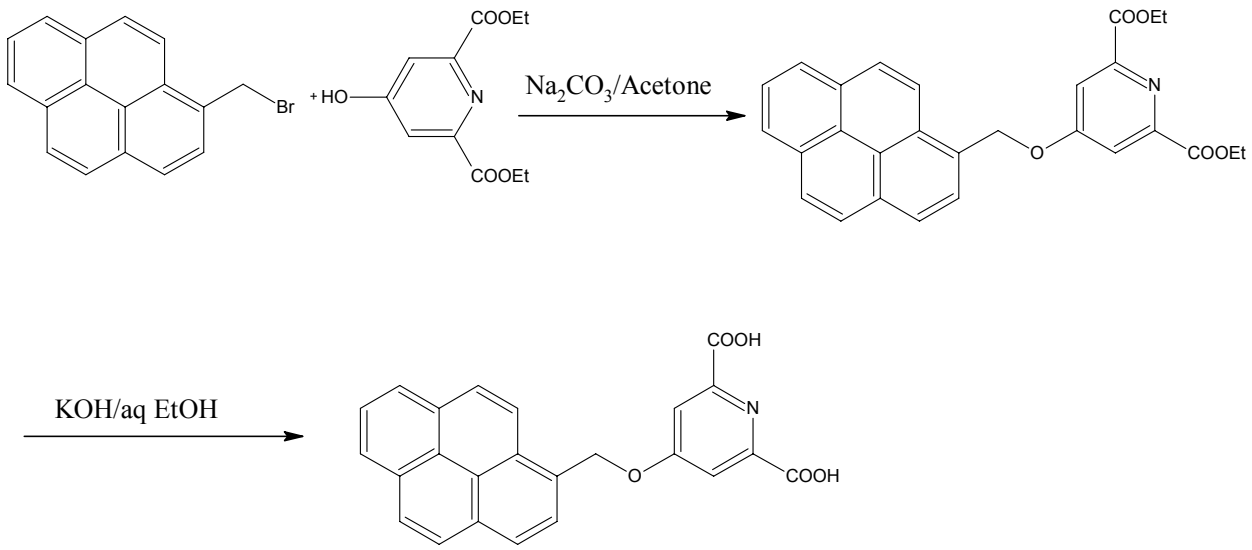

The spectra collected for 1-bromomethylpyrene and for Diethyl 4-hydroxypyridine-2,6-dicarboxylate have been previously displayed.

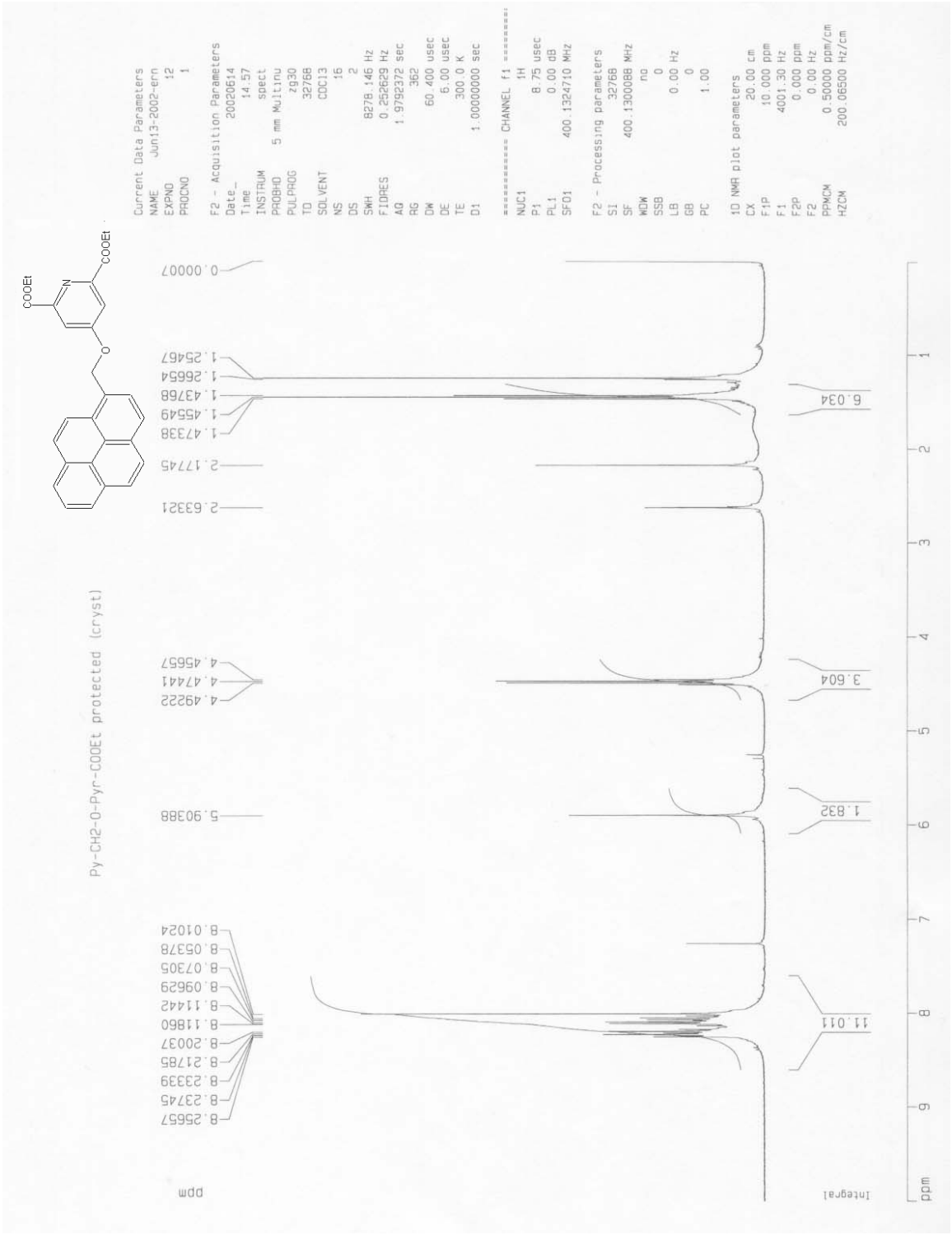
Py-CH2-O-Pyr-COOEt protected (cryst)
Current Data Parameters
NAME Jun13-2002-ern
EXPNO 12
PROCNO 1
F2 - Acquisition Parameters
Date_ 20020614
Time 14.57
INSTRUM spect
PROBHD 5 mm Multinu
PULPROG zg30
TD 32768
SOLVENT CDCl3
NS 16
DS 2
SWH 8278.146 Hz
FIDRES 0.252629 Hz
AQ 1.9792372 sec
RG 362
DW 60.400 usec
DE 6.00 usec
TE 300.0 K
D1 1.00000000 sec
========== CHANNEL f1 ==========
NUC1 1H
P1 8.75 usec
PL1 0.00 dB
SFO1 400.1324710 MHz
F2 - Processing parameters
SI 32768
SF 400.1300088 MHz
WDW no
SSB 0
LB 0.00 Hz
GB 0
PC 1.00
1D NMR plot parameters
CX 20.00 cm
F1P 10.000 ppm
F1 4001.30 Hz
F2P 0.000 ppm
F2 0.00 Hz
PPMCM 0.50000 ppm/cm
HZCM 200.06500 Hz/cm
COOEt
COOEt
O
N
7.00007
1.25467
1.26654
1.43768
1.45549
1.47338
2.17745
2.63321
4.45657
4.47441
4.49222
5.90388
8.01024
8.05378
8.07305
8.09629
8.11442
8.11860
8.20037
8.21785
8.23339
8.23745
8.25657
6.034
3.604
1.832
11.011
ppm
Integral

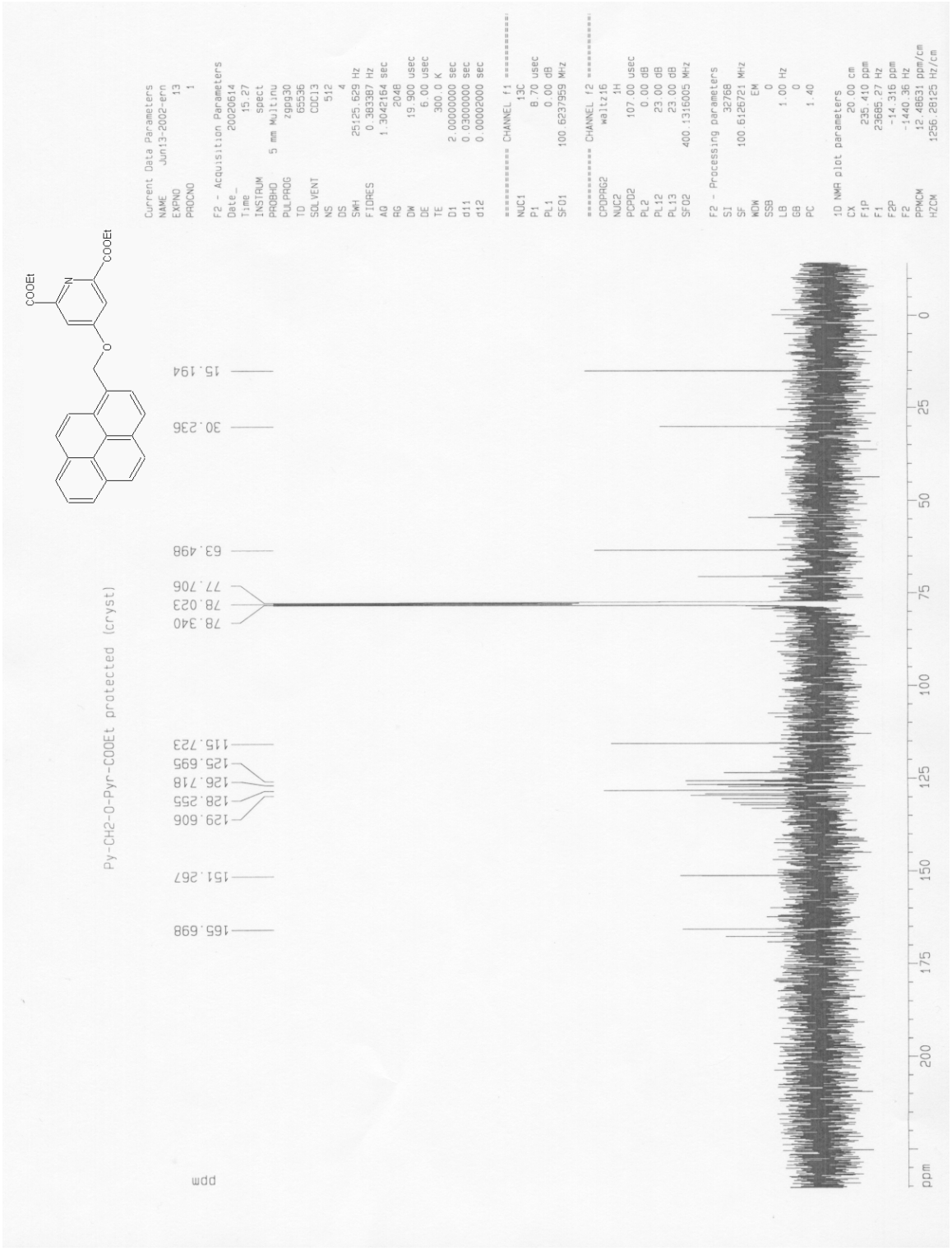
Py-CH2-O-Pyr-COOEt protected (cryst)
COOEt
COOEt
N
O
ppm
15.194
30.236
63.498
77.706
78.023
78.340
115.723
125.695
126.718
128.255
129.606
151.267
165.698
Current Data Parameters
NAME Jun13-2002-ern
EXPNO 13
PROCNO 1
F2 - Acquisition Parameters
Date_ 20020614
Time 15.27
INSTRUM spect
PROBHD 5 mm Multinu
PULPROG zgpg30
TD 65536
SOLVENT CDCl3
NS 512
DS 4
SWH 25125.629 Hz
FIDRES 0.383307 Hz
AQ 1.3042164 sec
RG 2048
DW 19.900 usec
DE 6.00 usec
TE 300.0 K
D1 2.00000000 sec
d11 0.03000000 sec
d12 0.00002000 sec
CHANNEL f1
NUC1 13C
P1 8.70 usec
PL1 0.00 dB
SFO1 100.6237959 MHz
CHANNEL f2
CPDPRG2 waltz16
NUC2 1H
PCPD2 107.00 usec
PL2 0.00 dB
PL12 23.00 dB
PL13 23.00 dB
SFO2 400.1316005 MHz
F2 - Processing parameters
SI 32768
SF 100.6126721 MHz
WDW EM
SSB 0
LB 1.00 Hz
GB 0
PC 1.40
1D NMR plot parameters
CX 20.00 cm
F1P 235.410 ppm
F1 23685.27 Hz
F2P -14.316 ppm
F2 -1440.36 Hz
PPMCM 12.48631 ppm/cm
HZCM 1256.28125 Hz/cm
ppm
0
25
50
75
100
125
150
175
200

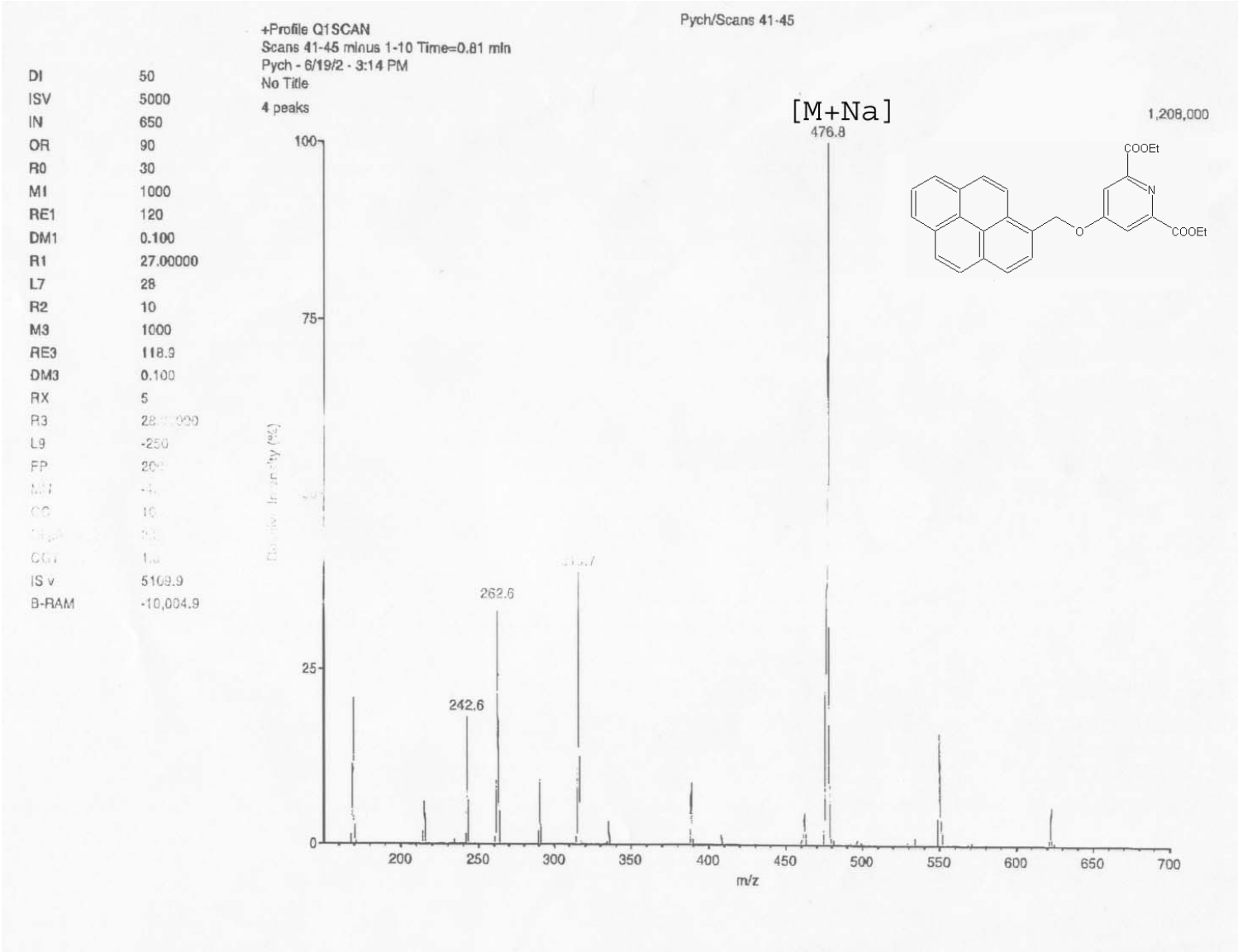
Pych/Scans 41-45
+Profile Q1SCAN
Scans 41-45 minus 1-10 Time=0.81 min
Pych - 6/19/2 - 3:14 PM
No Title
4 peaks
[M+Na]
476.8
1,208,000
COOEt
N
O
COOEt
262.6
242.6
100
75
25
0
200
250
300
350
400
450
500
550
600
650
700
m/z
DI 50
ISV 5000
IN 650
OR 90
R0 30
M1 1000
RE1 120
DM1 0.100
R1 27.00000
L7 28
R2 10
M3 1000
RE3 118.9
DM3 0.100
RX 5
L9 -250
IS v 5109.9
B-RAM -10,004.9

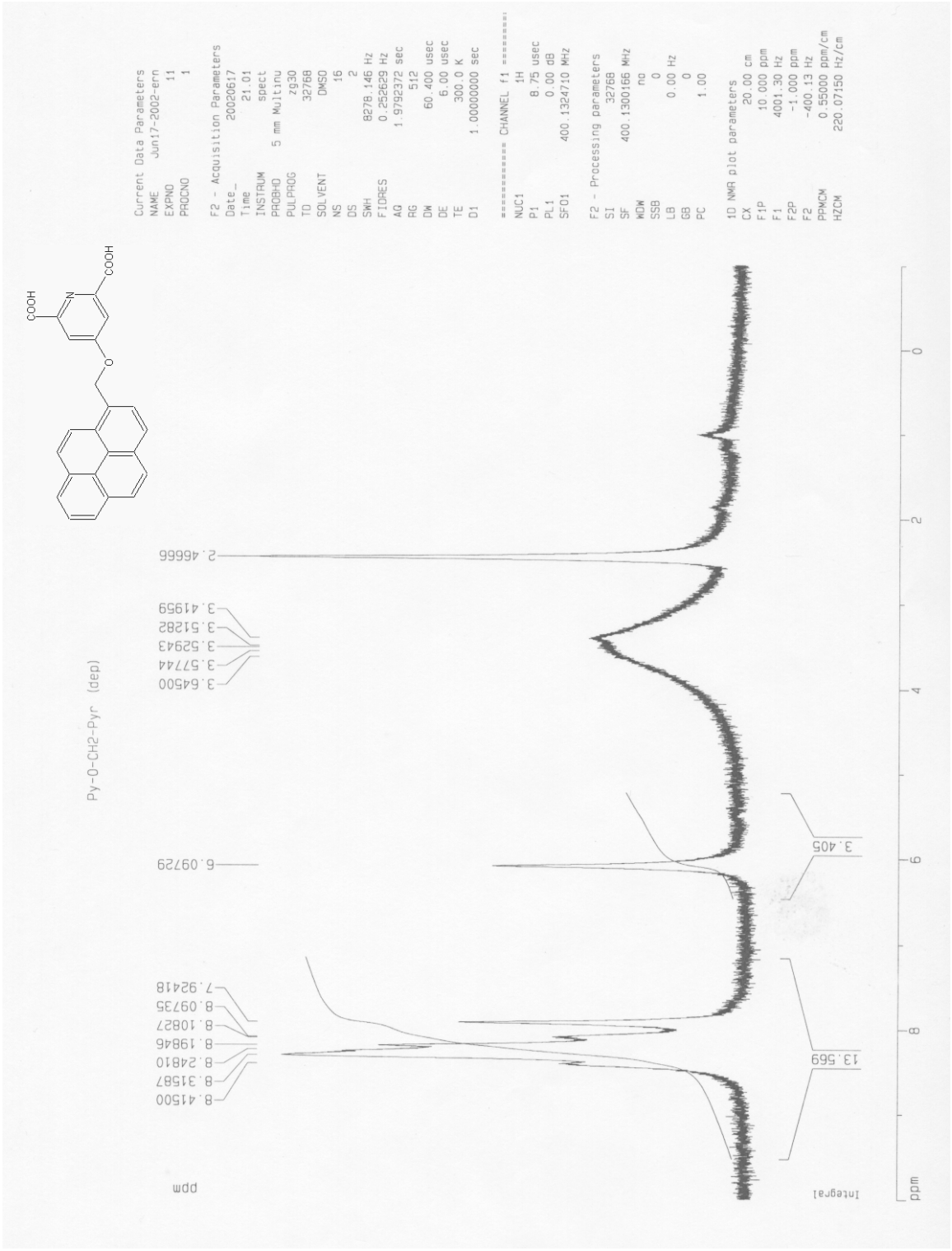
Current Data Parameters
NAME Jun17-2002-ern
EXPNO 11
PROCNO 1
F2 - Acquisition Parameters
Date_ 20020617
Time 21.01
INSTRUM spect
PROBHD 5 mm Multinu
PULPROG zg30
TD 32768
SOLVENT DMSO
NS 16
DS 2
SWH 8278.146 Hz
FIDRES 0.252629 Hz
AQ 1.9792372 sec
RG 512
DW 60.400 usec
DE 6.00 usec
TE 300.0 K
D1 1.00000000 sec
========== CHANNEL f1 ========
NUC1 1H
P1 8.75 usec
PL1 0.00 dB
SFO1 400.1324710 MHz
F2 - Processing parameters
SI 32768
SF 400.1300166 MHz
WDW no
SSB 0
LB 0.00 Hz
GB 0
PC 1.00
1D NMR plot parameters
CX 20.00 cm
F1P 10.000 ppm
F1 4001.30 Hz
F2P -1.000 ppm
F2 -400.13 Hz
PPMCM 0.55000 ppm/cm
HZCM 220.07150 Hz/cm
COOH
COOH
N
O
Py-O-CH2-Pyr (dep)
2.46666
3.41959
3.51282
3.52943
3.57744
3.64500
6.09729
7.92418
8.09735
8.10827
8.19846
8.24810
8.31587
8.41500
3.405
13.569
ppm
Integral
ppm

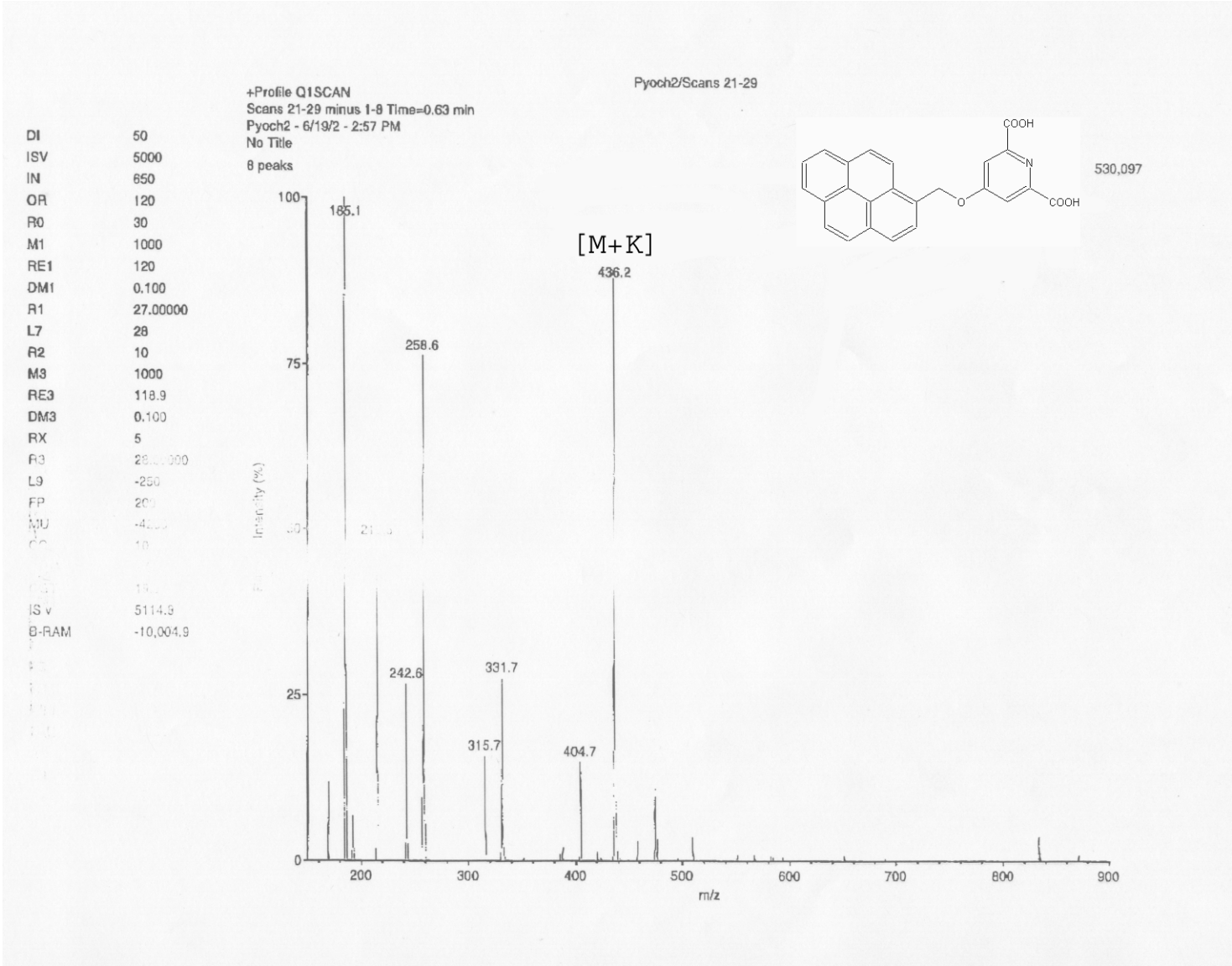
+Profile Q1SCAN
Scans 21-29 minus 1-8 Time=0.63 min
Pyoch2 - 6/19/2 - 2:57 PM
No Title
8 peaks
Pyoch2/Scans 21-29
530,097
[M+K]
436.2
185.1
258.6
242.6
331.7
315.7
404.7
Intensity (%)
m/z
DI 50
ISV 5000
IN 650
OR 120
R0 30
M1 1000
RE1 120
DM1 0.100
R1 27.00000
L7 28
R2 10
M3 1000
RE3 118.9
DM3 0.100
RX 5
L9 -250
IS v 5114.9
B-RAM -10,004.9

Scheme 8. Synthesis of Lipoamine-(Ala-Aib)$_6$-t-Boc-Pyrenyl Alanine

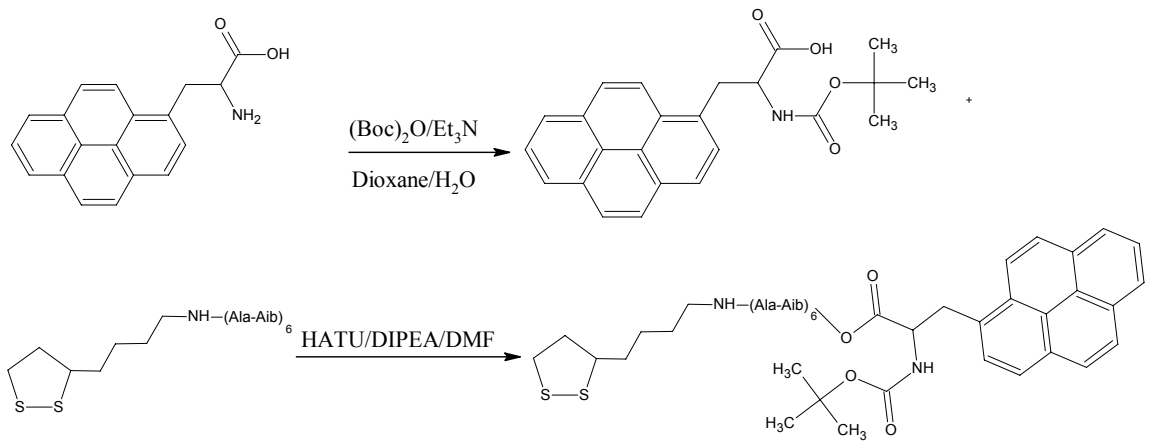

The spectra collected for pyrenyl alanine have been previously displayed.

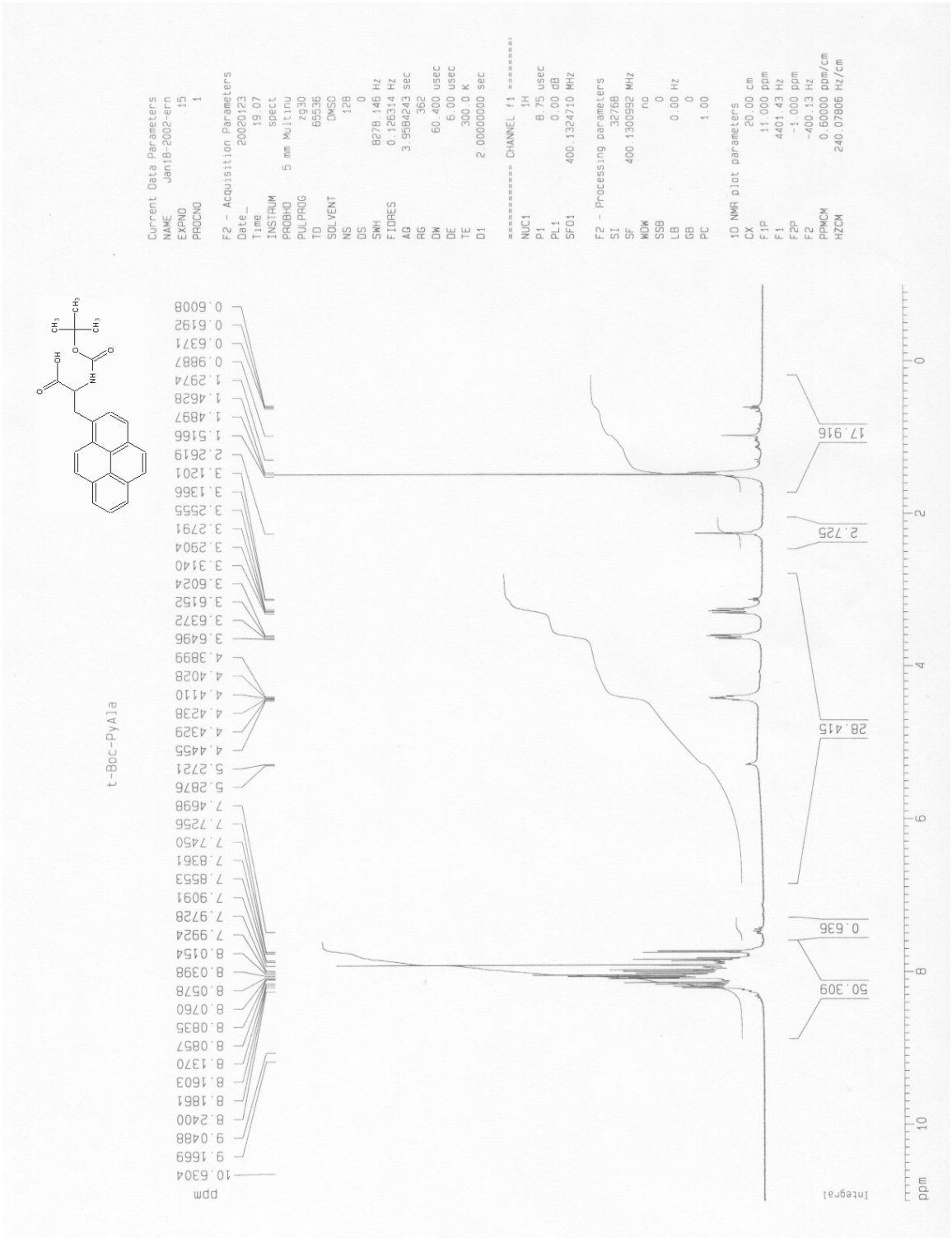
Current Data Parameters
NAME Jan18-2002-ern
EXPNO 15
PROCNO 1
F2 - Acquisition Parameters
Date_ 20020123
Time 19.07
INSTRUM spect
PROBHD 5 mm Multinu
PULPROG zg30
TD 65536
SOLVENT DMSO
NS 128
DS 0
SWH 8278.146 Hz
FIDRES 0.126314 Hz
AQ 3.9584243 sec
RG 362
DW 60.400 usec
DE 6.00 usec
TE 300.0 K
D1 2.00000000 sec
======== CHANNEL f1 ========
NUC1 1H
P1 8.75 usec
PL1 0.00 dB
SFO1 400.1324710 MHz
F2 - Processing parameters
SI 32768
SF 400.1300932 MHz
WDW no
SSB 0
LB 0.00 Hz
GB 0
PC 1.00
1D NMR plot parameters
CX 20.00 cm
F1P 11.000 ppm
F1 4401.43 Hz
F2P -1.000 ppm
F2 -400.13 Hz
PPMCM 0.60000 ppm/cm
HZCM 240.07806 Hz/cm
t-Boc-PyAla
ppm
Integral
17.916
2.725
28.415
0.636
50.309

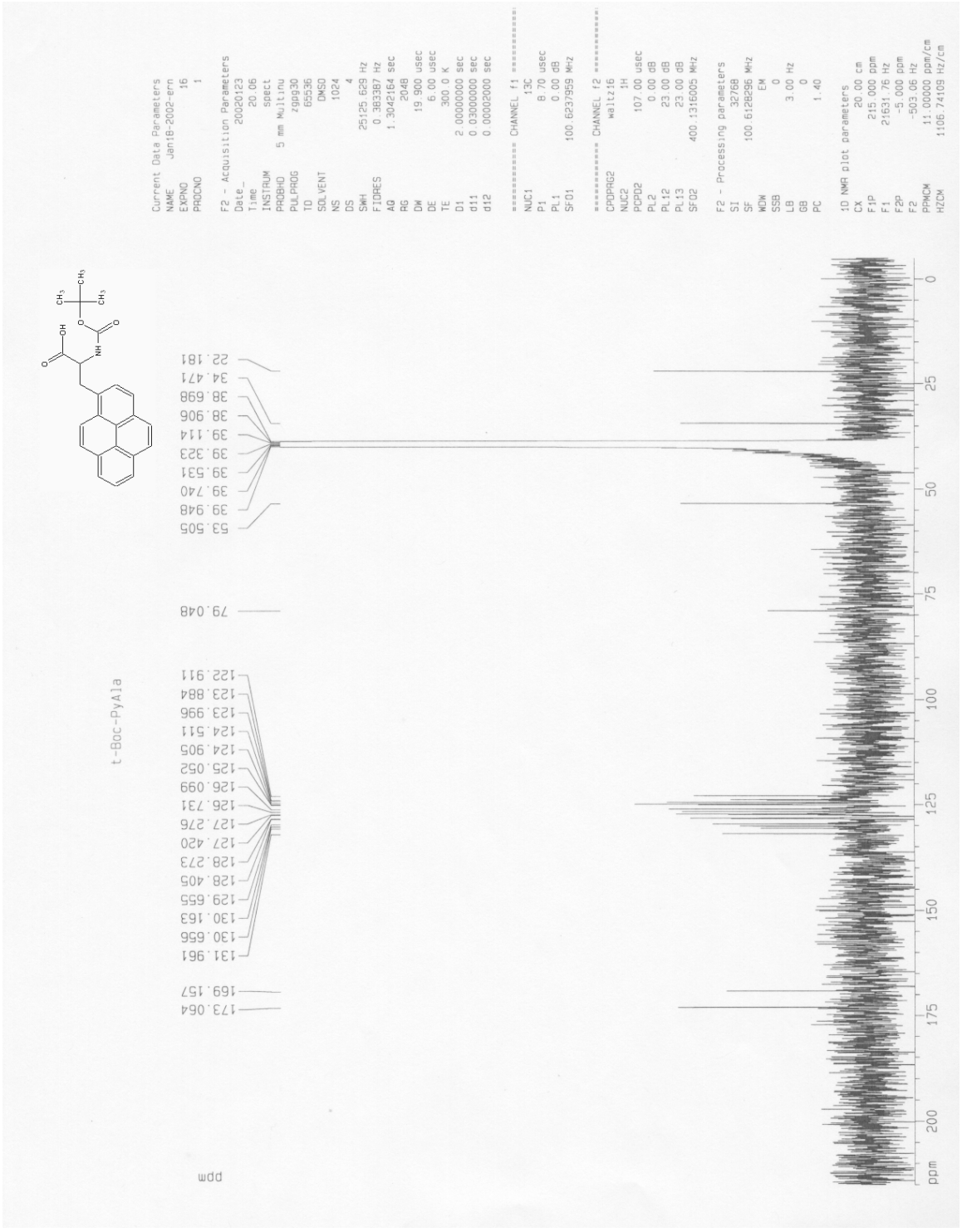
t-Boc-PyAla
ppm
22.181
34.471
38.698
38.906
39.114
39.323
39.531
39.740
39.948
53.505
79.048
122.911
123.884
123.996
124.511
124.905
125.052
126.099
126.731
127.276
127.420
128.273
128.405
129.655
130.163
130.656
131.961
169.157
173.064
Current Data Parameters
NAME Jan18-2002-ern
EXPNO 16
PROCNO 1
F2 - Acquisition Parameters
Date_ 20020123
Time 20.06
INSTRUM spect
PROBHD 5 mm Multinu
PULPROG zgpg30
TD 65536
SOLVENT DMSO
NS 1024
DS 4
SWH 25125.629 Hz
FIDRES 0.383387 Hz
AQ 1.3042164 sec
RG 2048
DW 19.900 usec
DE 6.00 usec
TE 300.0 K
D1 2.00000000 sec
d11 0.03000000 sec
d12 0.00002000 sec
CHANNEL f1
NUC1 13C
P1 8.70 usec
PL1 0.00 dB
SFO1 100.6237959 MHz
CHANNEL f2
CPDPRG2 waltz16
NUC2 1H
PCPD2 107.00 usec
PL2 0.00 dB
PL12 23.00 dB
PL13 23.00 dB
SFO2 400.1316005 MHz
F2 - Processing parameters
SI 32768
SF 100.6128296 MHz
WDW EM
SSB 0
LB 3.00 Hz
GB 0
PC 1.40
1D NMR plot parameters
CX 20.00 cm
F1P 215.000 ppm
F1 21631.76 Hz
F2P -5.000 ppm
F2 -503.06 Hz
PPMCM 11.00000 ppm/cm
HZCM 1106.74109 Hz/cm
ppm
200
175
150
125
100
75
50
25
0

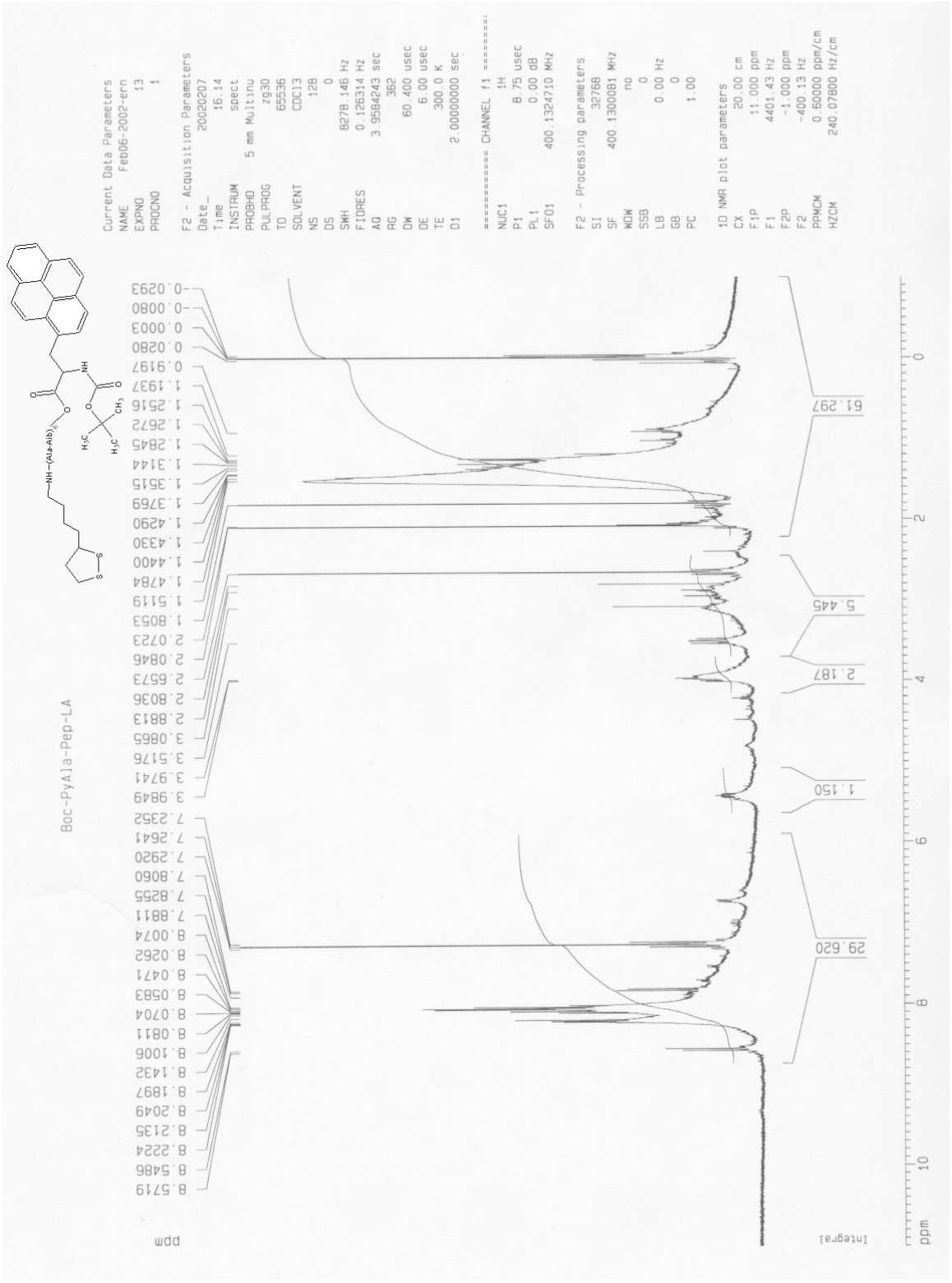
Boc-PyAla-Pep-LA
Current Data Parameters
NAME Feb06-2002-ern
EXPNO 13
PROCNO 1
F2 - Acquisition Parameters
Date_ 20020207
Time 16.14
INSTRUM spect
PROBHD 5 mm Multinu
PULPROG zg30
TD 65536
SOLVENT CDCl3
NS 128
DS 0
SWH 8278.146 Hz
FIDRES 0.126314 Hz
AQ 3.9584243 sec
RG 362
DW 60.400 usec
DE 6.00 usec
TE 300.0 K
D1 2.00000000 sec
========== CHANNEL f1 ========
NUC1 1H
P1 8.75 usec
PL1 0.00 dB
SFO1 400.1324710 MHz
F2 - Processing parameters
SI 32768
SF 400.1300081 MHz
WDW no
SSB 0
LB 0.00 Hz
GB 0
PC 1.00
1D NMR plot parameters
CX 20.00 cm
F1P 11.000 ppm
F1 4401.43 Hz
F2P -1.000 ppm
F2 -400.13 Hz
PPMCM 0.60000 ppm/cm
HZCM 240.07800 Hz/cm
61.297
5.445
2.187
1.150
29.620
ppm
Integral

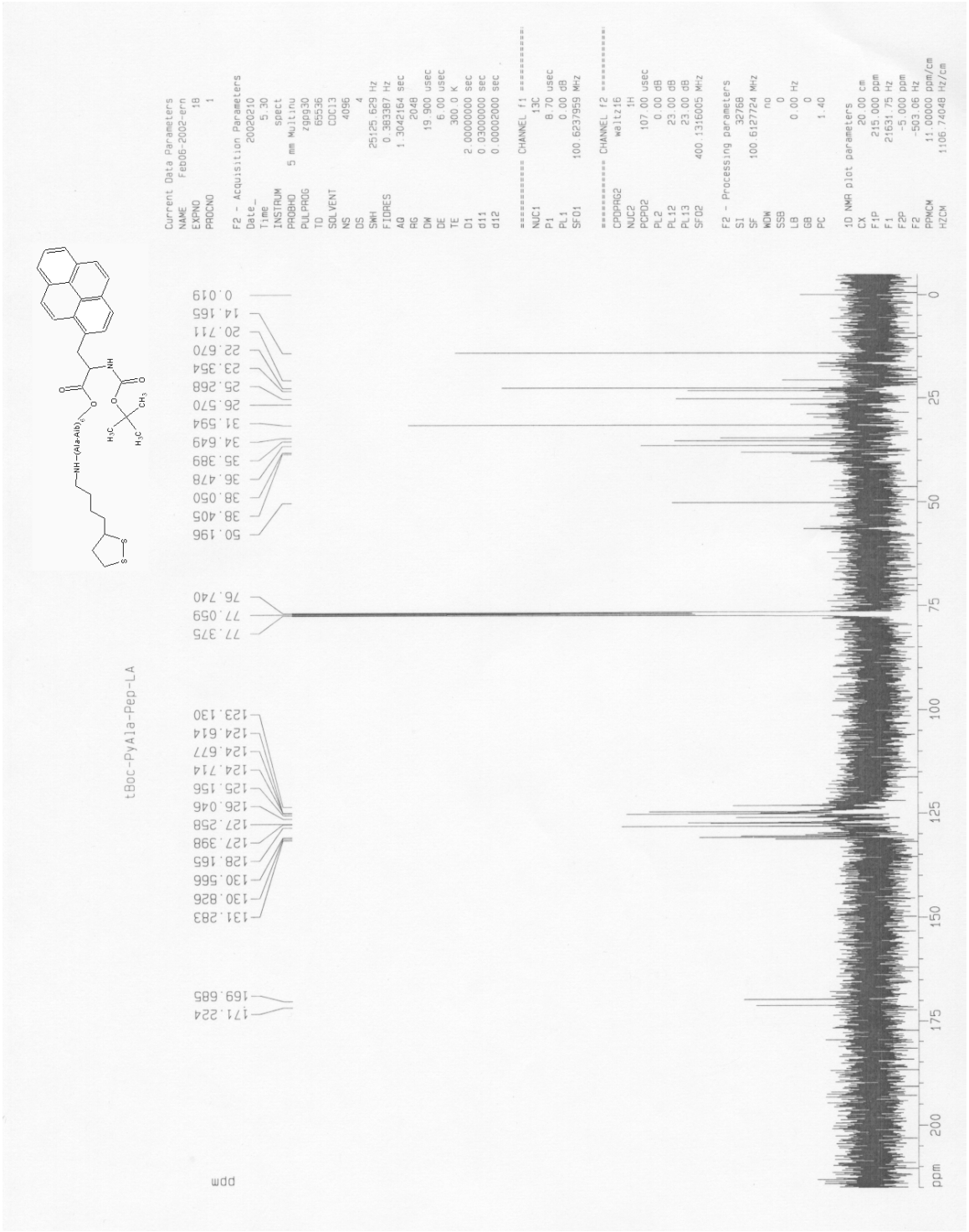
tBoc-PyAla-Pep-LA
Current Data Parameters
NAME FebO6-2002-ern
EXPNO 18
PROCNO 1
F2 - Acquisition Parameters
Date_ 20020210
Time 5.30
INSTRUM spect
PROBHD 5 mm Multinu
PULPROG zgpg30
TD 65536
SOLVENT CDCl3
NS 4096
DS 4
SWH 25125.629 Hz
FIDRES 0.383387 Hz
AQ 1.3042164 sec
RG 2048
DW 19.900 usec
DE 6.00 usec
TE 300.0 K
D1 2.00000000 sec
d11 0.03000000 sec
d12 0.00002000 sec
======== CHANNEL f1 ========
NUC1 13C
P1 8.70 usec
PL1 0.00 dB
SF01 100.6237959 MHz
======== CHANNEL f2 ========
CPDPRG2 waltz16
NUC2 1H
PCPD2 107.00 usec
PL2 0.00 dB
PL12 23.00 dB
PL13 23.00 dB
SF02 400.1316005 MHz
F2 - Processing parameters
SI 32768
SF 100.6127724 MHz
WDW no
SSB 0
LB 0.00 Hz
GB 0
PC 1.40
1D NMR plot parameters
CX 20.00 cm
F1P 215.000 ppm
F1 21631.75 Hz
F2P -5.000 ppm
F2 -503.06 Hz
PPMCM 11.00000 ppm/cm
HZCM 1106.74048 Hz/cm
ppm
0.019
14.165
20.711
22.670
23.354
25.268
26.570
31.594
34.649
35.389
36.478
38.050
38.405
50.196
77.375
77.059
76.740
123.130
124.614
124.677
124.714
125.156
126.046
127.258
127.398
128.165
130.566
130.826
131.283
169.685
171.224

Scheme 9. Synthesis of cis 2, 2'-Dipyridyl Ethylene

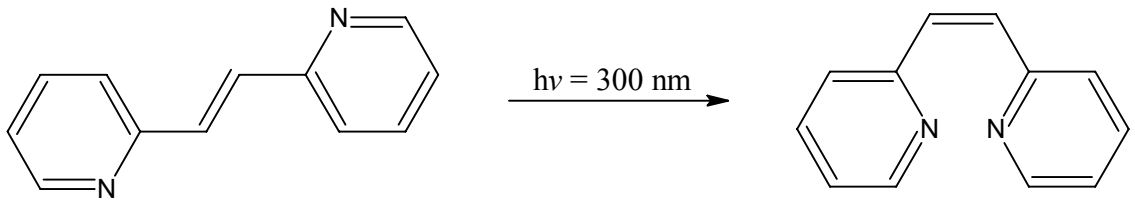

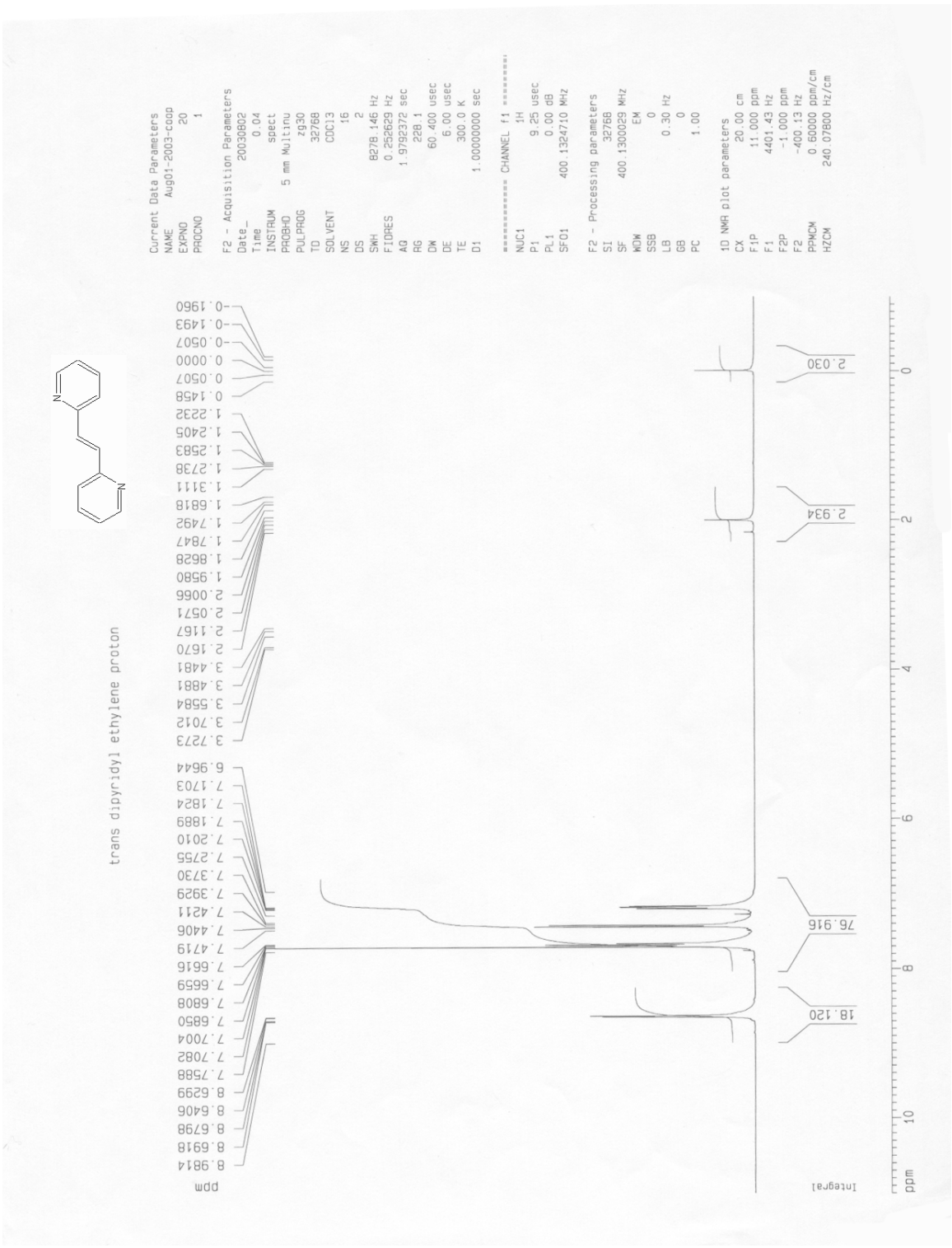
trans dipyridyl ethylene proton
Current Data Parameters
NAME Aug01-2003-coop
EXPNO 20
PROCNO 1
F2 - Acquisition Parameters
Date_ 20030802
Time 0.04
INSTRUM spect
PROBHD 5 mm Multinu
PULPROG zg30
TD 32768
SOLVENT CDCl3
NS 16
DS 2
SWH 8278.146 Hz
FIDRES 0.252629 Hz
AQ 1.9792372 sec
RG 228.1
DW 60.400 usec
DE 6.00 usec
TE 300.0 K
D1 1.00000000 sec
======== CHANNEL f1 ========
NUC1 1H
P1 9.25 usec
PL1 0.00 dB
SFO1 400.1324710 MHz
F2 - Processing parameters
SI 32768
SF 400.1300029 MHz
WDW EM
SSB 0
LB 0.30 Hz
GB 0
PC 1.00
1D NMR plot parameters
CX 20.00 cm
F1P 11.000 ppm
F1 4401.43 Hz
F2P -1.000 ppm
F2 -400.13 Hz
PPMCM 0.60000 ppm/cm
HZCM 240.07800 Hz/cm
ppm
8.9814
8.6918
8.6798
8.6406
8.6299
7.7588
7.7082
7.7004
7.6850
7.6808
7.6659
7.6616
7.4719
7.4406
7.4211
7.3929
7.3730
7.2755
7.2010
7.1889
7.1824
7.1703
6.9644
3.7273
3.7012
3.5584
3.4881
3.4481
2.1670
2.1167
2.0571
2.0066
1.9580
1.8628
1.7847
1.7492
1.6818
1.3111
1.2738
1.2583
1.2405
1.2232
0.1458
0.0507
0.0000
-0.0507
-0.1493
-0.1960
2.030
2.934
76.916
18.120
Integral
ppm
10
8
6
4
2
0


trans dipyridyl ethylen 13-C
77.133
77.451
77.768
123.081
123.789
132.109
137.087
150.181
155.386
ppm
Current Data Parameters
NAME Aug01-2003-coop
EXPNO 21
PROCNO 1
F2 - Acquisition Parameters
Date_ 20030802
Time 0.27
INSTRUM spect
PROBHD 5 mm Multinu
PULPROG zgpg30
TD 65536
SOLVENT CDCl3
NS 321
DS 4
SWH 25125.629 Hz
FIDRES 0.383307 Hz
AQ 1.3042164 sec
RG 4096
DW 19.900 usec
DE 6.00 usec
TE 300.0 K
D1 2.00000000 sec
d11 0.03000000 sec
d12 0.00002000 sec
========== CHANNEL f1 ==========
NUC1 13C
P1 8.70 usec
PL1 0.00 dB
SFO1 100.6237959 MHz
========== CHANNEL f2 ==========
CPDPRG2 waltz16
NUC2 1H
PCPD2 107.00 usec
PL2 0.00 dB
PL12 23.00 dB
PL13 23.00 dB
SFO2 400.1316005 MHz
F2 - Processing parameters
SI 32768
SF 100.6127290 MHz
WDW EM
SSB 0
LB 1.00 Hz
GB 0
PC 1.40
1D NMR plot parameters
CX 20.00 cm
F1P 215.000 ppm
F1 21631.74 Hz
F2P -5.000 ppm
F2 -503.06 Hz
PPMCM 11.00000 ppm/cm
HZCM 1106.73999 Hz/cm
ppm
200
175
150
125
100
75
50
25
0

GC/MS of trans dipridylethylene, retention time = 17.633 minutes

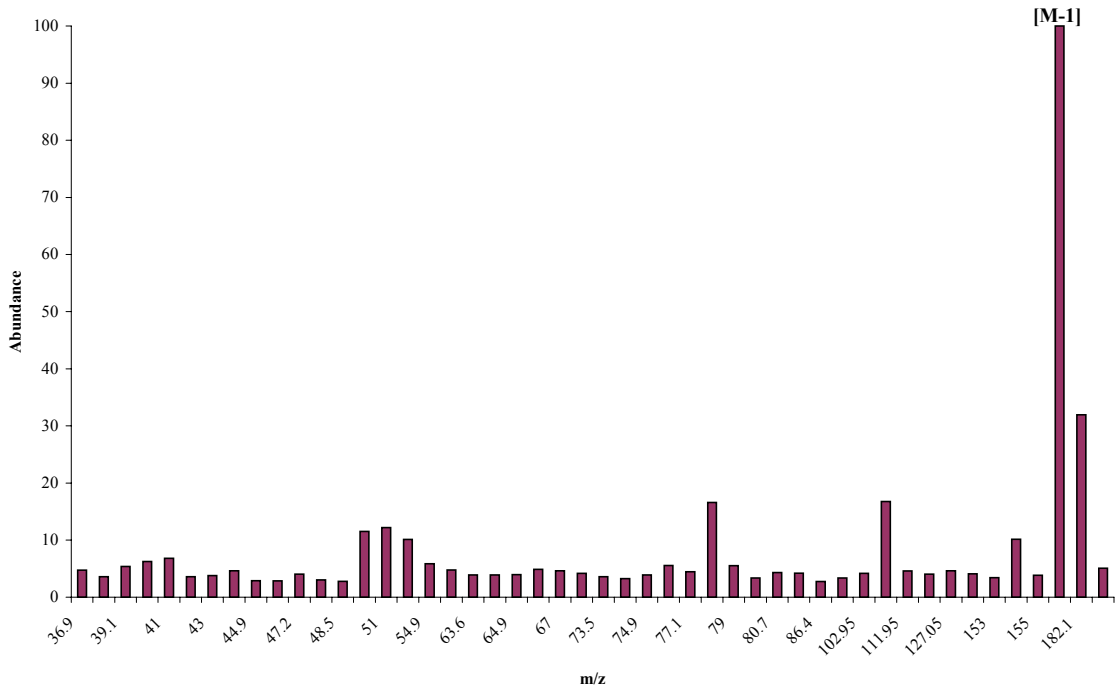

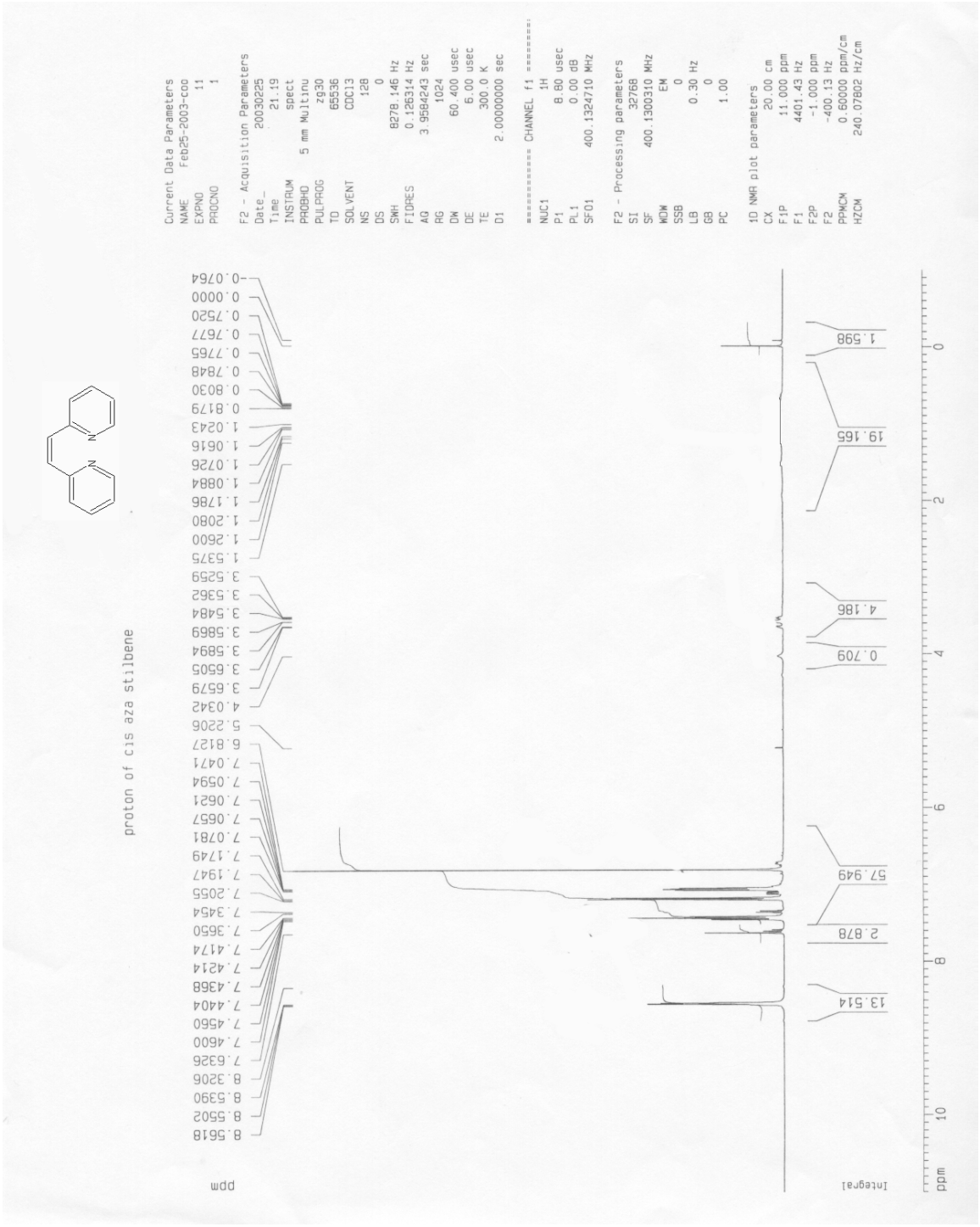
proton of cis aza stilbene
Current Data Parameters
NAME Feb25-2003-coo
EXPNO 11
PROCNO 1
F2 - Acquisition Parameters
Date_ 20030225
Time 21.19
INSTRUM spect
PROBHD 5 mm Multinu
PULPROG zg30
TD 65536
SOLVENT CDCl3
NS 128
DS 0
SWH 8278.146 Hz
FIDRES 0.126314 Hz
AQ 3.9584243 sec
RG 1024
DW 60.400 usec
DE 6.00 usec
TE 300.0 K
D1 2.00000000 sec
======== CHANNEL f1 ========
NUC1 1H
P1 8.80 usec
PL1 0.00 dB
SFO1 400.1324710 MHz
F2 - Processing parameters
SI 32768
SF 400.1300310 MHz
WDW EM
SSB 0
LB 0.30 Hz
GB 0
PC 1.00
1D NMR plot parameters
CX 20.00 cm
F1P 11.000 ppm
F1 4401.43 Hz
F2P -1.000 ppm
F2 -400.13 Hz
PPMCM 0.60000 ppm/cm
HZCM 240.07802 Hz/cm
ppm
Integral
8.5618
8.5502
8.5390
8.3206
7.6326
7.4600
7.4560
7.4404
7.4368
7.4214
7.4174
7.3650
7.3454
7.2055
7.1947
7.1749
7.0781
7.0657
7.0621
7.0594
7.0471
6.8127
5.2206
4.0342
3.6579
3.6505
3.5894
3.5869
3.5484
3.5362
3.5259
1.5375
1.2600
1.2080
1.1786
1.0884
1.0726
1.0616
1.0243
0.8179
0.8030
0.7848
0.7765
0.7677
0.7520
0.0000
-0.0764
13.514
2.878
57.949
0.709
4.186
19.165
1.598

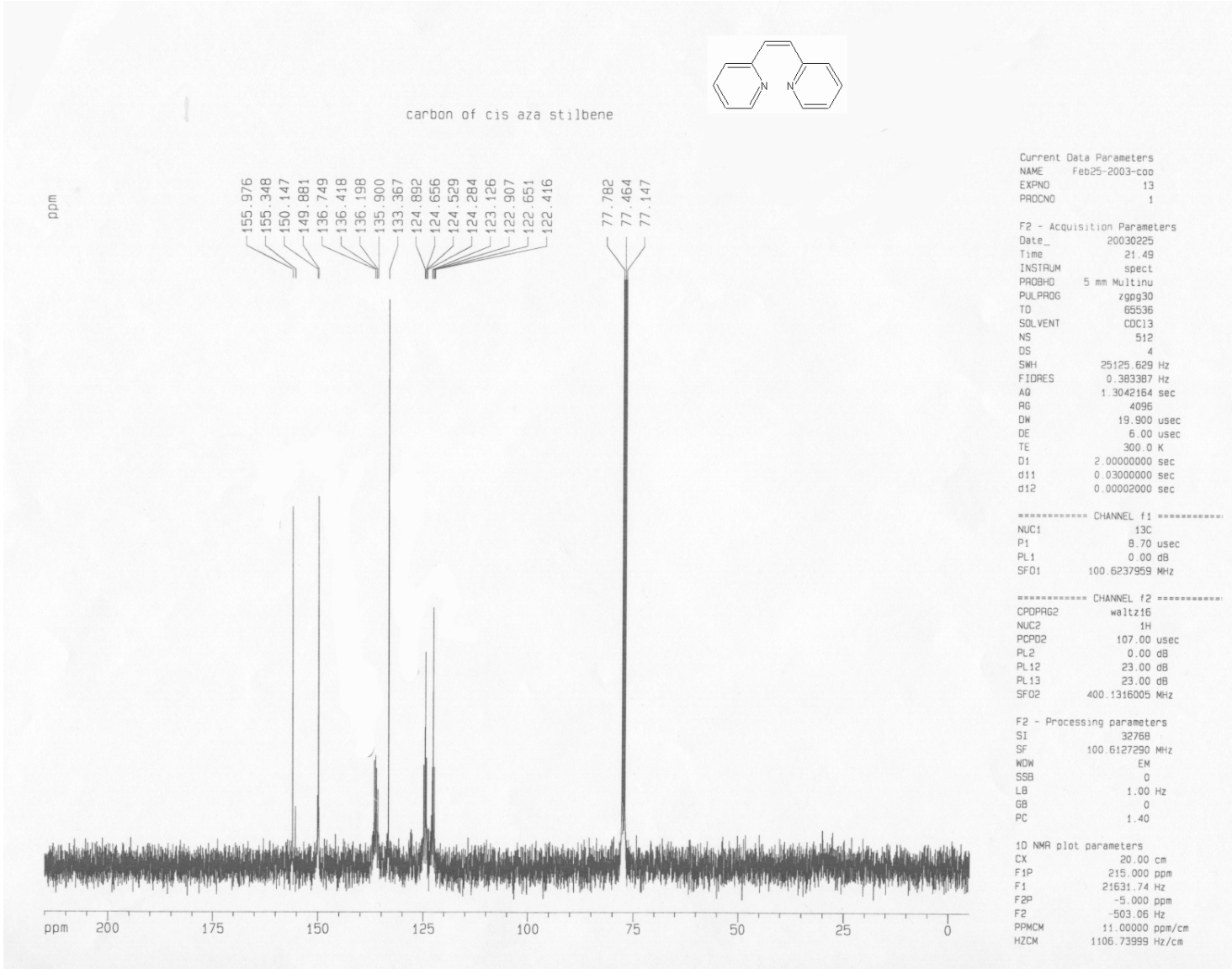
carbon of cis aza stilbene
ppm
155.976
155.348
150.147
149.881
136.749
136.418
136.198
135.900
133.367
124.892
124.656
124.529
124.284
123.126
122.907
122.651
122.416
77.782
77.464
77.147
ppm 200 175 150 125 100 75 50 25 0
Current Data Parameters
NAME Feb25-2003-coo
EXPNO 13
PROCNO 1
F2 - Acquisition Parameters
Date_ 20030225
Time 21.49
INSTRUM spect
PROBHD 5 mm Multinu
PULPROG zgpg30
TD 65536
SOLVENT CDCl3
NS 512
DS 4
SWH 25125.629 Hz
FIDRES 0.383387 Hz
AQ 1.3042164 sec
RG 4096
DW 19.900 usec
DE 6.00 usec
TE 300.0 K
D1 2.00000000 sec
d11 0.03000000 sec
d12 0.00002000 sec
CHANNEL f1
NUC1 13C
P1 8.70 usec
PL1 0.00 dB
SFO1 100.6237959 MHz
CHANNEL f2
CPDPRG2 waltz16
NUC2 1H
PCPD2 107.00 usec
PL2 0.00 dB
PL12 23.00 dB
PL13 23.00 dB
SFO2 400.1316005 MHz
F2 - Processing parameters
SI 32768
SF 100.6127290 MHz
WDW EM
SSB 0
LB 1.00 Hz
GB 0
PC 1.40
1D NMR plot parameters
CX 20.00 cm
F1P 215.000 ppm
F1 21631.74 Hz
F2P -5.000 ppm
F2 -503.06 Hz
PPMCM 11.00000 ppm/cm
HZCM 1106.73999 Hz/cm

GC/MS of cis dipyridyl ethylene, retention time = 10.63 minutes

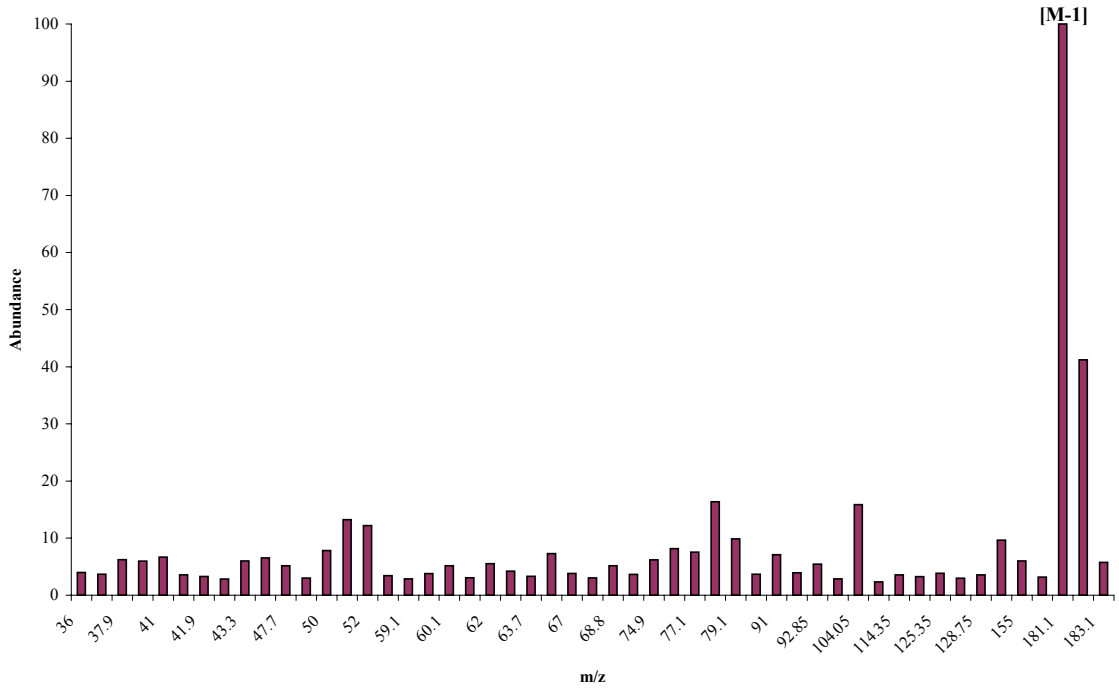

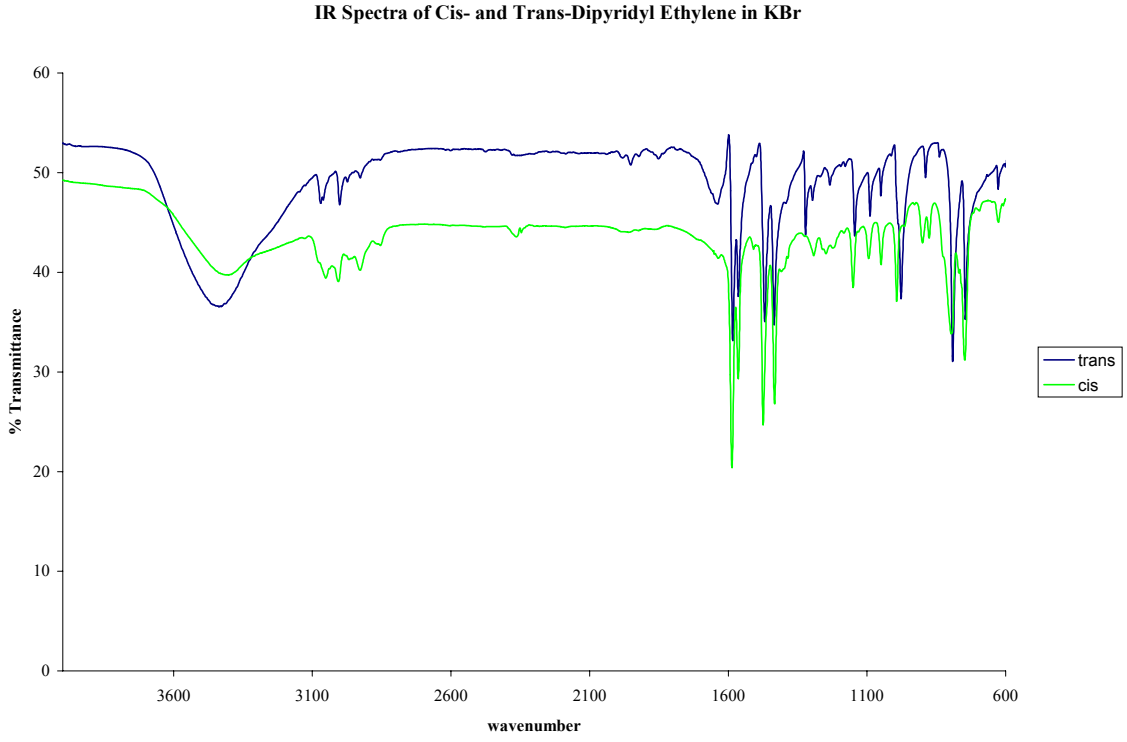
IR Spectra of Cis- and Trans-Dipyridyl Ethylene in KBr
% Transmittance
60
50
40
30
20
10
0
3600
3100
2600
2100
1600
1100
600
wavenumber
trans
cis

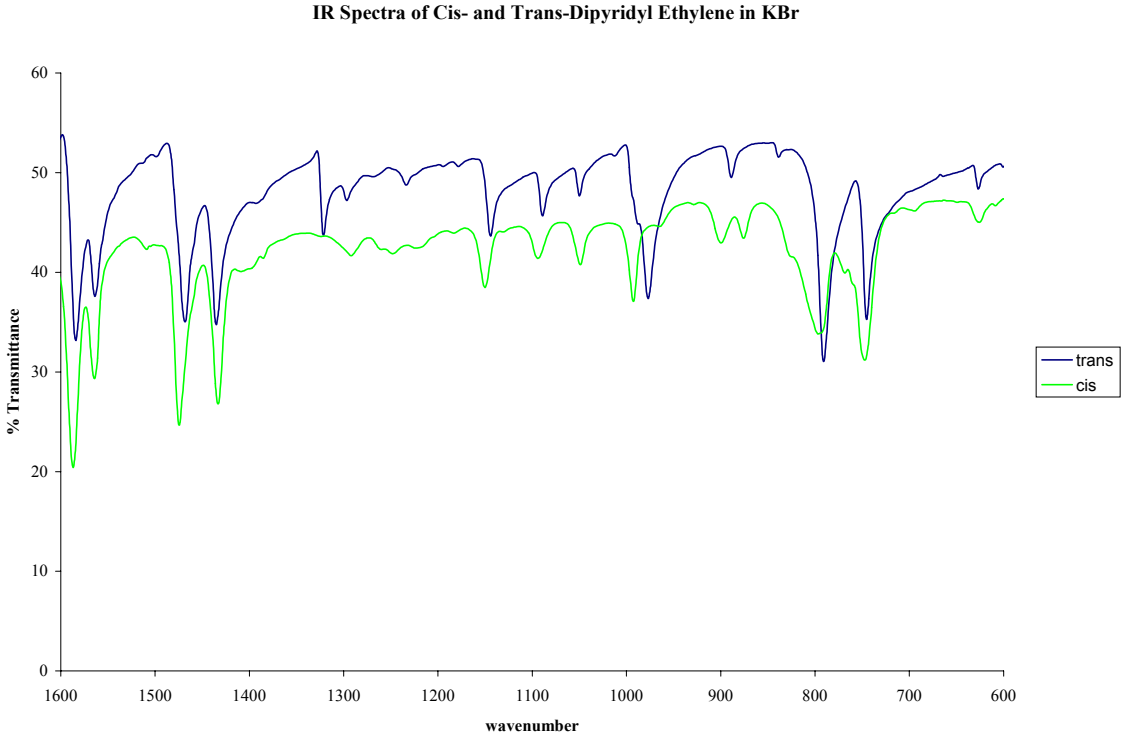
IR Spectra of Cis- and Trans-Dipyridyl Ethylene in KBr
% Transmittance
60
50
40
30
20
10
0
1600
1500
1400
1300
1200
1100
1000
900
800
700
600
wavenumber
trans
cis

Scheme 10. Synthesis of 4-[(2,6-dicarboxypyridin-4-yl)ethynyl]pyridine-2,6-dicarboxylic acid.

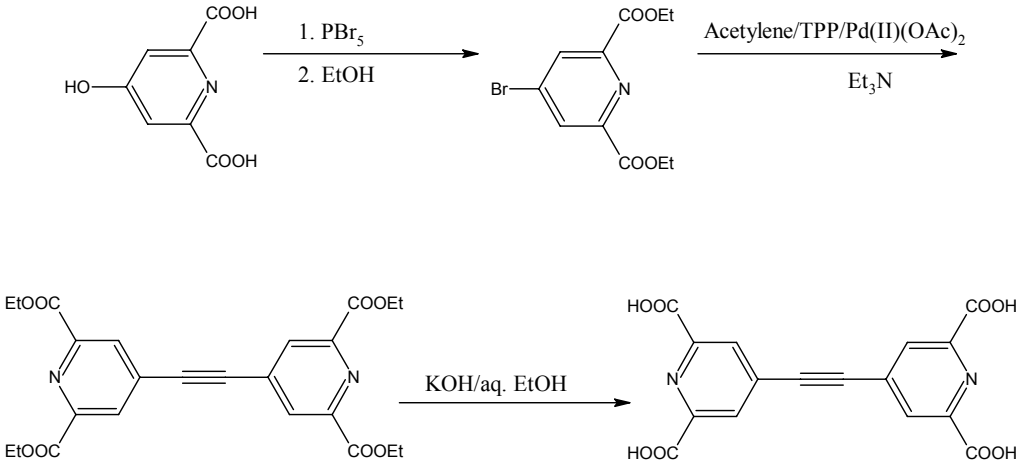

Note: The spectra collected for chelidamic acid have been previously displayed.

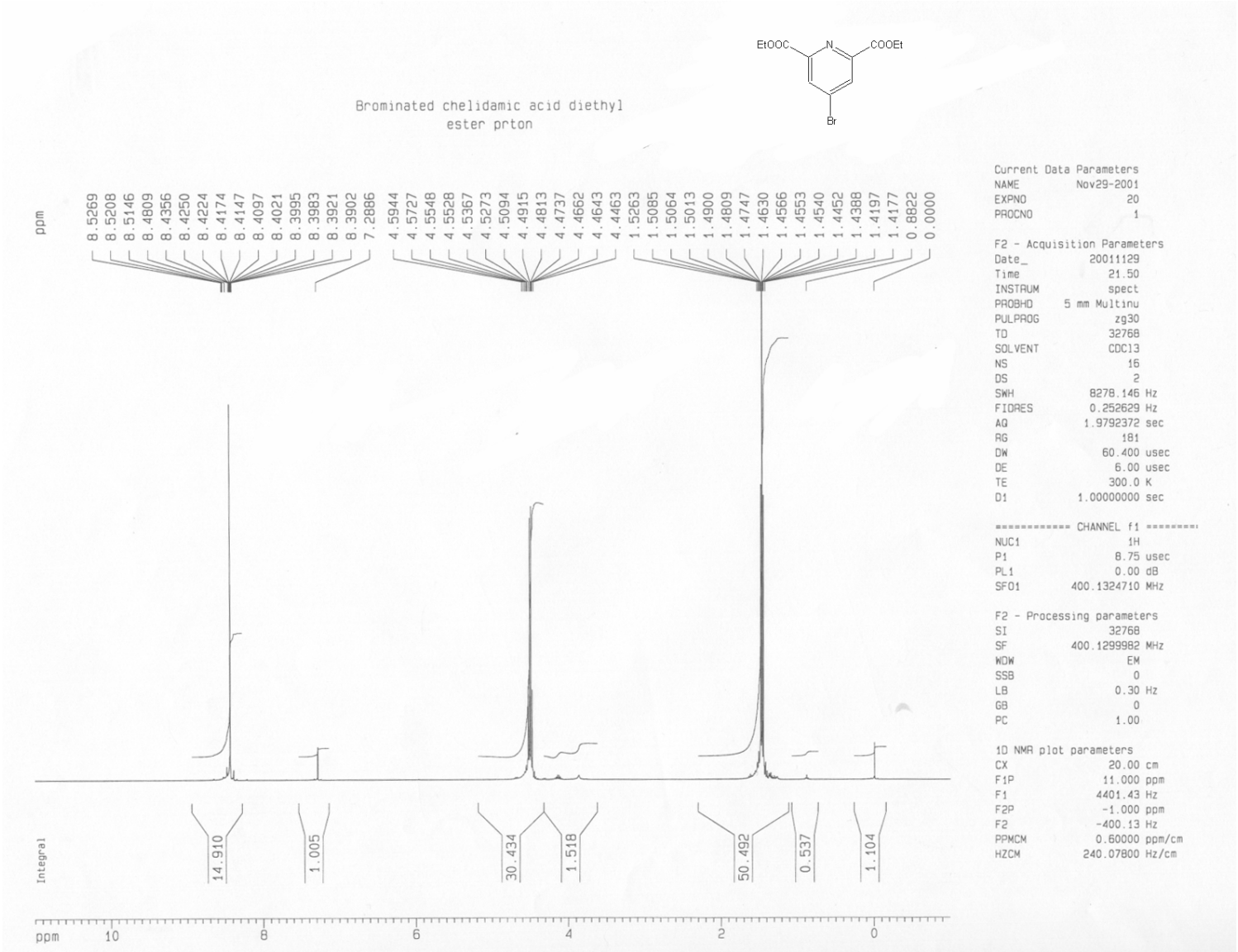
EtOOC
N
COOEt
Br
Brominated chelidamic acid diethyl
ester prton
ppm
8.5269
8.5208
8.5146
8.4809
8.4356
8.4250
8.4224
8.4174
8.4147
8.4097
8.4021
8.3995
8.3983
8.3921
8.3902
7.2886
4.5944
4.5727
4.5548
4.5528
4.5367
4.5273
4.5094
4.4915
4.4813
4.4737
4.4662
4.4643
4.4463
1.5263
1.5085
1.5064
1.5013
1.4900
1.4809
1.4747
1.4630
1.4566
1.4553
1.4540
1.4452
1.4388
1.4197
1.4177
0.8822
0.0000
Integral
14.910
1.005
30.434
1.518
50.492
0.537
1.104
ppm
10
8
6
4
2
0
Current Data Parameters
NAME Nov29-2001
EXPNO 20
PROCNO 1
F2 - Acquisition Parameters
Date_ 20011129
Time 21.50
INSTRUM spect
PROBHD 5 mm Multinu
PULPROG zg30
TD 32768
SOLVENT CDCl3
NS 16
DS 2
SWH 8278.146 Hz
FIDRES 0.252629 Hz
AQ 1.9792372 sec
RG 181
DW 60.400 usec
DE 6.00 usec
TE 300.0 K
D1 1.00000000 sec
========== CHANNEL f1 ========
NUC1 1H
P1 8.75 usec
PL1 0.00 dB
SFO1 400.1324710 MHz
F2 - Processing parameters
SI 32768
SF 400.1299982 MHz
WDW EM
SSB 0
LB 0.30 Hz
GB 0
PC 1.00
1D NMR plot parameters
CX 20.00 cm
F1P 11.000 ppm
F1 4401.43 Hz
F2P -1.000 ppm
F2 -400.13 Hz
PPMCM 0.60000 ppm/cm
HZCM 240.07800 Hz/cm

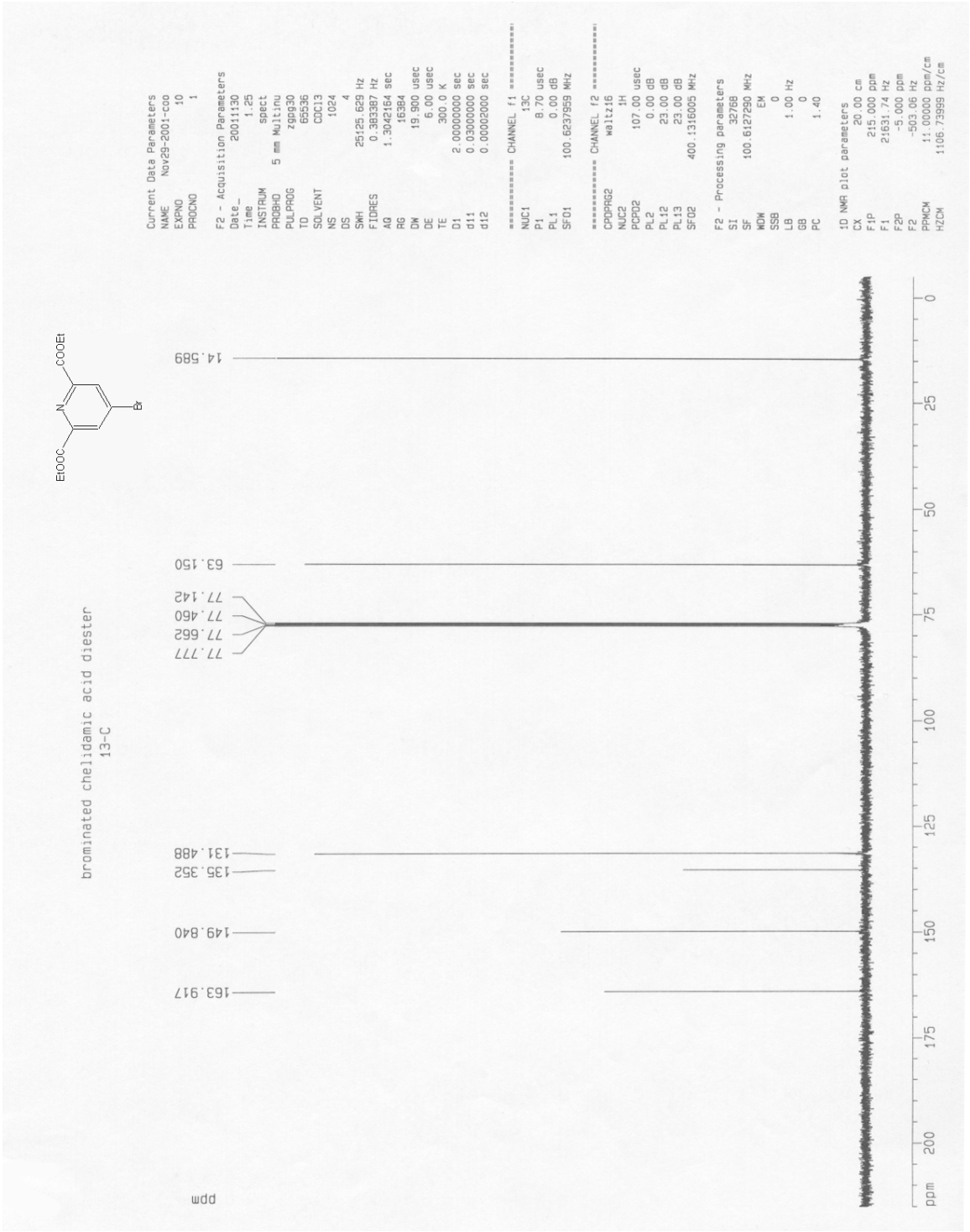
brominated chelidamic acid diester
13-C
EtOOC
COOEt
Br
14.589
63.150
77.142
77.460
77.662
77.777
131.488
135.352
149.840
163.917
ppm
Current Data Parameters
NAME Nov29-2001-coo
EXPNO 10
PROCNO 1
F2 - Acquisition Parameters
Date_ 20011130
Time 1.25
INSTRUM spect
PROBHD 5 mm Multinu
PULPROG zgpg30
TD 65536
SOLVENT CDCl3
NS 1024
DS 4
SWH 25125.629 Hz
FIDRES 0.383387 Hz
AQ 1.3042164 sec
RG 16384
DW 19.900 usec
DE 6.00 usec
TE 300.0 K
D1 2.00000000 sec
d11 0.03000000 sec
d12 0.00002000 sec
======== CHANNEL f1 ========
NUC1 13C
P1 8.70 usec
PL1 0.00 dB
SFO1 100.6237959 MHz
======== CHANNEL f2 ========
CPDPRG2 waltz16
NUC2 1H
PCPD2 107.00 usec
PL2 0.00 dB
PL12 23.00 dB
PL13 23.00 dB
SFO2 400.1316005 MHz
F2 - Processing parameters
SI 32768
SF 100.6127290 MHz
WDW EM
SSB 0
LB 1.00 Hz
GB 0
PC 1.40
1D NMR plot parameters
CX 20.00 cm
F1P 215.000 ppm
F1 21631.74 Hz
F2P -5.000 ppm
F2 -503.06 Hz
PPMCM 11.00000 ppm/cm
HZCM 1106.73999 Hz/cm
ppm
200
175
150
125
100
75
50
25
0

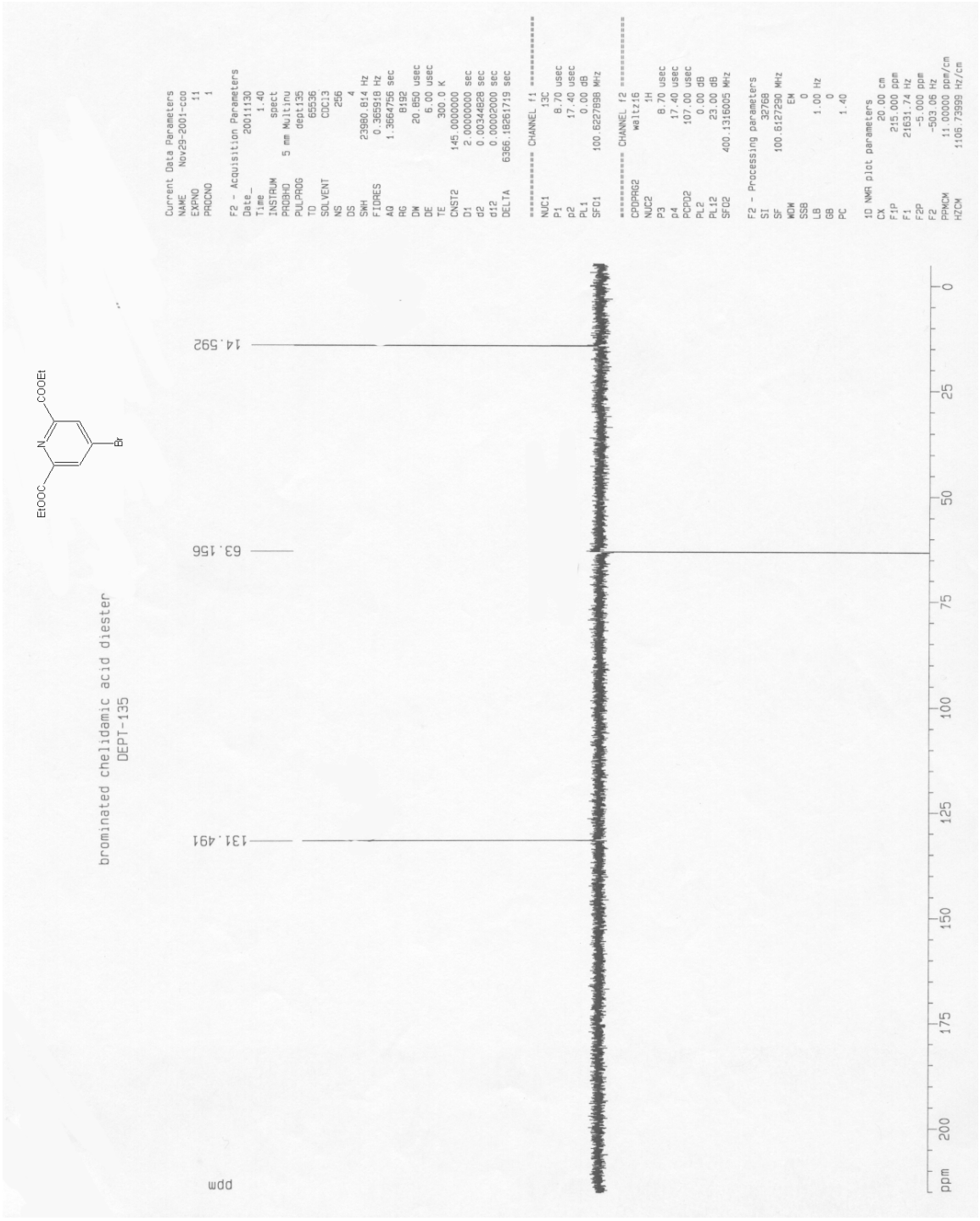
brominated chelidamic acid diester
DEPT-135
EtOOC
COOEt
Br
N
14.592
63.156
131.491
ppm
Current Data Parameters
NAME Nov29-2001-coo
EXPNO 11
PROCNO 1
F2 - Acquisition Parameters
Date_ 20011130
Time 1.40
INSTRUM spect
PROBHD 5 mm Multinu
PULPROG dept135
TD 65536
SOLVENT CDCl3
NS 256
DS 4
SWH 23980.814 Hz
FIDRES 0.365918 Hz
AQ 1.3664756 sec
RG 8192
DW 20.850 usec
DE 6.00 usec
TE 300.0 K
CNST2 145.0000000
D1 2.00000000 sec
d2 0.00344828 sec
d12 0.00002000 sec
DELTA 6366.18261719 sec
CHANNEL f1
NUC1 13C
P1 8.70 usec
p2 17.40 usec
PL1 0.00 dB
SFO1 100.6227898 MHz
CHANNEL f2
CPDPRG2 waltz16
NUC2 1H
P3 8.70 usec
p4 17.40 usec
PCPD2 107.00 usec
PL2 0.00 dB
PL12 23.00 dB
SFO2 400.1316005 MHz
F2 - Processing parameters
SI 32768
SF 100.6127290 MHz
WDW EM
SSB 0
LB 1.00 Hz
GB 0
PC 1.40
1D NMR plot parameters
CX 20.00 cm
F1P 215.000 ppm
F1 21631.74 Hz
F2P -5.000 ppm
F2 -503.06 Hz
PPMCM 11.00000 ppm/cm
HZCM 1106.73999 Hz/cm
ppm 200
175
150
125
100
75
50
25
0

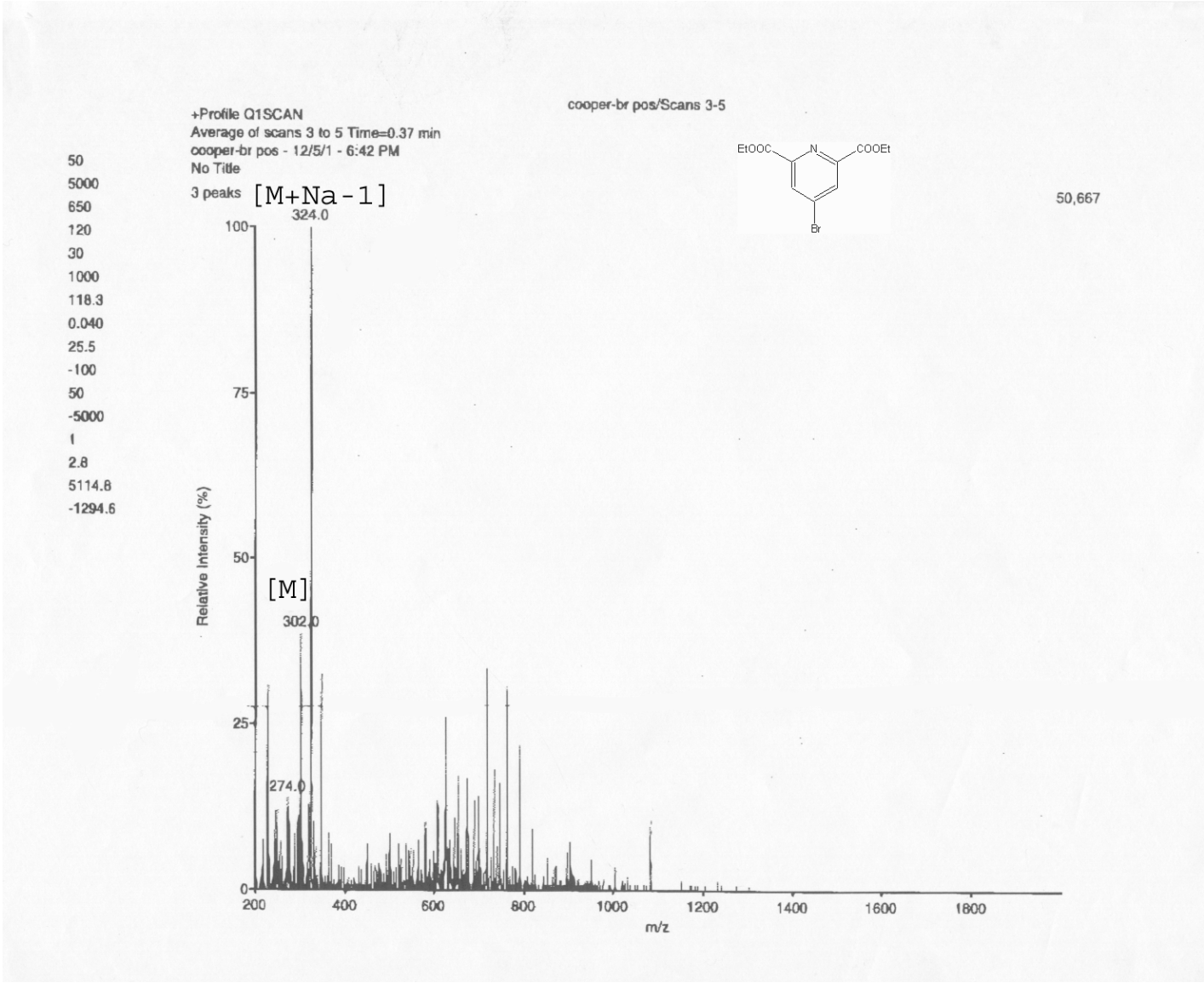
+Profile Q1SCAN
Average of scans 3 to 5 Time=0.37 min
cooper-br pos - 12/5/1 - 6:42 PM
No Title
3 peaks
cooper-br pos/Scans 3-5
50,667
EtOOC
N
COOEt
Br
50
5000
650
120
30
1000
118.3
0.040
25.5
-100
50
-5000
1
2.8
5114.8
-1294.6
[M+Na-1]
324.0
[M]
302.0
274.0
Relative Intensity (%)
m/z
0
25
50
75
100
200
400
600
800
1000
1200
1400
1600
1800

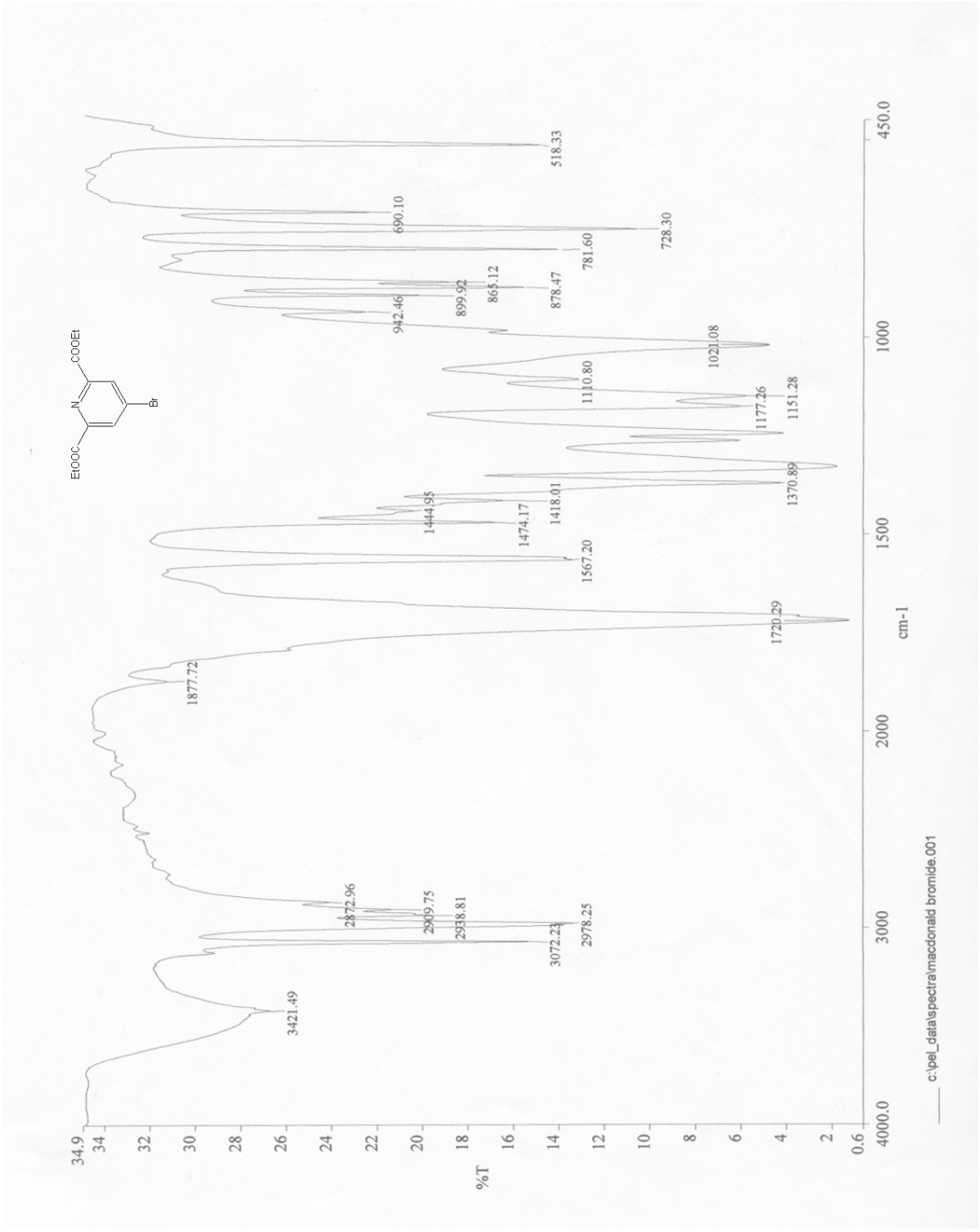
EtOOC
COOEt
N
Br
%T
cm-1
3421.49
3072.23
2978.25
2938.81
2909.75
2872.96
1877.72
1720.29
1567.20
1474.17
1444.95
1418.01
1370.89
1177.26
1151.28
1110.80
1021.08
942.46
899.92
865.12
878.47
781.60
728.30
690.10
518.33
c:\pel_data\spectra\macdonald bromide.001

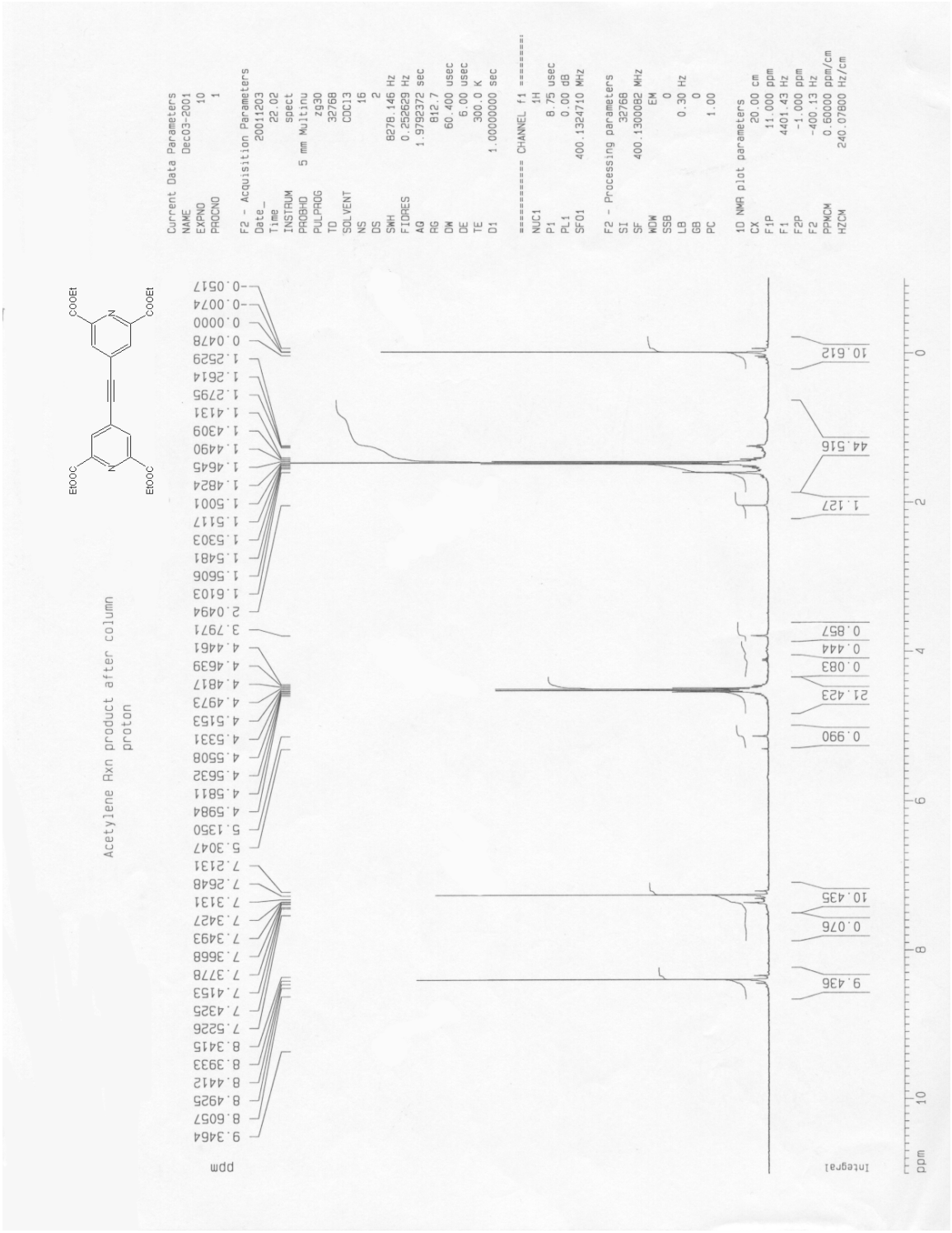
Current Data Parameters
NAME Dec03-2001
EXPNO 10
PROCNO 1
F2 - Acquisition Parameters
Date_ 20011203
Time 22.02
INSTRUM spect
PROBHD 5 mm Multinu
PULPROG zg30
TD 32768
SOLVENT CDCl3
NS 16
DS 2
SWH 8278.146 Hz
FIDRES 0.252629 Hz
AQ 1.9792372 sec
RG 812.7
DW 60.400 usec
DE 6.00 usec
TE 300.0 K
D1 1.00000000 sec
========== CHANNEL f1 ==========
NUC1 1H
P1 8.75 usec
PL1 0.00 dB
SF01 400.1324710 MHz
F2 - Processing parameters
SI 32768
SF 400.1300082 MHz
WDW EM
SSB 0
LB 0.30 Hz
GB 0
PC 1.00
1D NMR plot parameters
CX 20.00 cm
F1P 11.000 ppm
F1 4401.43 Hz
F2P -1.000 ppm
F2 -400.13 Hz
PPMCM 0.60000 ppm/cm
HZCM 240.07800 Hz/cm
Acetylene Rxn product after column
proton
EtOOC
COOEt
EtOOC
COOEt
ppm
9.346
8.605
8.492
8.441
8.393
8.341
7.522
7.432
7.415
7.377
7.366
7.349
7.342
7.313
7.264
7.213
5.304
5.135
4.598
4.581
4.563
4.550
4.533
4.515
4.497
4.481
4.463
4.446
3.797
2.049
1.610
1.560
1.548
1.530
1.511
1.500
1.482
1.464
1.449
1.430
1.413
1.279
1.261
1.252
0.047
0.000
-0.007
-0.051
Integral
10.612
44.516
1.127
0.857
0.444
0.083
21.423
0.990
10.435
0.076
9.436
ppm

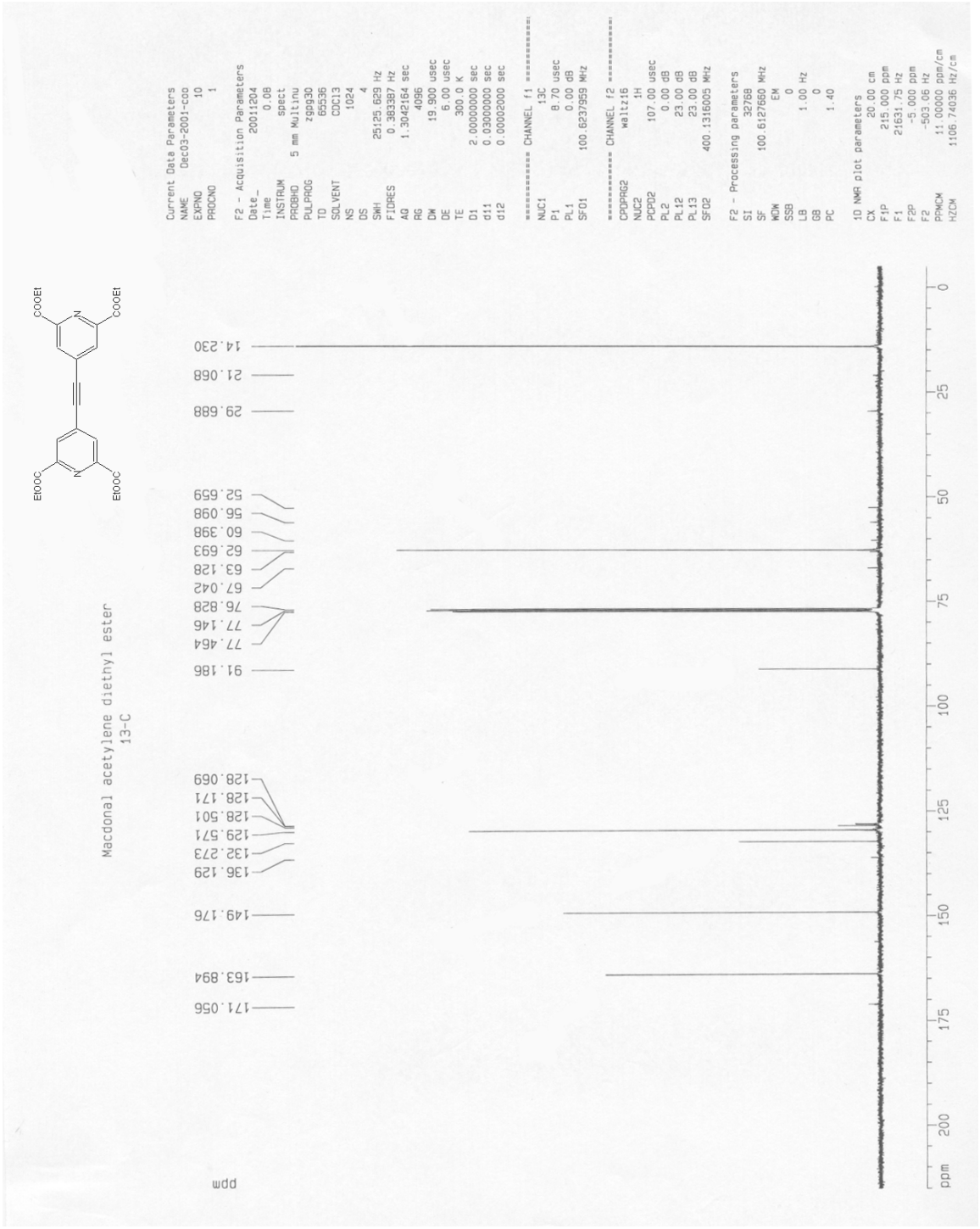
Macdonal acetylene diethyl ester
13-C
COOEt
COOEt
EtOOC
EtOOC
Current Data Parameters
NAME Dec03-2001-coo
EXPNO 10
PROCNO 1
F2 - Acquisition Parameters
Date_ 20011204
Time_ 0.08
INSTRUM spect
PROBHD 5 mm Multinu
PULPROG zgpg30
TD 65536
SOLVENT CDCl3
NS 1024
DS 4
SWH 25125.629 Hz
FIDRES 0.383387 Hz
AQ 1.3042164 sec
RG 4096
DW 19.900 usec
DE 6.00 usec
TE 300.0 K
D1 2.00000000 sec
d11 0.03000000 sec
d12 0.00002000 sec
========== CHANNEL f1 ==========
NUC1 13C
P1 8.70 usec
PL1 0.00 dB
SFO1 100.6237959 MHz
========== CHANNEL f2 ==========
CPDPRG2 waltz16
NUC2 1H
PCPD2 107.00 usec
PL2 0.00 dB
PL12 23.00 dB
PL13 23.00 dB
SFO2 400.1316005 MHz
F2 - Processing parameters
SI 32768
SF 100.6127660 MHz
WDW EM
SSB 0
LB 1.00 Hz
GB 0
PC 1.40
1D NMR plot parameters
CX 20.00 cm
F1P 215.000 ppm
F1 21631.75 Hz
F2P -5.000 ppm
F2 -503.06 Hz
PPMCM 11.00000 ppm/cm
HZCM 1106.74036 Hz/cm
14.230
21.068
29.688
52.659
56.098
60.398
62.693
63.128
67.042
76.828
77.146
77.464
91.186
128.069
128.171
128.501
129.571
132.273
136.129
149.176
163.894
171.056
ppm
200
175
150
125
100
75
50
25
0

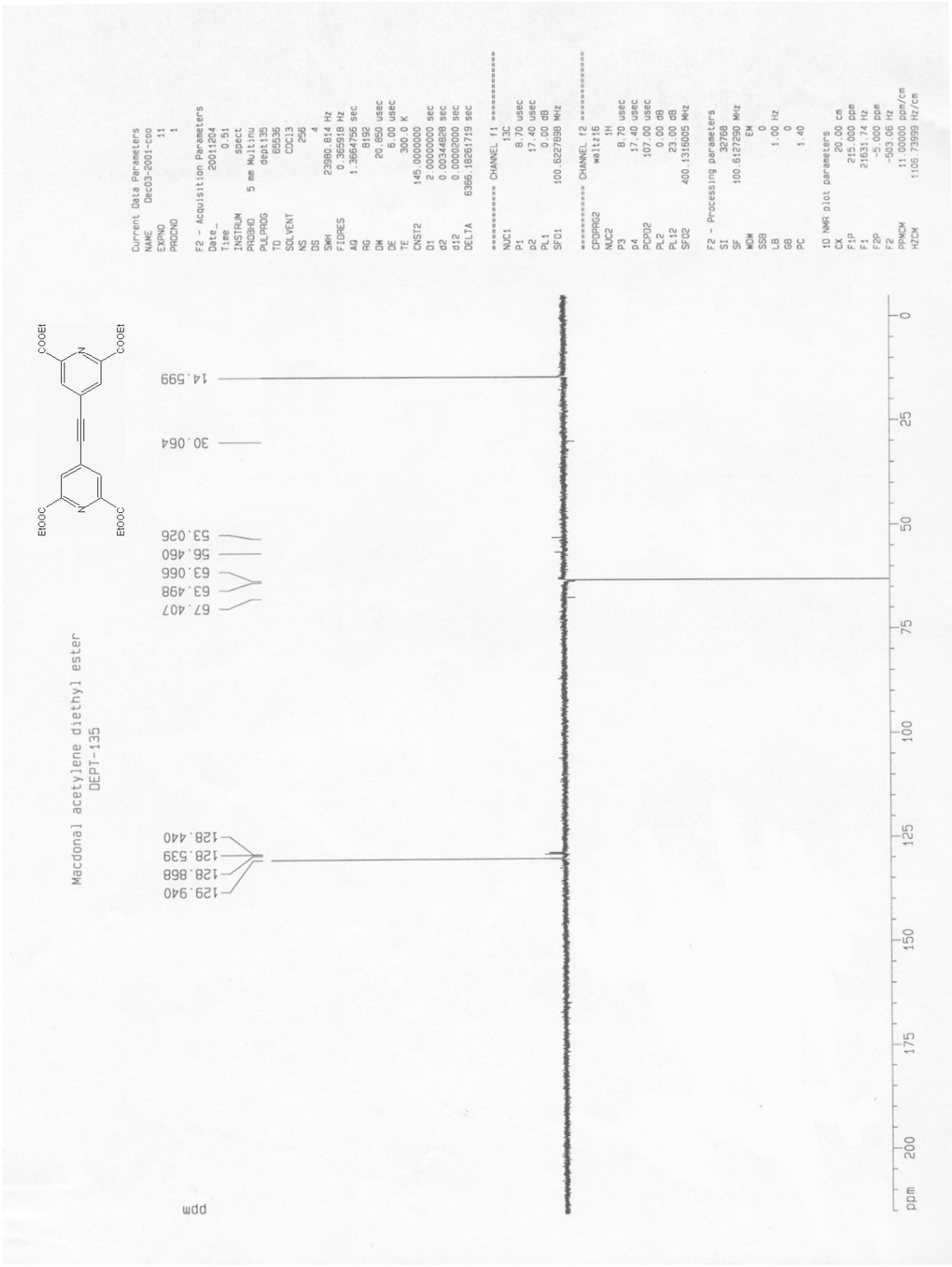
Macdonal acetylene diethyl ester
DEPT-135
129.940
128.868
128.539
128.440
67.407
63.498
63.066
56.460
53.026
30.064
14.599
COOEt
COOEt
EtOOC
EtOOC
Current Data Parameters
NAME Dec03-2001-coo
EXPNO 11
PROCNO 1
F2 - Acquisition Parameters
Date_ 20011204
Time_ 0.51
INSTRUM spect
PROBHD 5 mm Multinu
PULPROG dept135
TD 65536
SOLVENT CDCl3
NS 256
DS 4
SWH 23980.814 Hz
FIDRES 0.365918 Hz
AQ 1.3664756 sec
RG 8192
DW 20.850 usec
DE 6.00 usec
TE 300.0 K
CNST2 145.0000000
D1 2.00000000 sec
d2 0.00344828 sec
d12 0.00002000 sec
DELTA 6366.18261719 sec
========== CHANNEL f1 ==========
NUC1 13C
P1 8.70 usec
p2 17.40 usec
PL1 0.00 dB
SFO1 100.6227898 MHz
========== CHANNEL f2 ==========
CPDPRG2 waltz16
NUC2 1H
P3 8.70 usec
p4 17.40 usec
PCPD2 107.00 usec
PL2 0.00 dB
PL12 23.00 dB
SFO2 400.1316005 MHz
F2 - Processing parameters
SI 32768
SF 100.6127290 MHz
WDW EM
SSB 0
LB 1.00 Hz
GB 0
PC 1.40
1D NMR plot parameters
CX 20.00 cm
F1P 215.000 ppm
F1 21631.74 Hz
F2P -5.000 ppm
F2 -503.06 Hz
PPMCM 11.00000 ppm/cm
HZCM 1106.73999 Hz/cm
ppm
200
175
150
125
100
75
50
25
0

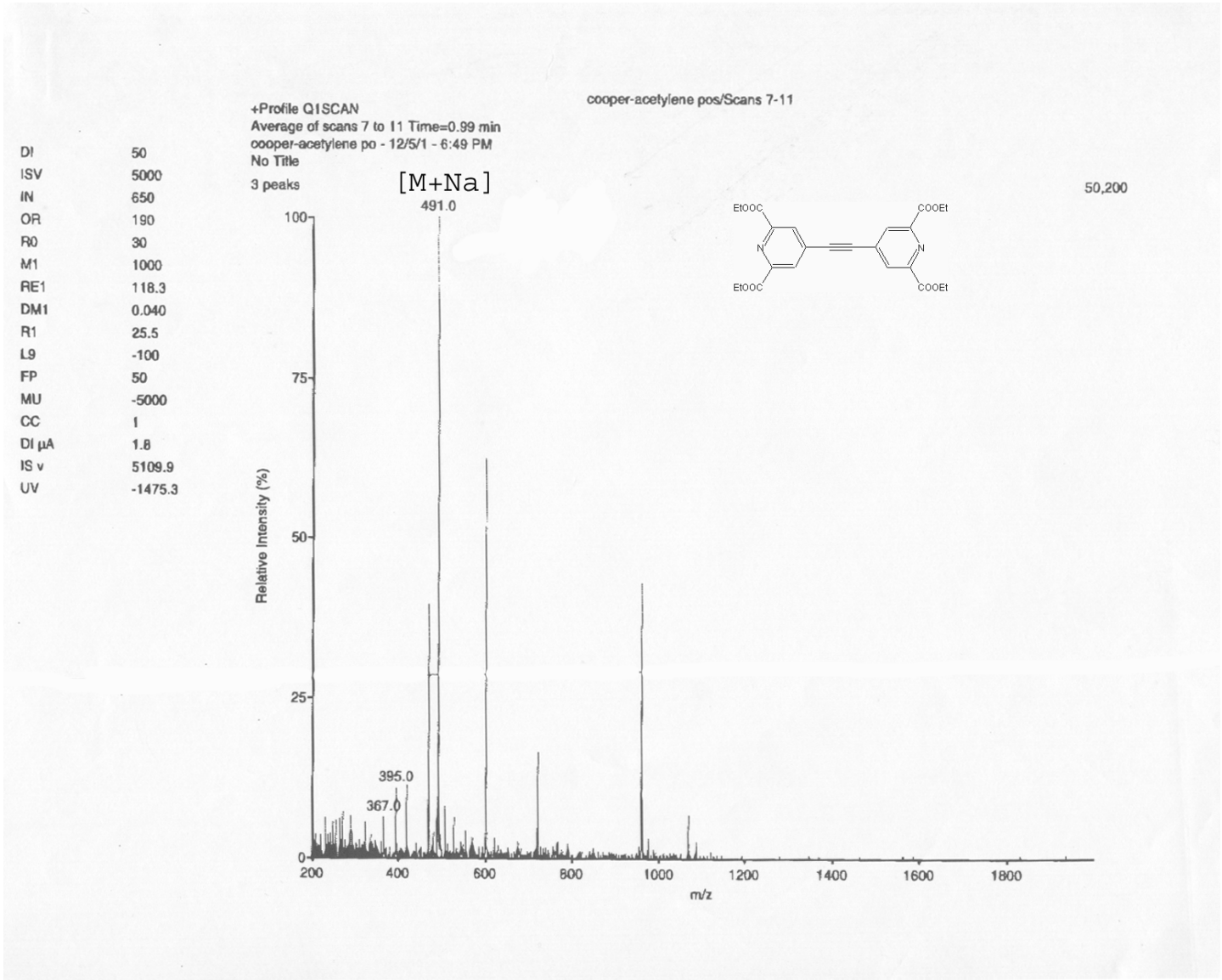
cooper-acetylene pos/Scans 7-11
+Profile Q1SCAN
Average of scans 7 to 11 Time=0.99 min
cooper-acetylene po - 12/5/1 - 6:49 PM
No Title
3 peaks
[M+Na]
491.0
50,200
DI 50
ISV 5000
IN 650
OR 190
R0 30
M1 1000
RE1 118.3
DM1 0.040
R1 25.5
L9 -100
FP 50
MU -5000
CC 1
DI µA 1.8
IS v 5109.9
UV -1475.3
EtOOC
COOEt
N
EtOOC
COOEt
N
Relative Intensity (%)
100
75
50
25
0
395.0
367.0
200
400
600
800
1000
1200
1400
1600
1800
m/z

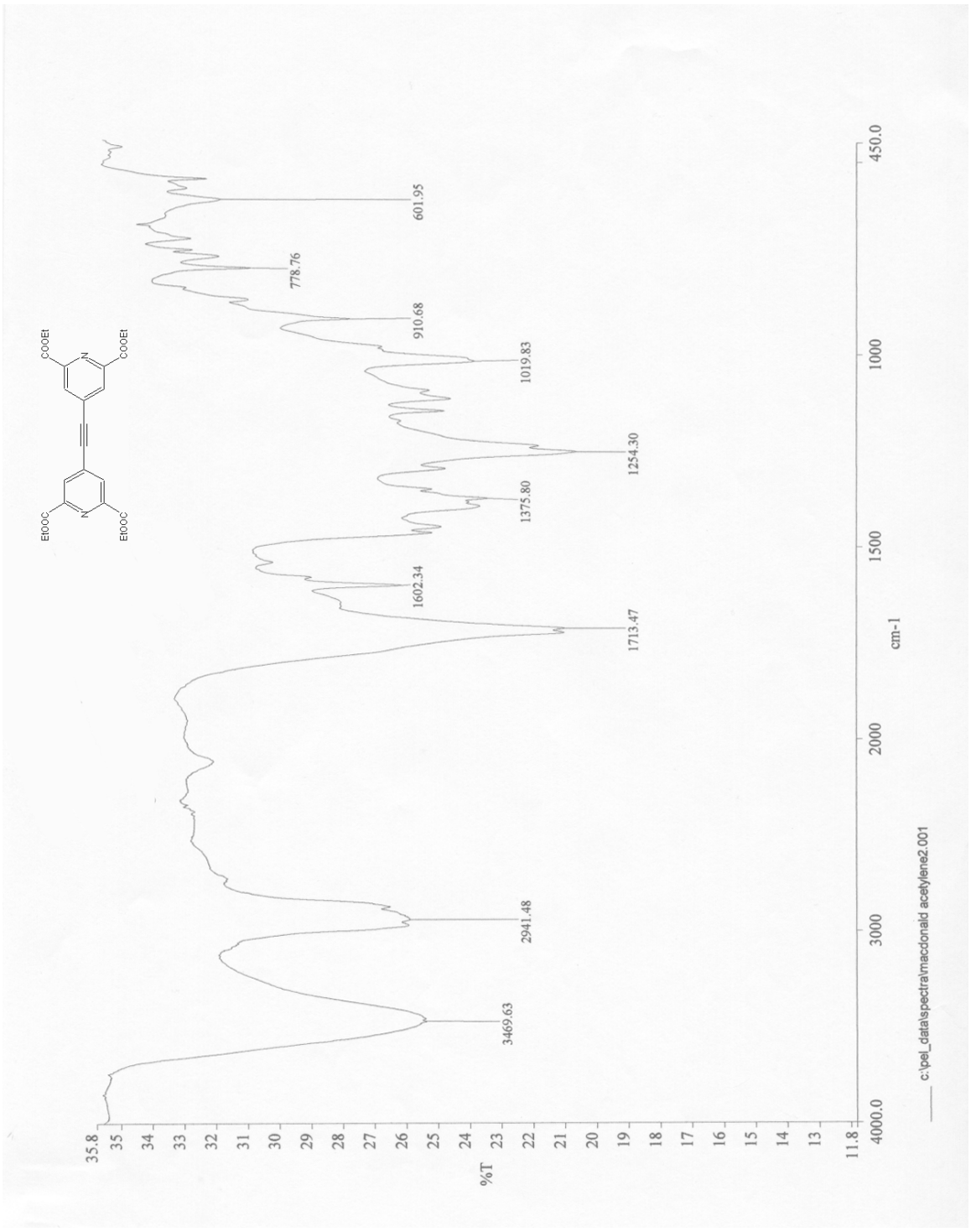
EtOOC
COOEt
N
N
EtOOC
COOEt
%T
cm-1
4000.0
3000
2000
1500
1000
450.0
35.8
35
34
33
32
31
30
29
28
27
26
25
24
23
22
21
20
19
18
17
16
15
14
13
11.8
3469.63
2941.48
1713.47
1602.34
1375.80
1254.30
1019.83
910.68
778.76
601.95
c:\pel_data\spectra\macdonald acetylene2.001

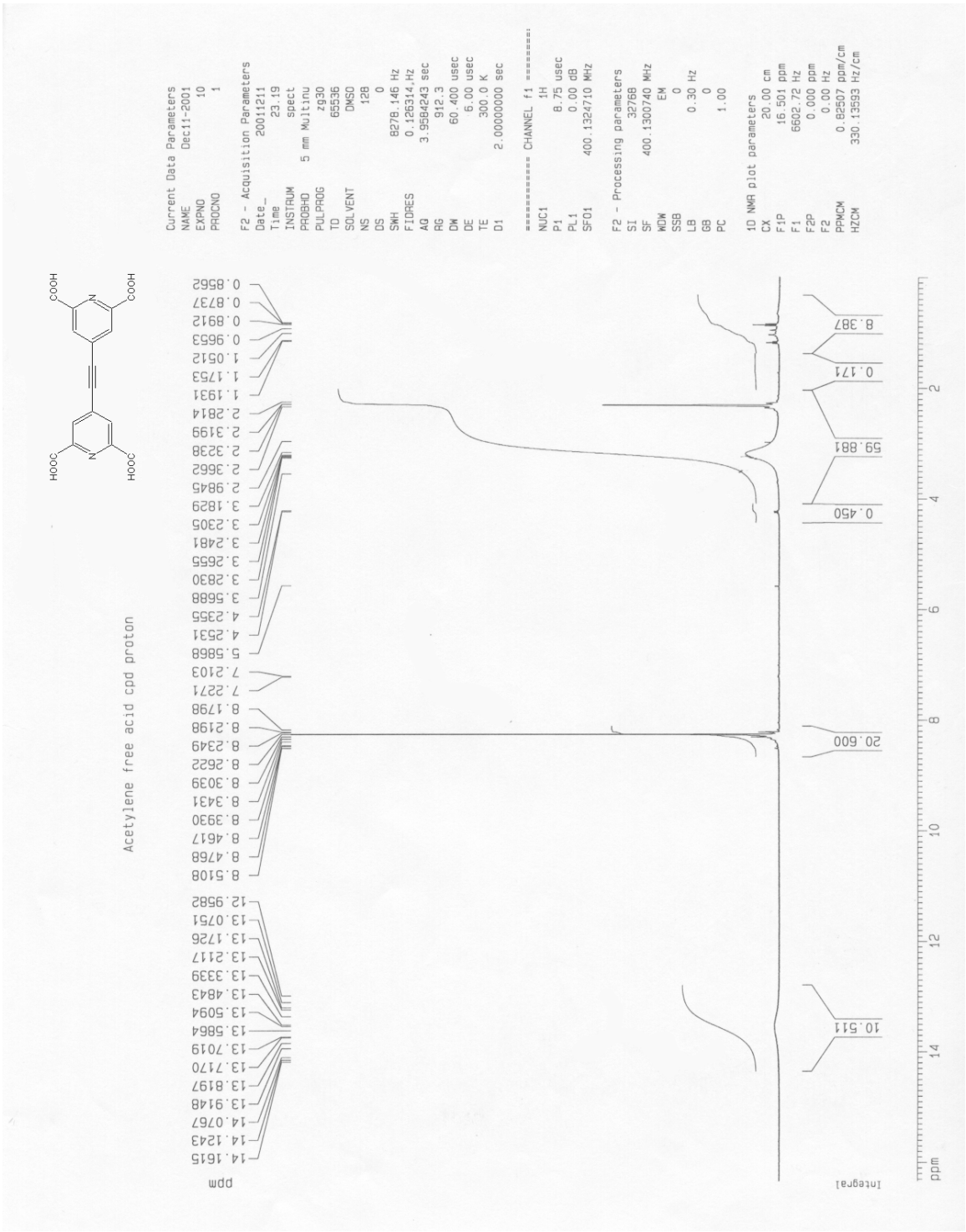
Acetylene free acid cpd proton
Current Data Parameters
NAME Dec11-2001
EXPNO 10
PROCNO 1
F2 - Acquisition Parameters
Date_ 20011211
Time 23.19
INSTRUM spect
PROBHD 5 mm Multinu
PULPROG zg30
TD 65536
SOLVENT DMSO
NS 128
DS 0
SWH 8278.146 Hz
FIDRES 0.126314 Hz
AQ 3.9584243 sec
RG 912.3
DW 60.400 usec
DE 6.00 usec
TE 300.0 K
D1 2.00000000 sec
======== CHANNEL f1 ========
NUC1 1H
P1 8.75 usec
PL1 0.00 dB
SFO1 400.1324710 MHz
F2 - Processing parameters
SI 32768
SF 400.1300740 MHz
WDW EM
SSB 0
LB 0.30 Hz
GB 0
PC 1.00
1D NMR plot parameters
CX 20.00 cm
F1P 16.501 ppm
F1 6602.72 Hz
F2P 0.000 ppm
F2 0.00 Hz
PPMCM 0.82507 ppm/cm
HZCM 330.13593 Hz/cm
ppm
Integral
0.8562
0.8737
0.8912
0.9653
1.0512
1.1753
1.1931
2.2814
2.3199
2.3238
2.3662
2.9845
3.1829
3.2305
3.2481
3.2655
3.2830
3.5688
4.2355
4.2531
5.5868
7.2103
7.2271
8.1798
8.2198
8.2349
8.2622
8.3039
8.3431
8.3930
8.4617
8.4768
8.5108
12.9582
13.0751
13.1726
13.2117
13.3339
13.4843
13.5094
13.5864
13.7019
13.7170
13.8197
13.9148
14.0767
14.1243
14.1615
10.511
20.600
0.450
59.881
0.171
8.387

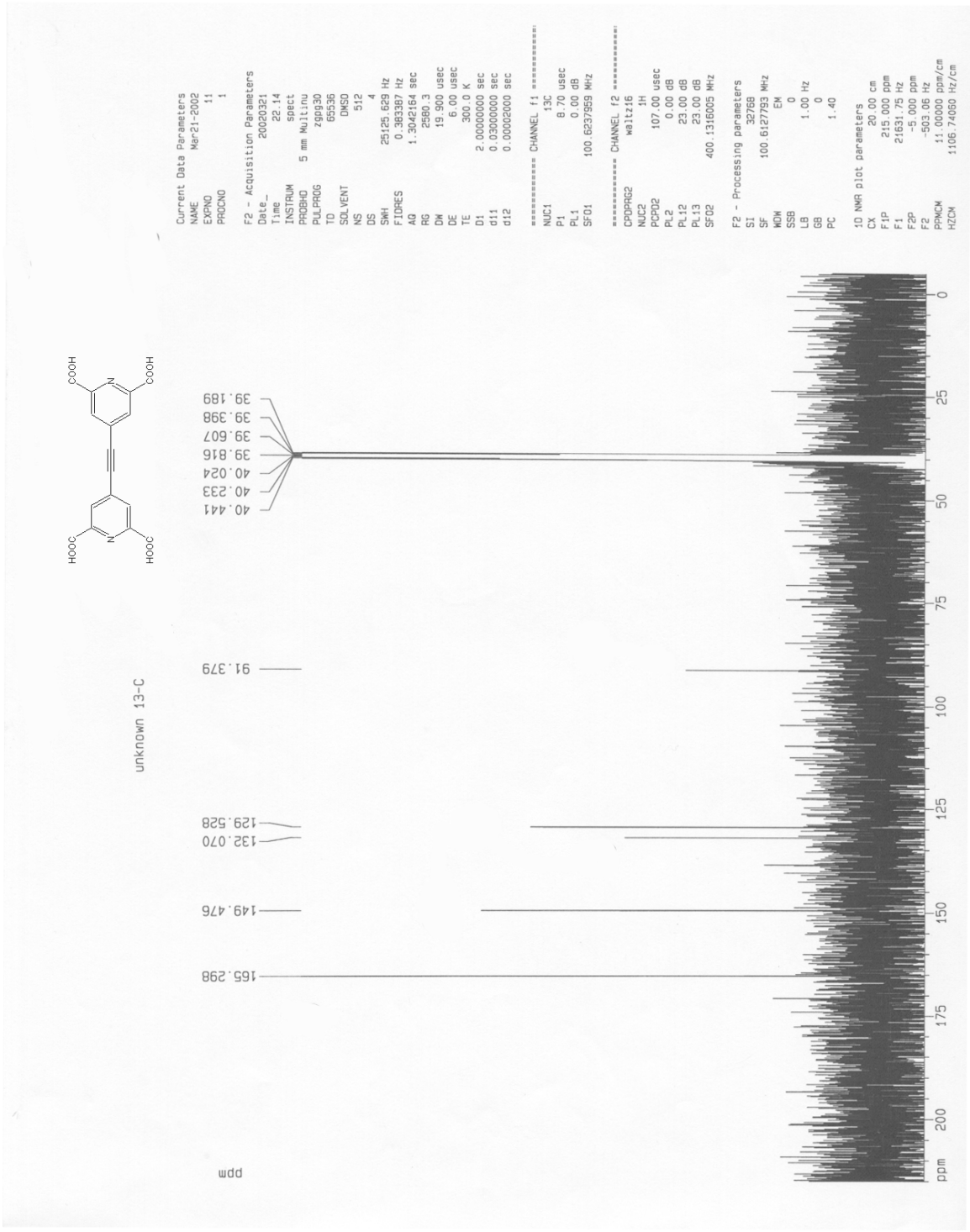
unknown 13-C
ppm
39.189
39.398
39.607
39.816
40.024
40.233
40.441
91.379
129.528
132.070
149.476
165.298
COOH
COOH
HOOC
HOOC
N
N
Current Data Parameters
NAME
EXPNO
PROCNO
F2 - Acquisition Parameters
Date_
Time
INSTRUM
PROBHD
PULPROG
TD
SOLVENT
NS
DS
SWH
FIDRES
AQ
RG
DW
DE
TE
D1
d11
d12
CHANNEL f1
NUC1
P1
PL1
SF01
CHANNEL f2
CPDPRG2
NUC2
PCPD2
PL2
PL12
PL13
SF02
F2 - Processing parameters
SI
SF
WDW
SSB
LB
GB
PC
1D NMR plot parameters
CX
F1P
F1
F2P
F2
PPMCM
HZCM
20021321
22.14
spect
5 mm Multinu
zgpg30
65536
DMSO
512
4
25125.629 Hz
0.38387 Hz
1.3042164 sec
2580.3
19.900 usec
6.00 usec
300.0 K
2.00000000 sec
0.03000000 sec
0.00002000 sec
13C
8.70 usec
0.00 dB
100.6237959 MHz
waltz16
1H
107.00 usec
0.00 dB
23.00 dB
23.00 dB
400.1316005 MHz
32768
100.6127793 MHz
EM
0
1.00 Hz
0
1.40
20.00 cm
215.000 ppm
21631.75 Hz
-5.000 ppm
-503.06 Hz
11.00000 ppm/cm
1106.74060 Hz/cm
0
25
50
75
100
125
150
175
200
ppm

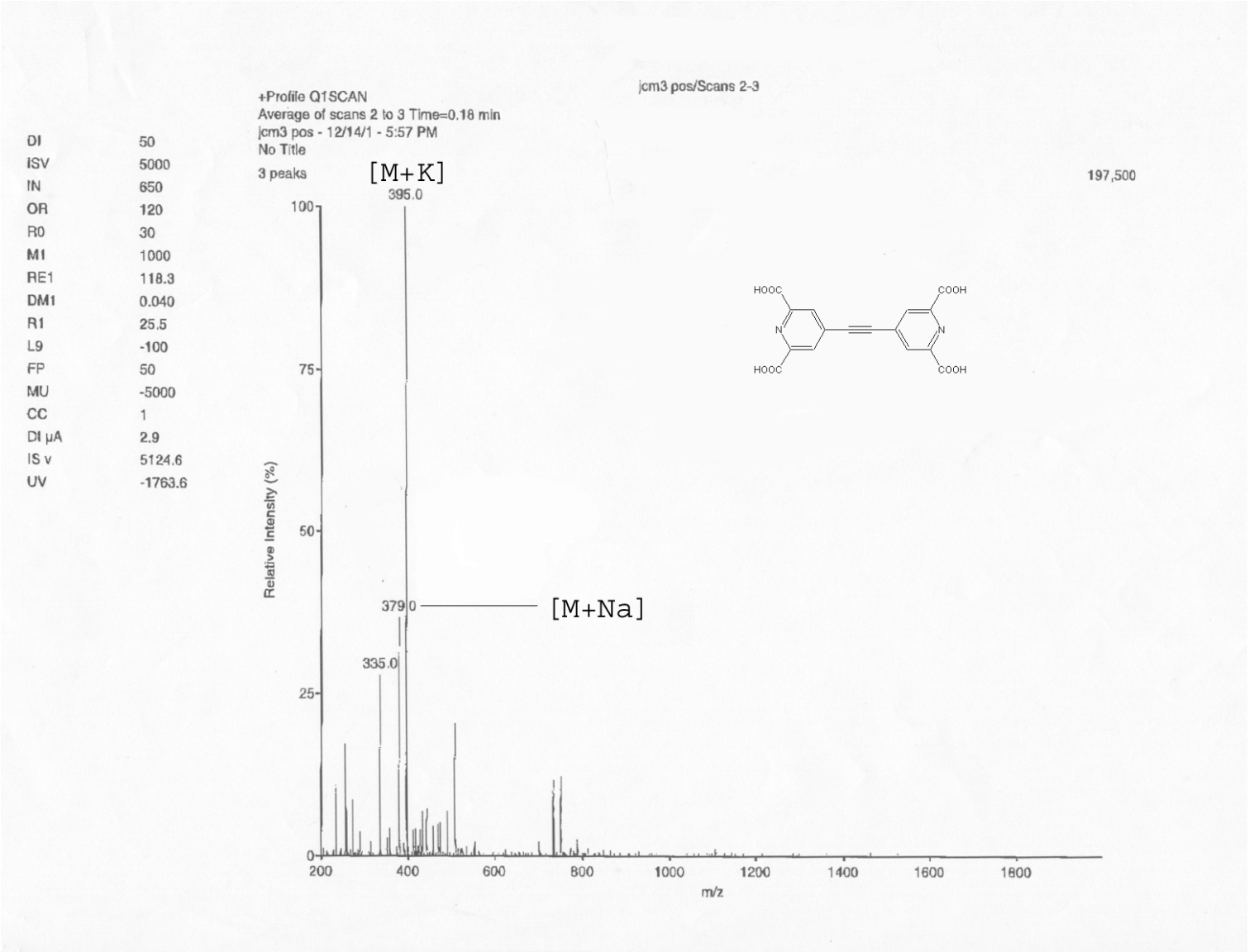
jcm3 pos/Scans 2-3
+Profile Q1SCAN
Average of scans 2 to 3 Time=0.16 min
jcm3 pos - 12/14/1 - 5:57 PM
No Title
3 peaks
DI 50
ISV 5000
IN 650
OR 120
R0 30
M1 1000
RE1 118.3
DM1 0.040
R1 25.5
L9 -100
FP 50
MU -5000
CC 1
DI µA 2.9
IS v 5124.6
UV -1763.6
[M+K]
395.0
379.0
[M+Na]
335.0
197,500
HOOC
COOH
N
Relative Intensity (%)
m/z
100
75
50
25
0
200
400
600
800
1000
1200
1400
1600
1800

Scheme 11. Synthesis of 10-bromo-1-decene

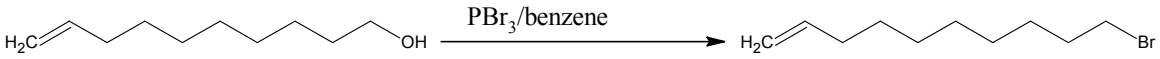

9 decen-1-ol proton
ppm
Integral
Current Data Parameters
NAME May08-2003-coo
EXPNO 13
PROCNO 1
F2 - Acquisition Parameters
Date_ 20030508
Time 22.56
INSTRUM spect
PROBHD 5 mm Multinu
PULPROG zg30
TD 65536
SOLVENT CDCl3
NS 128
DS 0
SWH 8278.146 Hz
FIDRES 0.126314 Hz
AG 3.9584243 sec
RG 20.2
DW 60.400 usec
DE 6.00 usec
TE 300.0 K
D1 2.00000000 sec
========== CHANNEL f1 ========
NUC1 1H
P1 9.25 usec
PL1 0.00 dB
SFO1 400.1324710 MHz
F2 - Processing parameters
SI 32768
SF 400.1299935 MHz
WDW EM
SSB 0
LB 0.30 Hz
GB 0
PC 1.00
1D NMR plot parameters
CX 20.00 cm
F1P 11.000 ppm
F1 4401.43 Hz
F2P -1.000 ppm
F2 -400.13 Hz
PPMCM 0.60000 ppm/cm
HZCM 240.07800 Hz/cm
7.29818
5.85464
5.83797
5.82929
5.82130
5.81236
5.79547
5.78659
5.77862
5.76985
5.75319
5.01035
5.00661
4.96760
4.96382
4.93552
4.92239
4.91017
3.61283
3.59616
3.57938
2.66211
2.06215
2.04523
2.02736
2.01030
1.56361
1.54659
1.52957
1.51288
1.38959
1.37183
1.35309
1.30428
0.88026
0.00000
12.676
2.101
1.097
2.097
2.016
1.000

9-decen-1-ol 13-C
OH
H2C
ppm
137.304
112.302
60.887
75.608
75.289
74.972
31.975
30.868
30.694
27.647
27.593
27.257
27.080
24.096
23.937
Current Data Parameters
NAME May08-2003-coo
EXPNO 18
PROCNO 1
F2 - Acquisition Parameters
Date_ 20030509
Time 1.04
INSTRUM spect
PROBHD 5 mm Multinu
PULPROG zgpg30
TD 65536
SOLVENT CDCl3
NS 512
DS 4
SWH 25125.629 Hz
FIDRES 0.383387 Hz
AQ 1.3042164 sec
RG 1625.5
DW 19.900 usec
DE 6.00 usec
TE 300.0 K
D1 2.00000000 sec
d11 0.03000000 sec
d12 0.00002000 sec
======== CHANNEL f1 ========
NUC1 13C
P1 8.70 usec
PL1 0.00 dB
SF01 100.6237959 MHz
======== CHANNEL f2 ========
CPDPRG2 waltz16
NUC2 1H
PCPD2 107.00 usec
PL2 0.00 dB
PL12 23.00 dB
PL13 23.00 dB
SF02 400.1316005 MHz
F2 - Processing parameters
SI 32768
SF 100.6129502 MHz
WDW EM
SSB 0
LB 1.00 Hz
GB 0
PC 1.40
1D NMR plot parameters
CX 20.00 cm
F1P 215.000 ppm
F1 21631.79 Hz
F2P -5.000 ppm
F2 -503.06 Hz
PPMCM 11.00000 ppm/cm
HZCM 1106.74243 Hz/cm
ppm 200 175 150 125 100 75 50 25 0

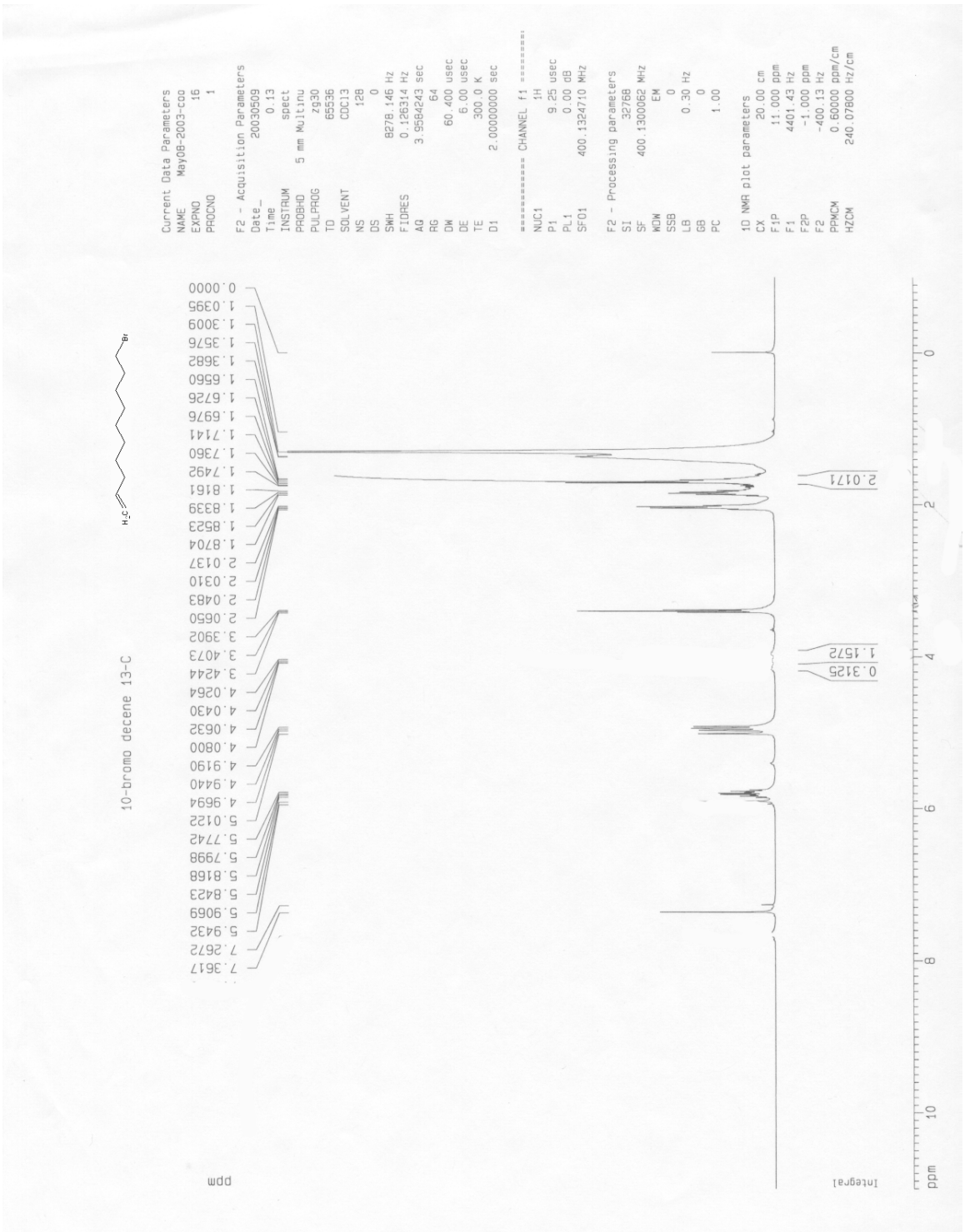
Current Data Parameters
NAME May08-2003-coo
EXPNO 16
PROCNO 1
F2 - Acquisition Parameters
Date_ 20030509
Time 0.13
INSTRUM spect
PROBHD 5 mm Multinu
PULPROG zg30
TD 65536
SOLVENT CDCl3
NS 128
DS 0
SWH 8278.146 Hz
FIDRES 0.126314 Hz
AQ 3.9584243 sec
RG 64
DW 60.400 usec
DE 6.00 usec
TE 300.0 K
D1 2.00000000 sec
========== CHANNEL f1 ========
NUC1 1H
P1 9.25 usec
PL1 0.00 dB
SFO1 400.1324710 MHz
F2 - Processing parameters
SI 32768
SF 400.1300062 MHz
WDW EM
SSB 0
LB 0.30 Hz
GB 0
PC 1.00
1D NMR plot parameters
CX 20.00 cm
F1P 11.000 ppm
F1 4401.43 Hz
F2P -1.000 ppm
F2 -400.13 Hz
PPMCM 0.60000 ppm/cm
HZCM 240.07800 Hz/cm
10-bromo decene 13-C
Br
H2C
ppm
0.0000
1.0395
1.3009
1.3576
1.3682
1.6560
1.6726
1.6976
1.7141
1.7360
1.7492
1.8161
1.8339
1.8523
1.8704
2.0137
2.0310
2.0483
2.0650
3.3902
3.4073
3.4244
4.0264
4.0430
4.0632
4.0800
4.9190
4.9440
4.9694
5.0122
5.7742
5.7998
5.8168
5.8423
5.9069
5.9432
7.2672
7.3617
2.0171
1.1572
0.3125
Integral
ppm
10
8
6
4
2
0

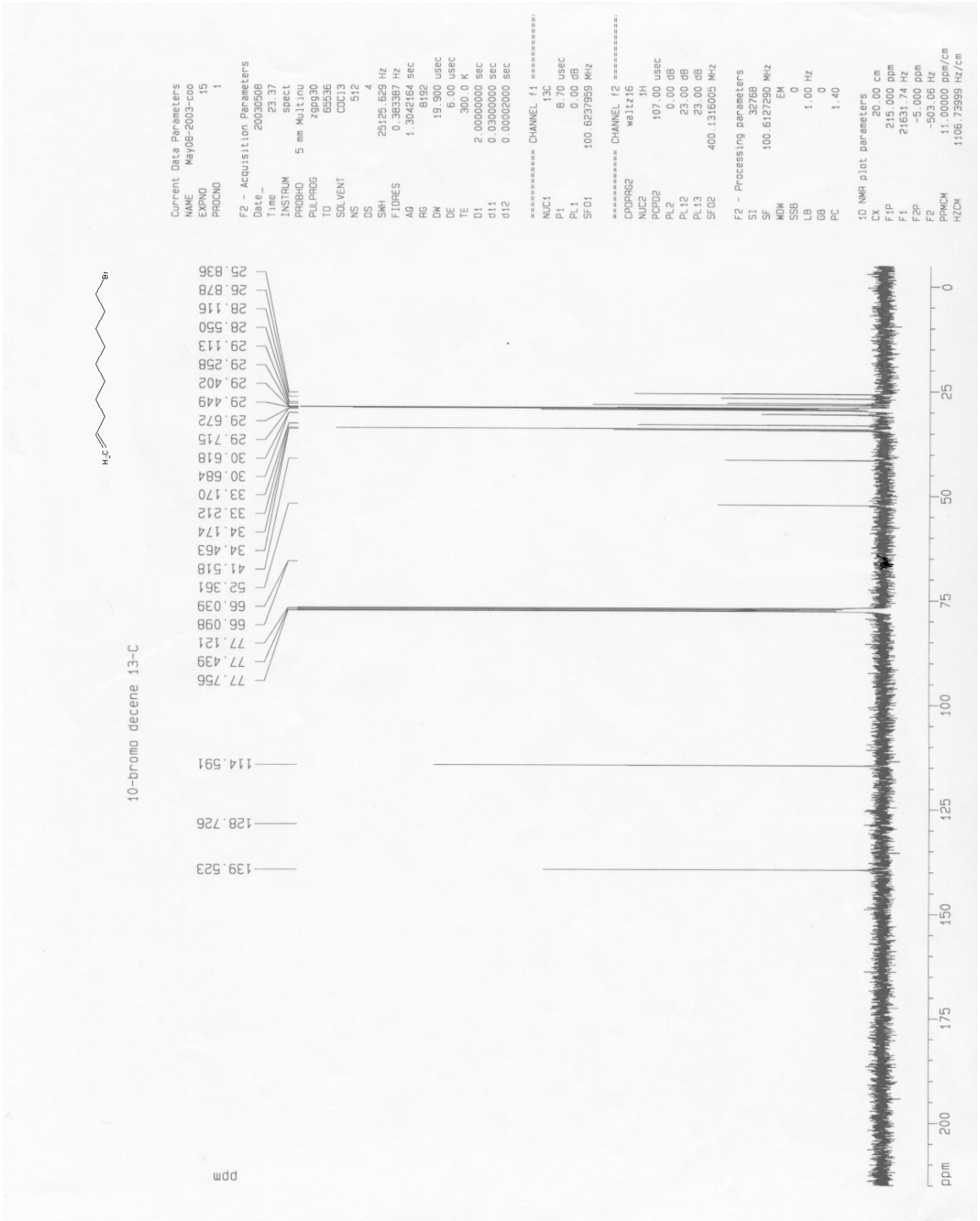
10-bromo decene 13-C
Current Data Parameters
NAME May06-2003-cao
EXPNO 15
PROCNO 1
F2 - Acquisition Parameters
Date_ 20030508
Time 23.37
INSTRUM spect
PROBHD 5 mm Multinu
PULPROG zgpg30
TD 65536
SOLVENT CDCl3
NS 512
DS 4
SWH 25125.629 Hz
FIDRES 0.383387 Hz
AQ 1.3042164 sec
RG 8192
DW 19.900 usec
DE 6.00 usec
TE 300.0 K
D1 2.00000000 sec
D11 0.03000000 sec
D12 0.00002000 sec
CHANNEL f1
NUC1 13C
P1 8.70 usec
PL1 0.00 dB
SFO1 100.6237959 MHz
CHANNEL f2
CPDPRG2 waltz16
NUC2 1H
PCPD2 107.00 usec
PL2 0.00 dB
PL12 23.00 dB
PL13 23.00 dB
SFO2 400.1316005 MHz
F2 - Processing parameters
SI 32768
SF 100.6127290 MHz
WDW EM
SSB 0
LB 1.00 Hz
GB 0
PC 1.40
1D NMR plot parameters
CX 20.00 cm
F1P 215.000 ppm
F1 21631.74 Hz
F2P -5.000 ppm
F2 -503.06 Hz
PPMCM 11.00000 ppm/cm
HZCM 1106.73999 Hz/cm
77.756
77.439
77.121
66.098
66.039
52.361
41.518
34.463
34.174
33.212
33.170
30.684
30.618
29.715
29.672
29.449
29.402
29.258
29.113
28.550
28.116
26.878
25.836
114.591
128.726
139.523
ppm
0
25
50
75
100
125
150
175
200

Mass Spectrum of 10-bromo-1-decene, retention time = 3.5 minutes

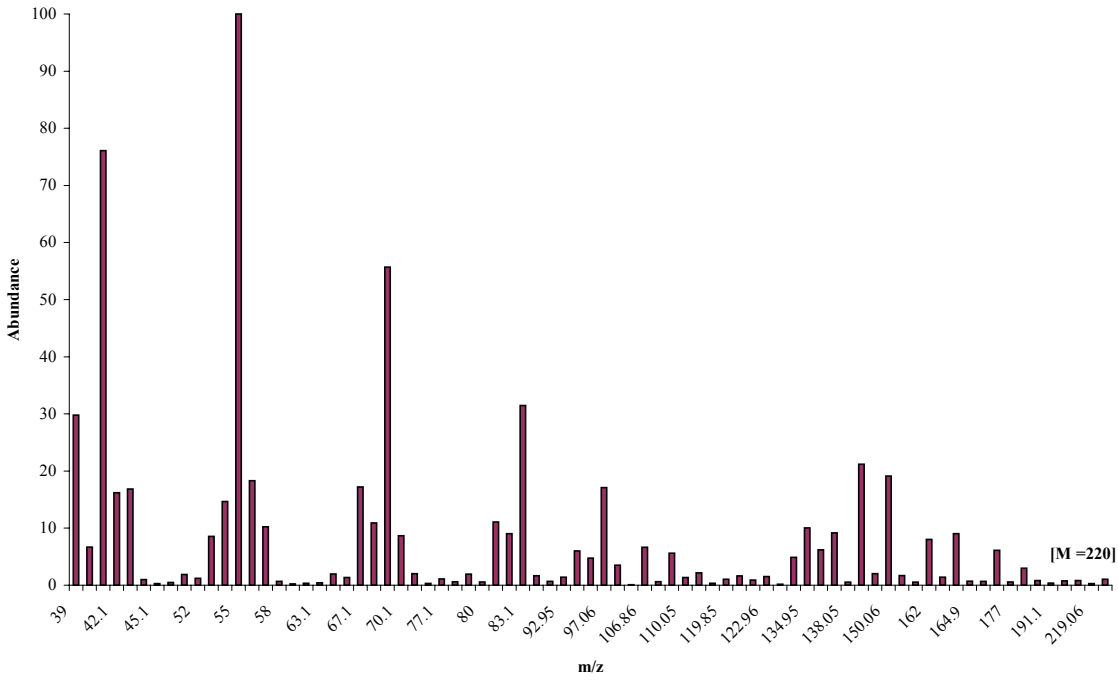

Scheme 12. Synthesis of Disubstituted Diaza 18-Crown-6 (7N-Anthrylmethyl, 16N-decyl(10-trichlorosilyl), 1,4,10,13-tetraoxa-7,16-diazacyclooctadecane)

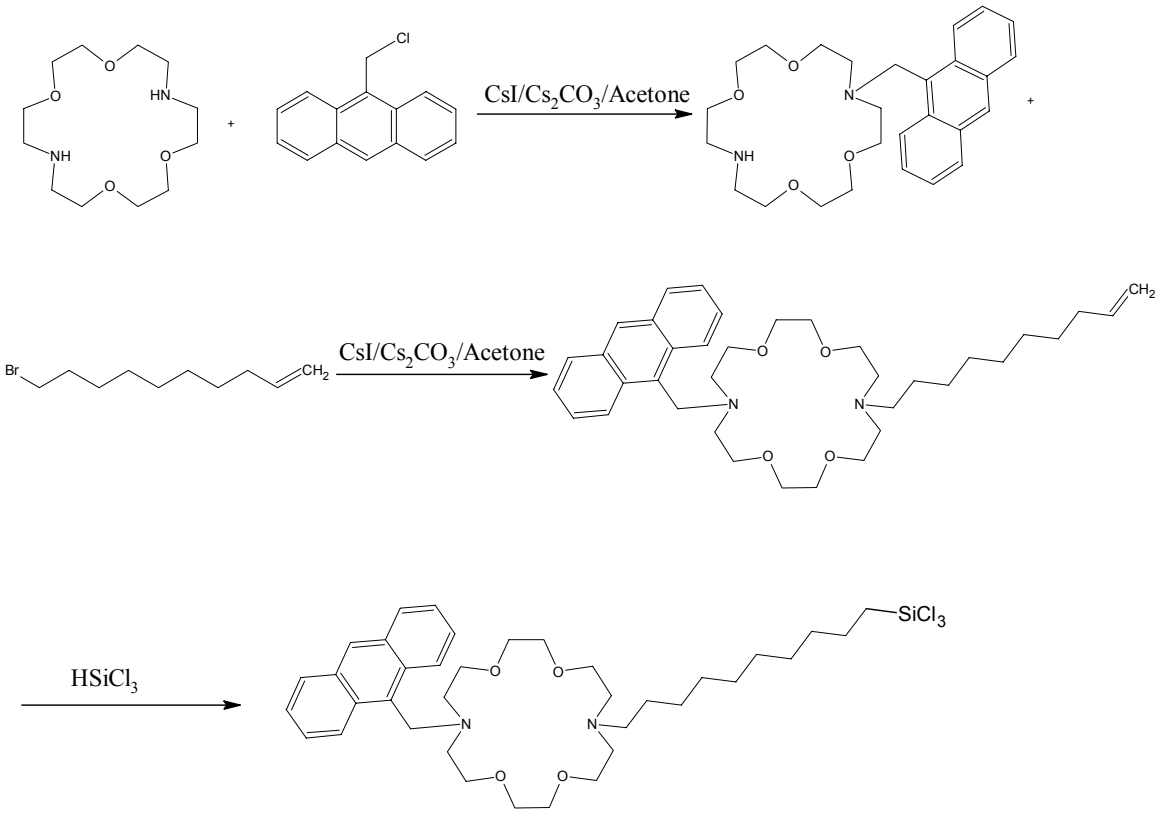

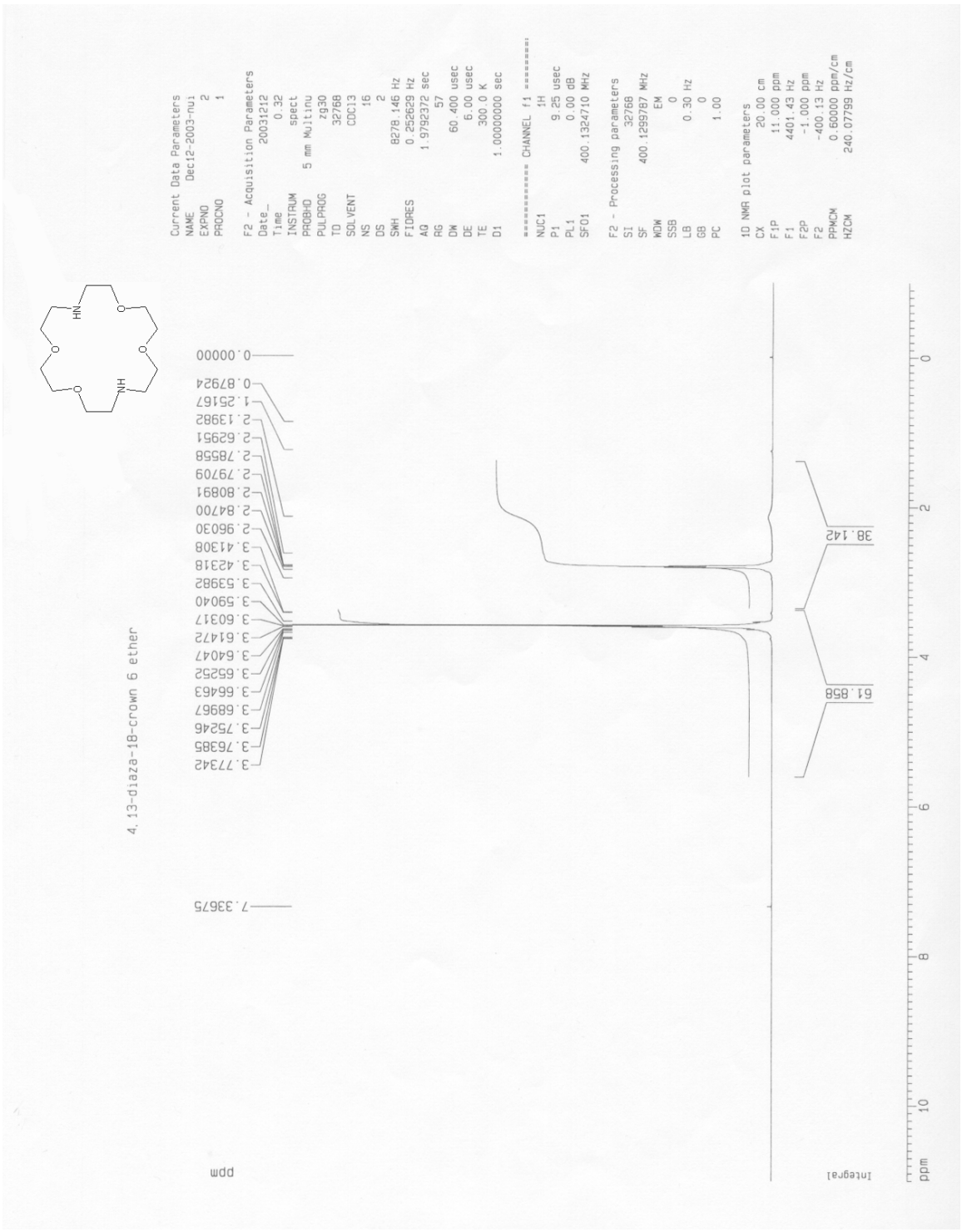
4,13-diaza-18-crown 6 ether
Current Data Parameters
NAME Dec12-2003-nui
EXPNO 2
PROCNO 1
F2 - Acquisition Parameters
Date_ 20031212
Time 0.32
INSTRUM spect
PROBHD 5 mm Multinu
PULPROG zg30
TD 32768
SOLVENT CDCl3
NS 16
DS 2
SWH 8278.146 Hz
FIDRES 0.252629 Hz
AQ 1.9792372 sec
RG 57
DW 60.400 usec
DE 6.00 usec
TE 300.0 K
D1 1.00000000 sec
======== CHANNEL f1 ========
NUC1 1H
P1 9.25 usec
PL1 0.00 dB
SF01 400.1324710 MHz
F2 - Processing parameters
SI 32768
SF 400.1299787 MHz
WDW EM
SSB 0
LB 0.30 Hz
GB 0
PC 1.00
1D NMR plot parameters
CX 20.00 cm
F1P 11.000 ppm
F1 4401.43 Hz
F2P -1.000 ppm
F2 -400.13 Hz
PPMCM 0.60000 ppm/cm
HZCM 240.07799 Hz/cm
0.00000
0.87924
1.25167
2.13982
2.62951
2.78558
2.79709
2.80891
2.84700
2.96030
3.41308
3.42318
3.53982
3.59040
3.60317
3.61472
3.64047
3.65252
3.66463
3.68967
3.75246
3.76385
3.77342
7.33675
38.142
61.858
ppm
Integral

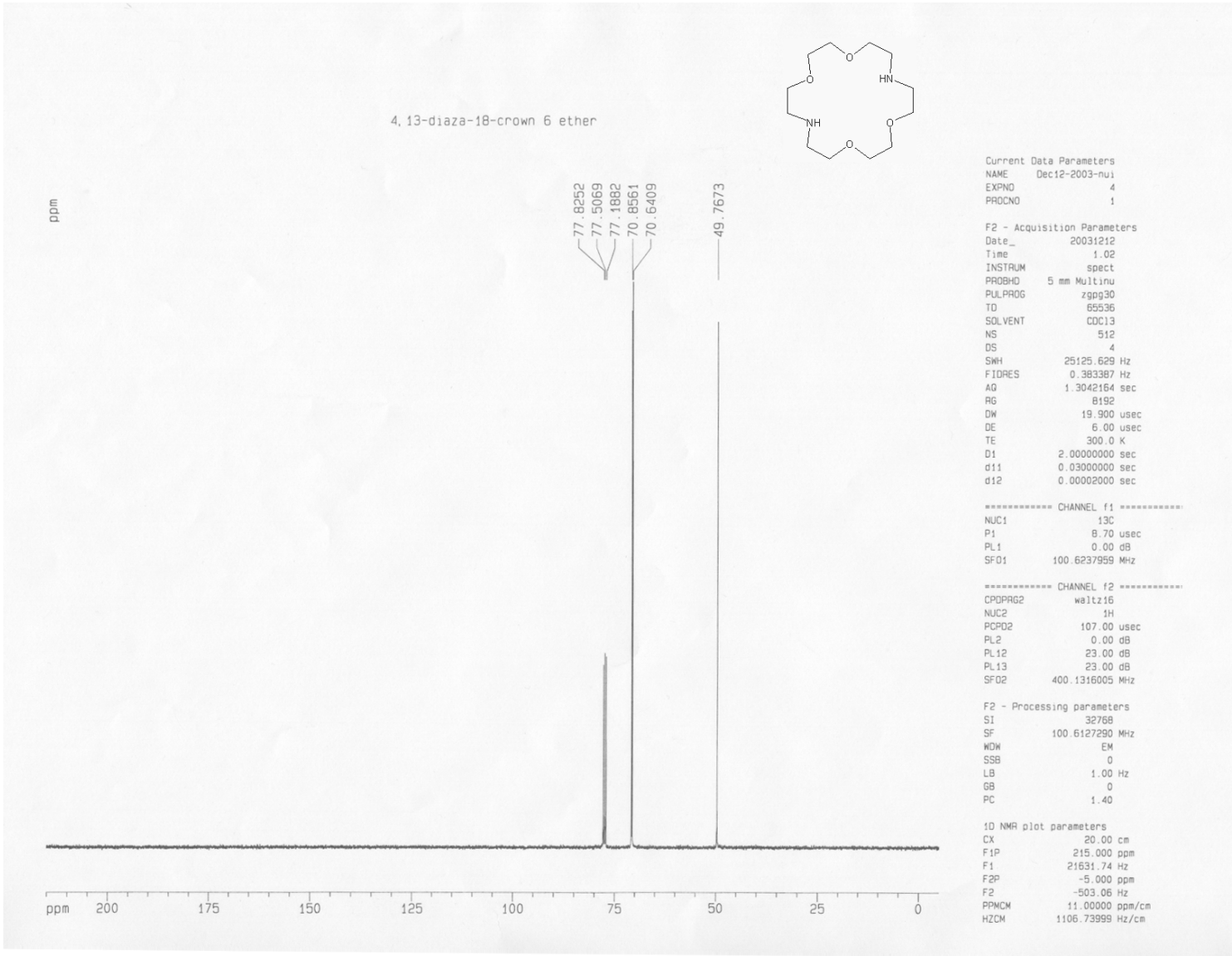
4, 13-diaza-18-crown 6 ether
O
HN
O
NH
O
O
ppm
77.8252
77.5069
77.1882
70.8561
70.6409
49.7673
ppm 200 175 150 125 100 75 50 25 0
Current Data Parameters
NAME Dec12-2003-nui
EXPNO 4
PROCNO 1
F2 - Acquisition Parameters
Date_ 20031212
Time 1.02
INSTRUM spect
PROBHD 5 mm Multinu
PULPROG zgpg30
TD 65536
SOLVENT CDCl3
NS 512
DS 4
SWH 25125.629 Hz
FIDRES 0.383387 Hz
AQ 1.3042164 sec
RG 8192
DW 19.900 usec
DE 6.00 usec
TE 300.0 K
D1 2.00000000 sec
d11 0.03000000 sec
d12 0.00002000 sec
========== CHANNEL f1 ==========
NUC1 13C
P1 8.70 usec
PL1 0.00 dB
SFO1 100.6237959 MHz
========== CHANNEL f2 ==========
CPDPRG2 waltz16
NUC2 1H
PCPD2 107.00 usec
PL2 0.00 dB
PL12 23.00 dB
PL13 23.00 dB
SFO2 400.1316005 MHz
F2 - Processing parameters
SI 32768
SF 100.6127290 MHz
WDW EM
SSB 0
LB 1.00 Hz
GB 0
PC 1.40
1D NMR plot parameters
CX 20.00 cm
F1P 215.000 ppm
F1 21631.74 Hz
F2P -5.000 ppm
F2 -503.06 Hz
PPMCM 11.00000 ppm/cm
HZCM 1106.73999 Hz/cm

Cl
Current Data Parameters
NAME May22-2003-tes
EXPNO 17
PROCNO 1
F2 - Acquisition Parameters
Date_ 20030523
Time_ 1.16
INSTRUM spect
PROBHD 5 mm Multinu
PULPROG zg30
TD 32768
SOLVENT CDCl3
NS 16
DS 2
SWH 8278.146 Hz
FIDRES 0.252629 Hz
AQ 1.9792372 sec
RG 406.4
DW 60.400 usec
DE 6.00 usec
TE 300.0 K
D1 1.00000000 sec
========== CHANNEL f1 ========
NUC1 1H
P1 9.25 usec
PL1 0.00 dB
SFO1 400.1324710 MHz
F2 - Processing parameters
SI 32768
SF 400.1300000 MHz
WDW no
SSB 0
LB 0.00 Hz
GB 0
PC 1.00
1D NMR plot parameters
CX 20.00 cm
F1P 11.000 ppm
F1 4401.43 Hz
F2P -1.000 ppm
F2 -400.13 Hz
PPMCM 0.60000 ppm/cm
HZCM 240.07800 Hz/cm
ppm
8.7867
8.5200
8.3569
8.3346
8.0751
8.0739
8.0538
8.0526
7.6650
7.6517
7.6485
7.6466
7.6427
7.6295
7.6264
7.5545
7.5357
7.5335
7.5187
7.5171
7.2830
5.6977
5.6786
5.6695
5.6467
5.6197
5.5965
5.4555
3.7352
3.2478
1.7602
1.6298
1.5791
1.5298
1.2228
0.1798
0.0851
0.0663
0.0561
0.0537
0.0422
0.0340
0.0258
0.0070
0.0045
0.0165
0.0410
ppm

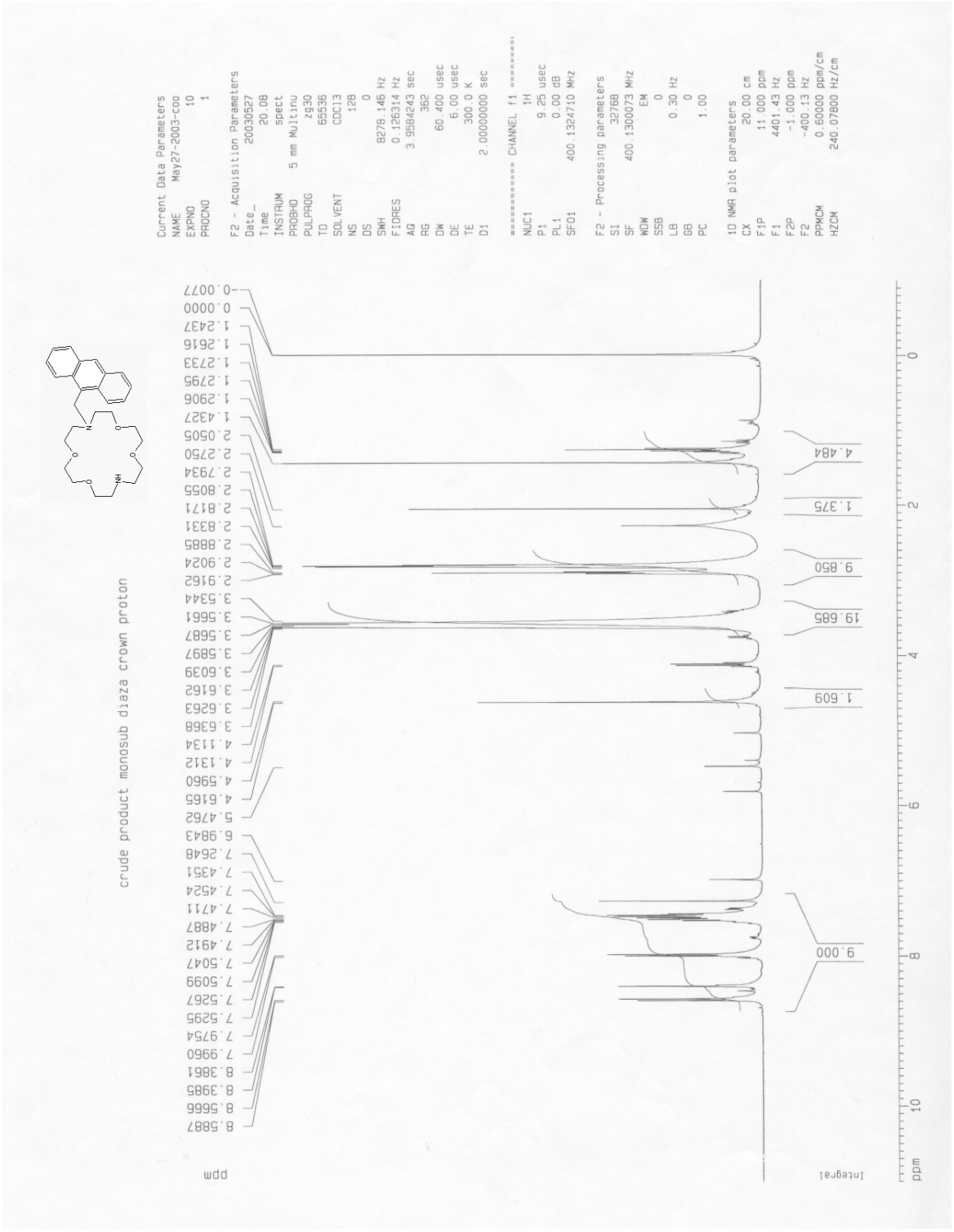
crude product monosub diaza crown proton
Current Data Parameters
NAME May27-2003-coo
EXPNO 10
PROCNO 1
F2 - Acquisition Parameters
Date_ 20030527
Time 20.08
INSTRUM spect
PROBHD 5 mm Multinu
PULPROG 2930
TD 65536
SOLVENT CDCl3
NS 128
DS 0
SWH 8278.146 Hz
FIDRES 0.126314 Hz
AQ 3.9584243 sec
RG 362
DW 60.400 usec
DE 6.00 usec
TE 300.0 K
D1 2.00000000 sec
========== CHANNEL f1 ========
NUC1 1H
P1 9.25 usec
PL1 0.00 dB
SFO1 400.1324710 MHz
F2 - Processing parameters
SI 32768
SF 400.1300073 MHz
WDW EM
SSB 0
LB 0.30 Hz
GB 0
PC 1.00
1D NMR plot parameters
CX 20.00 cm
F1P 11.000 ppm
F1 4401.43 Hz
F2P -1.000 ppm
F2 -400.13 Hz
PPMCM 0.60000 ppm/cm
HZCM 240.07800 Hz/cm
-0.0077
0.0000
1.2437
1.2616
1.2733
1.2795
1.2906
1.4327
2.0505
2.2750
2.7934
2.8055
2.8171
2.8331
2.8885
2.9024
2.9162
3.5344
3.5661
3.5687
3.5897
3.6039
3.6162
3.6263
3.6368
4.1134
4.1312
4.5960
4.6165
5.4762
6.9843
7.2648
7.4351
7.4524
7.4711
7.4887
7.4912
7.5047
7.5099
7.5267
7.5295
7.9754
7.9960
8.3861
8.3985
8.5666
8.5887
ppm
Integral
4.484
1.375
9.850
19.685
1.609
9.000
ppm

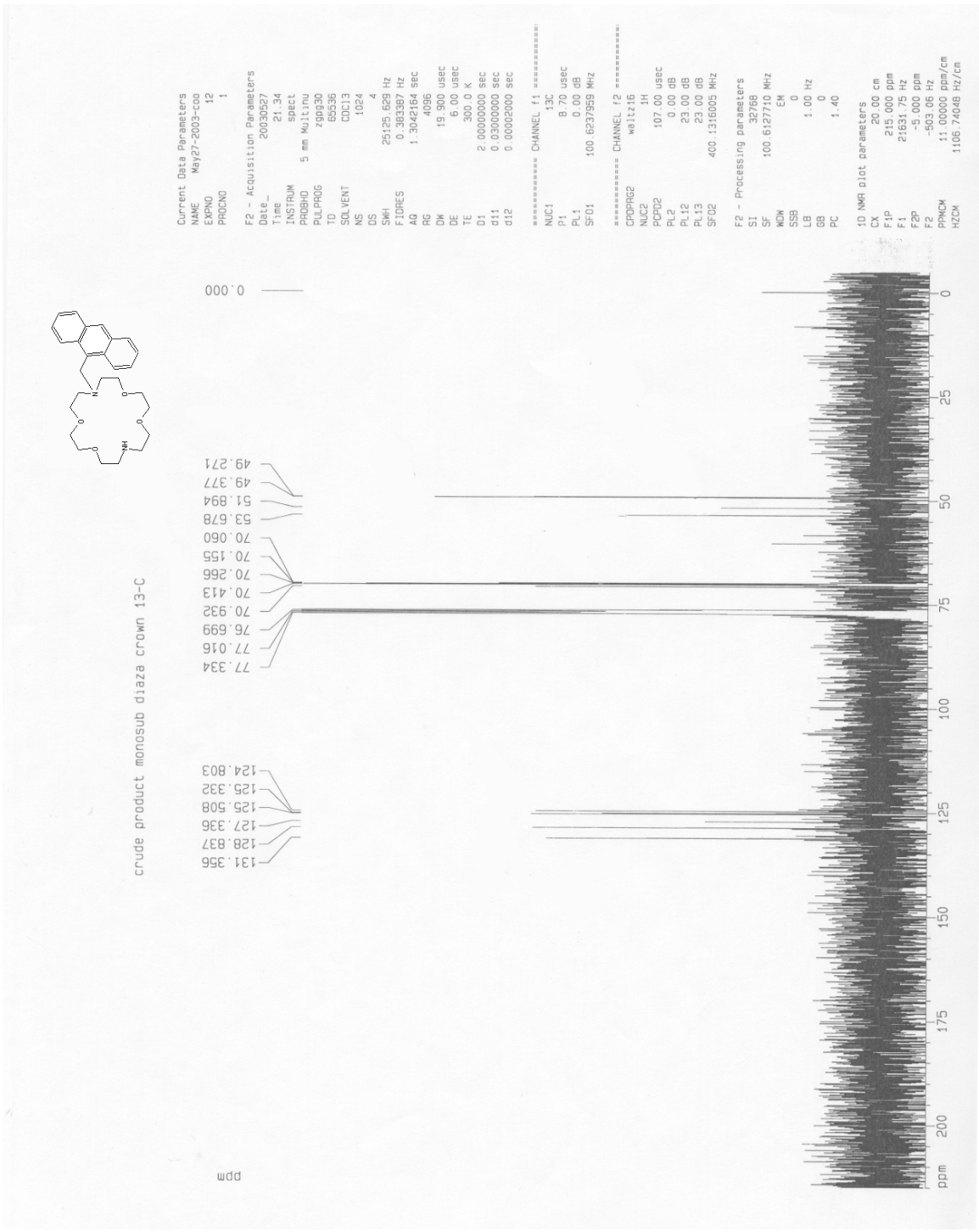
crude product monosub diaza crown 13-C
ppm
0.000
49.271
49.377
51.894
53.678
70.060
70.155
70.266
70.413
70.932
76.699
77.016
77.334
124.803
125.332
125.508
127.336
128.837
131.356
Current Data Parameters
NAME May27-2003-coo
EXPNO 12
PROCNO 1
F2 - Acquisition Parameters
Date_ 20030527
Time 21.34
INSTRUM spect
PROBHD 5 mm Multinu
PULPROG zgpg30
TD 65536
SOLVENT CDCl3
NS 1024
DS 4
SWH 25125.629 Hz
FIDRES 0.383387 Hz
AQ 1.3042164 sec
RG 4096
DW 19.900 usec
DE 6.00 usec
TE 300.0 K
D1 2.00000000 sec
d11 0.03000000 sec
d12 0.00002000 sec
======== CHANNEL f1 ========
NUC1 13C
P1 8.70 usec
PL1 0.00 dB
SFO1 100.6237959 MHz
======== CHANNEL f2 ========
CPDPRG2 waltz16
NUC2 1H
PCPD2 107.00 usec
PL2 0.00 dB
PL12 23.00 dB
PL13 23.00 dB
SFO2 400.1316005 MHz
F2 - Processing parameters
SI 32768
SF 100.6127710 MHz
WDW EM
SSB 0
LB 1.00 Hz
GB 0
PC 1.40
1D NMR plot parameters
CX 20.00 cm
F1P 215.000 ppm
F1 21631.75 Hz
F2P -5.000 ppm
F2 -503.06 Hz
PPMCM 11.00000 ppm/cm
HZCM 1106.74048 Hz/cm
ppm
0
25
50
75
100
125
150
175
200

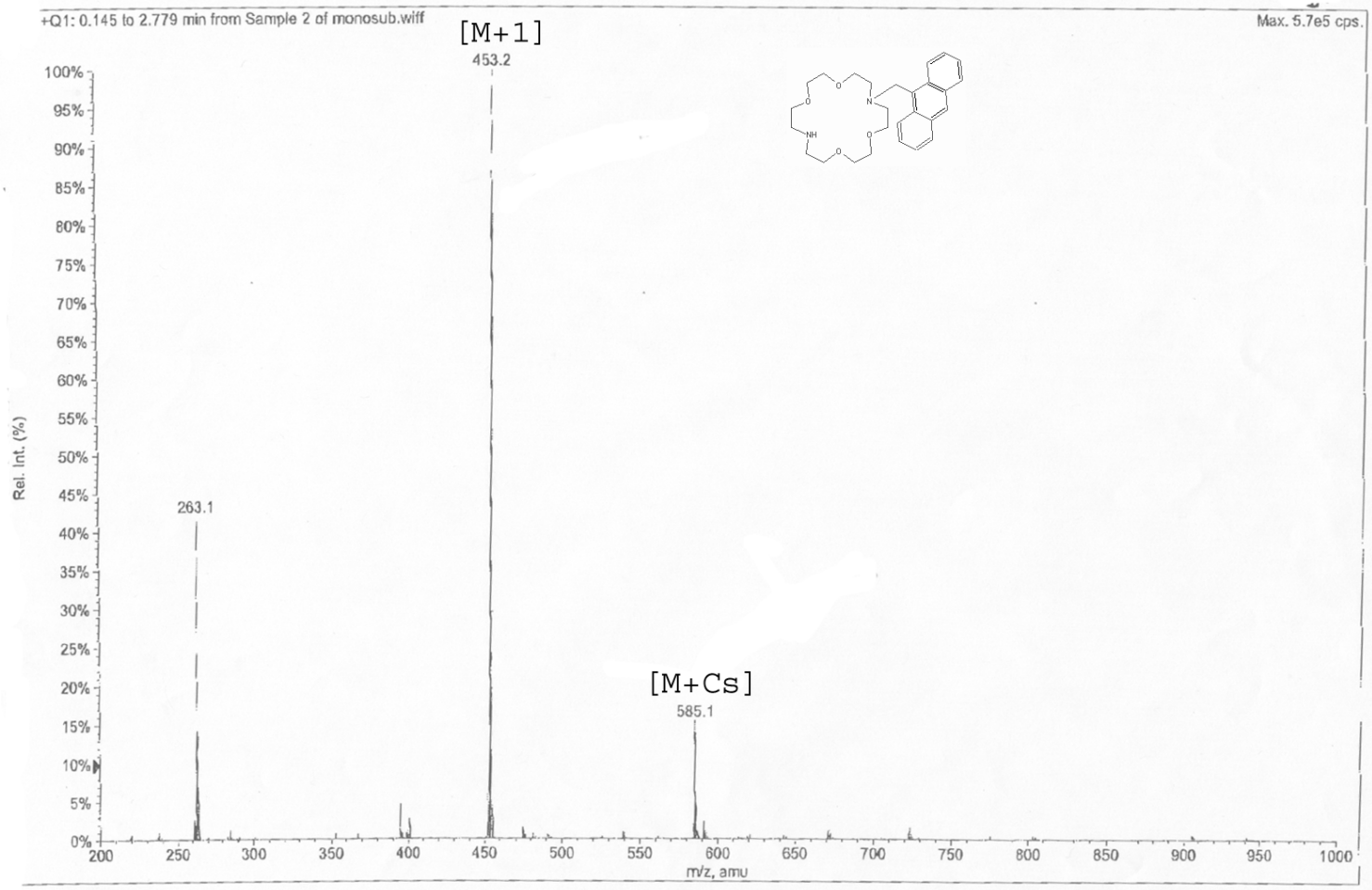
+Q1: 0.145 to 2.779 min from Sample 2 of monosub.wiff
Max. 5.7e5 cps.
[M+1]
453.2
263.1
[M+Cs]
585.1
Rel. Int. (%)
m/z, amu

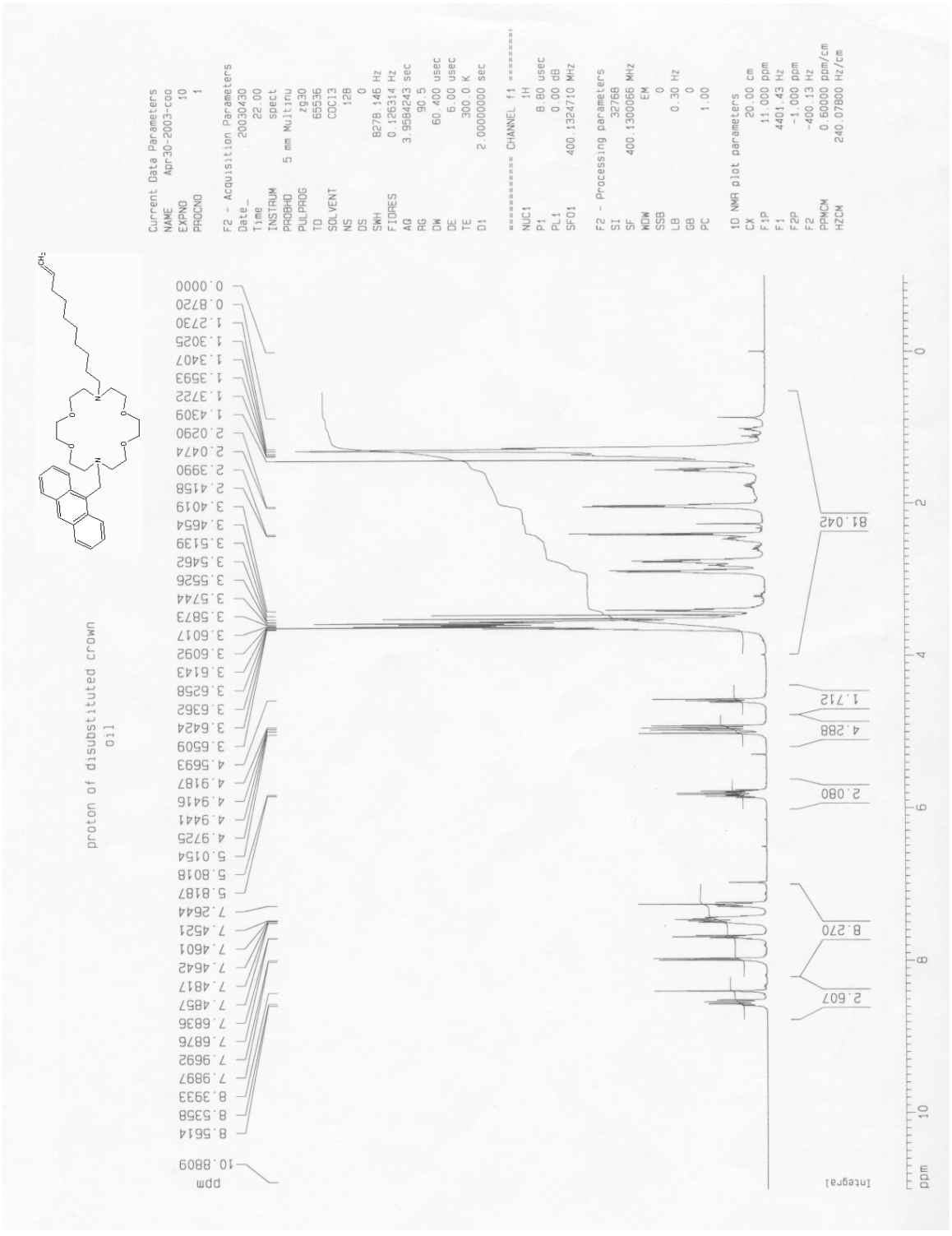
proton of disubstituted crown
oil
Current Data Parameters
NAME Apr30-2003-coo
EXPNO 10
PROCNO 1
F2 - Acquisition Parameters
Date_ 20030430
Time 22.00
INSTRUM spect
PROBHD 5 mm Multinu
PULPROG z930
TD 65536
SOLVENT CDCl3
NS 128
DS 0
SWH 8278.146 Hz
FIDRES 0.126314 Hz
AQ 3.9584243 sec
RG 90.5
DW 60.400 usec
DE 6.00 usec
TE 300.0 K
D1 2.00000000 sec
========== CHANNEL f1 ========
NUC1 1H
P1 8.80 usec
PL1 0.00 dB
SFO1 400.1324710 MHz
F2 - Processing parameters
SI 32768
SF 400.1300066 MHz
WDW EM
SSB 0
LB 0.30 Hz
GB 0
PC 1.00
1D NMR plot parameters
CX 20.00 cm
F1P 11.000 ppm
F1 4401.43 Hz
F2P -1.000 ppm
F2 -400.13 Hz
PPMCM 0.60000 ppm/cm
HZCM 240.07800 Hz/cm
ppm
Integral
81.042
4.288
2.080
1.712
8.270
2.607

13-C of disubstituted crown
oil
ppm
Current Data Parameters
NAME Apr30-2003-coo
EXPNO 11
PROCNO 1
F2 - Acquisition Parameters
Date_ 20030430
Time 22.07
INSTRUM spect
PROBHD 5 mm Multinu
PULPROG zgpg30
TD 65536
SOLVENT CDCl3
NS 512
DS 4
SWH 25125.629 Hz
FIDRES 0.383387 Hz
AQ 1.3042164 sec
RG 4096
DW 19.900 usec
DE 6.00 usec
TE 300.0 K
D1 2.00000000 sec
d11 0.03000000 sec
d12 0.00002000 sec
======== CHANNEL f1 ========
NUC1 13C
P1 8.70 usec
PL1 0.00 dB
SFO1 100.6237959 MHz
======== CHANNEL f2 ========
CPDPRG2 waltz16
NUC2 1H
PCPD2 107.00 usec
PL2 0.00 dB
PL12 23.00 dB
PL13 23.00 dB
SFO2 400.1316005 MHz
F2 - Processing parameters
SI 32768
SF 100.6127290 MHz
WDW EM
SSB 0
LB 1.00 Hz
GB 0
PC 1.40
1D NMR plot parameters
CX 20.00 cm
F1P 215.000 ppm
F1 21631.74 Hz
F2P -5.000 ppm
F2 -503.06 Hz
PPMCM 11.00000 ppm/cm
HZCM 1106.73999 Hz/cm
21.886
26.128
27.256
27.894
29.298
29.453
29.775
29.839
29.944
30.709
33.023
33.188
34.192
49.505
52.338
54.097
54.228
63.395
70.532
70.672
70.831
70.955
71.211
77.127
77.445
77.762
114.543
125.215
125.574
125.650
125.955
127.518
127.862
129.310
130.041
130.756
131.792
137.029
139.595
143.584
ppm
200
175
150
125
100
75
50
25
0

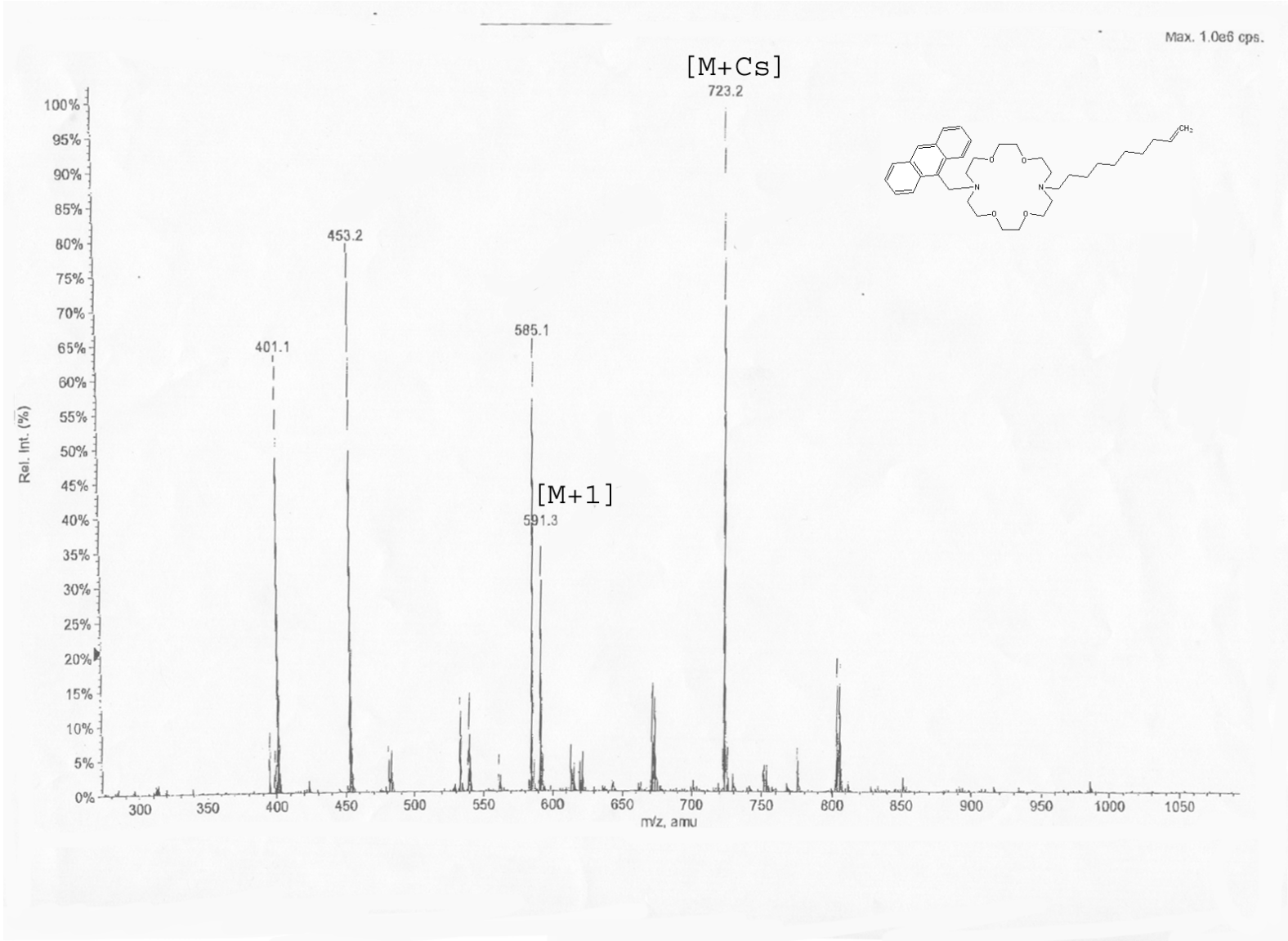
Max. 1.0e6 cps.
[M+Cs]
723.2
453.2
401.1
585.1
[M+1]
591.3
Rel. Int. (%)
m/z, amu

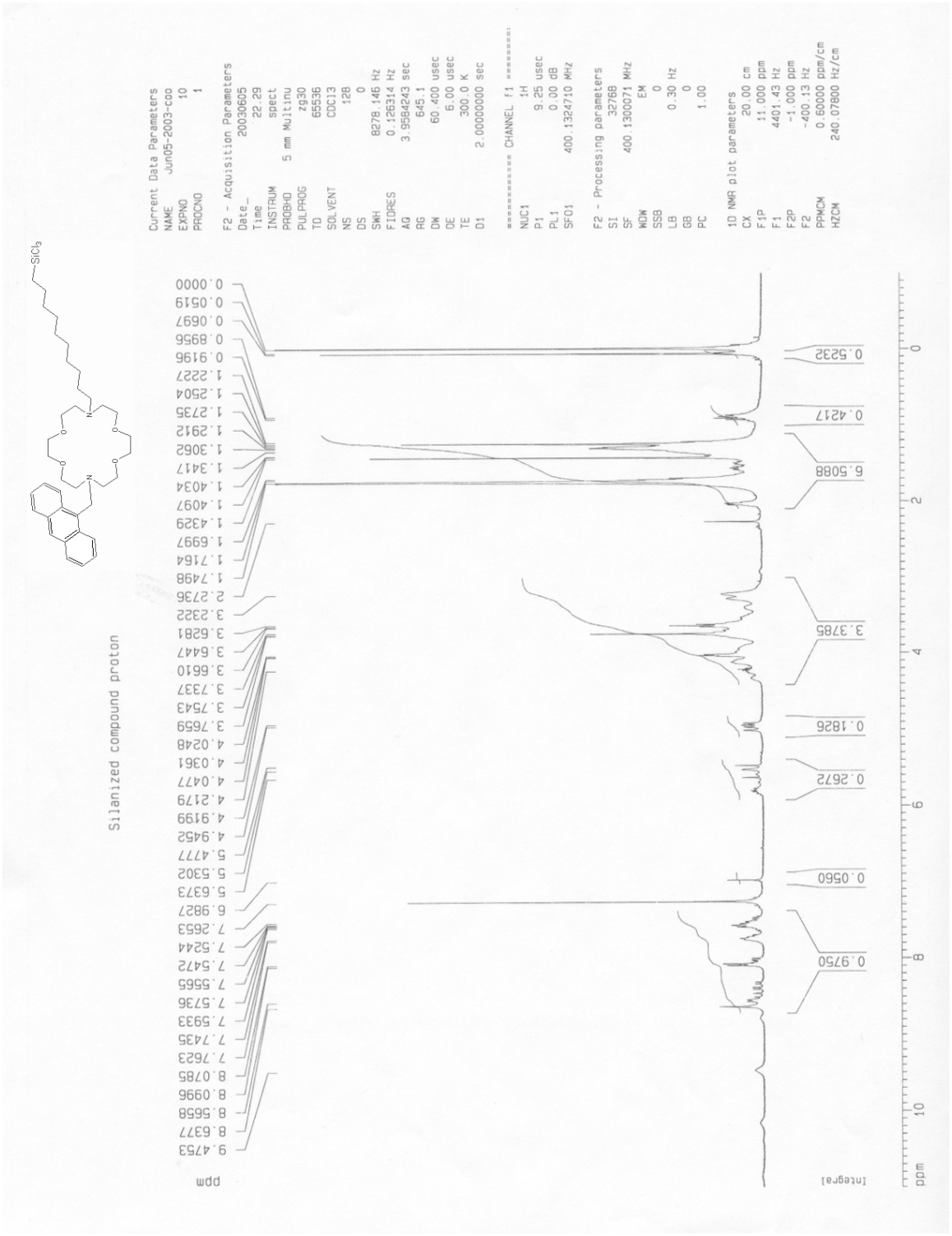

Due to a lack of stability, only a proton spectrum was collected for this product.

Synthesis of pyrenyl substituted Diketopiperazine

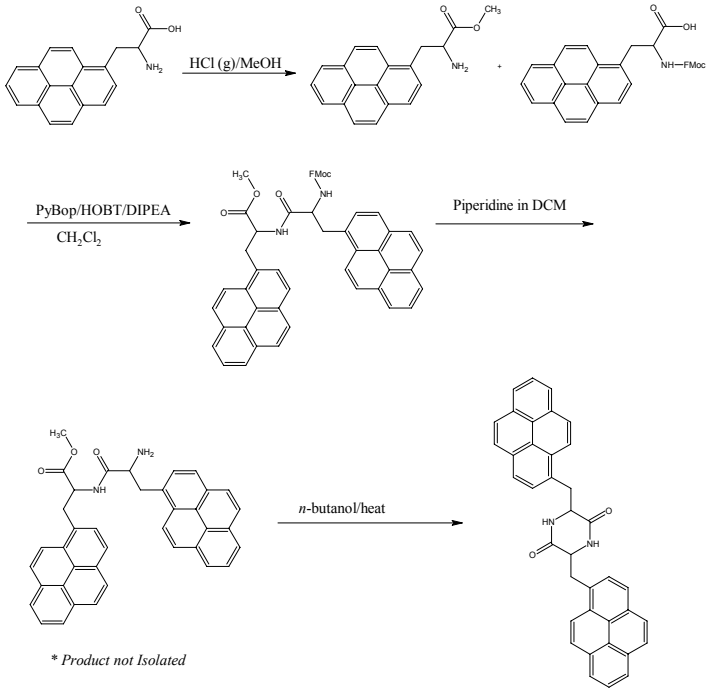

The spectra for N-Fmoc L, Pyrenyl alanine have been previously displayed. In addition, solubility problems made it impossible to obtain spectral data for the non-cyclic dipeptide intermediate.

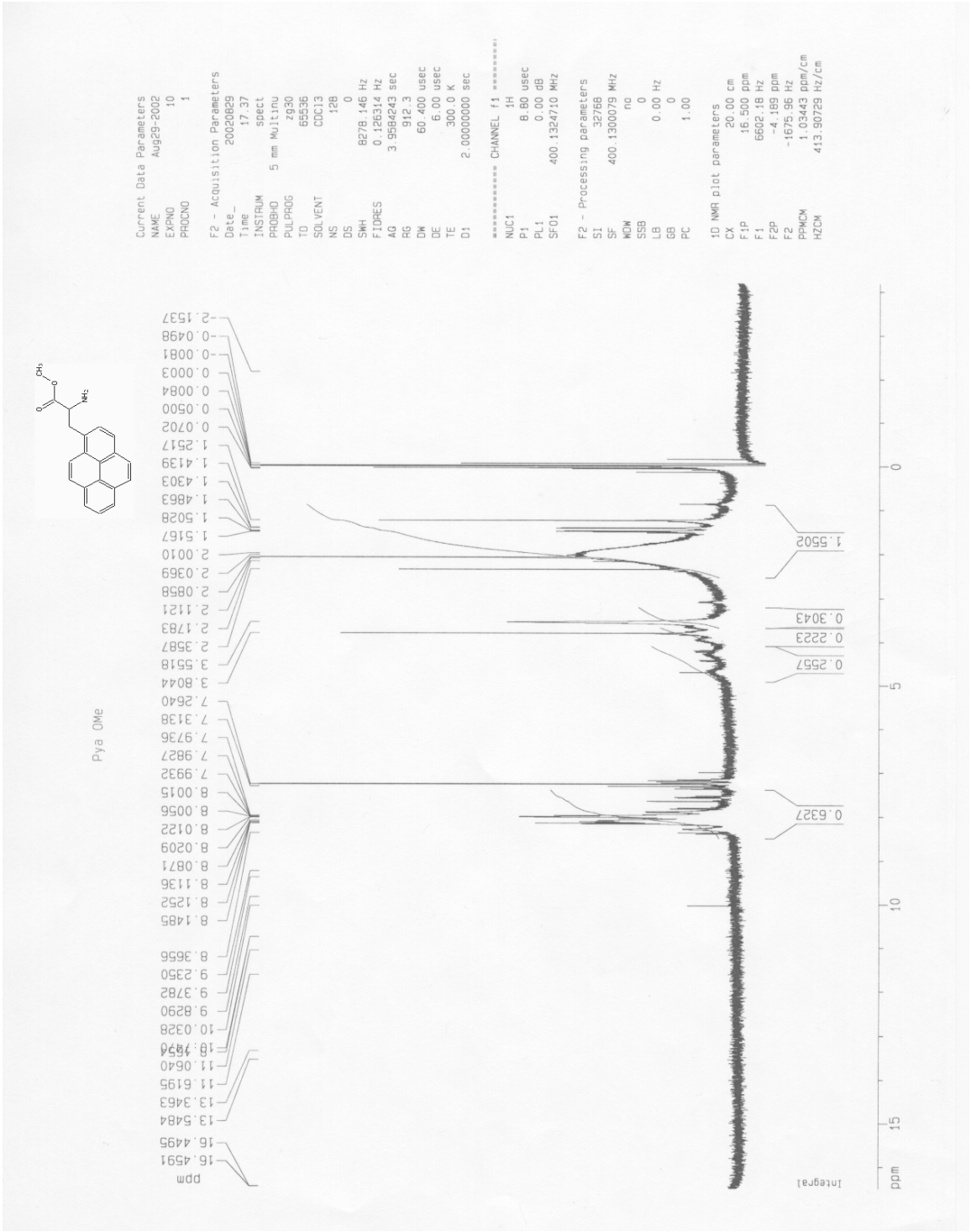
Current Data Parameters
NAME Aug29-2002
EXPNO 10
PROCNO 1
F2 - Acquisition Parameters
Date_ 20020829
Time 17.37
INSTRUM spect
PROBHD 5 mm Multinu
PULPROG zg30
TD 65536
SOLVENT CDCl3
NS 128
DS 0
SWH 8278.146 Hz
FIDRES 0.126314 Hz
AQ 3.9584243 sec
RG 912.3
DW 60.400 usec
DE 6.00 usec
TE 300.0 K
D1 2.00000000 sec
======== CHANNEL f1 ========
NUC1 1H
P1 8.80 usec
PL1 0.00 dB
SFO1 400.1324710 MHz
F2 - Processing parameters
SI 32768
SF 400.1300079 MHz
WDW no
SSB 0
LB 0.00 Hz
GB 0
PC 1.00
1D NMR plot parameters
CX 20.00 cm
F1P 16.500 ppm
F1 6602.18 Hz
F2P -4.169 ppm
F2 -1675.96 Hz
PPMCM 1.03443 ppm/cm
HZCM 413.90729 Hz/cm
Pya OMe
ppm
Integral
1.5502
0.3043
0.2223
0.2557
0.6327
ppm 15 10 5 0

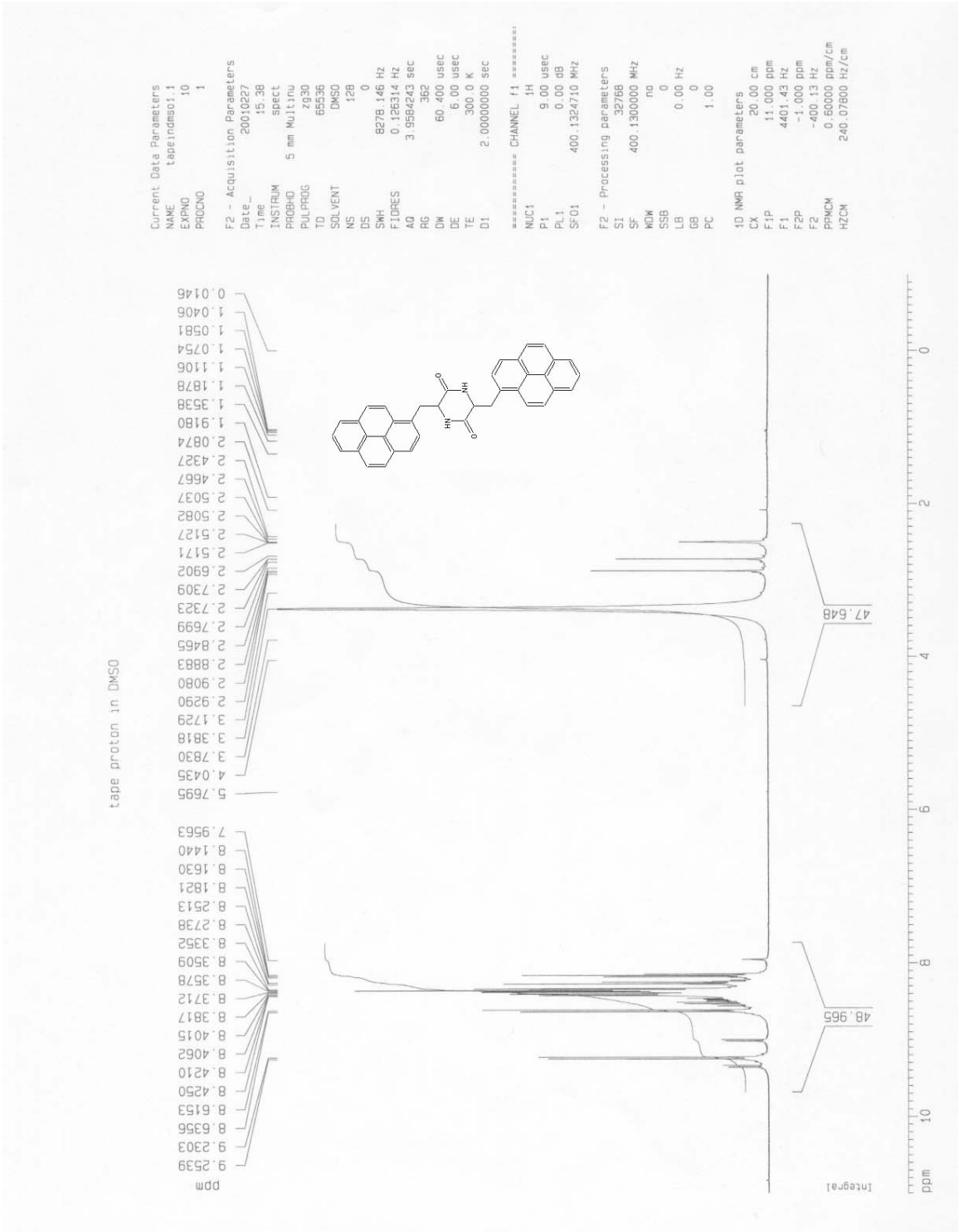
tape proton in DMSO
ppm
9.2539
9.2303
8.6356
8.6153
8.4250
8.4210
8.4062
8.4015
8.3817
8.3712
8.3578
8.3509
8.3352
8.2738
8.2513
8.1821
8.1630
8.1440
7.9563
5.7695
4.0435
3.7830
3.3818
3.1729
2.9290
2.9080
2.8883
2.8465
2.7699
2.7323
2.7309
2.6902
2.5171
2.5127
2.5082
2.5037
2.4667
2.4327
2.0874
1.9180
1.3538
1.1878
1.1106
1.0754
1.0581
1.0406
0.0146
Current Data Parameters
NAME tapeindmso1.1
EXPNO 10
PROCNO 1
F2 - Acquisition Parameters
Date_ 20010227
Time 15.38
INSTRUM spect
PROBHD 5 mm Multinu
PULPROG z930
TD 65536
SOLVENT DMSO
NS 128
DS 0
SWH 8278.146 Hz
FIDRES 0.126314 Hz
AQ 3.9584243 sec
RG 362
DW 60.400 usec
DE 6.00 usec
TE 300.0 K
D1 2.00000000 sec
========== CHANNEL f1 ========
NUC1 1H
P1 9.00 usec
PL1 0.00 dB
SFO1 400.1324710 MHz
F2 - Processing parameters
SI 32768
SF 400.1300000 MHz
WDW no
SSB 0
LB 0.00 Hz
GB 0
PC 1.00
1D NMR plot parameters
CX 20.00 cm
F1P 11.000 ppm
F1 4401.43 Hz
F2P -1.000 ppm
F2 -400.13 Hz
PPMCM 0.60000 ppm/cm
HZCM 240.07800 Hz/cm
NH
NH
O
O
47.648
48.965
Integral
ppm
10
8
6
4
2
0

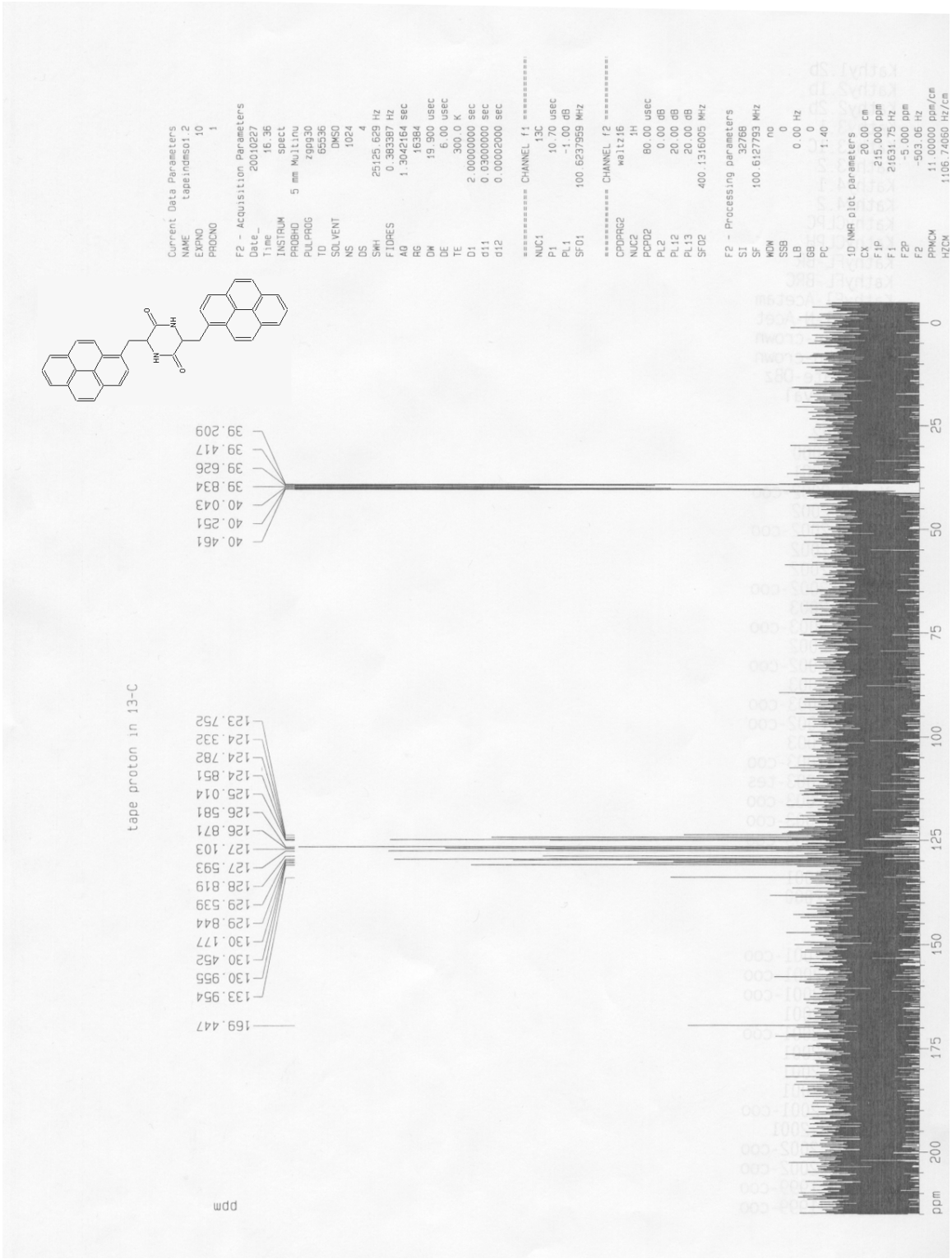
tape proton in 13-C
ppm
Current Data Parameters
NAME tapeindmso1.2
EXPNO 10
PROCNO 1
F2 - Acquisition Parameters
Date_ 20010227
Time 16.36
INSTRUM spect
PROBHD 5 mm Multinu
PULPROG zgpg30
TD 65536
SOLVENT DMSO
NS 1024
DS 4
SWH 25125.629 Hz
FIDRES 0.383387 Hz
AQ 1.3042164 sec
RG 16384
DW 19.900 usec
DE 6.00 usec
TE 300.0 K
D1 2.00000000 sec
d11 0.03000000 sec
d12 0.00002000 sec
CHANNEL f1
NUC1 13C
P1 10.70 usec
PL1 -1.00 dB
SF01 100.6237959 MHz
CHANNEL f2
CPDPRG2 waltz16
NUC2 1H
PCPD2 80.00 usec
PL2 0.00 dB
PL12 20.00 dB
PL13 20.00 dB
SF02 400.1316005 MHz
F2 - Processing parameters
SI 32768
SF 100.6127793 MHz
WDW no
SSB 0
LB 0.00 Hz
GB 0
PC 1.40
1D NMR plot parameters
CX 20.00 cm
F1P 215.000 ppm
F1 21631.75 Hz
F2P -5.000 ppm
F2 -503.06 Hz
PPMCM 11.00000 ppm/cm
HZCM 1106.74060 Hz/cm
39.209
39.417
39.626
39.834
40.043
40.251
40.461
123.752
124.332
124.782
124.851
125.014
126.581
126.871
127.103
127.593
128.819
129.539
129.844
130.177
130.452
130.955
133.954
169.447

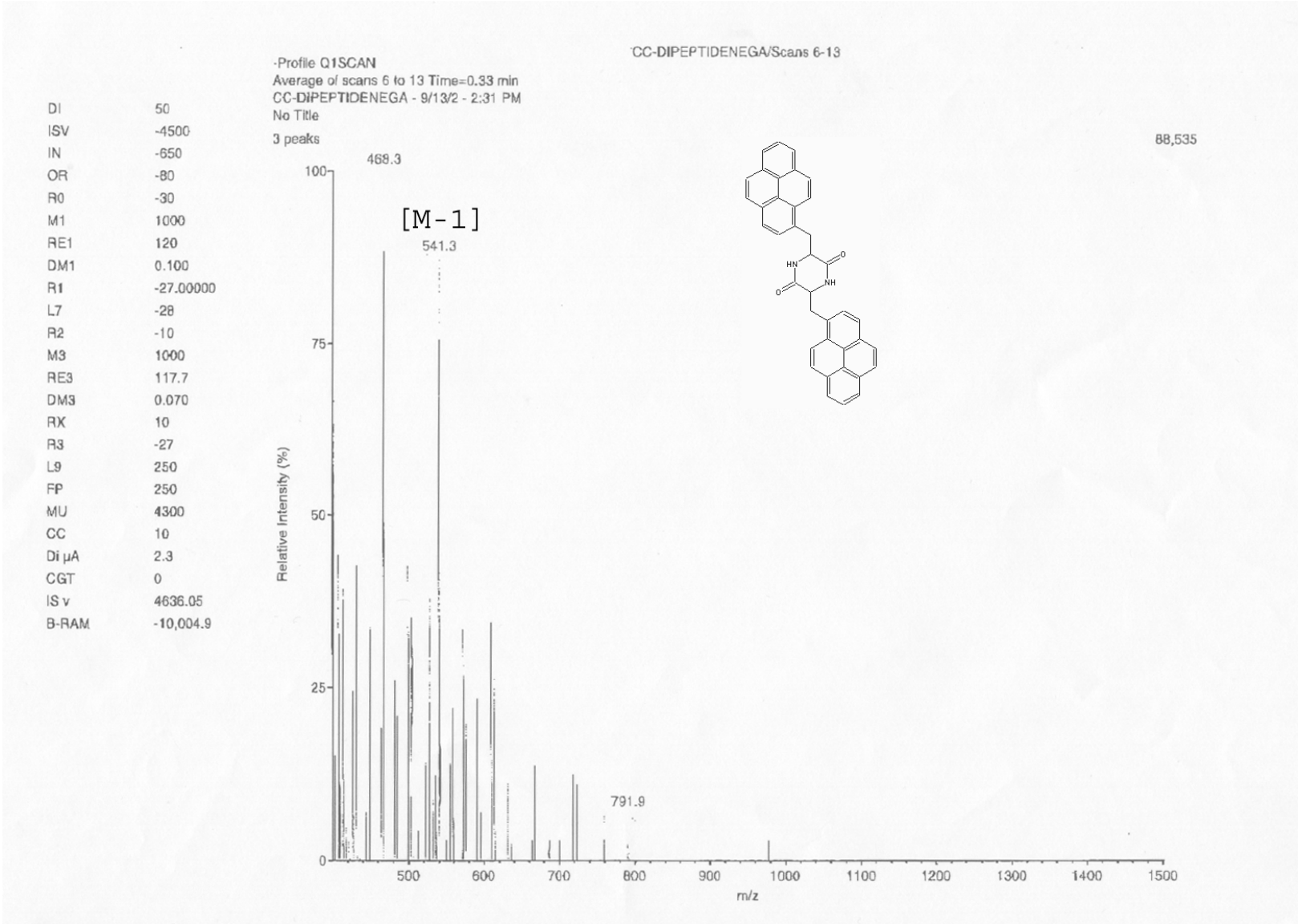
CC-DIPEPTIDENEGA/Scans 6-13
-Profile Q1SCAN
Average of scans 6 to 13 Time=0.33 min
CC-DIPEPTIDENEGA - 9/13/2 - 2:31 PM
No Title
3 peaks
88,535
DI 50
ISV -4500
IN -650
OR -80
R0 -30
M1 1000
RE1 120
DM1 0.100
R1 -27.00000
L7 -28
R2 -10
M3 1000
RE3 117.7
DM3 0.070
RX 10
R3 -27
L9 250
FP 250
MU 4300
CC 10
Di µA 2.3
CGT 0
IS v 4636.05
B-RAM -10,004.9
468.3
[M-1]
541.3
791.9
Relative Intensity (%)
m/z
100
75
50
25
0
500
600
700
800
900
1000
1100
1200
1300
1400
1500
HN
NH
O
O

2. REFERENCES

References:

[1] Feynman, R.P. "*There's Plenty of Room at the Bottom: An Invitation to Enter a New Field of Physics*" Published in *California Institute of Technologiy: Engineering and Science*, February, **1960**.
[2] Eigler, D.M.; Schweizer, E.K. *Nature*, **1990**, *344*, 524.
[3] Cuberes, M.T.; Gimzewski, J.K. *Appl. Phys. Lett.* **1996**, *69*, 3016.
[4] Drexler, K.E. *"Nanosystems: Molecular Machinery, Manufacturing, and Computation*". Wiley: New York, NY, **1992**.
[5] Merkle, R. *IEEE Spectrum*, **2001**, (2)*,* 19.
[6] Merkle, R. *Nanotech.*, **1997**, *8*, 149.
[7] Merkle, R.; Goddard, W.A.; Pery, J.; Musgrave, C. *Nanotech*., **1991**, *2*, 187.
[8] Drexler, K.E. *"Engines of Creation"*, Anchor Press/Double Day: Garden City, NY, **1986**.
[9] Whitesides, G.M. *Sci. Amer.*, **2001**, *285*, 78.
[10] Drexler, K.E.; Forrest, D.; Freitas, R.A.; Hall, J.S.; Jacobstein, N.; McKendree, T.; Merkle, R.; Peterson, C. *"A Debate About Assemblers"*, Insititute for Molecular Manufacturing, **2001**.
[11] Smalley, R.E.; Drexler, K.E. *Chem. Eng. News*, **2003**, *81*, 37.
[12] Reed, M.A.; Zhou, C.; Muller, C.J.; Burgin, T.P.; Tour, J.M. *Science*, 1997, *278*, 252.
[13] Facchetti, A.; Wnag, A.; Marks, T.J.; Sirringhaus, H.; Deng, Y.; Friend, R.H. *Polymer Mat. Sci. Eng.*, **2000**, *83*, 290.
[14] Mackowski, S.; Smith, L.M.; Jackson, H.E.; Heiss, W.; Kossut, J.; Karczewski, G. *Appl. Phys. Lett.*, **2003**, *83*, 254.
[15] Zhang, B.P.; Wang, W.X.; Yasuda, T.; Segawa, Y.; Yaguchi, H.; Onabe, K.; Edamatsu, K.; Itoh, T. *Mat. Sci. Eng.*, **1998**, *51*, 224.
[16] Yan, H.; Huang, W.; Cui, J. Veinot, J.G.C.; Kern, M.; Marks, T.J. *Advan. Mater.*, **2003**, *15*, 835.
[17] Pierson, H.O. *Handbook of Chemical Vapor Deposition: Principles, Technology, and Applications.* William Andrew Publishing: New York, NY., **1999**.
[18] Ulman, A. *An Introduction to Ultrathin Organic Films: From Langmuir-Blodgett to Self-assembly.* Academic Press: New York, NY., **1998**.
[19] Ulman, A. *Thin Films: Self-Assembled Monolayers of Thiols (Thin Films 24).* Academic Press: New York, NY., **1998**.
[20] Roberts, G.G. *Langmuir-Blodgett Films*. Plenum Press, **1990**.
[21] Langmuir, I. *J. Am. Chem. Soc.*, **1917**, *39*, 1848.
[22] Blodgett, K.B. *J. Am. Chem. Soc*, **1935**, *57*, 1007.
[23] Nuzzo, R.G.; Allara, D.L. *J. Am. Chem. Soc.* **1983**, *105*, 4481.
[24] Peterlinz, K.A.; Georgiadis, R. *Langmuir*, **1996**, *12*, 4731.
[25] Boubour, E.; Lennox, B.R. *Langmuir*, **2000**, *16*, 4222.
[26] Bard, A.J.; Kanoufi, F.; Cannes, C. *Langmuir*, **2002**, *18*, 8134.
[27] Laibinis, P.E.; Bain, C.D.; Nuzzo, R.G.; Whitesides, G.M. *J. Phys. Chem.*, **1995**, *99*, 7663.
[28] Patai, S.; Rappaport, Z. *The Chemistry of Organic Derivatives of Gold and Sulfur*. John Wiley and Sons: New York, **1999**.
[29] Fox, M.A.; Wooten, M.D. *Langmuir*, **1997**, *13*, 7099.
[30] Fox, M.A.; Weisin, L.; Lynch, V.; Thompson, H. *J. Am. Chem. Soc.* **1997**, *119*, 7211.
[31] Whitesides, G.M.; Wilbur, J.C.; Jackman, R.J. *Science*, **1995**, *269*, 664.
[32] Kuman, A.; Biebuyck, H.A.; Abbott, N.C.; Whitesides, G.M. *J. Am. Chem. Soc.*, **1992**, *114*, 9188.
[33] Chaudhury, M.K.; Whitesides, G.M. *Science*, **1992**, *256*, 1539.
[34] Laibinis, P.E.; Whitesides, G.M. *Langmuir*, **1990**, *6*, 87.
[35] Boubour, E.; Lennox, B.R. *Langmuir,*, **2000**, *16*, 7464.
[36] Boubour, E.; Lennox, B.R. *J. Phys. Chem. B.*, **2000**, *104*, 9004.
[37] Hong, H.G.; Mallouk, T.E. *Langmuir*, **1991**, *7*, 2362.
[38] Yang, H.L.; Aoki, K.; Hong, H.G.; Sackett, D.D.; Arendt, M.F.; Yau, S.L.; Bell, C.M.; Mallouk, T.E. *J. Am. Chem. Soc.* **1993**, *115*, 11855.
[39] Evans, D.S.; Ulman, A.; Goppert-Berarducci, K.E.; Gerenser, L. *J. Am. Chem. Soc.*, **1991**, *113*, 5866.
[40] Brust, M.; Blass, P.M.; Bard, A.J. *Langmuir*, **1997**, *13*, 5607.
[41] MacDonald, J.C.; Dorrestein, P.C.; Pilley, M.M. *Cryst. Growth and Design.* **2001**, *1*, 29.

[42] Bharathi, S.; Yengnaraman, V.; Rao, G.P. *Langmuir*, **1993**, *9*, 1614.
[43] Bharathi, S.; Nogami, M.; Ikeda, S. *Langmuir*, **2001**, *17*, 7468.
[44] Lin, C.; Kagan, C.R. *J. Am. Chem. Soc.*, **2003**, *125*, 336.
[45] Soto, E.; MacDonald, J.C.; Cooper, C.G.F.; McGimpsey, W.G. *J. Am. Chem. Soc.*, **2003**, *125*, 2838.
[46] MacDonald, J.C.; Dorrestein, P.C.; Pilley, M.M.; Foote, M.M.; Lundburg, J.L. Henning, R.W.; Schultz, A.J. Manson, J.L. *J. Am. Chem. Soc.*, **2000**, *122*, 11692.
[47] For other multilayer systems making use of ionic interactions see:
a. Ansell, M.A.; Zeppenfeld, A.C.; Yoshimoto, K.; Cogan, E.B.; Page, C.J. *Chem. Mater.*, **1996**, *8*, 591.
b. Lee, H.; Kepley, L.J.; Hong, H.G.; Mallouk, T.E. *J. Am. Chem. Soc.* **1988**, *110*, 618.
c. Hatzor, A.; Boom-Moav, T.V.; Yochelis, S.; Vaskevich, A.; Shanzer, A.; Rubinstein, I. *Langmuir*, **2000**, *16*, 4420.
d. Li, D.; Ratner, M.A.; Marks, T.J. *J. Am. Chem. Soc.*, **1990**, *112*, 1430.
e. Brust, M.; Blass, P.M.; Bard, A.J. *Langmuir*, **1997**, *103*, 5602.
[48] Nuzzo, R.G.; Dubois, L.H.; Allara, D.L.; Dhidsey, C.E.D. *J. Am. Chem. Soc.*, **1990**, *112*, 558.
[49] Hatzor, A.; Moav, T.; Cohen, H.; Matlis, S.; Libman, J.; Vaskevich, A.; Shanzer, A.; Rubinstein, I. *J. Am. Chem. Soc.*, **1998**, *120*, 13469.
[50] Ansell, M.; Cogan, E.; Page, C. *Langmuir*, **2000**, *16*, 1172.
[51] Uosaki, K.; Kondo, T.; Zhang, X.; Yanagida, M. *J. Am. Chem. Soc.*, **1997**, *119*, 8367.
[52] Morita, T.; Kimura, S.; Kobayashi, s.; Imanishi, Y. *J. Am. Chem. Soc.*, **2000**, *122*, 2850.
[53] Kondo, T.; Yanagida, M.; Nomura, S.; Ito, T.; Vosaki, K. *J. Electroanal. Chem*., **1997**, *438*, 121.
[54] Imahori, H.; Nishimura, Y.; Norieda, H.; Karita, H.; Yamazaki, I.; Sakata, Y.; Fukuzumi, S. *Chem. Comm.*, **2000**, 661.
[55] Imahori, H.; Norieda, H.; Nishimura, Y.; Yamazaki, I.; Higuchi, K.; Kato, N.; Motohiro, T.; Yamada, H.; Tamaki, K.; Arimura, M.; Sakata, Y. *J. Phys. Chem. B.*, **2000**, *104*, 1253.
[56] Imahori, H.; Norieda, H.; Yamada, H.; Nishimura, Y.; Yamazaki, I.; Sakata, Y.; Fukumuzi, S. *J. Am. Chem. Soc.*, **2001**, *123*, 100.
[57] Fujita, K.; Bunses, N.; Nakajima, K.; Hara, M.; Sasabe, H.; Knoll, W. *Langmuir*, **1998**, 6167.
[58] Nuzzo, R.G.; Dubois, L.H.; Allara, D.L.; Dhidsey, C.E.D. *J. Am. Chem. Soc.*, **1990**, *112*, 558.
[59] Whitesides, G.M.; Xia, Y. *Langmuir*, **1997**, *13*, 2059.
[60] Whitesides, G.M.; Laibinis, P.E. *Langmuir*, **1990**, *6*, 87.
[61] Abbott, S.; Ralston, J.; Reynolds, G.; Hayes, R. *Langmuir*, **1999**, *15*, 8923.
[62] Siewerski, L.M.; Brittain, W.J.; Petrash, S.; Foster, M.D. *Langmuir*, **1996**, *12*, 5838.
[63] Möller, G.; Harke, M.; Motschmann, H. *Langmuir*, **1998**, *14*, 4955.
[64] Ichimura, K.; Oh, S.; Nakagawa, M. *Science*, **2003**, *288*, 1624.
[65] Bayer, E.; Witte, E.G. *J. Coord. Chem.*, **1977**, *7*, 13.
[66] Vansant, J.; Toppet, S.; Smets, G. *J. Org. Chem.*, **1980**, *45*, 1565.
[67] Whitten, D.G.; McCall, M.T. *J. Am. Chem. Soc.*, **1968**, *91*, 5097.
[68] Chessa, G.; Scrivanti, A. *J. Chem. Soc. Perkin. Trans. I.*, **1996**, *4*, 307.
[69] Markees, D.G. *J. Org. Chem.*, **1964**, *29*, 3120.
[70] Huenig, S.; Wehner, I. *Synthesis*, **1989**, 552.
[71] Snyder, H.R.; Shekelton, J.F.; Lewis, C.D. *J. Am. Chem. Soc.*, **1945**, *67*, 310.
[72] Morrison, D.C. *J. Org. Chem.*, **1958**, *24*, 463.
[73] Nestor, J.J.; Ho, T.; Simpson, R.A.; Horner, B.L.; Jones, G.H.; McRae, G.I.; Vickery, B.H. *J. Med. Chem.*, **1982**, *9*, 1753.
[74] Leconite, L.; Rolland-Fulcrand, V.; Roumestant, M.L.; Viallefont, P.; Martinez, T. *Tetrahedron: Asymmetry*, **1998**, *9*, 1753.
[75] Colavita, P.E.; Doescher, M.S.; Molliet, A.; Evans, U.; Reddic, J.; Zhou, J.; Chen, D.; Miney, P.G.; Myrick, M.L. *Langmuir*, **2002**, *18*, 8503.
[76] Porter, M.D.; Bright, T.B.; Allara, D.L.; Chidsey, C.E.D. *J. Am. Chem. Soc.*, **1987**, *109*, 3559.
[77] Lehn, J.M. *Supramolecular Chemistry*, VCH, Weinheim, **1995**.
[78] Wu, C.G.; Bein, T. *Science*, **1994**, *264*, 757.
[79] Abrahams, B.F.; Hoskins, B.F.; Michail, D.M.; Robson, R. *Nature*, **1994**, *369*, 727.
[80] Granja, J.R.; Ghadiri, M.R. *J. Am. Chem. Soc.*, **1994**, *116*, 10785.
[81] Granja, J.R.; Buehler, L.K.; Ghadiri, M.R. *Nature*, **1994**, *369*, 301.
[82] Iijima, S. *Nautre*, **1991**, *354*, 56.

[83] Shnur, J.M. *Science*, **1993**, *262*, 1669.
[84] Harada, A.; Li, J.; Kamachi, M. *Nature (London)*, **1993**, *364*, 516.
[85] Kaiser, A.B. *Rep. Prog. Phy*, **2001**, *64*, 1.
[86] Vaccarini, L.; Goze, C.; Henard, L.; Hernandez, E.; Bernier, P.; Rubio, A. *Carbon*, **2000**, *38*, 1681.
[87] Barton, J.K.; Delaney, S. *J. Org. Chem.*, **2003**, *68*, 6475.
[88] Murphy, C.J.; Arkin, M.R.; Chatlia, N.D.; Bossmann, S.; Turro, N.J.; Barton, J.K. *Proc. Natl. Acad. Sci.,* **1994**, *91*, 5315.
[89] Holmlin, R.E.; Tong, R.T.; Barton, J.K. *J. Am. Chem.. Soc.*, **1998**, *120*, 9724.
[90] Williams, T.T.; Barton, J.K. *J. Am. Chem. Soc.*, **2002**, *124*, 1840.
[91] Desantis, P.; Morosetti, S.; Rizzo, R. *Macromolecules*, **1974**, *7*, 52.
[92] Ghadiri, M.R.; Granja, J.R.; Milligan, R.A.; McRee, D.E.; Khazanovich, N. *Nature*, **1993**, *366*, 324.
[93] Hartgerink, J.D.; Granja, J.R.; Milligan, R.A.; Ghadiri, M.R. *J. Am. Chem. Soc.*, **1996**, *118*, 43.
[94] Sun, X.; Lorenzi, G.P. *Helv. Chim. Acta*., **1994**, *77*, 1520.
[95] Granja, J.R.; Ghadiri, M.R. *J. Am. Chem. Soc.*, **1994**, *116*, 10785.
[96] Khazanovich, N. Granja, J.R.; McRee, D.E.; Milligan, R.A.; Ghadiri, M.R. *J. Am. Chem. Soc.,* **1994**, *116*, 6011.
[97] Engels, M.; Bashford, D.; Ghadiri, M.R. *J. Am. Chem. Soc.,* **1995**, *117*, 9151.
[98] Kobayashi, K.; Granja, J.R.; Ghadiri, M.R. *Angew. Chem. Int. Ed. Engl.,* **1995**, *34*, 95.
[99] Ghadiri, M.R.; Kobayashi, K.; Granja, J.R.; Chadha, R.K.; McRee, D.E. *Angew. Chem. Int. Ed. Engl.*, **1995**, *34*, 93.
[100] Bong, D.T.; Clark, T.D.; Granja, J.R.; Ghadiri, M.R. *Angew. Chem. Int. Ed. Engl.*, **2001**, *40*, 988.
[101] Kawahara, S.; Uchimaru, T.; Murata, S. *Chem. Commun.,* **1999**, 563.
[102] Tong, A.K.; Jockusch, S.; Li, Z.; Zhu, H.; Atkins, D.L.; Turro, N.J.; Ju, J. *J. Am. Chem. Soc.*, **2001**, *123*, 12923.
[103] Boon, E.N., Barton, J.K. *Curr.Op. Struct. Bio.*, **2002**, *12*, 320.
[104] Camerman, A.; Trotter, J. *Acta Crystallogr.*, **1965**, *18*, 636.
[105] Nishino, N.; Mihara, N.; Tanaka, Y. *Tet. Lett.*, **1992**, *33*, 570.
[106] Mihara, H.; Tanaka, Y.; Fujimoto, T.; Nisho, N. *J. Chem. Soc. Perkin 2.*, **1995**, *6*, 1133.
[107] Ono, S.; Kameda, N.; Fujii, R.; Yoshimura, T.; Shimasaki, C. *Pep. Chem.*, **1993**, *31*, 449.
[108] Foerster, T.; Kasper, K. *Z. Physik Chem. N.F.* **1954**, *1*, 275.
[109] Winnik, F.M. *Chem. Rev.* **1993**, *93*, 587.
[110] Hochstrasser, R.M. *Ann. Rev. Chem. Phys.,* **1966**, *17*, 466.
[111] Turro, N.J. *Modern Molecular Photochemistry*. University Science Books, California, **1991**, 142.
[112] Kryszewski, M.; Wojciechowski, P. *Mol, Cryst. Liq. Cryst.*, **1976**, *32*, 183.
[113] Bhowmik, B.B.; Bhattacharyya, A. *Spectrochim. Acta. A.*, **1986**, *42A*, 1361.
[114] Yoshihara, K.; Kasuya, T. *Chem. Phys. Lett.*, **1971**, *9*, 469.
[115] Chu, N.R.C.; Kawaoka, K.; Kearns, D.R. *J. Chem. Phys.*, **1971**, *55*, 3059.
[116] Klopffer, W.; Bauser, H.; Dolezalek, F.; Naundorf, G. *Molec. Cryst. Liq. Cryst,.* **1972**, *16*, 229.
[117] Strauss, J.; Paub, J. *Org. Lett.*, **2002**, *4*, 683.
[118] Soliehac, J.M.; Roques, B.P. *Anal. Biochem.*, **1996**, *241*, 120.
[119] Szmanska, A.; Wicz, W.; Lankiewicz, L. *Amino Acids*, **2001**, *21*, 265.
[120] For a comprehensive review of laboratory techniques see: White, P.; Dorner, B.; kSteinauer, R. *The NovaBiochem 2002-2003Catalog: Synthesis Notes*, NovaBiochem Publishing: CA, **2002**.
[121] Benz, H. *Tetrahedron*, **1993**, *49*, 11065.
[122] Buriak, J.K.; Ghadiri, M.R. *"Self-Assembly of Cyclic Peptide Based Nanotubes on Gold and Silicon* Dioxide Surfaces", 213th Meeting of the American Chemical Society, Book of Abstracts. **1997**, No. 0853.
[123] Kim, H.S.; Hartgerink, J.D.; Ghadiri, M.R. *J. Am. Chem. Soc.,* **1998**, *120*, 4417.
[124] Chin, D.N.; Simanek, E.E.; MacDonald, J.C.; Whitesides, G.M.; McBride, M.T.; Palmore, G.T. *J. Am. Chem. Soc.,* **1997**, *119*, 11807.
[125] Wooten, M.D.; Fox, M.A. *Langmuir*, **1997**, *13*, 7099.
[126] Atabekyan, L.S.; Astafev, P.N.; Roitman, G.P.; Romanovskaya, G.I.; Chibisov, A.K. *J. Phys. Chem.*, **1982**, *56*, 1618.
[127] Yokoyama, Y. *Chem. Rev.*, **2000**, *100*, 1717
[128] Neta, P.; Whillans, D.W. *Radiat. Res.*, **1977**, *70*, 325.

[129] McGimpsey, W.G.; Nienaber, H.A.; Dennen, K.; Benco, J.S. *J. Photochem. Photobiol. A.*, **2002**, *152*, 33.
[130] McGimpsey, W.G.; Nienaber, H.A.; Benco, J.S. *Sensors and Actuators B*, **2002**, *85*, 126.
[131] McGimpsey, W.G.; Nienaber, H.A.; Benco, J.S. *The Spectrum*, **2002**, *14*, 1.

3. Curriculum Vitae

Christopher Cooper

709 Franklin St. Apt.1 (508) 795-1470
Worcester, MA 01604
ccoo@wpi.edu

Objective To obtain a full-time position as a synthetic chemist.

Education

Worcester Polytechnic Institute, Worcester, MA
8/99-5/04 Doctorate in Chemistry

Connecticut College, New London, CT
8/95-5/99 ACS Certified Bachelor of Arts in Chemistry

Research Experience

Doctoral Thesis, Worcester, MA
"Self Assembling Systems for Molecular Device Applications"

- Synthesis and characterization of:
  - unnatural amino acids
  - self-assembled mono- and multilayers on gold
  - linear and cyclic peptides (by solution and solid phase methods)
  - crown ether monolayers on quartz
- Photophysical characterizations of polychromophoric systems
- Developed a novel supramolecular scaffold for the controlled growth of thin films

Senior Thesis, New London, CT
"Cluster Analysis and Molecular Mechanics of 14 Membered Macrolide Ring Systems and Cobalt(II) Containing 14 Membered Tetra aza Macrocycles."

- Molecular mechanics calculations were performed on large ring systems to determine substituent effects on ring conformations
- Monte Carlo simulations were employed to find idealized ring conformations.

Techniques/ Skills

Lab Techniques: Peptide synthesis, Asymmetric synthesis, Purification and structural characterization of organic compounds, Spectroscopic identification of unknown compounds, Photophysical characterizations

Instrumental Techniques: UV/Vis. spectroscopy, Fluorescence spectroscopy, Phosphorimetry, Laser Flash Photolysis, Infrared spectroscopy (including grazing angle), Nuclear magnetic resonance, Mass spectrometry, Gas chromatography, High performance liquid chromatography, Flash/column chromatography, Atomic Force Microscopy, Two-Photon Microscopy, Contact Angle Measurements, Cyclic Voltammetry, Impedance Spectroscopy, Ellipsometry

Computer Skills: MacroModel, MOPAC, MOE, Gaussian, HyperChem, ISIS Draw, ACD Chem Sketch, Chem Office, SciFinder Scholar, Beilstein

Commander, LabView, can operate LINUX and UNIX systems, Microsoft Office, Cricket Graph, KaleidaGraph

Experience

01/01-present **Worcester State College**, visiting lecturer, organic chemistry
01/02-present **Assumption College**, adjunct faculty member, organic chemistry
10/02-01/03 **Argose, Inc.**, visiting scientist, operator of the two photon microscopy lab

Publications

1. Cooper, C.G.F.; McGimpsey, W.G.M. "Self-assembled Peptide Nanotubes as Scaffolds for Molecular Wires". *Submitted*.
2. Cooper, C.G.F.; McGimpsey, W.G.M.; Guler, M.; Benco, J. "Singlet-Singlet and Triplet-Triplet Energy Transfer in Bichromophoric Peptides". *Submitted*.
3. Cooper, C.G.F.; McGimpsey, W.G.M.; Soto, E.; MacDonald, J.C. "Thin Films with Tunable Conductivity and Thickness: A Modular Approach". *Submitted.*
4. Cooper, C.G.F.; McGimpsey, W.G.M.; Soto, E.; MacDonald, J.C. "Anodic and Cathodic Photocurrent Generation from Modularly Assembled Thin Films". *Submitted.*
5. Cooper, C.G.F.; McGimpsey, W.G.M.; Soto, E.; MacDonald, J.C. "Non-Covalent Assembly of a Photoswitchable Surface". *J. Am. Chem. Soc. (Comm. Ed.), in press.*
6. Cooper, C.G.F.; McGimpsey, W.G.M.; Soto, E.; MacDonald, J.C. "A Non-Covalent Strategy for the Assembly of Supramolecular Photocurrent Generating Systems". *J. Am. Chem. Soc (Comm. Ed.)*. **2003**, *125*, 2838.
7. Cooper, C.G.F.; Zimmer, M. "Molecular Mechanical and Cluster Analysis of Fourteen-Membered Cobalt(III) Macrocyclic Complexes." *Structural Chem.*, **1999**, *10*, 17.

Conference Presentations

October 2003, Foresight Conference on Molecular Nanotechnology, San Francisco, CA
October 2002, Foresight Conference on Molecular Nanotechnology, Bethesda, MD
August 2002, ACA National Conference, San Antonio, TX
June 2001, NATO Conference, Spectroscopy of Spatially Confined Systems, Italy
August 1998, ACS National Meeting, Boston, MA

Awards

July 2002, Awarded ACA travel grant for crystallographic research
June 2001, Awarded NATO travel grant
May 2001, Poster Award for Outstanding research at WPI
May 1999-present, Awarded a variety of scholarships and stipends which have supported me to date.

Acitivities/ Interests

Teaching, Reading, Baseball, Running, Squash, Skiing, Playing Trumpet

References available upon request